Smelting of Iron Oxides Using Hydrogen Based Plasmas

An der Montanuniversität Leoben eingereichte Dissertation zur Erlangung des akademischen Grades eines Doktors der Montanistischen Wissenschaften

Verfasser: Karim Badr, B.Sc., M.Sc.

Leoben, November 2007

Eidesstattliche Erklärung

Ich erkläre an Eides Statt, dass ich die gegenständliche Dissertation selbstständig und ohne fremde Hilfe verfasst, andere als die angegebenen Quellen und Hilfsmittel nicht benutzt und die den benutzten Quellen wörtlich und inhaltlich entnommen Stellen als solche kenntlich gemacht habe.

Karim Badr

Acknowledgments

I would like to thank:

Prof. Dr.mont. Wilfried Krieger for his full support in helping to carry out the present work at the Chair of Metallurgy and his confidence in my work within ULCOS project.

Prof. Dr. techn. Harald Raupenstrauch, Chair of Thermal Processes, for his readiness to assess my work and his helpful suggestions.

Em O.Prof. Dr. mont. Herbert Hiebler, Chair of Metallurgy, for his continued support and advices during my research work.

Dipl.-Ing. Dr.mont. Eduard Bäck, In-House Consultant, for the fruitful discussions and the detailed review of my work.

Dipl.-Ing. Thomas Bürgler, voestalpine Stahl Linz, for his financial support during the first period of my work.

Dipl.-Ing. Dr.mont. Axel Sormann, voestalpine Stahl Donawitz, for his assistance in suppling the required raw materials and carring out the needed metal and slag chemical analysis (free of charge) within the company.

The technicians of the chair for their assistance in executing the experimental work.

My wife Ingy Abou Elkhair for her complete support during the completion of the research work.

Finally, I would like to thank the European Community for their financial support under contract no. 515960 within the framework of the European research project (ULCOS).

Schmelzreduktion von Eisenoxiden mit auf Wasserstoff basierendem Plasma

Kurzfassung

Wasserstoff-Plasma-Schmelzreduktion wurde als eine der möglichen innovativen Stahlerzeugungsrouten am Lehrstuhl für Metallurgie an der Montanuniversität Leoben seit nunmehr fast zwei Jahrzehnten untersucht. Es zeigte sich das Potenzial der Vermeidung direkter CO_2-Emissionen als Folge der Substitution fossiler Brennstoffe durch eine kohlenstofffreie Quelle (H_2-Plasma). Die vorliegende Arbeit zielt auf den Nachweis des Potenzials von H_2 - bzw. CH_4-haltigen Reduktionsmitteln in einem up-scaled Prozess als Alternative zu fossilen Reduktionsmitteln in konventionellen Prozessen ab. Einige Versuche wurden durchgeführt, um den Einfluss von Gasen wie CO, CO_2 und H_2O auf den Reduktionsprozess mit wasserstoffhaltigem Plasma zu untersuchen. Die kontinuierliche Feinerzzufuhr durch die Hohlelektrode wurde in einer Versuchsserie durchgeführt um den Einfluss auf die Plasmastabilität und die Reduktionskinetik zu beurteilen. Der Prozess wurde in Bezug auf die Thermodynamik und die Kinetik charakterisiert und in der vorliegenden Arbeit auch diskutiert.

Smelting of Iron Oxides Using Hydrogen Based Plasmas

Abstract

As one of the possible innovative steelmaking technologies, hydrogen plasma smelting reduction, HPSR, has been examined over almost two decades at the chair of metallurgy, University of Leoben. HPSR showed a potential due to its defining characteristic of no direct CO_2 emissions as a result of replacing fossil fuels by carbon free source (H_2-Plasma). The present work aimed at showing the potential of H_2/CH_4 in an up-scaled process as an alternative to fossil fuel in the conventional processes. Some experiments were done to investigate the influence of gases like CO, CO_2 and H_2O on the reduction behaviour of hydrogen plasma. Continuous feeding of fines ore through the hollow electrode was also conducted in a series of experiments to assess its influence on the plasma arc stability and the reduction kinetics. The characteristics of the process in terms of thermodynamics and kinetics was also examined and discussed within the thesis.

Table of contents

1 Introduction

1.1 Background

Climate change has become a dominating problem around the globe, and as a result has been a priority in the agendas of many industrial countries in the last decade. This global problem requires a global solution and policies to encourage improved energy efficiency and reduced CO_2 emissions in all fields. In that sense, the Kyoto protocol proved its potential due to the commitment of the participating countries to reduce CO_2 and five other greenhouse gases, or engage in emissions trading if they maintain or increase emissions of these gases. However, such policies of imposing extra taxes and charges on the Kyoto-countries merely results in a switch of production to other parts of the world. This is likely to increase, rather than reduce, global greenhouse gas concentrations. A competitive global industry, such as the steel industry requires new and imaginative approaches in the post-Kyoto period.

The steel industry has made significant reductions in its CO_2 emissions mainly within the EU since 1990. The iron and steel industry produces now just over 3 % of global green house gases (GHG) emissions, mainly CO_2, and is still committed to taking positive actions to achieve further reductions in its own CO_2 emissions. Moreover, the steel industry believes that the new policies should accommodate the production growth required to provide the world with the steel it needs. These policies became even more important with the increasing steel production in developing countries such as China and India, where a booming in the world production up to 1.24 billion tonnes of steel was achieved in 2006, [1].

Most CO_2 gases generated by the steel industry is produced from the reduction of iron ore by carbon in the blast furnace, i.e. 75 % of the total CO_2 emissions of the blast furnace-oxygen converter route (BF-BOF), [2]. However, it should be mentioned that the maturity and efficiency of the BF-BOF, as a conventional technology, means that in the most advanced facilities, the iron-reduction process operates close to thermodynamic limits. Therefore, by using conventional technologies, making substantial further reductions in CO_2 emissions will be almost impossible. Awareness of the need of breakthrough technologies for CO_2 mitigation recently arose on an international level.

1.2 Objective of the present work

Research and development for new technology solutions to radically reduce the level of CO_2 emissions into the atmosphere for each ton of steel produced has been recently undertaken by an EU project called ULCOS. ULCOS (Ultra Low CO_2 Steelmaking) is a "concept development" program that explored, fairly extensively, a wide array of steelmaking routes with a high potential for CO_2 mitigation. The technologies called for breakthrough innovation within the steel industry, as they will need extensive research & development to mature into commercial processes. The target is to develop new solutions, before the end of the 2010's, with 50 % less specific CO_2 emissions compared to the modern blast furnace. These solutions should be in a position to be rolled out into production plants 15 to 20 years from now. A second and third step should thus lead to the deployment of the ULCOS technologies in the post-Kyoto period, [3].

In the first phase of the project (2004-2006), many technologies have passed a first pre-screening. The technologies were mainly classified to the following sub-projects: (1) new carbon-based reduction concepts, making use of the shaft furnace but also (2) new smelting reduction processes with less common reactors; (3) natural gas based pre-reduction reactors (4) hydrogen-based reduction using hydrogen from CO_2 lean technologies; (5) direct production of steel by electrolysis, and (6) the use of biomass, which circulates carbon rapidly in the atmosphere. (7) CO_2 capture and storage will be included in the design, [4].

The contribution of the University of Leoben, chair of metallurgy was within the second sub-project, where introducing new smelting reduction processes was required. The priorities of the new processes were innovation in design, optimization of energy and the use of carbon-lean or renewable resources.

A smelting reduction process is generally a two stage process, followed by a refining stage to produce liquid steel. These two stages include a first pre-reduction/pre-heating stage, followed by a final stage, which takes place in a bath of liquid iron and slag, figure 1. In the case of carbon based processes, oxygen is also injected with the reductant. This second stage is the so called bath smelter, electric arc or hydrogen plasma reactor. Using fines ore, rather than pellets, lumps and sinter is a main advantage of the process, where raw materials pre-treatment and coking (in the case of carbon usage as a reductant) are ruled out.

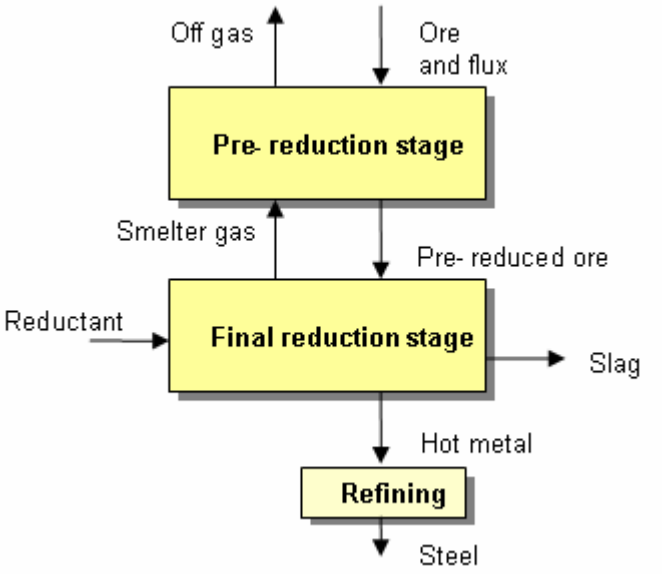

Fig. 1. Schematic diagram of a two stage smelting reduction process, [5]

The participation of the chair of metallurgy in the second sub-project was due to their experience in the field of hydrogen plasma smelting reduction, HPSR. It is should be noted that the development of HPSR, on a lab scale basis, has started within the chair of metallurgy since 1990, [6,7]. The objective of this participation was to show the potential of H_2/CH_4 as an alternative to fossil fuel, which is indispensable in the conventional processes both as heat source and reducing agent. The characteristics of the process in terms of thermodynamics, kinetics, and up-scalability potential were investigated and explained in details within the project.

1.3 Structure of the present work

The present work is classified into theoretical part and experimental part. In the theoretical part, a literature review to the relevant published work was carried out. Main topics covered are in the field of thermodynamical basics of iron ore reduction, kinetics results, and characteristics of direct current plasma. In the experimental part, the results of reduction experiments conducted in a plasma furnace are presented, discussed and compared with the previous conducted work.

In chapter 2, the thermodynamic principles of iron ore reduction are discussed. Fundamentals of ore reduction under plasma application and influence of the melt's electric charge on the thermodynamics behaviour are covered.

In chapter 3, a focus on the reduction kinetics of molten iron oxide by various reducing agents is discussed. Published work in the reduction rate of iron oxide by hydrogen at temperatures just above the melting temperature of FeO and at higher temperatures, using plasma facility, are presented. The published reduction rates of iron oxide by CO at temperatures just above the melting temperature of FeO are also included. In the end of that chapter, the reduction rate of molten iron oxide by solid carbon against that reduced by carbon dissolved in liquid iron are presented.

In chapter 4, the principles of a DC plasma is introduced. After defining briefly the meaning of plasma, published work is presented on the diagnostics of the plasma, i.e. plasma gas properties, velocity and arc classification. Moreover, mechanisms of heat transfer, effect of gas composition and metal vapours on the heat transfer are covered. Finally, the influence of plasma on the melt in terms of circulating flows in the melt and the depression pattern are discussed.

In chapter 5, the mechanism of H_2/H_2O solubility in liquid iron and slag is discussed. The importance of this subject is the susceptibility of liquid iron in the adopted process, hydrogen plasma, to relatively high hydrogen diffusion. This phenomenon is emphasized due to working with H_2 based gases plus dissociating atmosphere that is caused by arc / plasma.

Before starting the experimental part, thermodynamic calculations by FactSage 5.5, chapter 6, are carried out for better understanding of the thermodynamic characteristics of the reducing agents and oxidizing gases that were used in the experimental work. The influence of CaO additions and slag temperature on the liquidus temperature of the calculated phase diagrams are also investigated.

In chapter 7, the experimental work is presented. In the first section, 7.1, an overview of the experimental program is shown. While, the setups of the experiments conducted are described in other section, 7.2. Procedures of execution of experiments and the results evaluation are also demonstrated in section 7.3. Results of the experiments are finally presented and discussed in sections 7.4 and 7.5.

In chapter 8, the up-scaling potential of the prospective H_2/CH_4 plasma smelting reduction process is described. A conceptual design for an up-scaled production process of 1Mt/y is conducted by presenting a relevant flow-sheet and the corresponding heat and mass balance. A brief envisage is also introduced to the process parameters. The characteristics of the up-scaled process are in the end summarized by analysing its Strengths-Weaknesses-Opportunities-Threats (SWOT analysis).

In the last chapter, chapter 9, a conclusion of the experimental work is conducted. The main characteristics of an up-scaled process are also described exploiting the experimental results obtained. In the end, a proposal to the possible future experimental work is also introduced to widen the experience of the chair of metallurgy in terms of the process strengths.

2 Thermodynamical principles of iron oxide reduction

2.1 Thermodynamics at low temperatures

Bauer–Glaessner diagram shows the equilibrium between the iron oxide and H_2O/H_2 mixtures with respect to temperature, figure 2. CO/CO_2 equilibrium is also presented. The two leftmost equilibrium lines shown in the plot of the diagram represent the metallic iron /wustite equilibrium, reactions numbered with 3, whereas the two rightmost lines represent the hematite/magnetite equilibrium, reactions numbered with 1. The Bauer–Glaessner diagram provides two key properties describing the interaction between solid and gas phase in the shown reactions: Firstly, the equilibrium gas concentrations calculated for reactions of the investigated gaseous species with different iron oxides can be directly derived from the equilibrium lines shown in the diagram. Secondly, the relative position of the input gas concentrations indicates which equilibrium can be achieved with a certain reaction temperature.

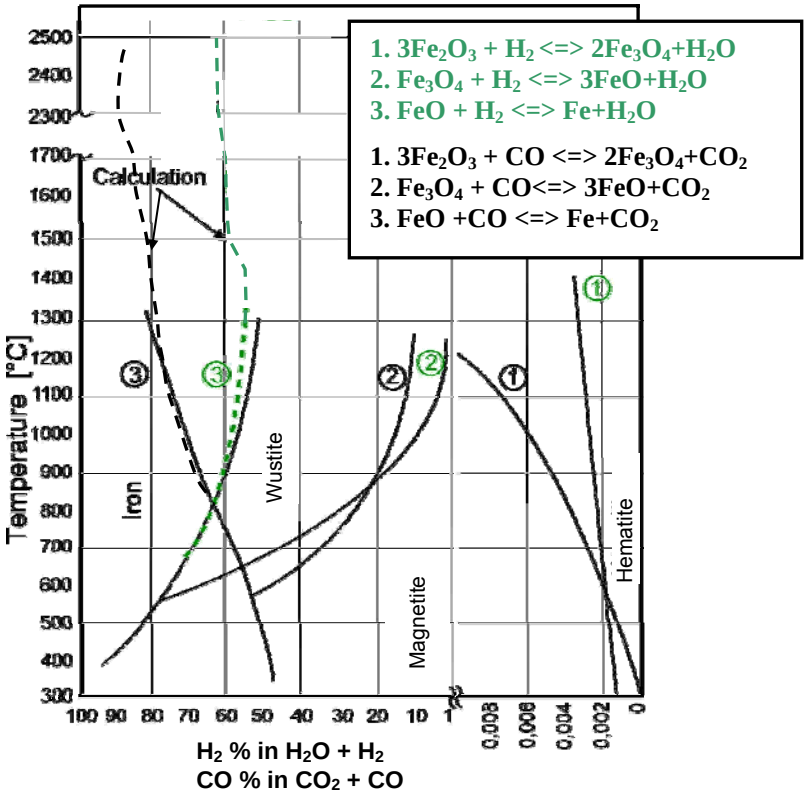

Fig. 2. Bauer-Glaessner diagram [8]

For instance at a temperature of 1300 °C, the equilibrium gas concentrations achieved with a reduction from wustite to iron would be 52 % H_2 / 48 % H_2O, and 82 % CO / 18 % CO_2, respectively. In other words, gas yields (degrees of gas utilisation) of input hydrogen and input CO of 48 % and 18 % are respectively obtained and an input gas having a H_2/H_2O ratio less than 52/48 and a CO/CO_2 ratio less than 82/18 will therefore not reduce wustite.

Extrapolating the equilibrium lines of FeO and H_2 / CO in figure 2 at higher temperatures (with molten phases) via calculations using FactSage program [9], indicates a constant degree of utilisation of H_2 of approximately 40 % up to 2500 ^oC. Moreover a slight variation between 10 and 15 % in the case of CO utilisation degree was found. It should be mentioned that above 2500 ^oC, further extrapolation of the equilibrium lines was not possible due to the significant evaporation of Fe and FeO. By conducting, however, equilibrium calculations of FeO and H_2 at higher temperatures (2600 ^oC - 2900 ^oC), an evolution of higher amounts of H_2O with respect to equilibrium at lower temperatures is obtained. It should be noted that this increase in H_2O amounts is not attributed to a change in the hydrogen reduction behaviour but to the shift of FeO from the liquid to the gas phase and its subsequent reaction with the existing molecular hydrogen to produce H_2O and gaseous Fe.

2.2 Thermodynamics at plasma temperatures

2.2.1 Fundamentals

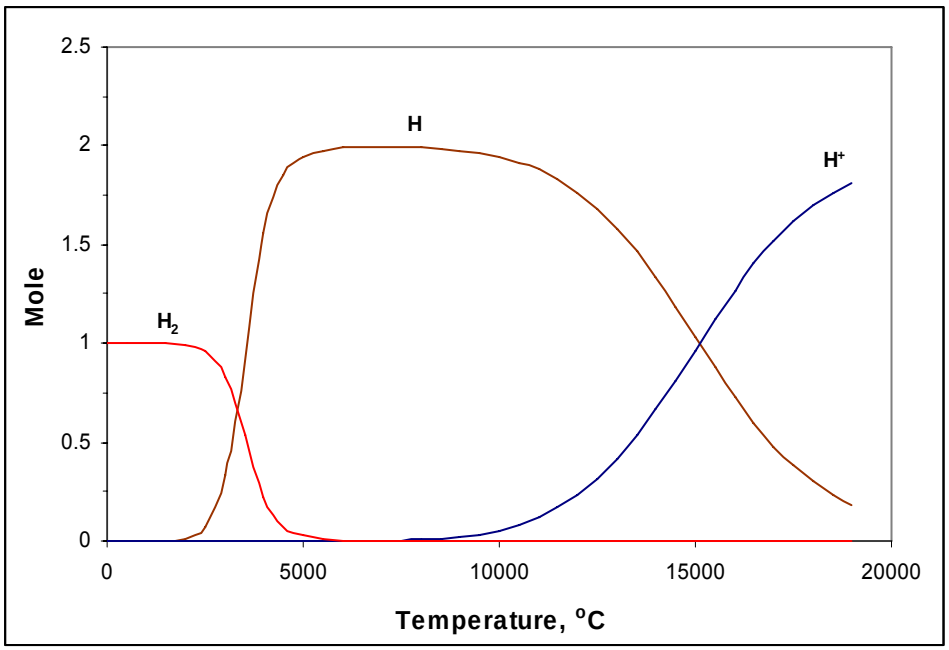

Fig. 3. Hydrogen dissociation and ionisation versus temperature, [10]

In plasma metallurgy, hydrogen can be chosen as a reducing gas for ore reduction purposes. Hydrogen under ambient temperature exists only in its molecular form, H_2, where the covalent bond between the two atoms is secured by a shared electron pair. At higher temperatures, H_2 starts to dissociate, as shown in figure 3, where the amount of H exceeds that of H_2 at approximately 3500 °C. Increasing the temperature furthermore leads to the ionisation of H into H^+. H^+ exceeds H at a temperature of 15500 °C.

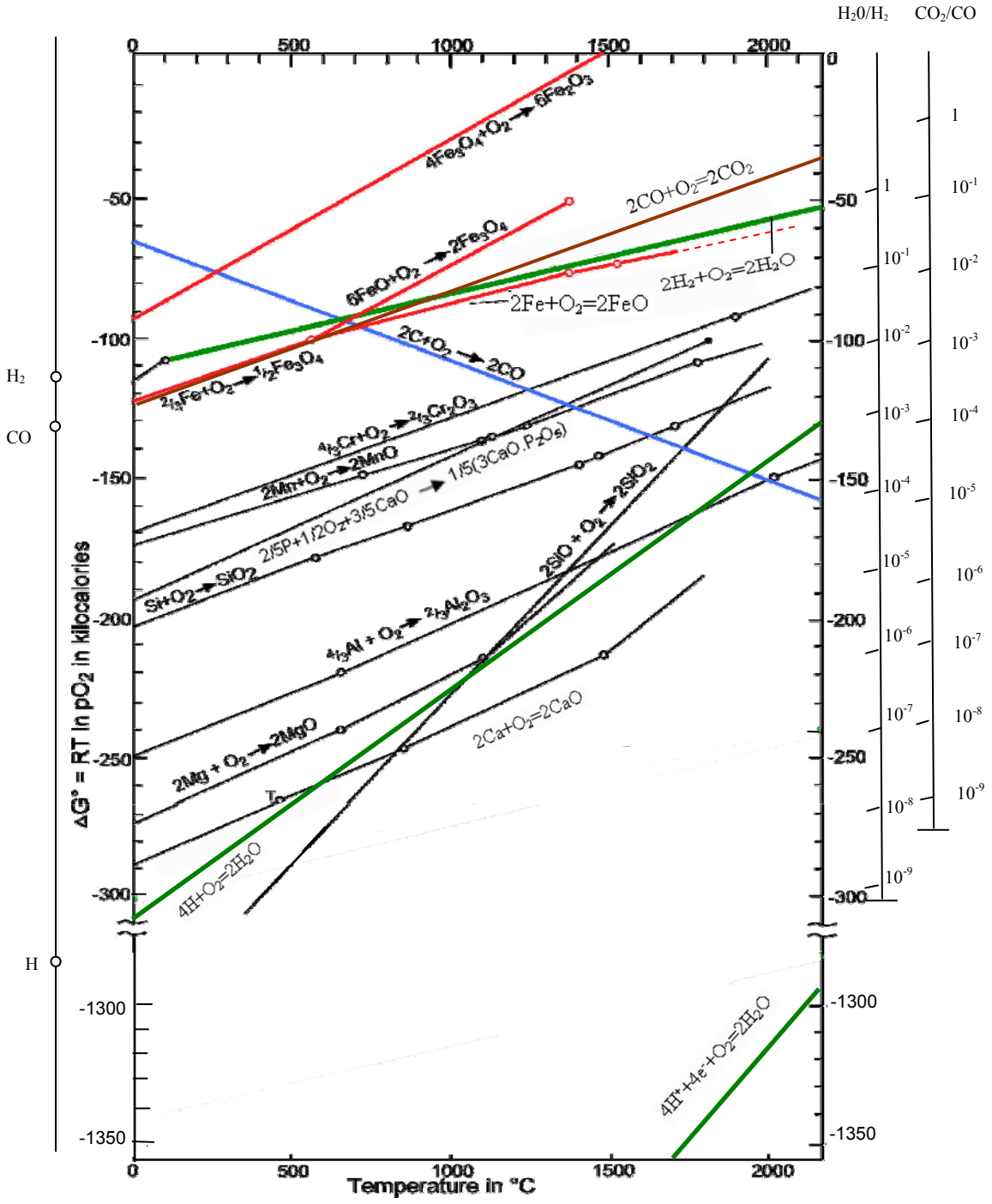

Fig. 4. Free energy of formation of various oxides, based on Ellingham - Richardson diagram, [11,12,13]

The Ellingham-Richardson diagram was explained in details in previous work [10,14]. However, a brief review of the diagram has been described in this work, where H and H^+ equilibrium calculations were corrected using FactSage program [14], with respect to the published calculations done by Dembovsky [15]. FeO-CO equilibrium line was also included.

The importance of the Ellingham-Richardson diagram, figure 4, in any set of compounds, such as oxides, is the possibility to readily determine the thermodynamics of all possible reactions. Important reactions and equilibriums can therefore be separated from those which are not important. Furthermore, the diagram can be used to quantitatively estimate how changes in temperature, pressure and composition affect the relevant chemical equilibrium.

The standard free energies of formation of various metal oxides, ΔG^o, are represented in figure 4 as a function of temperature. For temperatures at which the H_2/H_2O, CO/CO_2, C/CO equilibrium lines lie below the oxide lines, the corresponding reducing agent can reduce the oxides to their sub-oxides or elements. Furthermore, the ratios of H_2O/H_2 and CO_2/CO in equilibrium with any of the metal-metal oxide systems are easily determined using the right hand side scales shown in the diagram.

At higher temperatures, up to 20000 ^oC in the case of plasma application, where the existence of H_2, H and H^+ is possible, a potential reduction of extremely stable oxides, from the thermodynamical point of view, is obtained. In other words, the use of plasma shifts the ΔG^o values further towards the negative domain. This is evident from the shown free energies of formation of H_2O by means of H and H^+ with respect to H_2, [16]. However, practically speaking, in plasma metallurgy, homogeneous reactions (single phase) could not be guaranteed unless the processed material converts to a plasma state as well.

$$2H_{2(g)} + O_{2(g)} \leftrightarrow 2H_2O_{(g)} \qquad \Delta G^0_{298} = -474.38\ [kJ \cdot mol^{-1}] \qquad (1)$$

$$4H_{(g)} + O_{2(g)} \leftrightarrow 2H_2O_{(g)} \qquad \Delta G^0_{298} = -1287.55\ [kJ \cdot mol^{-1}] \qquad (2)$$

$$4H^+_{(g)} + O_{2(g)} + 4e^- \leftrightarrow 2H_2O_{(g)} \qquad \Delta G^0_{298} = -6512.24\ [kJ \cdot mol^{-1}] \qquad (3)$$

2.2.2 Influence of the melt polarity on thermodynamics

In the reduction processes, the reactions take place in heterogeneous systems, where the reducing gas is in the plasma phase while the processed material is in the solid or liquid

phase. A scheme of such a system, as shown in figure 5, showing the transport of active particles from the plasma to the surface of the material was presented by Dembovsky, [17].

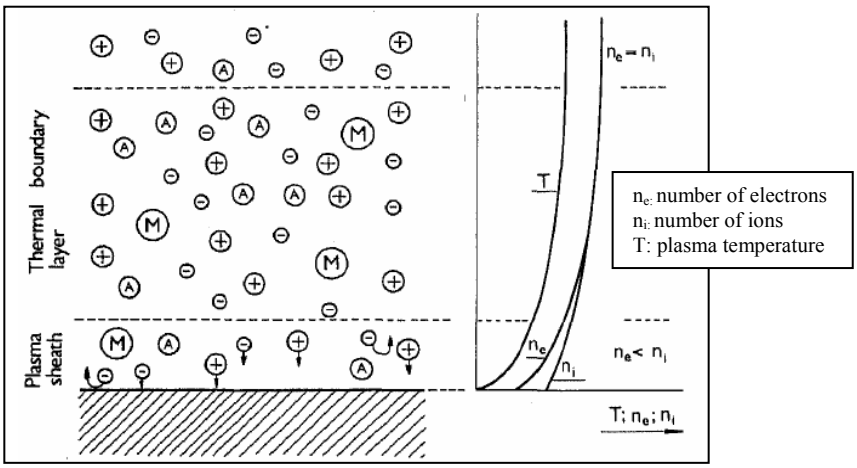

Fig. 5. Transport of active particles to the reacting surface, in the absence of an external electric field, Ⓜ : molecule, Ⓐ: atom, [17]

At the interface between the relatively cool charge material and the plasma, there will always be a boundary layer marked by an abrupt temperature gradient. In this layer atomic and electrically charged particles will tend to recombine. Recombination will reduce the concentration of the atomic and ionic particles, while increasing the concentration of electrically neutral or already recombined particles. Therefore, the zone adjacent to the cool surface will also be a region of concentration gradients, where the declining concentration of active particles causes ions and electrons to diffuse towards the reacting surface. As the coefficient of diffusion for electrons is much higher than that of ions, this might seem to imply that the electron flow will exceed the ion flow, but the electrically insulated surface of the charge material will not allow such development. A negative potential is formed which repels electrons and attracts positive ions until the flows are balanced. This process is localized in a narrow layer known as the plasma sheath, where the plasma is deprived of its electrically quasi neutral character as the positive and negative components no longer cancel each other.

When the electrically conductive charge surface is incorporated in the plasma torch circuit, or when a voltage is applied across this surface and the plasma stream, the situation that arises conforms essentially to that shown in figures 6 or 7, depending on the polarity of the surface charge.

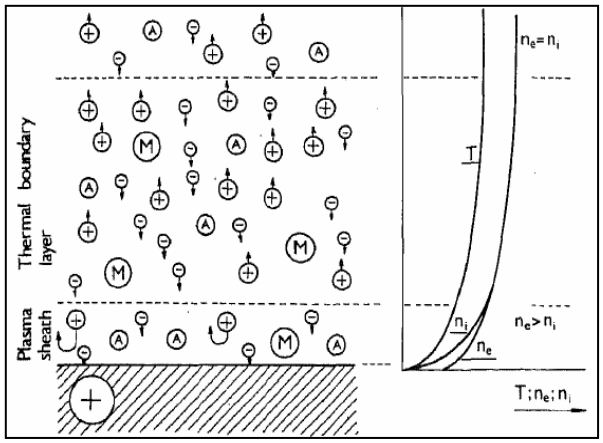

Fig. 6. Transport of active particles to the reacting surface with positive polarity, [17]

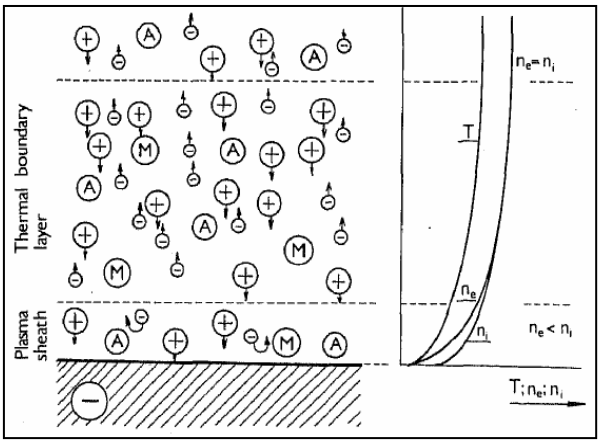

Fig. 7. Transport of active particles to the reacting surface with negative polarity, [17]

When the surface charge has a positive polarity, the current density, j, is delivered via the electrons, while the opposite takes place when the polarity is negative, i.e. the current density is transferred to the surface via the flow of ions.

Dembovsky [17] has examined the situation arising in the absence and the existence of an external applied electric field. The resultant electric field is found to accelerate particles with a polarity opposite to that of the surface, so that in effect the charge material attracts particles of the opposite polarity and repels particles which share its own polarity. A positively charged surface will attract electrons, but repel positive ions; consequently, the particles reacting with that surface will be neutral atoms and molecules. Conversely, a negatively charged surface will repel electrons and will therefore react only with positive ions and electrically neutral atoms and molecules.

Figure 8 shows the changes in the standard free energy, ΔG^o, at various temperatures of the reacting surface of iron oxide when it is reduced by hydrogen at 10,000 K, in a reaction described by:

$$FeO_l + xH_2 + 2yH + 2zH^+ + 2ze \rightarrow Fe + H_2O \qquad (4)$$

Dembovsky demonstrates in the diagram that a positive polarity of the reacting surface reduces the thermodynamic potential of this reaction with respect to the state with no external electric field application. On the other hand, the reaction proceeds much better, i.e. more negative ΔG^o, in the case of the surface negative polarity.

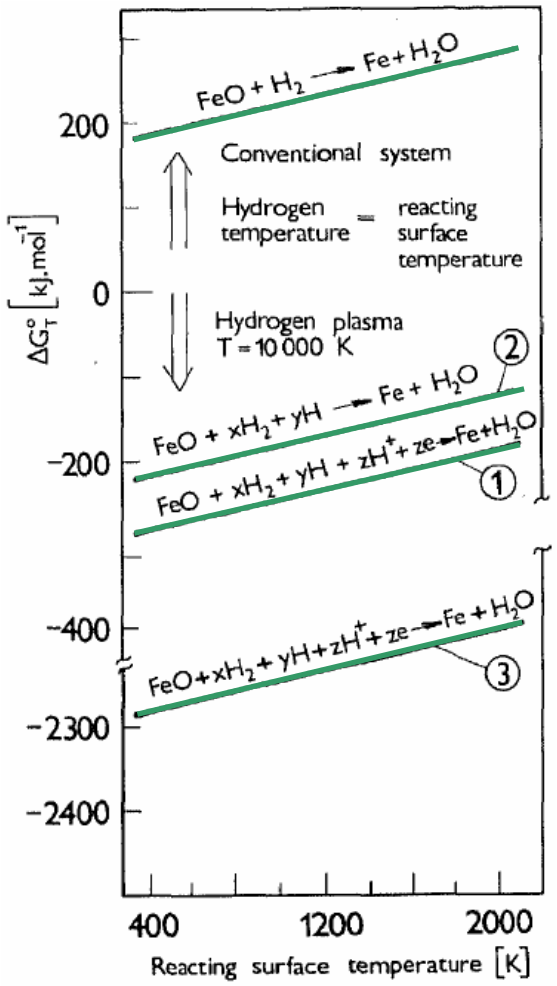

Fig. 8. ΔG^{o} versus surface temperature for FeO reduction by hydrogen plasma, [17]

1-no applied electric field, 2- surface with positive polarity, 3- surface with negative polarity

3 Kinetics of molten iron oxide reduction

For a chemical reaction to occur, the reacting particles must first collide, i.e. come into physical contact with one another with enough kinetic energy to climb the activation energy barrier. As the temperature of the system increases, the number of molecules that carry enough energy, to react when they collide, also increases. However, mutual contact is not all that is needed. Many reactions are restricted to rates far lower than the limit imposed by the frequency of collisions. By varying the concentrations of some of the reagents, we can not only influence the reaction rate, but also identify the slowest event in the mechanism, that restricts the overall reaction rate.

Mechanisms of the reduction in heterogeneous gas liquid system for iron oxide reduction by hydrogen plasma are governed by the following steps as summarized by Kamiya et al, [18]:

1. Mass transfer of hydrogen through a gas film from the bulk phase to the reaction interface between plasma gas and molten iron oxide or FeO bearing slag.
2. Mass transfer of oxygen through a liquid film from molten iron oxide or molten FeO bearing slag bulk to the reaction interface.
3. Adsorption of the molecular or atomic hydrogen at the reaction interface.
4. Adsorption with dissociation of FeO at the reaction interface.
5. Chemical reaction at the reaction interface.
6. Desorption of H_2O from the reaction interface.
7. Mass transfer of H_2O through a gas film from the reaction interface to the bulk phase.

3.1 Reduction rate of molten iron oxide by hydrogen

3.1.1 Reduction rate by hydrogen at low temperatures

A lot of studies have been made on the kinetics of the reduction of solid iron ores for the understanding of the conventional iron making processes. However, fundamental research on the kinetics of the reduction of molten iron oxide using hydrogen is still insufficient. A study, done by Ban-Ya et al.[19] was conducted to investigate the kinetics of hydrogen reduction in molten iron oxide contained in an iron crucible. The experimental work was measured using a thermo-balance, as illustrated in figure 9. The sample was heated and melted by a SiC resistance furnace at 1673 K. It was then reduced by purging a H_2-Ar or H_2-He mixture onto the surface of the melt. The reduction rate was determined by continuously recording the weight decrease.The partial pressure of H_2 and the gas flow rate were varied in the ranges between 20 to 0.3 kPa and 0.4 to 28 l/min, respectively.

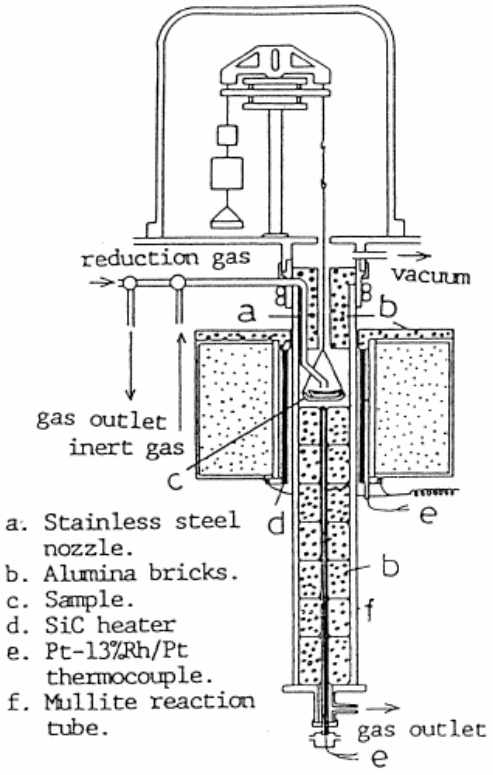

Fig. 9. Schematic diagram of the experimental setup, [19]

Throughout the experimental runs, the reduction rate was directly proportional to the partial pressure of H_2 in the H_2-Ar and H_2-He gaseous mixtures. It was expressed as follows:

$$r = k_a[H_2].p_{H_2} \quad \text{(kg-oxygen/m}^2\text{s)} \qquad (5)$$

where r is the specific reduction rate

$k_a[H_2]$ is the apparent rate constant for hydrogen reduction (kg-oxygen/m^2s Pa)

p_{H_2} is the H_2 partial pressure

The apparent rate constant obtained, $k_a[H_2]$, was found to be 1.6 x 10^{-6} (kg-oxygen/m^2s Pa) at 1673 K when the reduction rate was governed by the chemical reaction rate. The specific reduction rate, r, was accordingly determined to be 1.6 x 10^{-1} (kg-oxygen/m^2s) by using pure hydrogen.

Other work by Hayashi et al.[20] has measured the chemical reaction rate of hydrogen reduction in pure liquid FeO. A vertical type of cylindrical reactor was prepared as shown in figure 10. It was maintained at a constant temperature 1723 to 1823 K by heating a spiral SiC element. N_2-H_2 mixtures were flowed downwards through the reactor.

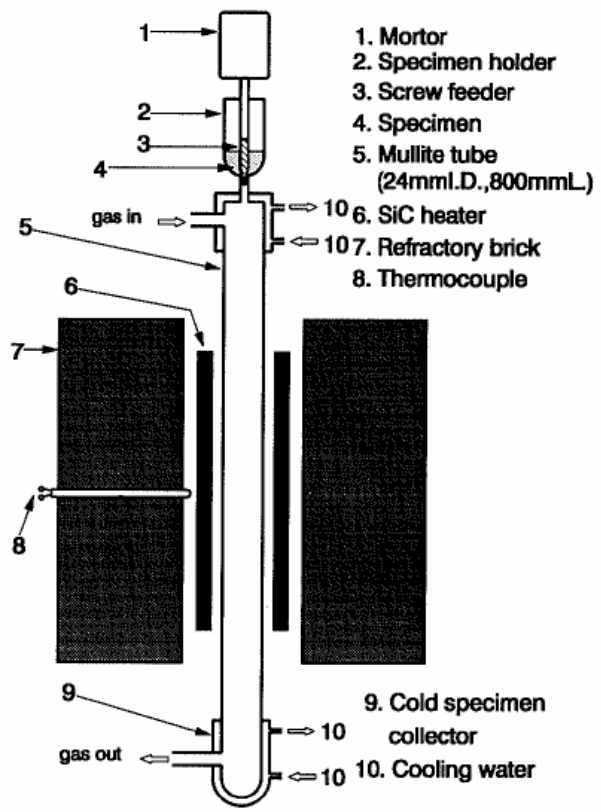

Fig. 10. Schematic diagram of the cylindrical reactor, [20]

A batch of pure spherical wustite particles (average diameter 58 μm) was fed into the upper part of the reactor at a small constant rate by means of a screw feeder. The feed ratio of particles to hydrogen was selected to be between 0.035 ~ 0.25 g/Nl, which allowed an extremely dilute particle-gas conveyance system to be realized. During the falling of these particles, they are melted, reduced, solidified and finally collected in a cold trap. The residence time of particles in the isothermal zone and the overall reduction rate can be controlled by shifting both flow rate and hydrogen content of gas mixtures in the range of Q = 0.6 ~ 3.0 Nl/min and 5 ~ 30 % H_2, respectively.

Results were obtained at 5 % H_2 where the chemical reaction should limit the overall reduction rates. It was found that the reaction rate constant decreased at higher % H_2 due to the increase of the diffusion resistance within the liquid phase. The results showed a specific reduction rate of 1.58 x 10^{-1} (kg-oxygen/m^2s) at 1773 K. The results obtained were slightly at elevated temperatures but showed good agreement with the previous shown work of Ban-Ya ,[19].

3.1.2 Reduction rate by hydrogen at plasma temperatures

Utilisation of plasma technology in the smelting of ores has been investigated since the late 1970's [21-33] and was summarized in a previous work [13]. However, the studies concerned with the reduction kinetics of molten FeO with hydrogen plasma are briefly reviewed in this section.

Kamiya et al. [18] have prepared a simple experimental apparatus for the study of iron ore reduction rate, figure 11. It is composed of a DC plasma torch with thoriated tungsten electrode, water cooled copper anode and water cooled copper crucible. The ore was partially melted by non transferred Ar plasma and then melted down by a transferred Ar plasma. The plasma gas was then switched to a H_2-Ar mixture. The ore varied between 25 to 75 g, the flow rate of the mixture was 20 Nl/min and the input DC power 8.3 kW.

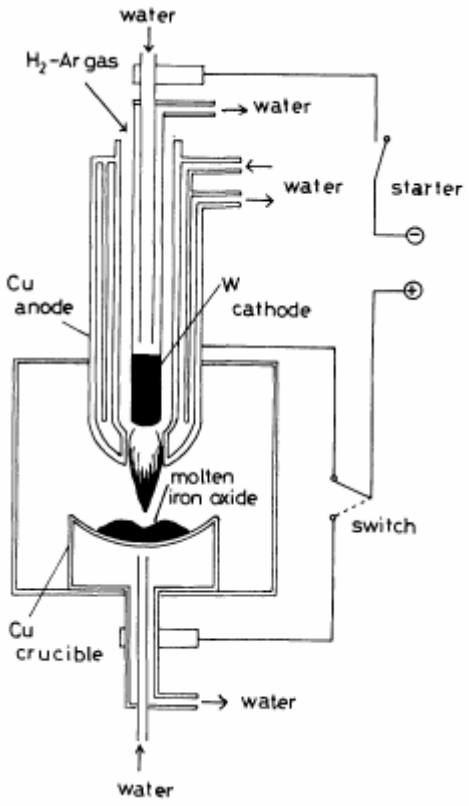

Fig. 11. Schematic diagram of the experimental apparatus, [18]

The results obtained showed a degree of hydrogen utilisation of approximately 44 %. This conforms to the reduction of FeO by molecular H_2 from the equilibrium point of view. The specific reduction rate of FeO, r, was also determined to be 0.3 kg-oxygen/m^2s. On the other hand, higher degree of hydrogen utilisation (60 – 70 %) at low concentrations of inlet H_2, less

than 20 % H_2 in Ar-H_2 mixtures was found. This phenomenon of having a higher degree of hydrogen utilisation at low % H_2 was also found in the work of Nakamura [29]. Nakamura attributed this in part to the dissociated hydrogen presented in the plasma. Moreover, he presumed that the separation of the oxide melt from the reduced iron might improve the reduction behaviour, i.e. iron oxide alone reacts with hydrogen. Lemperle [21] reported that the novel effect of atomic hydrogen, i.e. higher utilisation degree, might appear at low concentrations of H_2 but then disappears when the rate of recombination of atomic hydrogen increases (at higher concentrations of H_2).

The studies conducted by Nakamura et al. [29] and Lemperle [21], using principally a symmetric experimental setup like that shown in figure 11, showed specific reduction rates, r, of about 0.3 and 0.28 kg-oxygen/m^2s respectively, as was reported by Lemperle. These results are in good agreement with that of Kamiya [18]. However, a slight deviation in the results obtained should be expected due to the approximation of the reaction area (the arc melt interface) in the works conducted.

The published reduction rate of FeO by hydrogen in the solid phase, in the liquid phase (above the melting point of FeO) and at a higher temperature under plasma application are summarized in figure 12. It is clear that the reduction potential of hydrogen increases almost two orders of magnitudes just above the FeO melting point, with respect to that of the wustite phase. However, increasing the temperature up to the plasma temperature does improve the reduction rate but within the same order of magnitude.

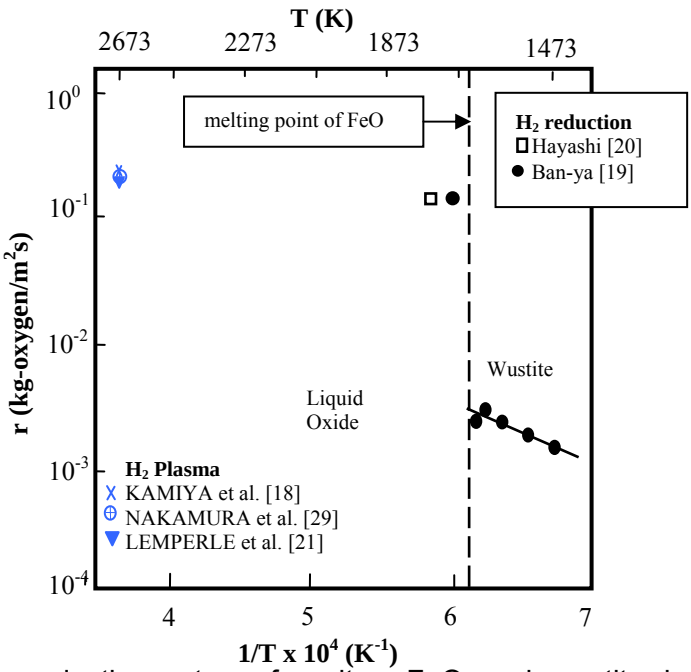

Fig. 12. Specific reduction rates of molten FeO and wustite by pure H_2 at various temperatures, [34]

3.2 Reduction rate of molten iron oxide by CO at low temperatures

The reduction of molten iron oxide by CO has been the subject of several investigations [36-39]. Nagasaka et al. [40] have reported the most of the previous work in figure 13. The results agree with each other except for those of Kato et al. [36]. Kato et al. reported a very fast rate of CO reduction of pure liquid FeO which was later corrected by Soma [37]. Tsukihashi et al. [38] have studied the rate of reduction of liquid iron oxide droplets in a CO gas conveyor system and the specific rate of reaction was determined to be 2.8 x 10^{-3} kg-oxygen/m^2s at 1873 K. Moreover, Nagasaka et al. [39] studied the reduction of liquid iron oxide by CO using a thermo-gravimetric technique. The results showed an agreement with Tsukihashi's work, i.e. a specific reduction rate of 1.93 x 10^{-3} kg-oxygen/m^2s at 1673 K. Both results were controlled by an interfacial chemical step.

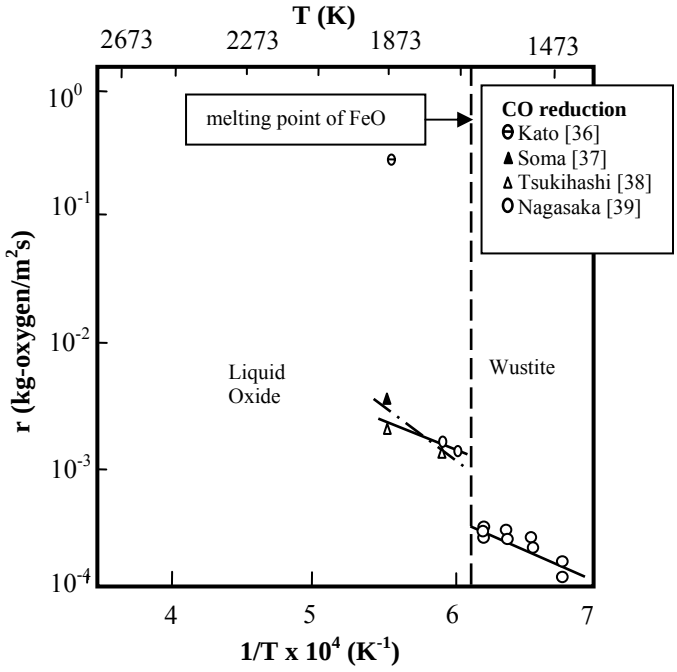

Fig. 13. Specific reduction rates of molten FeO by pure CO at various temperatures, [40]

It is clear that the reduction potential of CO increases by almost one order of magnitude just above the FeO melting point, with respect to the wustite phase. The reduction behaviour of CO at higher temperatures (under transferred arc plasma) has not been examined in a previous work. The corresponding results will be presented in the experimental section.

3.3 Reduction rate of molten iron oxide by carbon at low temperatures

3.3.1 Reduction rate by solid carbon

Many kinetic studies have been reported in the literature on the reduction of molten FeO by solid carbon because this reaction plays an important role in smelting reduction processes and blast furnaces [41-46]. Nagasaka et al. [40] have published a good review on the subject. They showed the temperature dependence of the specific reduction rate of pure liquid FeO with solid carbon, figure 14. It is clear from the figure that the reported results are in good agreement except with those of Ryozenkov et al. [41] and Kondakov et al. [42] due to the short reaction times.

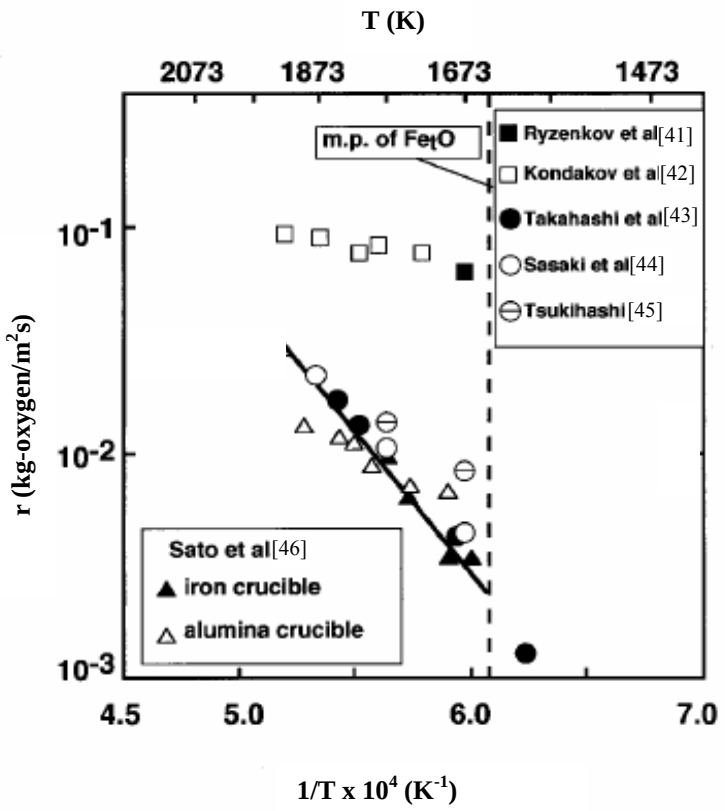

Fig. 14. Specific reduction rates of molten FeO with solid carbon, [40]

One of the representative studies was conducted by Sato et al. [46]. They melted iron oxide in iron and Al_2O_3 crucibles and immersed a rotating carbon rod in the molten FeO bath. The reduction rate was measured from the amount of CO gas evolved. They reported that the reduction rate in an Al_2O_3 crucible was slightly slower than that in an iron crucible due to the dissolution of Al_2O_3 in to the liquid FeO. However, the reduction rates obtained using the solid carbon showed results between 3.36×10^{-3} and 1.31×10^{-2} kg-oxygen/m^2s at 1693 and 1893 K respectively.

3.3.2 Reduction rate by carbon dissolved in liquid iron

Nagasaka et al. [40] plotted a graph, figure 15 , showing the reduction of molten iron oxide by carbon in the molten iron. The figure demonstrates the temperature dependence of the reported specific reduction rates of pure liquid FeO with hot metal. Results were obtained from literature for carbon contents from 3 % up to saturation levels, [47-50]. It is clear from the figure that the difference between the reduction rates obtained exceeded one order of magnitude.

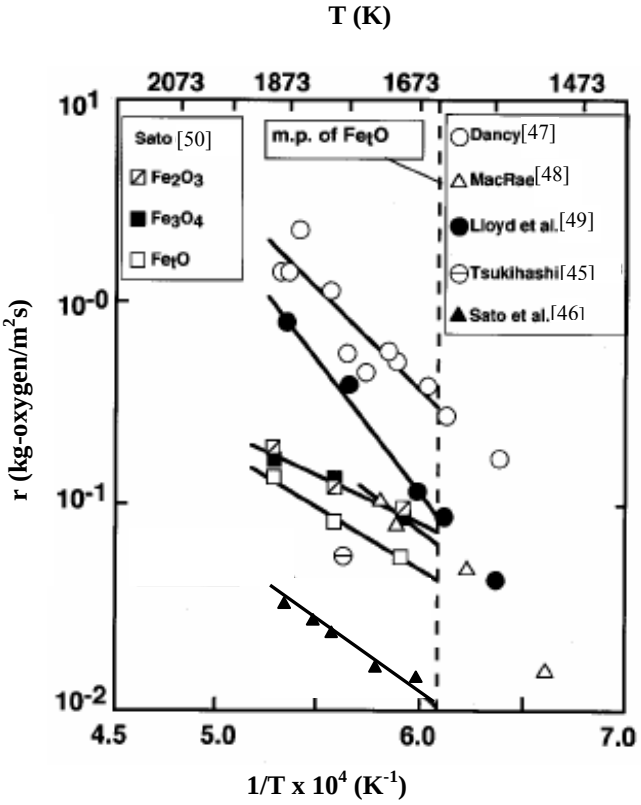

Fig. 15. Specific reduction rates of molten FeO with carbon dissolved in liquid iron, [40]

All of the experiments were conducted by dropping solid iron oxide into the bath of a molten Fe-C alloy and kept at the targeted temperature except the work of Sato et al. [46]. The disadvantage of the former experiments that the dropped iron oxide samples were reduced, in the solid state except for the later stage of the reduction, even by driving the samples to higher temperature than that of the melting point of FeO. On the contrary, Sato et al. [46] have managed to melt completely the iron oxide before the start of the reduction experiments. Therefore, Sato et al.'s results were considered as the most reliable as reported by Nagasaka et al. [40]. The corresponding reduction rates obtained using carbon in the molten iron showed results between 1.76 x 10^{-2} and 5.28 x 10^{-2} kg-oxygen/m^{2}s at 1693 and 1893 K respectively. It should be noted that the reduction rate of liquid iron oxide by

Fe-C is higher than that of solid carbon up to 1893 K. The reduction behaviour of carbon at higher temperatures (under plasma application) has not been examined in previous work. The corresponding results will be presented in the experimental section.

4 Characteristics of plasma

4.1 Definition of plasma

Plasmas are mainly generated by passing an electric current through a gas. While a gas at room temperature is an excellent insulator, a small percentage of charge carriers, ions and electrons, can be sufficient to make the gas electrically conducting. Plasma gas comprises molecules, atoms, ions, electrons and photons. However, overall, it is electrically neutral.

Plasma is principally divided into two types. The first type is the cold or non equilibrium plasma. It is characterised by high electron temperatures and low temperatures of heavy particles. The second type is the thermal or equilibrium plasma. In contrast to the cold plasma, it is characterised by an approximate equality between heavy particle (neutrals and ions) and electron temperatures, i.e. the thermodynamic state of the plasma approaches equilibrium, or more precisely, local thermal equilibrium (LTE).

The thermal plasma, which is adopted in the current research work, is chosen to provide high energy fluxes to the system. It is characterised by relatively high pressure (above 0.1 bar). As a result of the high pressure (high gas density), the collision frequency between the electrons and the heavy ions is high and an equilibrium state is attained ($T_e = T_h$). Typical temperatures and ionisation degrees of thermal plasma are in the range between 5×10^3 - 50×10^3 K and 5 -100 % respectively.

Maintaining an arc requires at least two electrodes to complete the path of the charge carriers (electrons and ions) into and out of the gas space of the arc [51]. At any given time, one electrode is the anode (electrons enter the electrode from the arc) while the second is the cathode (electrons leave the electrode). In a direct current (DC) arc, the function of the anode or cathode is maintained. In the alternating current (AC) arc, an electrode is successively anode and cathode at the frequency of power supply. If one electrode is tubular, from which gas emerges, and the other electrode is the material to be heated and melted, the plasma arc is said to be of the transferred type. Otherwise, a plasma torch is used, without heating the material, and the arc is called non transferred in that case.

4.2 Diagnostics of plasma

In plasma metallurgy, Ar, with low ionisation potential, is widely employed for stabilizing the arc discharges from plasma torches and electrodes. On the other hand, H_2 is used mainly for reduction purposes, but its physical properties make it also an excellent medium for

increasing the heat content of plasma. In the DC plasma arc, the properties of the gas used influence to a great extent the temperature, momentum and the heat transfer to the system.

4.2.1 Properties of plasma gas

Figure 16 shows the specific heat (calculated by FactSage [9]), viscosity, thermal conductivity and electrical conductivity of Ar, H_2 and CH_4*, [52, 53]. It is clear that Ar has the lowest specific heat and thermal conductivity of all these gases. The specific heat of CH_4, averaged throughout the temperature range presented, is approximately 2.5 times that of H_2. H_2 has the lowest viscosity, with some increase in the case of CH_4, and a much larger increase in the case of Ar. All gases have almost similar electrical conductivity.

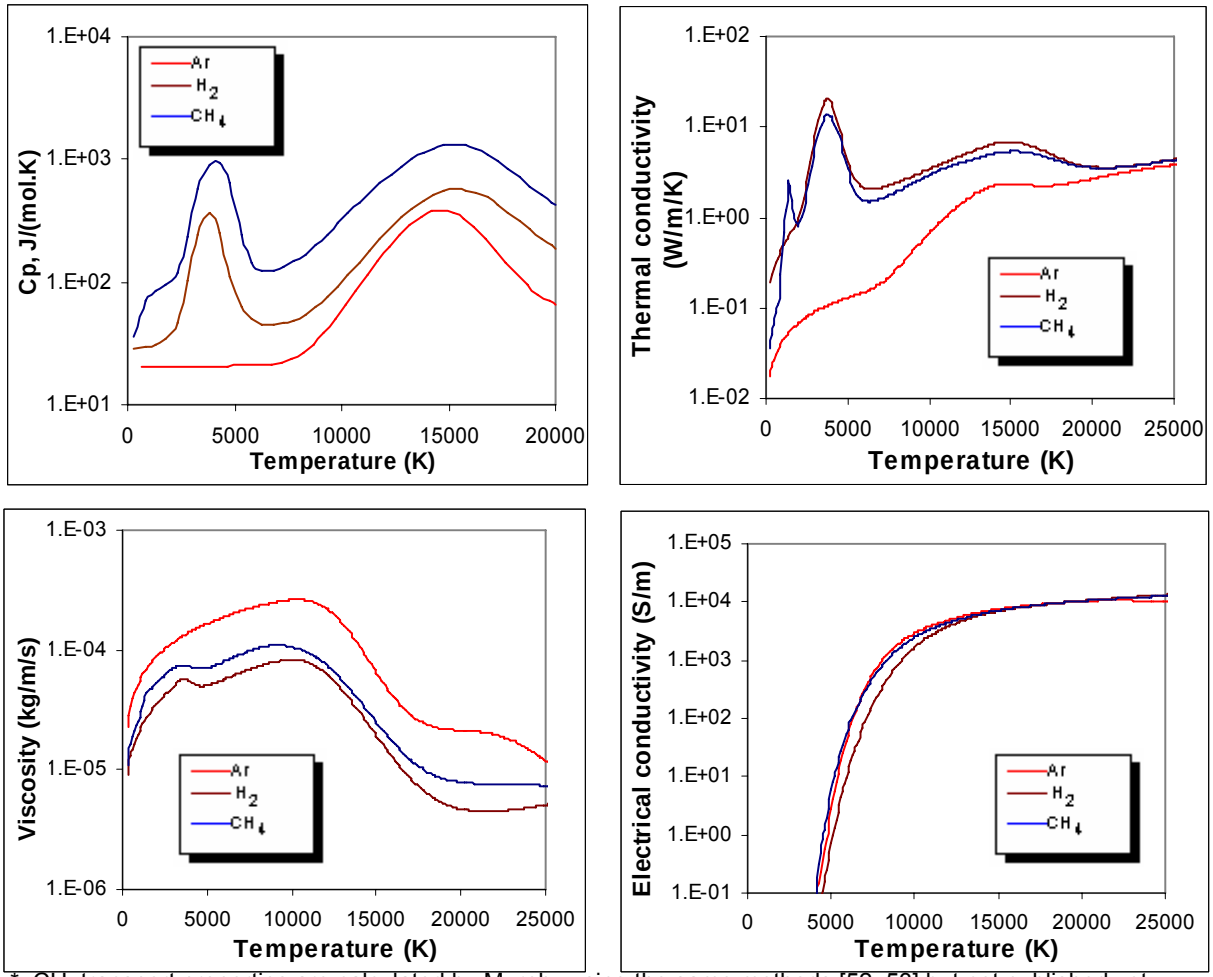

*: CH_4 transport properties are calculated by Murphy using the same methods [52, 53] but not published yet

Fig. 16. Specific heat, [9], viscosity, thermal conductivity and electrical conductivity of Ar, H_2 and CH_4 [52, 53]

4.2.2 Influence of gas properties on plasma

Figure 17 shows the calculated arc temperature in Ar and H_2 that was done by Murphy, [54]. This work was done by a computational model of TIG welding at a gas flow rate of 10 Nl/min, arc current of 150 A and atmospheric pressure. It is clear from the figure that the arc

properties are strongly dependent on the properties of the gases, where an increase in the arc temperature and the arc constriction was obtained by switching from Ar to H_2. This study was aimed at determining the main gas properties that are responsible for the changes in the arc behaviour. This has been done by modelling arcs with artificial thermodynamic and transport properties. In each case, all the properties of argon were used but only one property was replaced by an equivalent property of He like specific heat, thermal conductivity, electrical conductivity, etc.

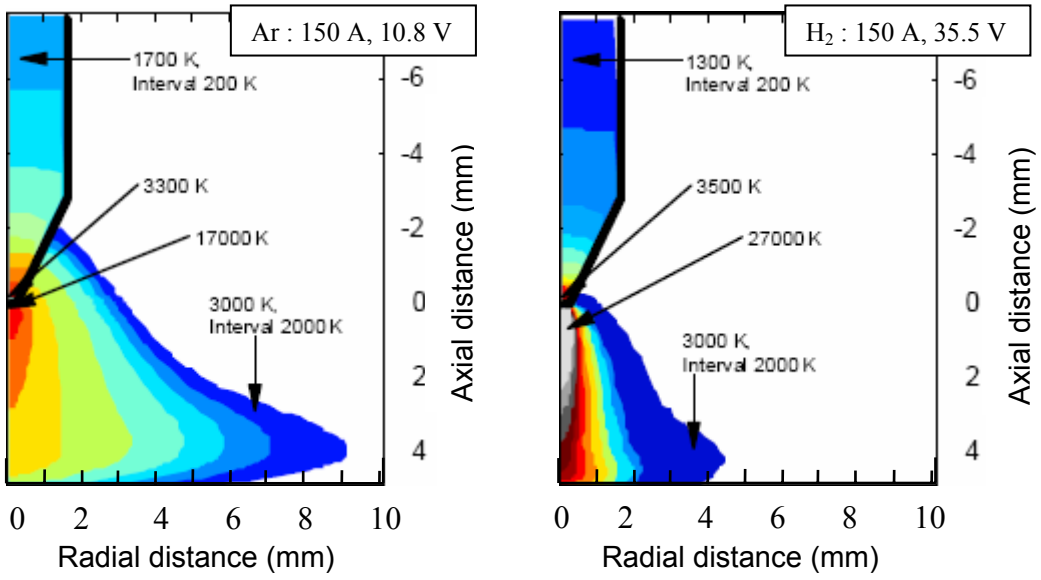

Fig. 17. Temperature fields for arcs in Ar and H_2, [54]

It was found that a higher specific heat leads to an increased constriction of the arc and a consequent increase in the maximum arc temperature. The mechanism by which increasing the specific heat constricts the arc has been discussed by Tanaka and Lowke, [55]. They argued that at any axial position, the total enthalpy of the plasma flowing towards the melt can be approximated by the product of the arc current I, and the potential difference V between the cathode and the plasma at the axial position. This neglects the low heat losses in case of the encountered small arc gap. Tanaka and Lowke then used the formula:

$$IV \approx \overline{\rho}.\overline{h}.\overline{v}.A \qquad (6)$$

,where $\overline{\rho}$, $\overline{h}$ and $\overline{v}$ are respectively density, enthalpy and velocity averaged over the arc cross-sectional area A.

They claimed that the term $\overline{\rho}.\overline{h}.\overline{v}$ increases by switching from Ar to H_2. This is attributed mainly to the increase of the enthalpy delivered by H_2, by approximately a factor of 10, and to the approximate neutral effect of the term $\overline{\rho}.\overline{v}$. Therefore, for almost 3 times higher voltage,

in the case of H_2, arc voltage = 35.5 V, a decrease in cross sectional area, A, is expected to balance the formula, and hence create a more constricted arc.

Back to the work of Murphy [54], he also found that the lower electrical conductivity, but to a lesser extent with respect to the specific heat effect, leads to an increased arc constriction. This was due to the restriction of the area through which the current flows, i.e. increasing current density, j, near the arc axis. By examining the influence of a higher thermal conductivity, an opposite effect by modelling was obtained (broadening of the arc). This is contrary to the previous arguments [56] that stated that increasing the thermal conductivity will increase the current density, j, near the arc axis and accordingly increase the arc constriction.

4.2.3 Plasma velocity

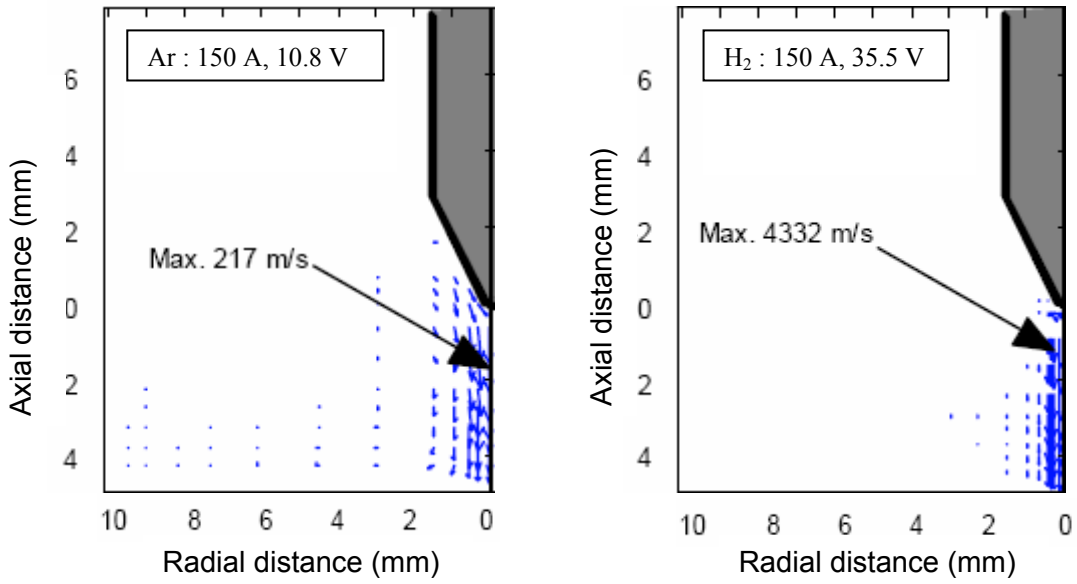

Fig. 18. Velocity fields for arcs in Ar and H_2, [54]

Figure 18 shows the calculated plasma axial velocity in Ar and H_2, [54]. It is clear that the increase in the axial velocity of H_2 is dramatic. As clarified in section 4.2.2, the delivery of H_2 decreases the arc cross sectional area compared to Ar. This constriction leads to the increase of current density near the cathode and consequently to an increase in the j x B force or Lorentz force, where j is the current density in the arc and B is applied magnetic field. The Lorentz force tends to squeeze the arc and increase the pressure on the arc axis. This pressure is the driving mechanism for the convective flow in the arc as it causes a strong axial flow away from the electrode towards the melt (pinch effect), [55].

4.2.4 Classification of arcs

In view of arc applications, a classification in terms of stabilization of the arc column appears to be useful. There is a direct link between the method of stabilizing the arc column and the options available for the design of arc devices [51]. Most electric arcs require some kind of stabilizing mechanism, which must be either provided externally or which may be produced by the arc itself. Here the term stabilization refers to a particular mechanism that keeps the arc column in a given, stable position. Existing stabilization mechanisms like wall stabilized arcs, vortex stabilised arcs, self stabilized arcs and forced convection stabilized arcs are common examples for the arc stabilizing mechanisms.

In free burning arcs [51], a classical type of arc, no external stabilizing mechanism is imposed on the arc. However, this does not exclude that the arc generates its own stabilizing mechanism. Although high intensity arcs may be operated in the free burning mode, they are frequently classified as self stabilized arcs. Stability can also be achieved by superimposing an axial flow to unstable arc as in the case of the forced convection stabilized arcs. The temperature is then reduced by the convective heat transfer from the arc to the cold gas shroud surrounding the arc. As a result, the electrical conductivity is dropped at this location and the arc in short will be forced to return to the equilibrium position towards the arc axis.

4.2.5 Striking behaviour of arcs

The method of arc striking at the anode, as described by Coudert et al. [57], is one of three types. The first type is cathode jet dominated (CJD) with a bell shape arc and a rather uniform heat transfer to the anode. The second type is anode jet dominated (AJD) with a severe constriction at the anode. The third type is that with erratic attachments with many constricted unstable arc spots leading to large voltage fluctuations. The AJD and erratic attachments result in a high local thermal flux that is unwanted in melting processes, where the arc attachment at the anode has to be the CJD type. The fluctuations of arc voltage with time in the transferred arc are caused mainly by the change of the anode spot positions. In the case of CJD, the arc is very stable and the anode spot position is fixed at the centre of the anode plane, which leads to small fluctuations of arc voltage with time. On the contrary, in the case of the erratic attachments, many constricted anode spots exist and the arc is very unstable, resulting in very large fluctuations of arc voltage with time. In the case of AJD, anode spots are severely constricted and continuously moved on the anode plane due to evaporation effects of anode material, which leads to smaller fluctuations of arc voltage with time than the erratic attachments but larger than the CJD.

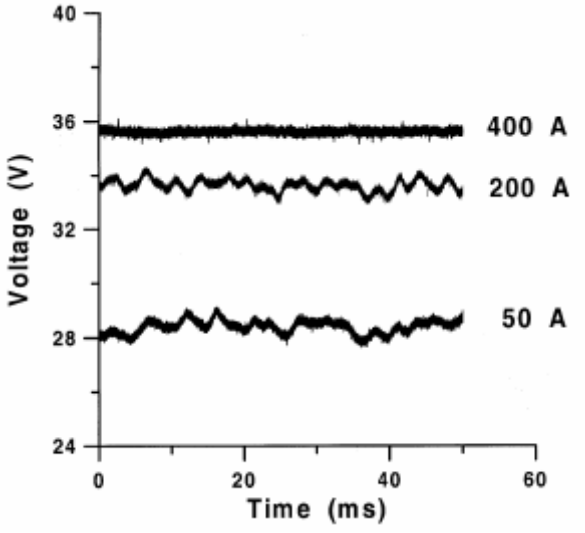

Fig. 19. Voltage fluctuations at arc gap: 2 cm, [58]

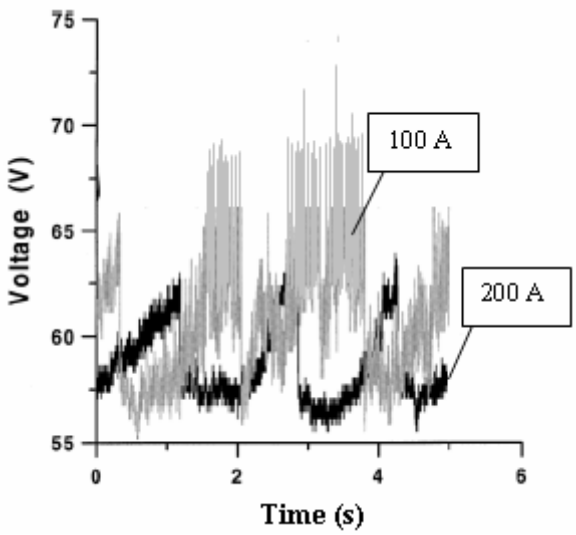

Fig. 20. Voltage fluctuations at arc gap: 5 cm, [58]

Hur et al. [58] made some measurements for a 15 Nl/min Ar gas flow in a transferred plasma torch, figure 19, 20. It is clear from figure 19 that the fluctuations of arc voltage are reduced with higher arc current, which means that a CJD arc can be easily acquired at higher current. On the other hand, the fluctuations of arc voltage, with larger arc gap in figure 20, are much greater than those with a short one in figure19. The increase of arc gap reduces the cathode jet and the arc transforms from a CJD to an AJD type or erratic attachments type.

4.3 Plasma heat transfer

4.3.1 Mechanisms of heat transfer

In the transferred plasma arc, the arc gap is relatively large with respect to the DC/AC electric arcs. This leads to a large heat flux to the furnace at the expense of that goes to the melt. Heat transferred by plasma arc is carried out by the following three different mechanisms [51]:

- Radiation from arc plasma
- Convection by gases propelled by the arc
- Electrode effect at anode and cathode

Figure 21 shows an estimation of the distribution of the arc power. The three mechanisms combine in different ways to deliver the arc heat, in part to the melt and in part to the furnace

(i.e. to the walls, the roof and the electrode itself). A portion of the heat delivered to the furnace will be reradiated to the melt.

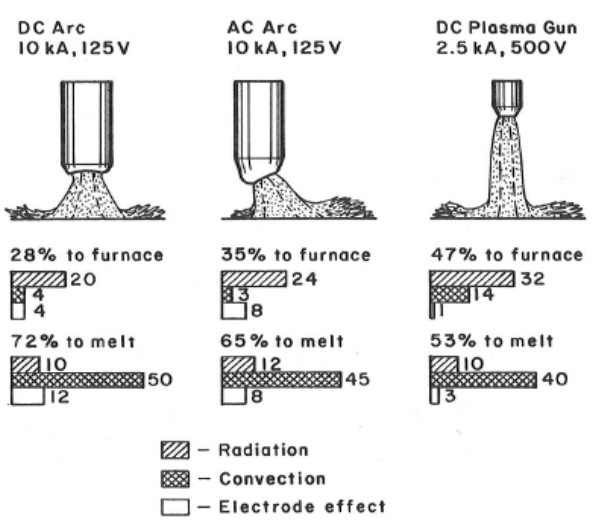

Fig. 21. Arc heating power distribution, [51]

Convection, as the main heat transfer mechanism, depends to a considerable degree on the plasma gas delivered. However, the heat transferred by radiation is significantly high in the plasma arc mode due to the high voltage / long arc operation. The heat transferred to the electrodes (electrode effect) is a minor mechanism in the case of plasma arc as it is proportional to the arc current, which is low with respect to the DC/AC electric arcs.

In plasma gas, excitation occurs when an atom or a molecule in its ground state absorbs sufficient energy through a collision with another heavy particle, an electron or a photon. In this process, one of its electrons passes to a higher level of energy. The excited states are limited in lifetime and rapidly decay to a lower energy state emitting one or several photons. It should be noted that the emitted photons do not have electric charge or rest mass but they act as carriers of the electromagnetic field. Absorption of photons might occur during their travel through the plasmas. This absorption process heats the gas by converting energy from radiation to kinetic energy. The reverse process, emission process, takes place by releasing this energy in the form of photons and cools the gas by converting the kinetic energy of atoms to energy in the form of radiation. The absorption, however, is only met in large volumes or extremely dense plasmas (optically thick plasmas). Since laboratory and industrial plasmas are usually small (a few centimetres in diameter), and not sufficiently

dense, therefore the emitted radiation intensity is generally significant, i.e. most of the photons are not reabsorbed in the plasma (optically thin plasma), [51, 59].

As an arc efficiency determinant, it should be noted that the radiation mechanism is a complicated process due to the interaction behaviour of the matter with radiated energy made up by photons. Photons energy, as a quantum of energy of electromagnetic radiation, is the product of Planck's constant and the frequency of the electromagnetic field. It ranges from high-energy gamma rays and X rays to low-energy infrared and radio waves, though all travel at the same speed, the speed of light, [59].

4.3.2 Distribution of the heat transfer

No modelling so far has been carried out for a transferred arc using pure H_2 gas for the reduction of iron ore. All published modelling works have handled other applications like metal melting, plasma welding, and plasma spraying. Theses publications were conducted either under pure Ar or a mixture of Ar and other gases like H_2 and He. However, to get a better understanding of the plasma characteristics in terms of heat transfer, it was decided to review the previous work.

An important study that examined the heat transfer by transferred Ar arc was conducted by Holt [60]. The heat transfer of 300 kW graphite lined plasma reactor with three 45 ^{o} tilted and 120 mm long arcs was used. A current and Ar flow rate of 500 A and 30 Nl/min were respectively used to melt silicon metal fines. A cold model that was equipped with the same torches, as the real hot reactor, was adopted to measure the heat flux distribution calorimetrically. A numerical simulation of the reactor heat transfer, including a thermal lining, was also done. Radiation from the arcs to the surrounding surfaces (including the melt) was calculated to be 31 % of the electric power input. It was stressed that the radiation transfer to the melt is likely to be better with tilted arcs than with one single axisymmetrically positioned arc. This is attributed to the increase of the view factors from the hot cathode end of the arc, which makes the net radiation flux to the melt less dependant on the wall to melt radiation. It was also stated that a better arc configuration could be obtained by an optimization between an efficient convective heat transfer obtained with a vertical arc and a possibly higher radiation to the melt by tilted arcs. In that sense, Esser [61] claimed that the higher heat transfer efficiency to the melt by the tilted arcs with respect to the vertical arc is attributed to their better convective heat transport in the melt. However, it was agreed in both studies that the tilted arc orientation is better than the axial arc in terms of heat transfer efficiency to the melt. Another experimental setup for calorimetric measurement was carried out by Bini et al.

[62] to assess the energy distribution in an Ar transferred arc for welding applications. The arc is developed between a thoriated tungsten electrode and copper anode. A maximum power of almost 3 kW and maximum Ar flow of 12 Nl/min was adopted. The results measured showed an arc efficiency of 75 % at 10 mm arc gap, which dropped to 64 % by increasing the power to almost 4 kW and the arc gap to 20 mm. This was attributed to a significant increase in radiation heat losses to the chamber walls.

A third energy balance was carried out for an experimental setup, for welding applications, with an arc current of 150 A, arc voltage of 10.4 V, and arc gap of 5 mm by Tanaka and Lowke, [55]. A water cooled copper anode at atmospheric pressure in Ar was used. The arc efficiency has been experimentally measured and also modelled to show a value of 82 %. It is obvious in that case that the arc efficiency is relatively high due to the small arc gap adopted in this experimental setup.

4.3.3 Effect of gas composition on the heat transfer

In section 4.3.2, the work presented was corresponding to pure Ar. Mixing some other gases with Ar, for example H_2, would enhance the arc efficiency. This is attributed to the H_2 higher specific heat with respect to Ar, which means more arc constriction and higher current density as clarified in section 4.2.2. This consequently leads to higher heat intensity to the melt in the case of H_2 as shown in figure 22. The effect of arc constriction on the heat intensity to the melt for various gases was examined by Tanaka and Lowke [55].

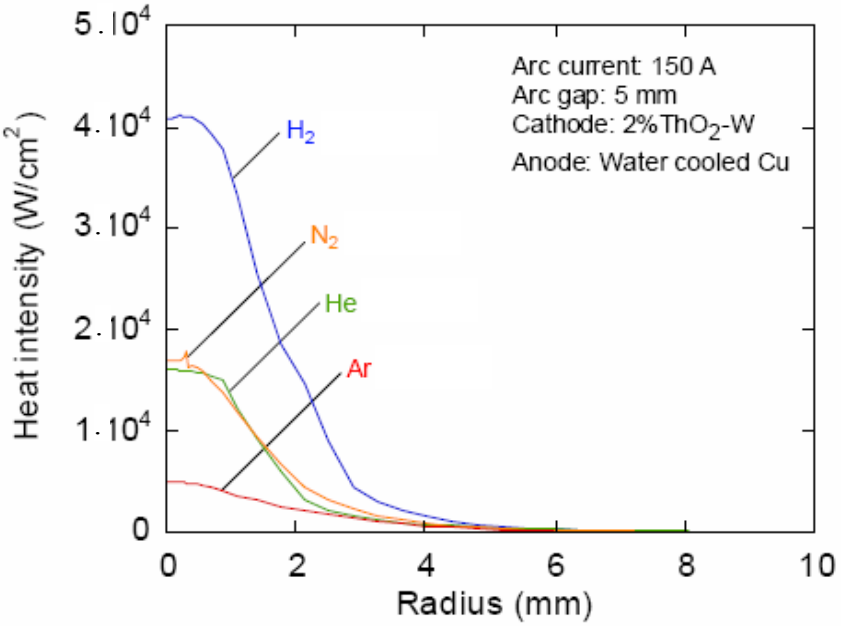

Fig. 22. Radial distribution of the heat flux density to the melt for different gases, [54]

One of the methods used to calculate radiative transfer in thermal plasmas is the net emission coefficient, a method proposed by Lowke [63]. This coefficient is a function of the temperature, pressure and radius of the plasma column and is suited to numerical studies. It is defined as the power radiated per unit volume and solid angle, on the axis of isothermal column, which escapes from the plasma of radius R. Cram [64] proposed a statistical method to calculate this coefficient to be applied to any atomic species. Figure 23 shows the net emission coefficients calculations done by Murphy [65] at atmospheric pressure for Ar, H_2 and CH_4. It is clear again, at high temperature ranges, that the power radiated per unit volume by Ar has the highest values, while that of H_2 has the lowest ones.

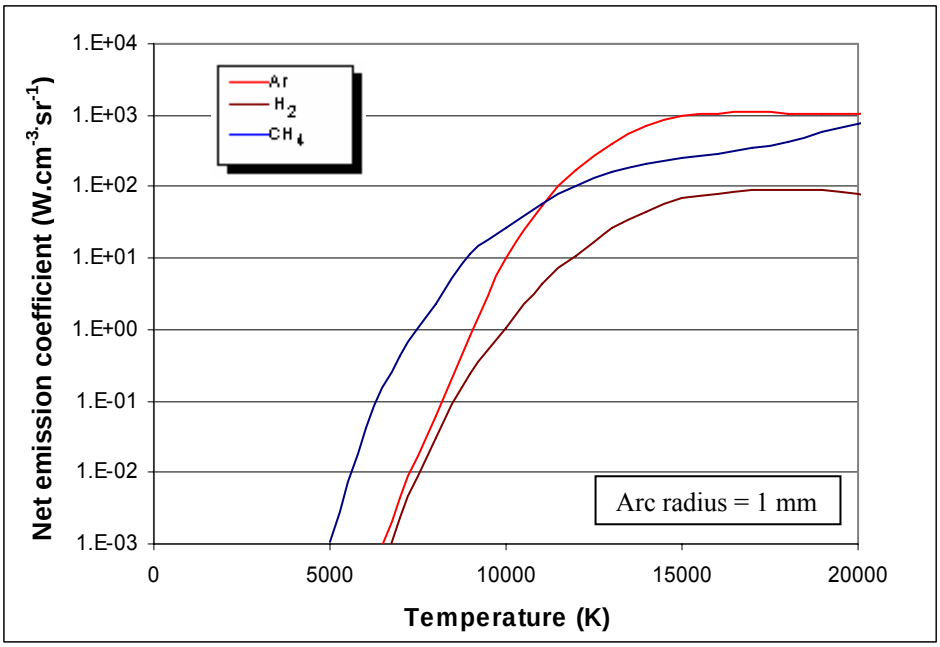

Fig. 23. Net emission coefficients of Ar, H_2 and CH_4 , [65]

4.3.4 Effect of metal vapours on the heat transfer

Discrepancies between computed and measured heat fluxes and arc voltages could in many cases be attributed to infiltration of small amounts of metal vapour originating from the electrodes particularly when a metal pool is serving as anode for a transferred arc and the pool is contaminated with low boiling elements as found by the modelling work of Bakken [66]. These elements tend to increase the electrical conductivity and thus reduce the arc voltage at low concentrations, for example, up to a concentration of 1 % Si. However, at higher concentrations, the associated radiation losses decrease the local temperatures, i.e. make the arc colder and thus decrease the conductivity and increase the voltage.

Another example was carried out by Essoltani [67] to evaluate the influence of the various concentrations of Ar-iron vapour mixtures on the radiative losses. He assessed the

volumetric radiation losses, Q_r, for atmospheric pressure plasma and produced figure 24. It is worth noting that even for concentrations of 0.001 %, the iron dominates the radiative losses for temperatures less than 9000 K. However, Ar has a rather strong influence at higher temperatures as the high energy excited levels of Ar begin to significantly dominate the results.

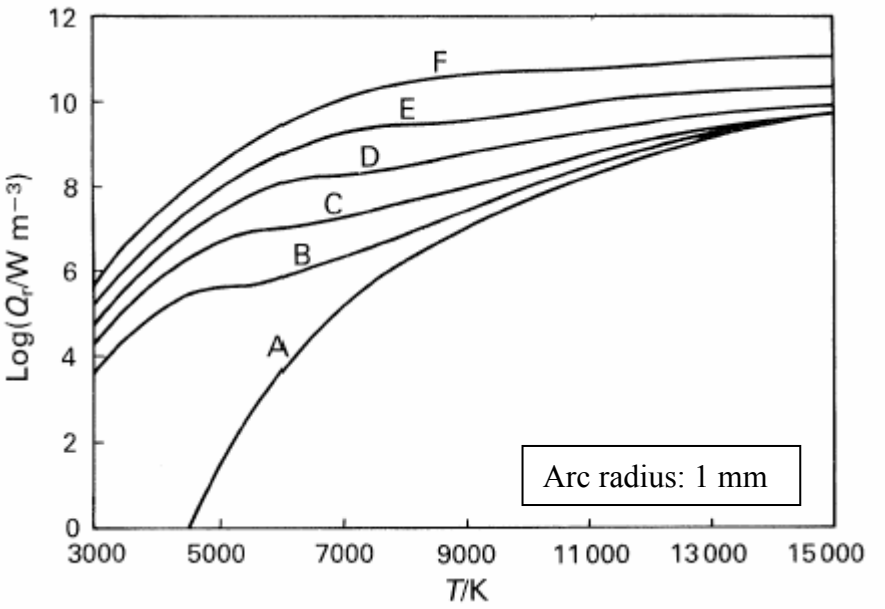

Fig. 24. Effect of iron vapour concentration on the total radiation of an Ar – Fe plasma: A, pure Ar; B, 0.001 %; C, 0.01 %; D, 0.1 %; E, 1 %; and F, 10 % Fe, [67]

4.4 Melt plasma interactions

4.4.1 Circulating flows in the melt

Understanding of the behaviour of fluid flow and heat transfer in an anodic melt is very important in arc welding and steelmaking applications using a DC arc. The circulating flow in the melt pool is driven by a combination of Lorentz/electromagnetic forces due to the passage of the arc current, drag forces caused by the cathode jet/pinch effect, shear forces due to buoyancy and Marangoni force. Marangoni force is initiated due to existence of surface tension gradients, where the flow is driven from lower surface tension regions (at high temperatures at the arc foot) to higher surface tension regions (at cold temperatures at the interface with the arc outer zones).

A numerical model was implemented by Tanaka et al. [68] to calculate the temperature and flow velocity of a stainless-steel (SUS 304) anode, figure 25. The calculations were made under conditions of welding current of 150 A and arc gap of 5 mm. In the case of Ar arc, it was found that the convective flow in the anode pool is an outward fluid flow. It is dominated

by the drag force and the Marangoni force compared with the other two driving forces (Lorentz and shear forces). A maximum calculated velocity of the cathode jet of 215 m/s is obtained. This cathode jet changes its direction in front of the anode surface, and then its radial component of the fluid flow drags the surface of the weld pool.

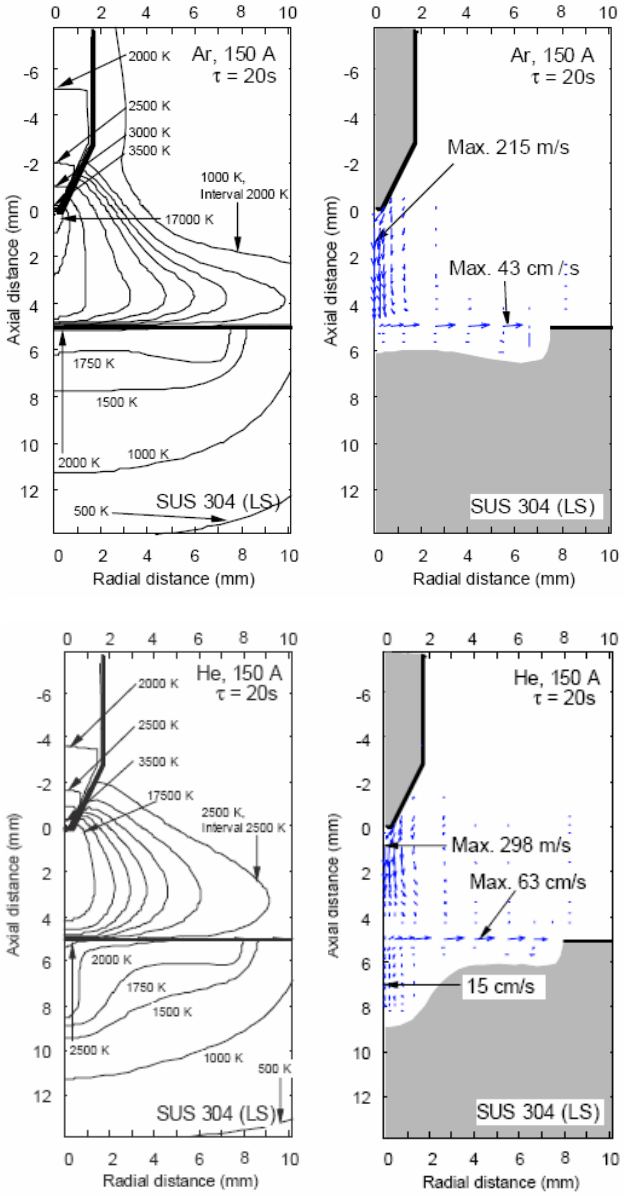

Fig. 25. Temperature and fluid flow velocity at 20 s after arc ignition in Ar, He gas tungsten arc welding of SUS 304, [68]

Helium was also modelled [68] as clear in the figure to investigate the change in temperature and flow velocities. It is clear that the calculated convective flow in the melt is dominated by two re-circulatory flows, namely an outward flow at the surface of the melt and inward fluid flow close to the centre at the inner of the melt. The outward one is principally caused by the Marangoni force. The inward fluid flow is caused by the electromagnetic force and leads to

the obvious melt penetration geometry obtained in the figure. The significant electromagnetic force was attributed to the smaller electrical conductivity of He with respect to Ar at low plasma temperatures. This consequently leads to a constriction of helium arc close to the anode surface and an increase in its current density. It is obvious from the work done that the balance of the driving forces could change the direction of the re-circulatory flow in the melt and changes the melt penetration geometry.

4.4.2 Melt depression

In the published numerical models of transferred and free burning arcs, the anode surface is assumed to be flat, [55,60]. It is well known, as clarified in last section, that the arc exerts electromagnetic force on the melt at its interface with the arc thus causing a depression of considerable depth. This depression most probably influences the arc voltage and energy transfer characteristics and should be considered in modelling work on industrial high current arcs.

Jones et al. [69] assessed the melt depression with depressed cavity of paraboloidal shape. They used Maecker's empirical correlation that specifies the dependence of the electromagnetic thrust on current flow for long arcs, and it was adopted as follows:

$$T = 1.16 \cdot 10^{-7} \cdot I^2 \qquad (7)$$

where T: electromagnetic thrust, N,

I: arc current, A

Having a displaced slag of a parabolic shape, a volume of depression may be expressed as:

$$V = \frac{\pi}{2} \cdot r^2 \cdot h \qquad (8)$$

where V: volume of paraboloid, m^3

r: radius of paraboloid depression, m

h: height or depth of paraboloid depression, m

The buoyancy force generated at the cavity can be taken as the depression volume multiplied by the melt density and gravitational acceleration. The buoyancy force may be equated to the electromagnetic thrust in order to provide an expression relating h to r.

$$1.16 \cdot 10^{-7} \cdot I^2 = \pi / 2 \cdot \rho \cdot g \cdot r^2 \cdot h \qquad (9)$$

where ρ: melt density, kg/m^3

g: standard gravitational acceleration, m/s^2

5 Solubility of hydrogen in liquid iron and slag

The control of hydrogen content in liquid steel is an important task for steelmakers because of its generally detrimental effects on processing characteristics and service performance of steel products. Just a few parts per million of hydrogen dissolved in iron can cause hairline cracks (flakes), hydrogen embrittlement, and loss of tensile ductility. Understanding the mechanism of hydrogen solubility in liquid iron and slag is sensible especially in the hydrogen based processes like that discussed in the present work, i.e. hydrogen plasma smelting reduction.

5.1 Hydrogen solubility in liquid iron

5.1.1 Solubility of molecular hydrogen

Diatomic gases such as H_2, N_2 and O_2 dissolve in liquid metals in the atomic form as follows:

$$1/2\,X_2(g) = [X] \quad \text{(ppm) in liquid metal} \tag{10}$$

The concentration of X, for example hydrogen, is directly proportional to the square root of the equilibrium gas partial pressure; this is known as Sievert's law, [70]:

$$[\%H] = K_{H_2} \cdot p_{H_2}^{\,1/2} \tag{11}$$

Where K_{H_2} and p_{H_2} are the equilibrium constant and the hydrogen partial pressure respectively.

For the solute content in ppm (by mass) and the gas pressure in atm, the temperature dependence (in K) of the equilibrium constant for H_2 solubility in liquid iron has been given by Turkodogan [71]:

$$\log\frac{[\text{ppmH}]}{(p_{H_2})^{1/2}} = -\frac{1900}{T} + 2.423 \tag{12}$$

5.1.2 Solubility of hydrogen in the plasma state

5.1.2.1 Mechanism of hydrogen absorption

Theoretical and experimental studies have been conducted to examine the solubilities of gases in liquid iron subjected to a plasma [72-74]. The studies stated that higher values than the equilibrium solubilities are attainable for the same gases. This means that a portion of the gas will enter the melt in a dissociated or ionised state due to the plasma application. In that case, the use of Sievert's law (based on equilibrium absorption of diatomic gas) is then invalid.

Dembovsky [72] described the hydrogen dissolution in the molten metal, in the plasma state where molecules, atoms, positive ions and electrons are dissolved, and in the case of absence of any applied electric field, by the following equation:

$$[\%H] = K_{H_2} \cdot p_{H_2}^{1/2} + K_H \cdot p_H + K_{H^+} \cdot (p_{H^+}^2 + p_e) \qquad (13)$$

where K_H and K_{H^+} are constants that apply to the dissolution of gas from its dissociated atomic and ionised states respectively and p_H, p_{H^+}, p_e are the partial pressures of the atomic, ionised particles and electrons respectively.

The derivation of the third term in the equation, $K_{H^+} \cdot (p_{H^+}^2 + p_e)$, was not clarified in the corresponding work. It is believed that it was wrongly presented and should be replaced by the term $K_{H^+} \cdot (p_{H^+} \cdot p_e)$ based on the mechanism of H^+ dissolution as shown in figure 26.c.

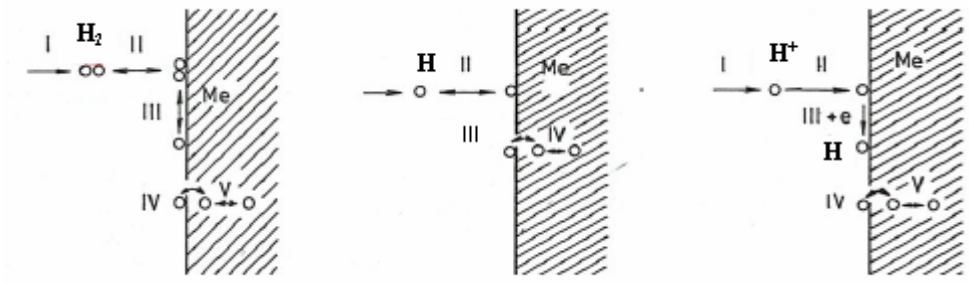

a b c

Fig. 26. Absorption of hydrogen supplied in a) molecular state, b) atomic state, c) ionic state [16]

Figure 26 shows the mechanism of hydrogen absorption into the melt. The schemes indicate the stages of hydrogen dissolution in the molecular, atomic and ionic states. In the molecular state, hydrogen is dissolved as described previously in equation (10). This reaction involves the following stages:

I.	Diffusion of H_2,	H_2 is free gas molecule
II.	$H_2 \Leftrightarrow H_{2\ (ads)}$,	$H_{2\ (ads)}$ is adsorbed gas molecule
III.	$H_2 \Leftrightarrow 2H_{\ (ads)}$,	$H_{\ (ads)}$ is adsorbed gas atom
IV.	$H_{\ (ads)} \Leftrightarrow [H]$	[H] is dissolved gas atom
V.	Diffusion of [H]	

The mechanism of absorption of atomic hydrogen is different compared to that of molecular hydrogen, figure 26.b. The atoms are adsorbed directly. Therefore, stage III in the above mechanism is omitted and the mechanism then comprises the following stages:

I.	Diffusion of H	III.	$H_{\ (ads)} \Leftrightarrow [H]$
II.	$H \Leftrightarrow H_{\ (ads)}$	IV.	Diffusion of [H]

When the hydrogen atoms are ionised, H^+, their dissolution differs from that of electrically neutral gas particles by an extra side reaction, which is the recombination of ions adsorbed at the metal surface. As clear from figure 26.c, the mechanism changes again to:

I.	Diffusion of H^+	IV.	$H_{\ (ads)} \Leftrightarrow [H]$
II.	$H^+ \Leftrightarrow H^+_{\ (ads)}$	V.	Diffusion of [H]
III.	$H^+_{\ (ads)} + e \Leftrightarrow H_{\ (ads)}$, where e is a negative charge (electron)		

Dembovsky [72] concluded that the dissociated gases in their atomic or ionised state have low activation energies for dissolution, which should make it possible to accelerate their dissolution in the liquid iron. It is therefore quite important to take into account the participation of active particles when examining the reactions involved in the dissolution of gases in their plasma state. On the other hand, it should be noted that the absorption of gas by molten metal, in the presence of an electric field, is governed not only by the partial pressure of the gas but also by the degree of its ionisation, by polarity of the metal surface and by the intensity of current that transports ions to the metal surface.

5.1.2.2 Equilibrium of atomic hydrogen with liquid iron

Gedeon and Eagar [73] have reviewed the previous research work in hydrogen absorption in arc welding applications. They stated that using the results from the diffusible hydrogen measurements, rather than the calculated absorbed hydrogen, can lead to significant errors. This is attributed to the significant amount of the total hydrogen that would be lost through the diffusion of hydrogen outside the melt, within seconds, during solidification.

It was found that although many researchers fitted their data points according to Sievert's law, figure 27 , the calculated reaction temperature was unreasonable. The calculated values were found to be much higher than 2500°C, the maximum temperature obtainable in steel arc welding. Even if Terasaki's theoretical analysis was applied to correct the measured diffusible hydrogen to that which was initially absorbed, one cannot quantitatively reconcile the Sievert's law with the experimental data, [75]. Geodeon and Eagar [73] stated that the researchers who used Sievert's law were unable to explain their results in terms of realistic reaction temperatures. Therefore, they proposed a model that considers the atomic hydrogen absorption. The model considers the dissociation of hydrogen in the plasma and the absorption of atomic hydrogen at the liquid interface.

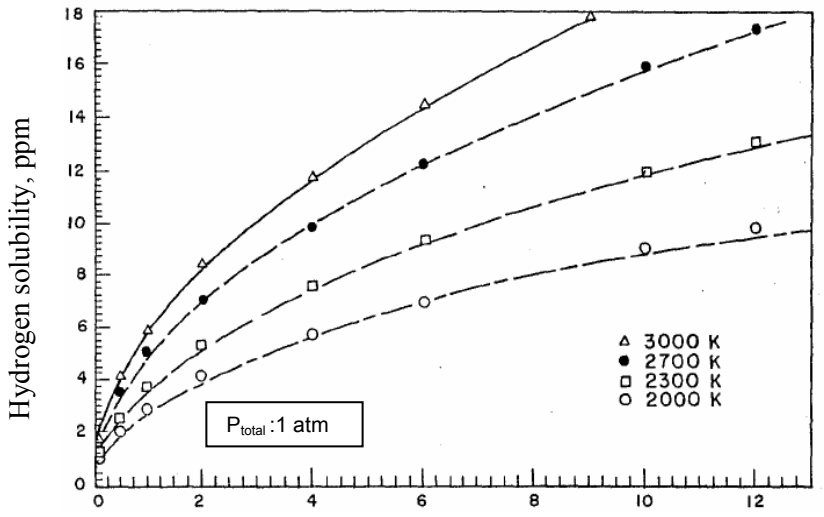

Fig. 27. Hydrogen solubility versus molecular hydrogen partial pressure, [73]

The dissociation of hydrogen can be presented by following reactions, (14) and (15), for which thermodynamic data are known. By combining these reactions, the absorption of atomic hydrogen can be expressed according to reaction (16), [73]:

$$1/2\,H_2(g) = [H] \quad (14)$$

$$H_2(g) = 2H(g) \quad (15)$$

$$H(g) = [H]\ ,\ \Delta G = -44780 + 3.38T \quad (16)$$

From the above reaction, one can obtain the amount of absorbed hydrogen as a function of the partial pressure of atomic hydrogen for various reaction temperatures as shown in figure 28.

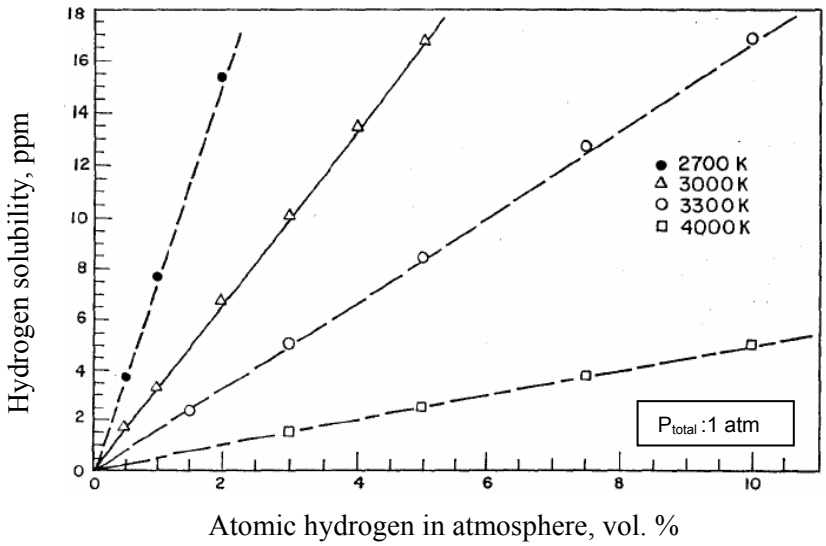

Fig. 28. Hydrogen solubility versus atomic hydrogen partial pressure, [73]

It is clear from figure 28 that the trend of absorption for atomic hydrogen is different from that of molecular hydrogen (figure 27).The amount of absorbed hydrogen decreases with temperature rather than increases, which means that this model can explain the experimental results obtained, without reaching high melt temperatures like in the case of the application of Sievert's law.

5.2 Hydrogen solubility in slag

The hydrogen solubilities of binary, ternary and quaternary slag systems were studied by different research groups. Researchers found that the solubility of the water dissolved in the oxide melt is proportional to the square root of the partial pressure of water vapour, [76-79].

$$(H) = C.\sqrt{p_{H_2O}} \qquad (17)$$

Where, (H) denotes the hydrogen content in the oxide melt (ppm), P_{H_2O} the partial pressure of water vapour and C is constant that may change depending upon the composition of the oxide and temperature.

The mode of solution varies according to the kind of melt as explained by the following equations, [70]:

In acidic melts and network building systems, for example acidic silicate, H_2O vapour reacts with double bonded oxygen (bridging oxygen), O^o, and depolymerises the melt to form hydroxyl radical, thus

$$-\overset{|}{\underset{|}{Si}}\text{-O-}\overset{|}{\underset{|}{Si}}- + H_2O\,(g) = -\overset{|}{\underset{|}{Si}}\text{-OH HO-}\overset{|}{\underset{|}{Si}}- \qquad (18)$$

In basic melts, H_2O reacts with free oxygen ions, O^{2-}, to form a hydroxyl ion according to the following reaction:

$$O^{2-} + H_2O = 2(OH)^- \qquad (19)$$

For both acidic and basic melts, the overall reaction is represented by:

$$O^* + H_2O = 2(OH^*) \qquad (20)$$

Where O* represents double bonded oxygen, single bonded oxygen (O^-), or O^{2-} , and OH* is single bonded to silicon or as a free ion. In this sense, hydroxyl radicals increase with double bonded oxygen while hydroxyl ions increase with single bonded or free oxygen. In these modes of solution, water behaves similar to basic oxides against acidic silicate, that is, it breaks a network structure in reaction with double bonded oxygen in silicate, and it also acts as an acid oxide against a basic silicate.

The equilibrium constant for a given melt composition is known as the hydroxyl capacity, $C_{OH,}$ and is expressed as:

$$C_{OH} = (\%H_2O)/(p_{H_2O})^{1/2} \quad (21)$$

where the $\%H_2O$ is the weight percentage of H_2O in the melt, and p_{H_2O} is the partial pressure of water vapour in bar.

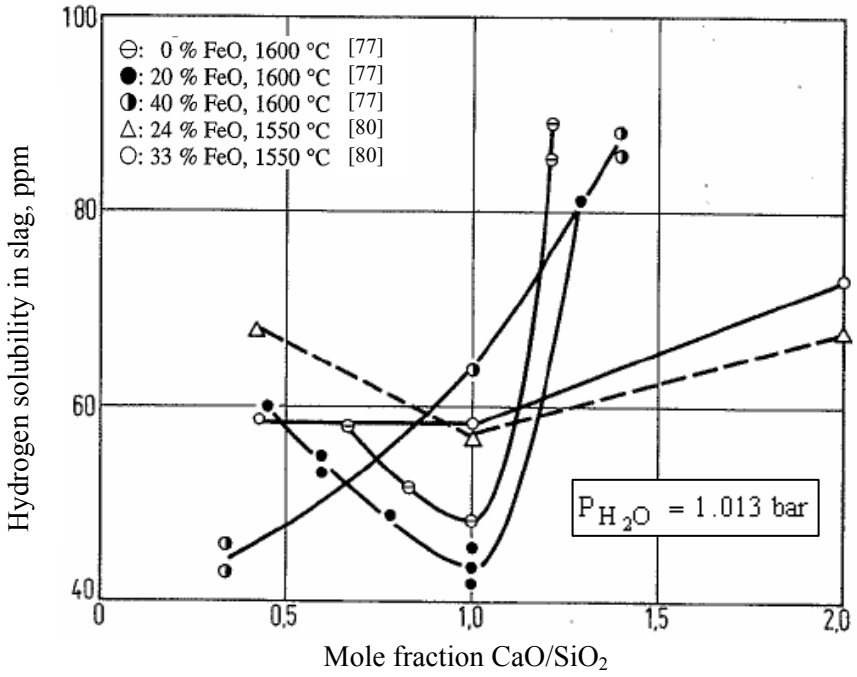

Fig. 29. Hydrogen solubility in CaO-FeO-SiO_2 melts in relation to CaO/SiO_2 ratios, [77]

Wahlster and Reichel [77] have studied in details the effect of the slag basicity on the H_2/H_2O solubility in the melt. In the binary system CaO-SiO_2, they found a minimum hydrogen solubility in the slag of CaO/SiO_2 = 1. The hydrogen solubility increases, however, in both directions on the basic and the acidic side. In the basic slag, hydrogen dissolves according to reaction (19) due to the increment of free oxygen ions, while in acidic slag hydrogen dissolves according to reaction (18) with an increase of double bonded oxygen existing in the silicate. Moreover, the rate of increment of hydrogen solubility in the basic slag was found to be higher than that in the acidic slag.

The influence of % FeO (0 – 40 %) in a CaO-FeO-SiO_2 system has been also investigated by Imai et al. [80] and Wahlster and Reichel [77], figure 29. Again, a minimum hydrogen solubility was obtained in the slag of CaO/SiO_2 = 1 in both studies. However, Imai [80] found that the hydrogen solubility remained constant (at 33 % FeO, in the acidic slag side) with respect to that at CaO/SiO_2 = 1. At higher levels of FeO in the slag, 40 %, Wahlster and Reichel found that the lowest hydrogen solubility is in the acidic slag. They attributed this finding to the highly obtained ratio of Fe^{3+}/Fe^{2+}, where the increment of hydrogen solubility in the acidic side could be hampered due to the low hydrogen solubility of Fe_2O_3. However, this justification is clearly not reliable where the presumed existence of Fe^{3+} in an acidic slag contradicts with the fact that Fe^{3+} increases on the basic side, [81].

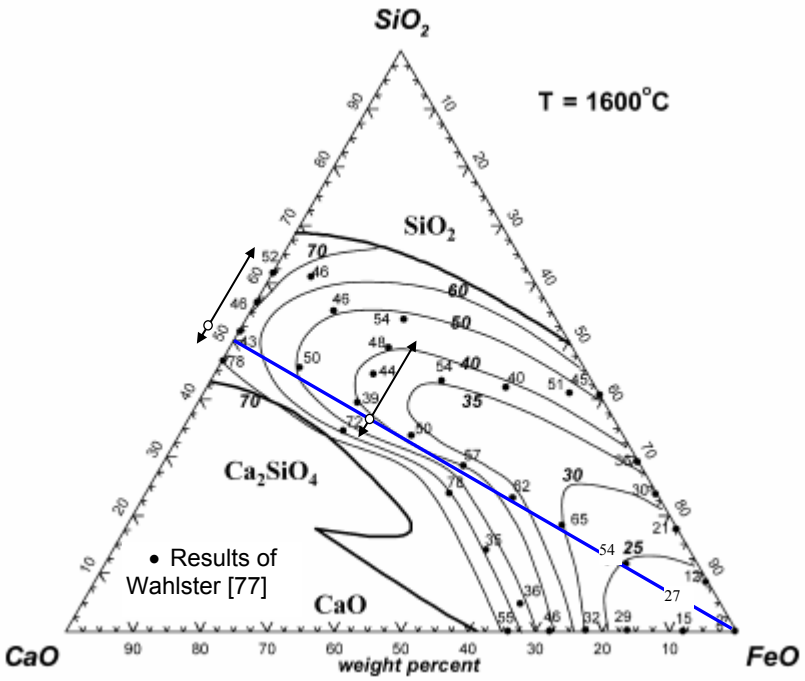

Fig. 30. Calculated C_{OH} lines against those measured for a CaO-FeO-SiO_2 system, (C_{OH} x 10^3), [82]

Recent modelling work has been carried out by Jung [82] to predict the hydroxyl capacity, C_{OH}, in a CaO-FeO-SiO_2 system. The results of the modelling work were presented in one diagram and compared with that measured by Wahlster and Reichel [77], figure 30. It is clear from the figure that the calculations are in fair agreement with the experimental data in the region between the double sided arrows. The agreement was in the hydroxyl capacity profiles, where almost minimum values were observed at 50 % SiO_2 at the CaO-SiO_2 binary side to FeO apex, the blue line. An increase of C_{OH} towards higher basic and acidic sides, with higher increment rate in the basic side, was also noticed. However, the calculations failed to agree with the measured values on the blue line at higher values of FeO. This discrepancy was shown by the continuous decrease of calculated C_{OH} with increasing

% FeO, whereas the measured C_{OH} increased by increasing % FeO approximately up to 65 % and then decreased again to approximately 0 % at 100 % FeO. Jung [82] has also divided the dissolved forms of water in the CaO-FeO-SiO_2 system into four different sections, figure 31. He demonstrated that the minimum water solubility values appear at the interface between the two different dissolution mechanisms of water. It is clear from the figure in the slag composition beneath the dashed blue line that water mainly dissolved in the form of $Ca(OH)_2$ hydroxyl ion and that the formation of $Fe(OH)_2$ was very rare. On the other hand, at slag compositions above the dashed blue line, water mainly dissolved in the form of (Si-O-H) hydroxyl radicals.

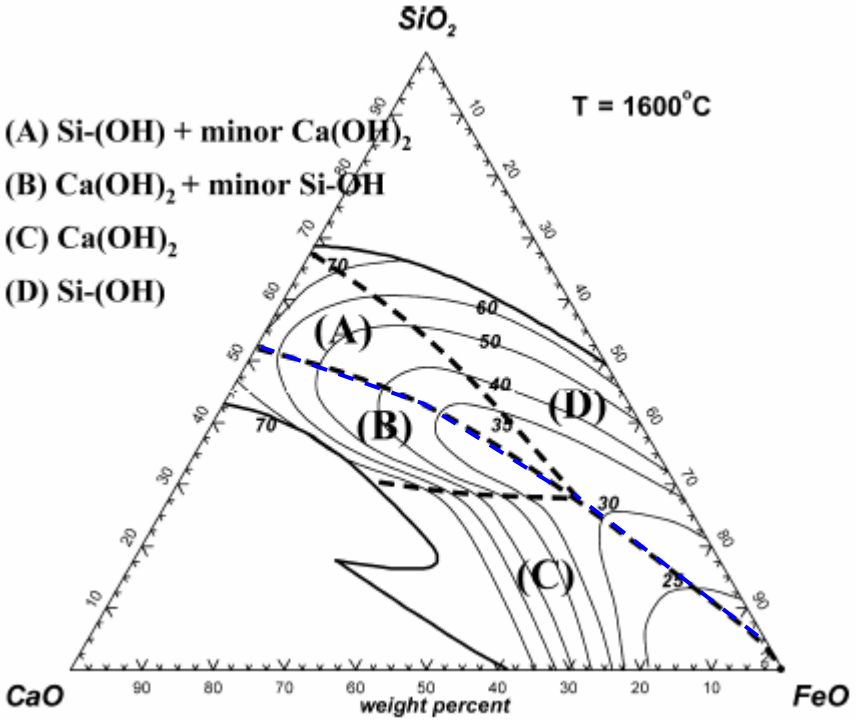

Fig. 31. Major dissolved forms of water in the CaO-FeO-SiO_2 slag as calculated, [82]

5.3 Phase boundary reactions in hydrogen plasma smelting reduction process

Hydrogen dissolves in molten slag in the form of hydroxyl ion or hydroxyl radical depending on the slag basicity. Provided that the process will be operated at a slag basicity $B_2 = 1$, then minimum water solubility could be obtained as shown in the last section. However, by working at this operation point, a transient status between the delivery of free oxygen ions and double bonded oxygen will result.

Figure 32 shows the phase boundary reactions in both basic and acidic slag to form hydroxyl ions and hydroxyl radicals respectively. These reactions provide the mechanism for H_2O transfer from gas phase to metal phase through the overlaying slag layer. In the case of plasma application, an additional phase, the plasma phase, should also be added above the gas phase. In that phase, an additional dissociation reaction takes place, where H_2O or H_2 are converted to hydrogen atoms that diffuse readily into the slag.

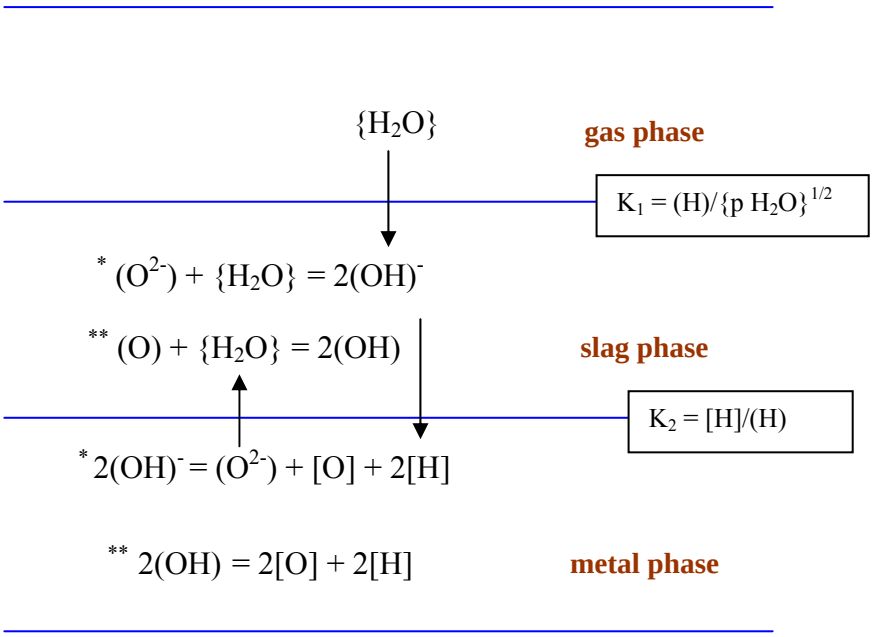

*: Basic slag, **: Acidic slag

Fig. 32. Phase boundary reactions

6 Implementation of thermodynamical calculations

6.1 Thermodynamic equilibrium of iron oxide and reducing /oxidising agents

The equilibrium of iron oxide with various reducing gases has been assessed by the thermodynamical program FactSage 5.5 [9]. Moreover, the reduction behaviour of H_2 under the supply of CO_2 and H_2O was examined. Evaluation of the reduction of iron oxide by carbon rather than reducing gases was also done. The calculations done were carried out in a temperature range from 1600 ^oC – 2600 ^oC, corresponding to the molten phase of iron oxide. The chosen temperature range covers the temperatures at the interface between the oxide melt and the plasma arc, 2000 ^oC – 2600 ^oC, as measured in previous works, [14, 21].

6.1.1 FeO-H_2

Figure 33 shows the thermodynamic equilibrium between 1 mole FeO and 1 mole H_2 over a temperature range from 1600 ^oC to 2600 ^oC. The calculations show that the reduced oxygen of 1 mole FeO by 1 mole H_2 is relatively stable, but shows a slight decrease of H_2O over temperature and some OH development, at higher temperatures. The reduced O (summation of H_2O and OH) varies between 0.42 and 0.38 moles at 1600 ^oC and 2600 ^oC respectively.

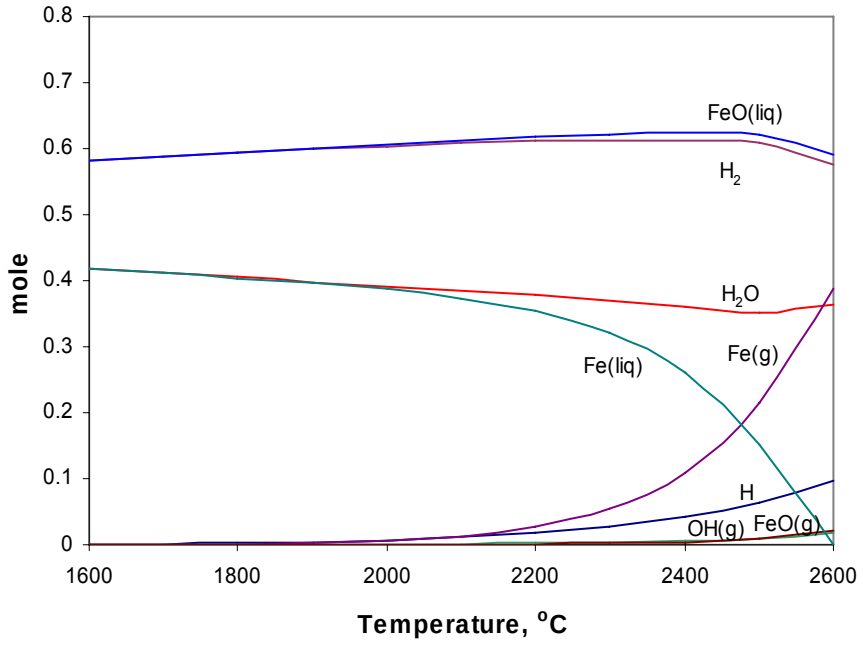

Fig. 33. Equilibrium of 1 mole FeO - 1 mole H_2

Above 2000 °C, Fe starts obviously to vaporise and H_2 starts to dissociate. It should be noted that up to the maximum temperature of 2600 °C, at the melt arc interface, the dissociated hydrogen obtained is fairly low with respect to the molecular hydrogen, i.e. approximately 0.1 moles of H. In other words, at this relative low temperature, the shown amount of H is not enough to speed up the reduction rate of FeO.

6.1.2 FeO-CH_4

Figure 34 shows the thermodynamic equilibrium between 4 moles FeO and 1 mole CH_4 over a temperature range from 1600 °C to 2600 °C. The calculations show a total reduced oxygen, O, of 1.99 moles at 1600 °C (summation of H_2O, OH, CO and CO_2) which decreased to 1.79 moles at 2600 °C. Whereas, the reduced oxygen of 1 mole FeO by 1 mole of H_2 at 1600 °C and 2600 °C is 0.42 and 0.38 moles respectively, as clarified in the previous section. In other words, the CH_4 reduction rate is about 4.75 times the H_2 over the stated temperature range.

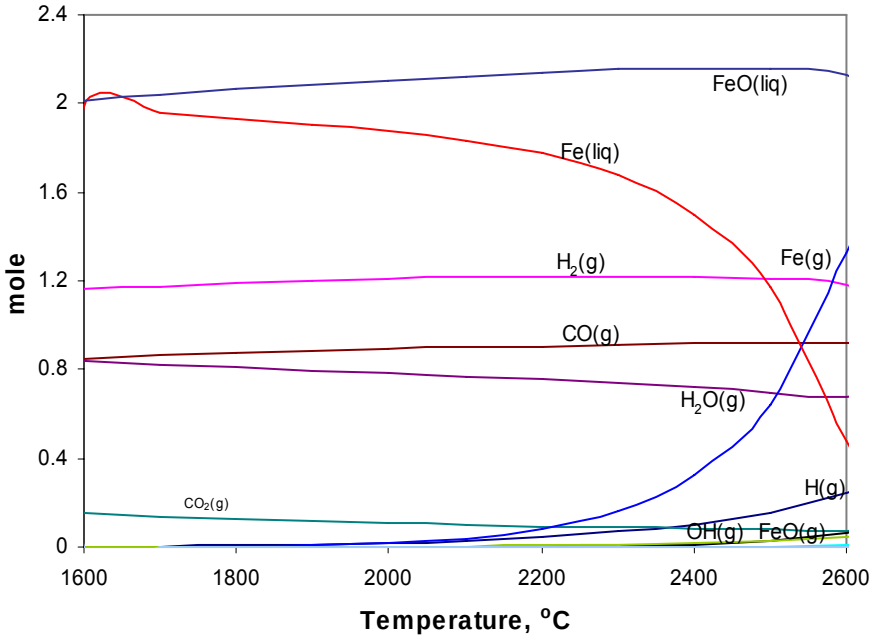

Fig. 34. Equilibrium of 4 moles FeO - 1 mole CH_4

Examining the contribution of H_2 contained in CH_4, in the reduction of FeO, it is clear from the figure that the reduced oxygen via the 2 moles of H_2 varies between 0.84 and 0.71 moles (summation of H_2O, OH) at the left- and rightmost temperatures of the diagram, i.e. 1600 °C and 2600 °C respectively. This means that the oxygen reduced by 1 mole of H_2 over the shown temperatures approximately varies between 0.42 and 0.36 moles.

From the contribution of carbon contained in CH_4, 1 mole of carbon is converted mainly to CO that varies between 0.85 and 0.92 moles and partially to CO_2 that varies between 0.15 and 0.08 moles, at the left- and rightmost temperatures of the diagram respectively. This means that the reduced O by 1 mole of carbon over the shown temperatures varies between 1.15 and 1.08 moles.

From the shown results for H_2 and carbon contained in CH_4, a carbon reduction rate was found to be approximately 1.45 times that of H_2 over the shown temperature range. It is advantageous then to use CH_4 as an alternative to H_2 from a thermodynamic point of view due to its carbon reduction potential.

6.1.3 FeO-CO

Figure 35 shows the thermodynamic equilibrium between 1 mole FeO and 1 mole CO over a temperature range from 1600 °C to 2600 °C. The calculations show that 0.15 moles of CO takes place in the reduction process at 1600 °C and converts to CO_2. Some decrease of the utilised CO is observed at higher temperatures up to 2400 °C. However, CO contribution goes up again, i.e. 0.15 moles of CO are converted to CO_2.

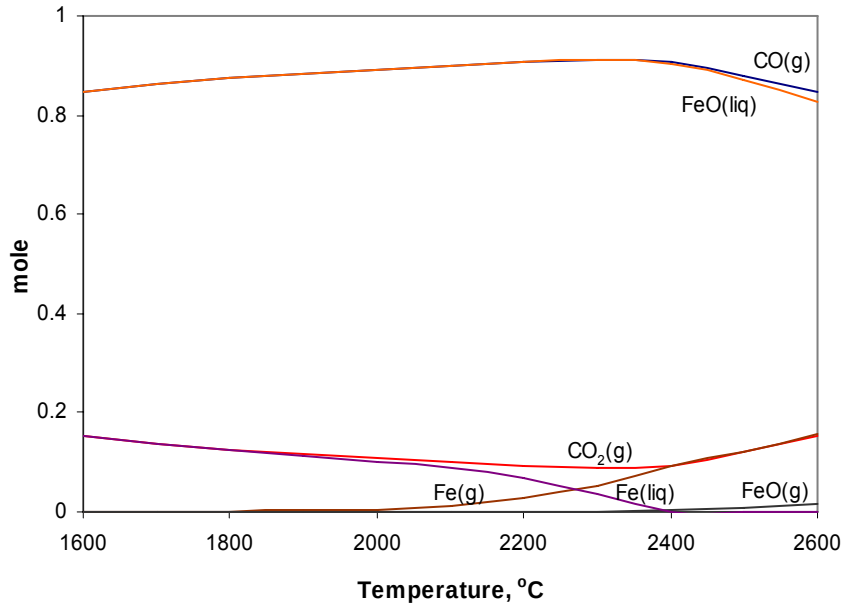

Fig. 35. Equilibrium of 1 mole FeO - 1 mole CO

From the equilibrium calculations obtained, FeO-CO, and the previous calculations of FeO-H_2, it was found that the potential of H_2 reduction is 2.5 times faster than CO. However,

looking at the CO reduction rates as experimentally attained in the literature, results turned to be far from equilibrium calculations at low temperature (1400 – 1600 ^{o}C). This was previously clarified in the literature review in sections 3.1 and 3.2, where the rate of H_2 reduction of liquid iron oxide was almost two orders of magnitude faster than CO.

6.1.4 FeO-H_2-CO_2

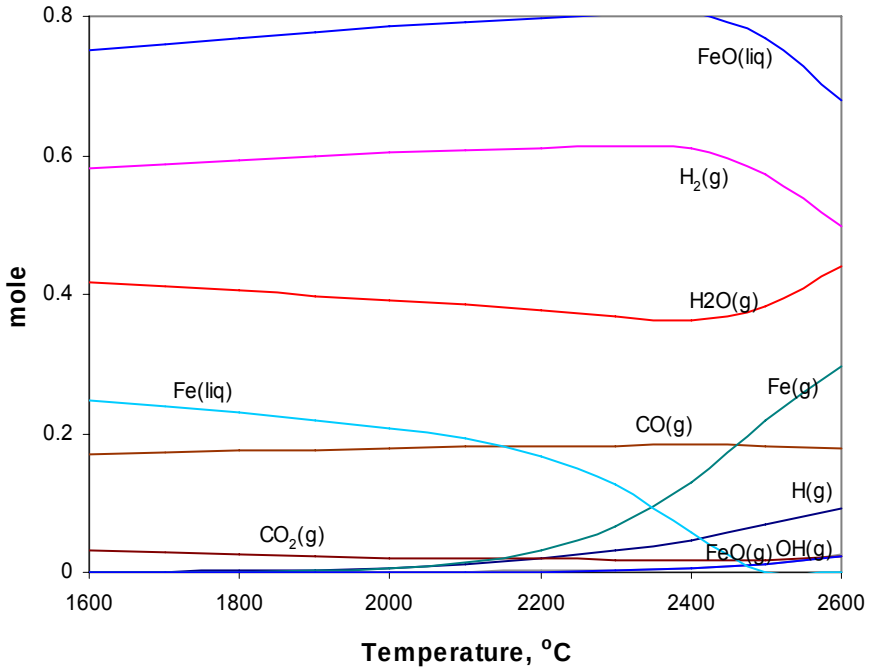

Fig. 36. Equilibrium of 1 mole FeO - 1 mole H_2 - 0.2 mole CO_2

Figure 36 shows the thermodynamic equilibrium between 1 mole FeO, 1 mole H_2 and 0.2 moles of CO_2 over a temperature range from 1600 ^{o}C to 2600 ^{o}C. The target of having this combination of gases is to assess the reduction rate of liquid FeO by H_2 under the usage of CO_2 with a chosen ratio of CO_2/H_2 = 0.2, as an extreme ratio in a real process. It was found that 0.2 moles of CO_2 decreases the reduced O by pure H_2 from 0.42 moles, shown previously in section 6.1.1, to 0.25 moles at 1600 ^{o}C. In other words, it decreases the rate of reduction by up to 40 % but this retardation effect diminishes further at high temperatures to a reduction rate drop of approximately 24 % at 2600 ^{o}C. It is clear from the results obtained that CO_2 has a significant influence on the retardation of the reduction rate adopted by H_2 and accordingly to the limitations of H_2 utilised in the process.

6.1.5 FeO-H_2-H_2O

An equilibrium calculation between 1 mole FeO, 1 mole H_2 and 0.2 moles of H_2O over a temperature range from 1600 ^oC to 2600 ^oC was conducted as shown in figure 37. The objective of this calculation was again to study the influence of adding an oxidising gas, H_2O, on the reduction of liquid FeO by H_2.

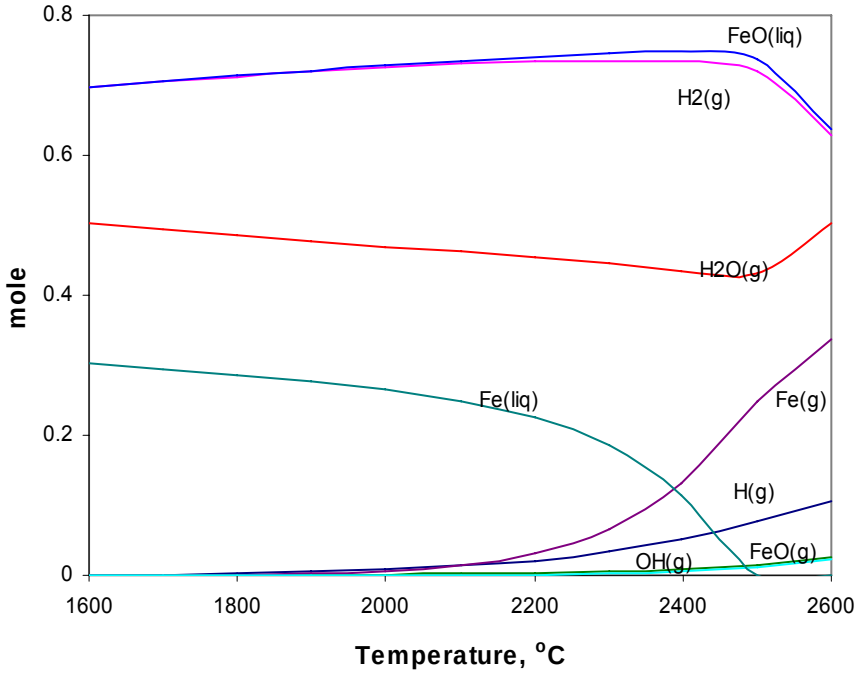

Fig. 37. Equilibrium of 1 mole FeO - 1 mole H_2 - 0.2 mole H_2O

It was found that 0.2 moles of H_2O decreases the reduced O by pure H_2 from 0.42 moles, shown previously in section 6.1.1, to 0.30 moles at 1600 ^oC. This means that the rate of reduction decreases due to the existence of 0.2 moles of H_2O by approximately 28 % at 1600 ^oC. However, only a drop in reduction potential of H_2 of 14 % with respect to pure H_2 is found at 2600 ^oC.

Figure 38 was produced to examine the negative influence of H_2O on the reduction behaviour of liquid FeO by H_2 against that of CO_2. It is obvious that the influence of CO_2 in retarding the reduction rate is higher than that of H_2O, i.e. there is less reduced oxygen in the case of CO_2 compared to H_2O over the shown temperature range.

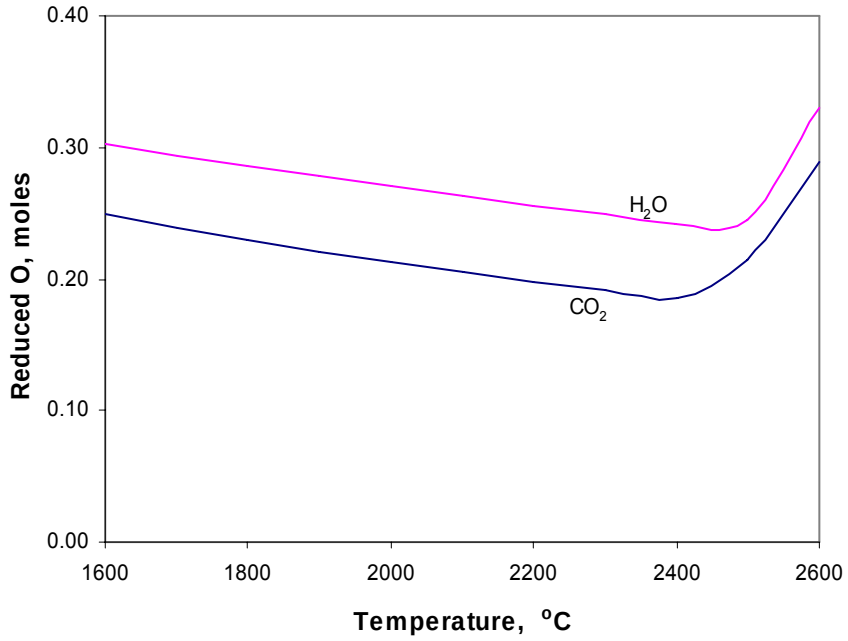

Fig. 38. Reduced oxygen in 1 mole FeO by 1 mole H_2 and 0.2 moles H_2O / CO_2

6.1.6 FeO-C

Figure 39 shows the thermodynamic equilibrium between 2 moles FeO and 1 mole C over a temperature range from 1600 °C to 2600 °C. From CO and CO_2 equilibrium lines, a total reduced O of 1.15 and 1.08 moles at 1600 °C and 2600 °C respectively was found.

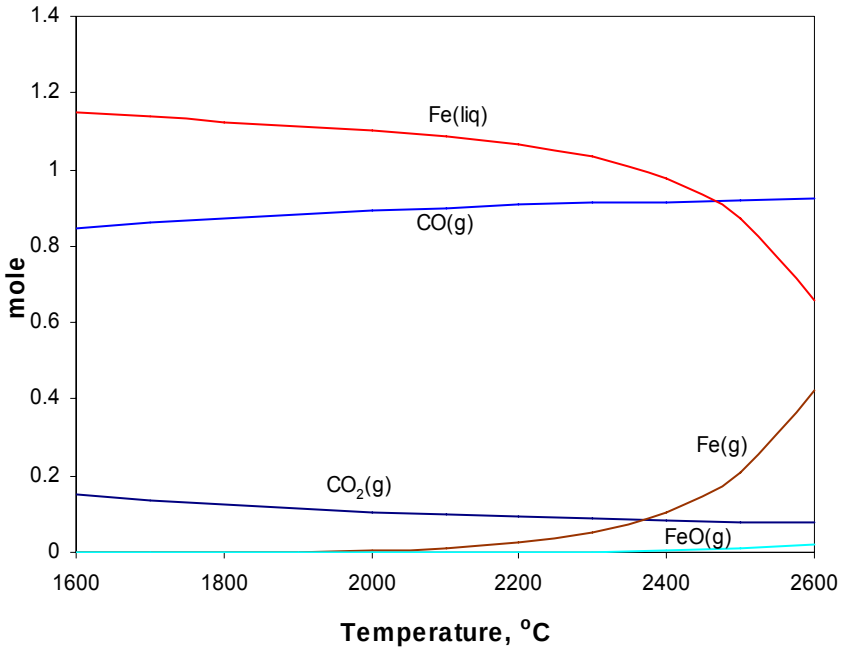

Fig. 39. Equilibrium of 2 moles FeO - 1 mole C

From the shown results and the results of FeO-H_2 in section 6.1.1, the carbon reduction rate was found approximately to be 2.85 times that of H_2 over the shown temperature range. Therefore, it is clear again that the carbon has a significant role compared to H_2 in the reduction process.

6.2 Thermodynamic calculation of slag diagrams at various % CaO

During the experimental work with hematite ore with acidic gangue material, a partial solidification of the slag is faced at the last phase of the reduction. This is obviously due to the diminished FeO amount in the slag. The partial solidification phenomenon leads to the decrease of the reduction rate where the rate limiting determinant becomes the oxygen transport to the reaction interface. It was therefore important to investigate the influence of slag temperature and basicity during the reduction of the ore on the solidification profile.

Plaul [10] has calculated the slag lines for various ores on a quaternary oxide system with constant concentration of 10 % wt. CaO using the FactSage Program [9]. The slag lines were plotted by producing equilibrium calculations between each ore and H_2 supplied, with increasing fixed steps, till complete reduction, reduction degree > 99 %. The results obtained were then normalised to 100 % for the main components of the slag (FeO-SiO_2-Al_2O_3). This procedure was done to enable the display of the slag lines on the quaternary oxide system. An important finding, as shown in figure 40, was the possibility to reduce the slag up to a reduction degree of approximately 99 % (10 % FeO) without encountering a problem of solidification.

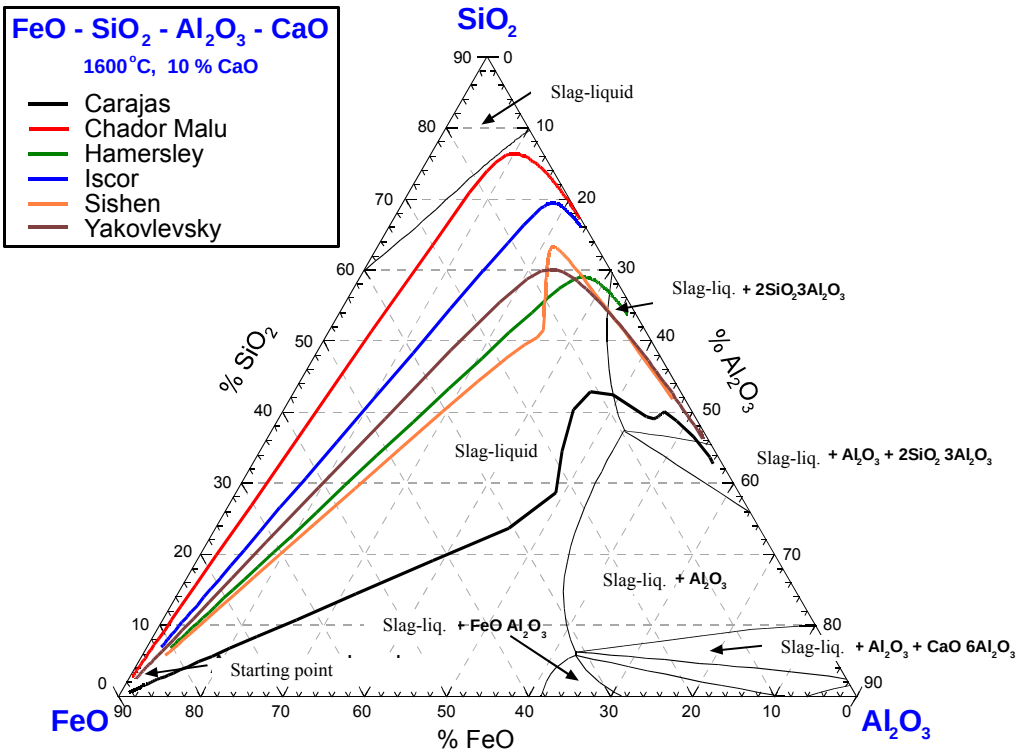

Fig. 40. Quaternary oxide system FeO-SiO_2-Al_2O_3-CaO and the calculated slag lines during reduction, [10]

In a continuous process, the slag line however would not be driven to the binary system SiO_2 – Al_2O_3 (0 % FeO), otherwise, the utilised amount of H_2 (hydrogen utilisation degree) according to the thermodynamical calculations will drop dramatically. This finding is explained in section 8.3.1, where the content of FeO in the slag was chosen to be 32 % to obtain a reduction degree of 98 %. According to these operation parameters, a determination of an optimum slag basicity and temperature was also sensible to obtain better data for an up-scaled process.

A set of calculations by FactSage 5.5 [9] was carried out to introduce the liquidus temperature of the oxide system FeO-SiO_2-Al_2O_3, wt. %, with various additions of CaO (0 %, 10 % and 20 %) and temperatures of 1500 and 1600 °C. The calculations were conducted adopting a hematite ore, Carajas, which was reduced by H_2 to obtain FeO in the slag up to approximately 30 %. Figure 41 shows the liquidus temperature of the ternary oxide system FeO-SiO_2-Al_2O_3, without CaO additions. It is clear from the figure that by reducing the slag to the required FeO in the slag that a solidification problem at 1500 °C would occur, i.e. further ore reduction is hindered. Whereas this problem could be avoided by increasing the temperature further up to 1600 °C.

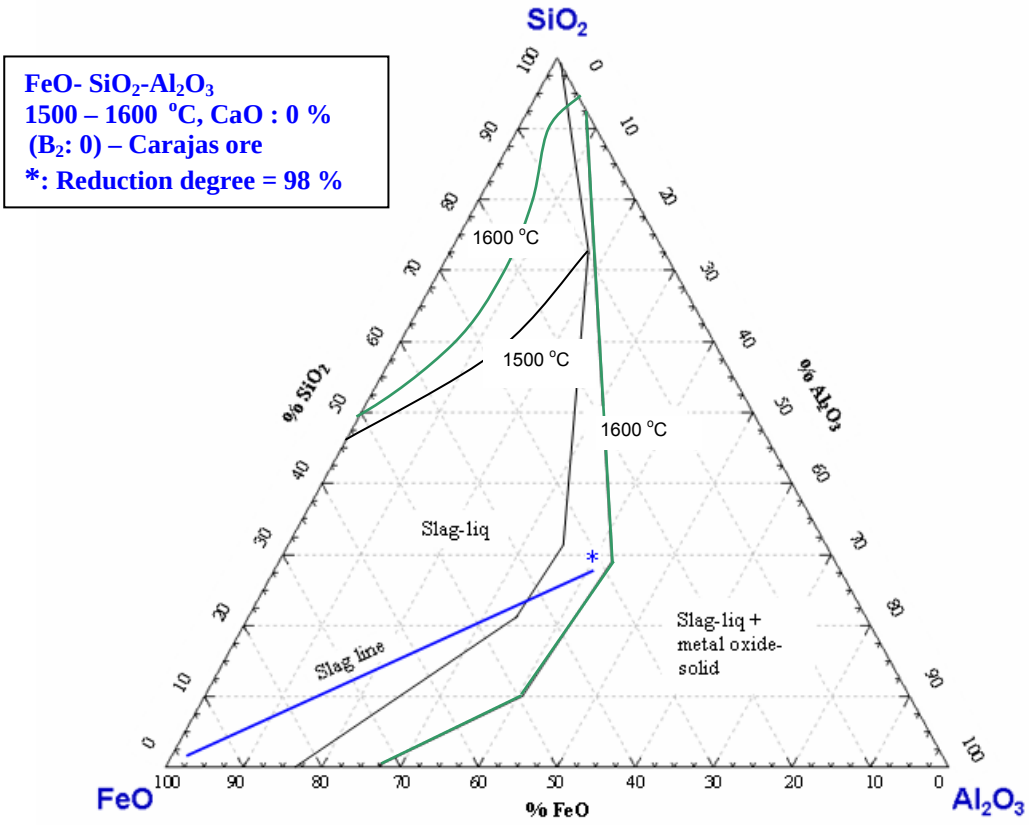

Fig. 41. Ternary oxide system FeO-SiO_2-Al_2O_3 and the liquidus temperatures

The feasibility of working with a slag temperature of 1500 °C but with higher basicity, 10 % CaO (B_2 ~ 0.5), was examined. The slag also ended up in a solidified region, as shown in the appendix. By increasing the slag basicity furthermore to 20 % CaO (B_2 ~1), figure 42 was obtained, where all the slag was diluted and the reduction process was feasible up to the required degree of reduction (98 %).

From the results obtained, it should be noted that the solidification behaviour should not be a problem in the up-scaled process as long as the slag temperature is kept at 1600 °C or above, as shown in the appendix. Operating at lower slag temperatures, T = 1500 °C, obviously entails the control of slag basicity at a minimum B_2 = 1. Provided that an acidic slag would not influence the refractory lifetime and that the phosphorous will not be handled in the reduction reactor, it is then preferred to work with slightly higher temperature (1600 °C) but with lower basicity (B_2 = 0 – 0.25), i.e. lower energy consumption and better operation of the process.

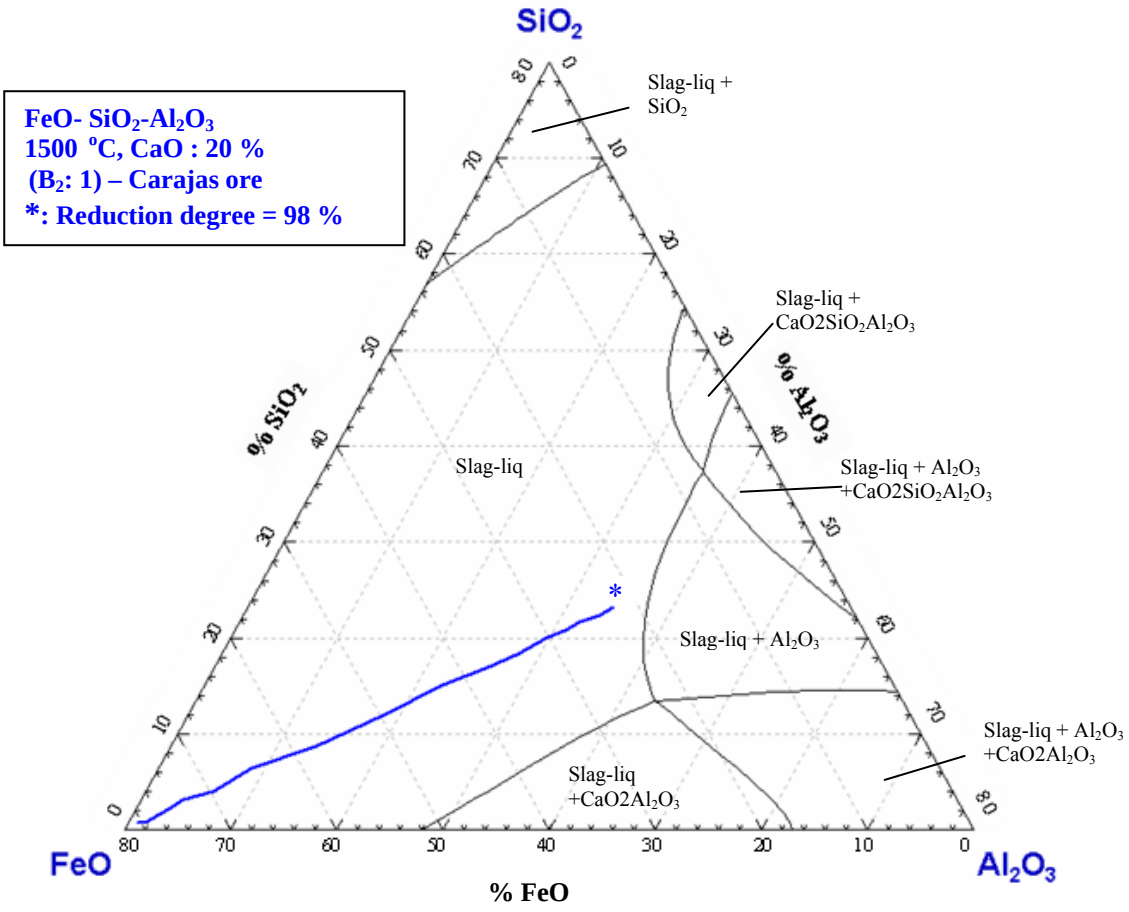

Fig. 42. Quaternary oxide system FeO-SiO_2-Al_2O_3-CaO and the calculated slag line during reduction

7 Experimental work

7.1 Experimental program

By the usage of the mass spectrometer (MS) “Basic Cube” produced by “Balzers Pfeiffer”, fluctuating readings of hydrogen as a light gas during the experimental work of Bäck [14] was faced. This has dedicated the chair of Metallurgy to buy a new MS “GAM 200” that was produced by “In Process Instruments”. The new MS is characterised by its high detection limits of light gases like hydrogen and helium.

Start up of the MS and implementation of on-line evaluation program has been carried out successfully within the current experimental work. A review of the H_2-Ar experiments has been carried out to examine the MS and use the results obtained for comparison purpose with the results of the main experimental program.

The process parameters of the main experimental program is summarised in figure 43.

1. Reduction, graphite vs. tungsten electrodes *graphite* / *tungsten* 30 % H_2 / 30 % H_2 40 % H_2 / 40 % H_2 50 % H_2 / 50 % H_2 Flow: 5 Nl/min, bal. Ar, 100 g Carajas	**2. Reduction by lateral supply of H_2** 15 % H_2-lat. 20 % H_2-lat. 25 % H_2-lat. Flow: 5 Nl/min, 40 % H_2, bal. Ar, 100 g Carajas	**3. CH_4-Ar reduction** 10 % CH_4 15 % CH_4 20 % CH_4 25 % CH_4 Flow: 5 Nl/min, bal. Ar, 100 g Carajas	**4. Reduction at various basicities** B_2: 0.06 B_2: 1 B_2: 1.5 B_2: 2 B_2:2.5 Flow: 5 Nl/min, 40 % H_2, bal. Ar, 100 g Hamersley
5. Magnetite reduction 30 % H_2 40 % H_2 50 % H_2 Flow: 5 Nl/min, bal. Ar, 100 g Kiruna	**6. Pre-reduced ore reduction** 30 % H_2 40 % H_2 50 % H_2 60 % H_2 Flow: 5 Nl/min, bal. Ar, 100 g reduced LKAB	**7. CO-H_2-Ar reduction** 5 % CO, 33 % H_2 7 % CO, 33 % H_2 8 % CO, 33 % H_2 10% CO, 33 % H_2 Flow: 6 Nl/min, bal. Ar, 100 g Carajas	**8. CO-Ar reduction** 50 % CO 60 % CO 70 % CO Flow: 5 Nl/min, bal. Ar, 100 g Carajas
9. CO_2-H_2-Ar reduction 3 % CO_2, 33 % H_2 5 % CO_2, 33 % H_2 7 % CO_2, 33 % H_2 8 % CO_2, 33 % H_2 Flow: 6 Nl/min, bal. Ar, 100 g Carajas	**10. H_2O-H_2-Ar reduction** 4 % H_2O, 38 % H_2 7 % H_2O, 37 % H_2 9 % H_2O, 36 % H_2 11 % H_2O, 35 % H_2 Flow: 5.2 - 5.7 Nl/min, bal. Ar, 100 g Carajas	**11. H_2-Ar reduction with coke additions** 2.5 g coke, 5 g coke, 10 g coke, 15 g coke 1.33 g/min coke Flow: 5 Nl/min, 40 % H_2, bal. Ar, 100 g Carajas	**12. Continuous feeding of ore during reduction** 30 % H_2 40 % H_2 50 % H_2 55 % H_2 Flow: 5 Nl/min, bal. Ar 4.55 g/min Carajas

bal.: Balance

Fig. 43. Experimental program

Carajas fines ore was used in most of the conducted experiments. Hamersley, Kiruna and pre-reduced LKAB were also used as shown below in some series of experiments.

Reference experiments were conducted first using a graphite electrode. After that, experiments with a tungsten electrode with the same process parameters were done. The objective of these experiments was to assess the *hydrogen utilisation degree* with carbon contribution predominating from the graphite electrode against the *actual hydrogen utilisation degree* without carbon contribution by the usage of a tungsten electrode.

Lateral supply of hydrogen through a ceramic pipe, rather than being supplied through a hollow electrode were conducted in a second series of experiments. The objective of these experiments was to investigate the hydrogen reduction behaviour at reaction zones with lower temperature ranges (non plasma zone) where absence of dissociated hydrogen is quite obvious.

Methane has been used instead of hydrogen as an alternative reducing gas in a series of experiments. The advantage of methane with respect to hydrogen is firstly saving a H_2 production unit in the case of up-scaling. Secondly is the utilisation of the existing carbon in the methane as a superior reductant in the process. Experiments at various concentrations of methane have been conducted and compared with the results of hydrogen experiments at the same amount of supplied H_2.

Basicity of the ore has been controlled by varying CaO amount in a set of reduction experiments. The target was to evaluate the reduction behaviour with CaO additions and investigate the behaviour of phosphorous in the process up to the di-calcium silicate phase of the slag.

Magnetite ore has been adopted in a set of experiments (rather than hematite). The same process parameters were kept to compare the influence of the ore characteristics on the reduction behaviour.

LKAB ore has been reduced almost to a divalent iron phase with the assistance of the LKAB company to carry out experiments using pre-reduced ore. It has been charged in a set of experiments under various concentrations of hydrogen to investigate the influence of the ore pre-reduction on the reduction behaviour.

All the following series of experiments were planned to deepen the perception of an up-scaled process as a main task within our contribution part in an EU project (ULCOS).

In up-scaled processes, where graphite electrode reactions, calcination products from the used additives and products from the reduction process take place, accompanying gases like CO, CO_2 and H_2O would exist in the system. Some experiments have been carried out as shown in the following four series of experiments to investigate the effect of these gases on the reduction behaviour:

1. CO was varied in Ar-H_2 mixture to evaluate the influence of CO on hydrogen reduction behaviour.
2. Absolute reduction rate of CO at various concentrations was evaluated in another series of experiments. Higher concentrations of CO without the usage of hydrogen were used in these experiments to assess precisely the CO reduction kinetics under plasma application.
3. CO_2 was varied in Ar-H_2 mixture to evaluate the influence of CO_2 on the retardation of hydrogen reduction rate.
4. H_2O was varied in Ar-H_2 mixture to evaluate the influence of H_2O on the retardation of hydrogen reduction rate.

In the study phase of up-scaled process, a hybrid application of coke and hydrogen plasma was used as an option. Coke has been mixed with the ore and placed in the crucible in a series of experiments to evaluate the influence of coke on the reduction behaviour of hydrogen plasma. Additionally, the development of slag foaming via coke additions was a phenomenon to be observed. In the end, in order to have representative results and longer time of evaluation to the coke reduction behaviour, continuous feeding of coke by a screw conveyor through the hollow electrode was conducted.

In the last series of experiments, continuous feeding of fines ore, instead of charging it in the crucible before the experiments, was carried out. The objective of this series of experiments was to investigate the plasma stability and the reduction behaviour under continuous feeding of ore. The necessity of these experiments was to study the feasibility of the continuous feeding of ore via the electrodes in an up-scaled process as this option might have a positive effect on the in-flight reduction or the arc heat load to the furnace walls.

7.2 Setup of the laboratory furnace system

7.2.1 Basic setup of the hydrogen plasma facility

Detailed explanation of the system setup was shown in previous work, Bäck [14] and Plaul [10]. However, a brief overview of the system is shown in figure 44. The lab-scale plasma facility consists mainly of a *direct current supply unit* (PC-Plasmette) that was produced by "Messer Griesheim" and designed for plasma cutting purposes. The plasmette unit is working with one transformer with a maximum power of 8 kW, a voltage of 110 V and a current of 70 A. *Mass flow meters / controllers* (Bronkhorst type) are set to measure and control the gas flow up to 10 Nl/min, independent of pressure and temperature changes. The used gases are mixed in a mixing chamber in the plasmette and fed to the *plasma reactor* through a graphite / tungsten hollow electrode. A *quadrupole mass spectrometer* (MS), GAM 200, which was delivered by "In Process Instruments", is used to analyse the off-gas and evaluate the reduction rates. This basic setup was applied in the experiment series 1, 3, 4, 5, 6, 8 and 11 (as classified in figure 43). An additional flow meter has been used in the experiment series 7 and 9, while some modifications, as clarified later on, were carried out in the rest of the experiments, (2, 10, and 12).

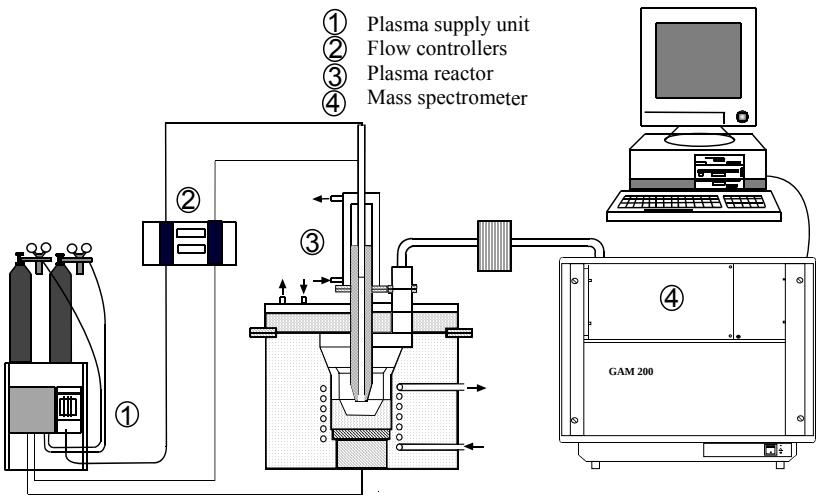

Fig. 44. Schematic overview of the plasma facility

7.2.2 Lateral supply of hydrogen via a ceramic lance

In the standard experiments, hydrogen is mixed with argon in the mixing chamber of the plasma device before being fed to the plasma reactor. However, in the experiment series 2, hydrogen was partitioned into two parts. The first part was via mixing hydrogen with argon as practiced in the standard experiments. The second part was through supplying hydrogen laterally through an installed ceramic lance with inner diameter of 5 mm, figure 45. With such

an experimental setup the blown hydrogen was injected to the oxide melt at room temperature, rather than the plasma temperature. The lance was fixed ~20 mm apart from the bath surface in the conducted series of experiments. Increasing the distance to 40 mm was also done to investigate the pulse effect of hydrogen.

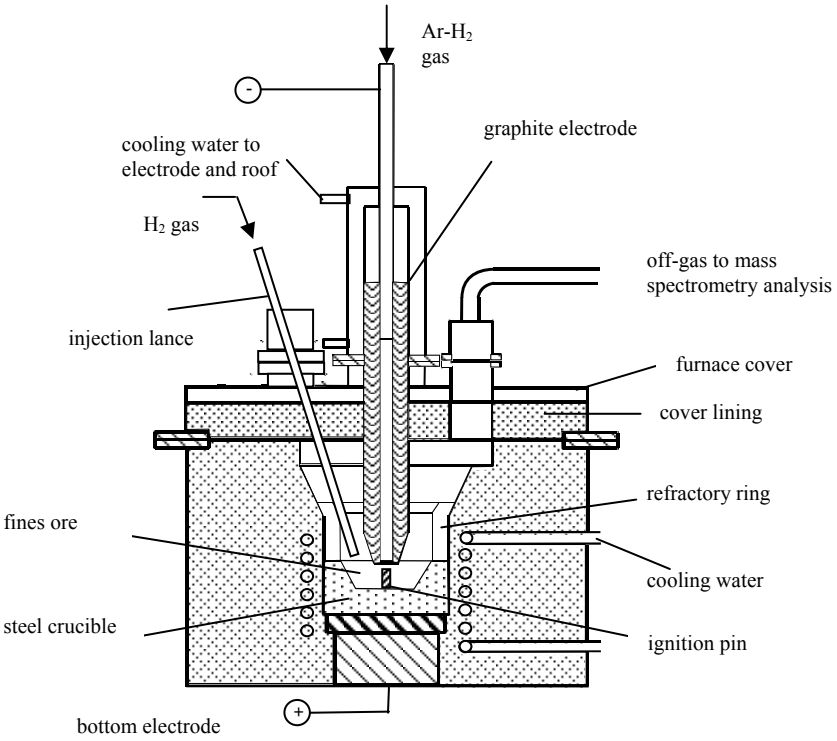

Fig. 45. Furnace layout with lateral injection of H_2

7.2.3 Steam addition to the existing Ar-H_2 supply facility

Steam was mixed to the Ar-H_2 mixture in the experiment series 10 before being fed to the plasma reactor. Steam production is achieved through the usage of an evaporator system (Bronkhorst type), figure 46. Water is fed through a liquid flow meter (LFM) that is pressurised by an inert gas (Ar) while the carrier gas (Ar) is fed through a gas flow controller. Water and the carrier gas are mixed in a mixture valve and then evaporated by a heater in a controlled evaporator mixer system (CEM). Two readout units are used. One is used to measure and control the carrier gas flow while the other is used to measure and control both the water flow and the process temperature. Further heating of the produced steam is done with an additional heated line till a delivery point where mixture with Ar-H_2 takes place directly before gas injection to the hollow electrode.

Before every start up, the piping system is purged with argon from both sides (the liquid flow meter side and the gas flow meter side). The water supply tank is then pressurised. The system is filled with water and the process is ready for operation after venting all gas bubbles.

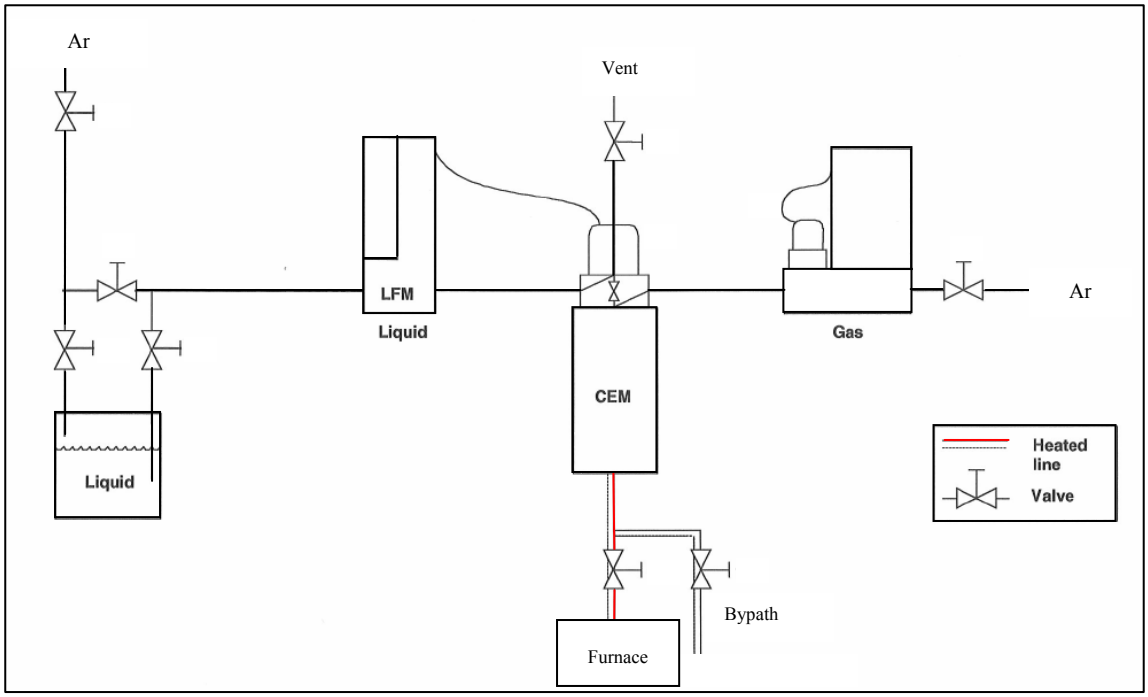

Fig. 46. Evaporator layout

The control of the process parameters is carried out by setting up the gas flow, the water flow and the CEM heater to the required temperature via the installed readout units. Minimum required temperature to guarantee evaporation with respect to the set water flow is calculated by the Bronkhorst designed software, Fluidat [83]. After reaching the stabilisation phase, the steam is switched from the bypath line to the process. The steam quantity is controllable up to 30 g/hr.

7.2.4 Fines ore continuous feeding system

A continuous feeding system was prepared to supply fines ore in the experiment series 12. Ready made systems of low feeding rate (grams per minute) were not available in the market. Therefore, the design and assembly of the system have been carried out within the chair of metallurgy. The fabrication of a screw conveyor that delivers the required feed rate has been outsourced. A general layout of the screw conveyor system is shown in figure 47.

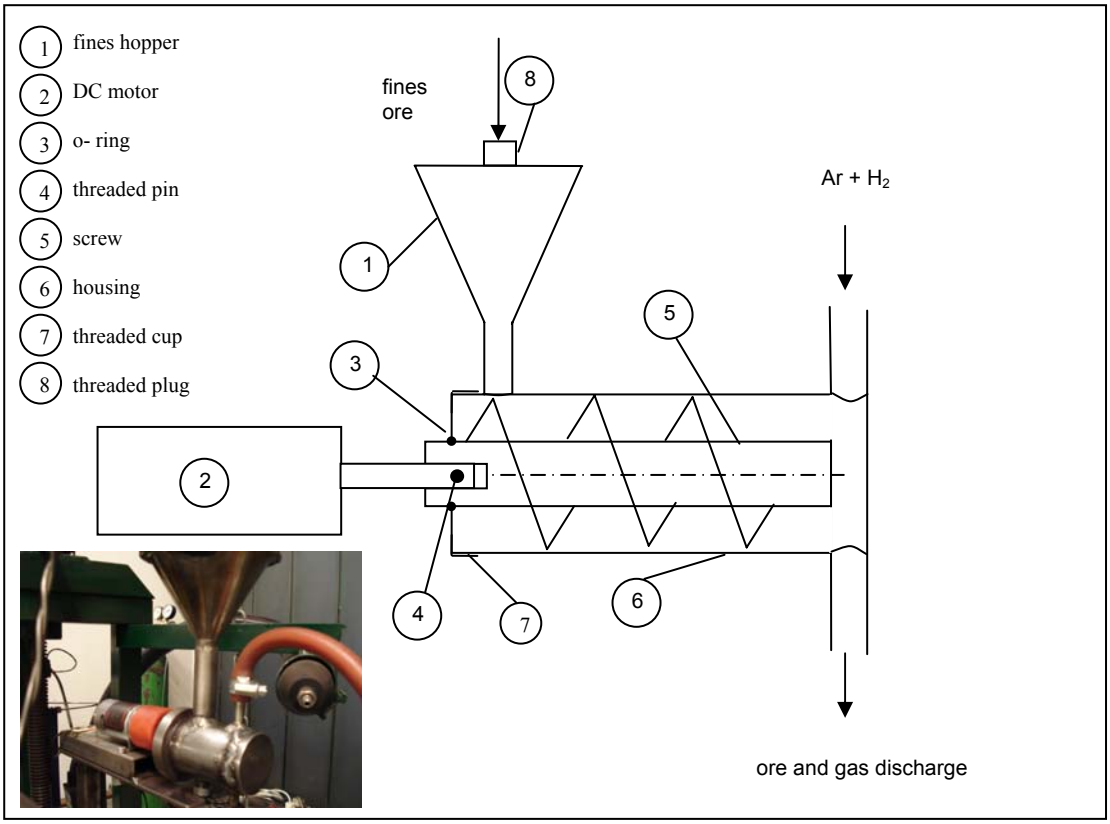

Fig. 47. Screw conveyor system

The shown system consists of an adjustable voltage transformer, DC geared motor of operation voltage (4.5 – 15 V) and rotation speed (8 – 25 rpm), fines ore hopper, ϕ30 mm screw, screw housing welded to 2 x ϕ7 mm pipes for the handling of gas and fines. Fines are conveyed by the screw, mixed with gas and discharged together into the hollow metallic rod coupled to the hollow graphite electrode. A plastic hose is used as a spacer and mounted between the discharge pipe and the hollow rod to avoid an electrical short that in turn will deteriorate the plasma arc initiation.

The system is gas sealed by an o-ring mounted between the threaded cup and the screw shaft. Moreover, for further sealing, a cover is welded to the hopper and only a small opening port is prepared for fines addition and then plugged. Feeding rate of the used fines was 4.55 g/min in the conducted series of experiments. The system was used as well to convey coke instead of fines ore with 1.33 g/min feeding rate.

7.3 Experimental procedures

This section is aiming at explaining the procedures of the conducted experiments. The main practices in terms of MS calibration, preparation of experiments and furnace operation are the same as the work done and explained in details in previous works, [10,14]. However, the evaluation of the results varied from one series to another. Amendments in the main calculation procedures were considered to assess the change in reduction behaviour with the changing parameters.

7.3.1 Preparation of fines ore

In the conducted experiments, hematite ore (Carajas, Hamersley), magnetite ore (Kiruna) and pre-reduced hematite ore (LKAB) were used according to the following chemical analysis, table 1. The size of ore used was varying between 0.01 and 1 mm.

		Carajas (hematite)	Hamersley (hematite)	Kiruna (magnetite)	LKAB (pre-reduced hematite)
$Fe_{tot.}$	%	67.66	60	69.83	74.39
FeO	%	0.4	0.14	29.25	78.17*
CaO	%	0.01	0.33	0.45	0.91
MgO	%	0.02	1.61	0.50	0.73
SiO_2	%	0.56	5.4	0.18	0.91
Al_2O_3	%	0.84	2.32	0.15	0.18
Mn	%	0.31	0.23	0.08	0.06
P	%	0.037	0.075	0.040	0.026
S		0.01	0.024	-	-
TiO_2	%	-	-	-	0.17
Na_2O	%	<0.01	<0.01	0.03	0.05
K_2O	%	0.13	0.10	0.07	-
V_2O_5	%	-	-	-	0.21
LOI		1.5	4.03	1.39	-

* FeO content is equivalent to (28.14 % Fe_3O_4 and 69.43 % FeO)

Table 1. Chemical analysis of the fines ores

Carajas ore was used as an ore with low slag content in most of the conducted experiments. Hamersley was used in a test run, as an ore with relatively higher phosphorous content with respect to Carajas. It was mixed with CaO (chemical analysis is shown in the appendix) to study the potential of dephosphorisation.

To study the reduction behaviour of magnetite ore against hematite ore, Kiruna ore (almost pure magnetite) was used in one series of experiments.

Wustite equivalent pre-reduced ore has been prepared at LKAB laboratory to carry out reduction experiments of Fe^{2+} containing ore. Hematite pellets were prepared, reduced mainly to wustite and then crushed to fines. The reducing gases were set at 830 ^{o}C and at vol. composition of 40/20/15/25 % - H_2/CO/CO_2/H_2O respectively. Reduction has been run until no weight loss of the sample was observed.

7.3.2 Preparation and execution of experiments

Before each experiment, fines ore, a steel crucible and a refractory ring (made of MgO) are weighted for a mass balance and then set in the furnace. The furnace cover is fitted to the furnace housing by a lifting crane and fastened by latch clamps. The electrode is manually derived downwards till being contacted to the ignition pin. Subsequently electric resistance is measured between the electrode and the furnace bottom part. The electric resistance is confirmed in each experiment to be less than 5 Ohm. The lifting arm of the electrode is then fixed to the electrode to control the movement mechanism of the electrode via a lifting spindle during the experiment. As a final stage in the furnace preparation, the MS heated capillary hose is coupled to the furnace off-gas duct.

In order to start furnace purging, the electromagnetic operated valves are switched on by starting the main switch button of the plasma device. Ar flow is then controlled up to 3 Nl/min and gas analysis is monitored till N_2 decreases to ppm range and Ar increases to more than 98 %. Cooling water is delivered to the furnace housing, roof, bottom part and the electrode jacket.

Before starting the experiment, contact between the electrode and the ignition pin has to be confirmed. The process parameters are set in an evaluation program for the sake of on-line monitoring of the reduction progress. The current supply is then switched on, electrode is lifted up, arc initiates and melting starts. After a melting phase of approximately 3 minutes, H_2 is supplied to the furnace according to the set process parameters. Meanwhile, the evaluation program is started. Current and voltage (across the arc) are monitored throughout the experiment. On-line measurements for voltage and current are carried out in some experiments for a better monitoring of the plasma stability in terms of voltage/current fluctuations. MS is used throughout the experiment to analyse the off-gas and calculate the reduction behaviour in terms of reduction degree and H_2 utilisation degree using the designated evaluation program.

After fulfilling the criteria of experiment completion, H_2 flow is cut off and current supply is switched off. Furnace cooling down under Ar is carried out for approximately 10 minutes till the reddish colour of the reduced metal disappears. Ar is then cut off and furnace roof is lifted up to get rid (as much as possible) of the remaining steam existing in the castable. To conduct the mass balance, the crucible and refractory ring are weighed after the experiment.

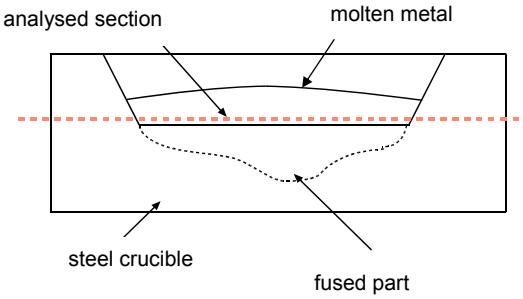

Fig. 48. Cross section of a crucible after an experiment

Finally, slag is removed from the crucible and the metal is chemically analysed. The procedure of metal analysis is carried out either by cutting or turning the crucible up to a flat section as shown in figure 48 and analysed by a radio spectrometer.

7.3.3 Evaluation of experiments

Based on the conducted gas analysis by the MS, the reduced amount of oxygen can be calculated. Having a new model of MS (GAM 200) and reliable readings of light gases like H_2, setting the measuring cycle (t_{cycle}) to low values of approximately 2.4 s is possible. As a result of reducing the fines ore by H_2, steam (H_2O) as a component in the off-gas is monitored. However, a significant portion of H_2 remains in the off-gas due to the thermodynamic equilibrium, where some of the H_2 supplied is un-reacted.

In the conducted experimental program as discussed earlier on, the process parameters were obviously different. The changes in process parameters were confined between the reducing agent (gas or solid), the type of fines ore, type of electrode, way of H_2 supply, batch wise or continuous feeding of ore or coke. However, in the Ar-H_2 based experiments (test series 1, 2, 4, 5, 6), as classified in figure 43, the calculation procedures of Bäck [14] were used and are clarified in the following section. Necessary changes in the calculations of other experiments will be then individually clarified.

7.3.3.1 Ar-H_2 reduction experiments

In the conducted experiments (test series 1, 2, 4, 5, 6 in figure 43), H_2 and Ar are used as plasma gas. Since the electrode used is made of graphite, CO and CO_2 are produced in addition to the expected H_2, H_2O and Ar. These gas components stem from the following reactions:

1. Due to the reaction between the steam formed by reduction and carbon from the used graphite electrode, CO is formed as follows:

$$\{H_2O\} + C_{electrode} \leftrightarrow \{H_2\} + \{CO\} \quad (22)$$

2. By the splash of oxide melt that settles on the electrode tip and reacts as follows:

$$(FeO_x) + x\,C \leftrightarrow Fe_{(l)} + x\{CO\} \quad (23)$$

3. Due to the partial melting of the crucible, the carbon contained (~0.04 %) reacts with the oxide melt. In case of iron carburisation by electrode reaction, (23), the corresponding carbon will also reduce the oxide melt as follows:

$$x\,[C] + (FeO_x) \leftrightarrow x\{CO\} + Fe_{(l)} \quad (24)$$

4. CO_2 develops due to the reaction between the formed CO and the oxide melt:

$$x\{CO\} + (FeO_x) \leftrightarrow x\{CO_2\} + Fe_{(l)} \quad (25)$$

5. CO_2 also develops due to the reaction between CO and H_2O according to the water gas shift reaction:

$$\{CO\} + \{H_2O\} \leftrightarrow \{CO_2\} + \{H_2\} \quad (26)$$

Evaluation of the reduction kinetics in these series of experiments is carried out via the MS software. The excel program was also designed to have more flexibility to change the parameters as practiced in the rest of the experimental program. To run the program, the following input data are required:

- Ar inlet flow by the flow meter (FM), V_{Ar}^{FM}, Nl/min
- H_2 inlet flow, $V_{H_2}^{FM}$, Nl/min
- $m_{o,red.}$, reducible amount of oxygen in the ore, g
- Duration of the measuring cycle, s
- Off-gas analyses (Ar, H_2, H_2O, CO, CO_2, N_2, O_2).

The off-gas analysis is used to calculate the gas flow per measuring cycle in Nl/cycle according to the following equations. The calculations are based on the inlet flow per cycle of Ar, V_{Ar}^{inlet}, which is equal to outlet flow of Ar as it does not contribute to the reduction process.

$$V_{Ar}^{inlet} = \frac{V_{Ar}^{FM}}{60} \cdot t_{cycle} \ [Nl/cycle] \quad (27)$$

$$V_{CO} = \frac{V_{Ar}^{inlet}}{\%Ar} \cdot \%CO \ [Nl/cycle] \quad (28)$$

$$V_{CO_2} = \frac{V_{Ar}^{inlet}}{\%Ar} \cdot \%CO_2 \ [Nl/cycle] \quad (29)$$

$$V_{H_2} = \frac{V_{Ar}^{inlet}}{\%Ar} \cdot \%H_2 \ [Nl/cycle] \quad (30)$$

$$V_{H_2O} = \frac{V_{Ar}^{inlet}}{\%Ar} \cdot \%H_2O \ [Nl/\ cycle] \quad (31)$$

Calculation of the total flow of each off-gas component is carried out by the summation of the obtained gas flow (Nl/cycle) throughout the whole period of the experiment, i.e. cycle= 1 to n.

$$V_{CO,tot.} = \sum_{c=1}^{n} V_{CO} \ [Nl] \quad (32)$$

$$V_{CO_2,tot.} = \sum_{c=1}^{n} V_{CO_2} \ [Nl] \quad (33)$$

$$V_{H_2,tot.} = \sum_{c=1}^{n} V_{H_2} \ [Nl] \quad (34)$$

$$V_{H_2O,tot.} = \sum_{c=1}^{n} V_{H_2O} \ [Nl] \quad (35)$$

By converting the obtained volumes of gases into moles and multiplying it by the atomic mass of oxygen, the reduced amount of oxygen in grams that is the found in off-gas is calculated.

$$m_{O,H_2O} = \frac{V_{H_2O,tot.}}{22.41} \cdot 16 \ [g] \quad (36)$$

$$m_{O,CO} = \frac{V_{CO,tot.}}{22.41} \cdot 16 \ [g] \quad (37)$$

$$m_{O,CO_2} = \frac{V_{CO_2,tot.}}{22.41} \cdot 32 \ [g] \quad (38)$$

By conducting a H_2 balance during the beginning of the experiment, a H_2 deficit is noticed. Whereas some time later a H_2 surplus is found. This is due to the relative low temperature of the furnace lining and the high steam partial pressure at the beginning of the experiment. This developing steam diffuses in the pores of the lining. Later, at higher lining temperature, steam gets out of the lining and shows up in the off-gas. To handle this error in the actual emitted steam, a correction term via the H_2 balance is calculated. This correction term ($m_{O,H2O,\ corr.}$) is positive at the beginning of the experiment but becomes negative at later stages of the experiment.

$$V_{H_2O,corr.} = V_{H_2}^{inlet} - V_{H_2O} - V_{H_2} \quad [Nl/cycle] \tag{39}$$

$$V_{H_2O,corr.,tot.} = \sum_{c=1}^{n} V_{H_2O,corr.} \quad [Nl] \tag{40}$$

$$m_{O,H_2O,corr.} = V_{H_2O,corr.,tot.} \cdot \frac{16}{22.41} \quad [g] \tag{41}$$

$$m_{O,tot.} = m_{O,H_2O} + m_{O,H_2O,corr.} + m_{O,CO} + m_{O,CO_2} \quad [g], \tag{42}$$

where $V_{H_2}^{inlet}$ is the inlet H_2 (Nl/cycle) and $m_{O,tot.}$ is the total amount of reduced oxygen.

The apparent contribution of H_2 and CO in the reduction is the reduced oxygen in g found in H_2O, CO and CO_2 divided by the reducible oxygen existing in the ore, $m_{O,red.}$ and assessed as individual reduction degrees in %.

$$\Delta RD_{H_2O} = \frac{m_{O,H_2O} + m_{O,H_2O,corr}}{m_{o,red.}} \cdot 100 \quad [\%] \tag{43}$$

$$\Delta RD_{CO} = \frac{m_{O,CO}}{m_{O,red.}} \cdot 100 \quad [\%] \tag{44}$$

$$\Delta RD_{CO_2} = \frac{m_{O,CO_2}}{m_{O,red.}} \cdot 100 \quad [\%] \tag{45}$$

The total reduction degree is then calculated as follows:

$$\Delta RD_{tot} = \Delta RD_{H_2O} + \Delta RD_{CO} + \Delta RD_{CO_2} \quad [\%] \tag{46}$$

To examine the thermodynamics equilibrium of the process, the degree of utilisation of H_2 (η_{H_2}) and the total utilisation degree of H_2 ($\eta_{tot.}$) per cycle are evaluated. Moreover, the rate of reduced oxygen $dm_{o,red.}/dt$ (g/cycle) is calculated to assess the reduction kinetics. The mentioned parameters are monitored via the evaluation program and defined as follows:

$$\eta_{H_2} = \frac{V_{H_2O} + V_{H_2O,corr}}{V_{H_2}^{inlet}} \cdot 100 \ [\%] \qquad (47)$$

The H_2 utilisation degree (η_{H_2}) per cycle is the measure of the H_2O produced in the off-gas from the H_2 supplied $V_{H_2}^{inlet}$ throughout a measuring cycle of the MS. The steam produced is the summation of the steam found in the off-gas V_{H_2O} and the steam received/produced by the furnace lining $V_{H_2O,corr}$ and calculated via the H_2 balance.

The total utilisation degree of H_2 $(\eta_{tot.})$ per cycle is calculated as follows:

$$\eta_{tot.} = \frac{V_{H_2O} + V_{H_2O,corr} + V_{CO} + 2 \cdot V_{CO_2}}{V_{H_2}^{inlet}} \cdot 100 \ [\%] \qquad (48)$$

In the analysed off-gas, oxygen is found mainly in H_2O. However, it is found in CO and CO_2 as well. It should be mentioned that some of the oxygen witnessed in CO and CO_2 stems from reactions (22) and (26) while the rest is produced by the reduction potential of CO according to the reaction (25). Therefore, the actual H_2 utilisation degree is some value between the H_2 utilisation degree and the total utilisation degree.

Finally, the reduction rate of oxygen $dm_{o,red.}/dt$ (g/cycle) is calculated as follows:

$$dm_{O,red.}/dt = (V_{H_2O} + V_{H_2O,corr} + V_{CO} + 2.V_{CO_2}).\frac{16}{22.41} \ [\text{g/cycle}] \qquad (49)$$

7.3.3.2 CH_4-Ar reduction experiments

CH_4 decomposes mainly to solid carbon and hydrogen molecules at the arc-melt interface according to the following reaction:

$$\{CH_4\} \Leftrightarrow C(s) + 2\ \{H_2\} \qquad (50)$$

Evaluation of the Ar-CH_4 experiments, experiment series 3, entails the input of inlet flow of CH_4 (Nl/cycle) and the same input data that was shown in the previous section. However, the previous calculations of $m_{O,H2O,corr}$ and the utilisation degrees are amended as follows:

$$V_{H_2O,corr.} = 2.V_{CH_4}^{inlet} - V_{H_2O} - V_{H_2} \ [\text{Nl/cycle}] \qquad (51)$$

$$\eta_{H_2} = \frac{V_{H_2O} + V_{H_2O,corr.}}{2.V_{CH_4}^{inlet}} \cdot 100 \ [\%] \quad (52)$$

$$\eta_C = \frac{0.5.V_{CO} + V_{CO_2}}{V_{CH_4}^{inlet}} \cdot 100 \ [\%] \quad (53)$$

7.3.3.3 CO-H_2-Ar and CO-Ar reduction experiments

Inlet flow of CO (V_{CO}^{inlet}), Nl/cycle is set within the input data in experiment series 7, 8. However, the previous calculations of $m_{O,tot.}$ and $dm_{O,red.}/dt$ are changed as shown below. Moreover, the total utilisation degree of H_2 is substituted by CO utilisation degree.

$$m_{O,COinlet.} = \sum_{c=1}^{n} V_{CO}^{inlet} \cdot \frac{16}{22.41} \ [g] \quad (54)$$

$$m_{O,tot.} = m_{O,H_2O} + m_{O,H_2O,corr} + m_{O,CO} + m_{O,CO_2} - m_{O,COinlet} \ [g] \quad (55)$$

$$\eta_{CO} = \frac{V_{CO_2}}{V_{CO}^{inlet}} \cdot 100 \ [\%] \quad (56)$$

$$dm_{O,red.}/dt = (V_{H_2O} + V_{H_2O,corr} + V_{CO} + 2.V_{CO_2} - V_{CO}^{inlet}).\frac{16}{22.41} \ [g/cycle] \quad (57)$$

7.3.3.4 CO_2-H_2-Ar reduction experiments

Inlet flow of CO_2 ($V_{CO_2}^{inlet}$), Nl/cycle is set within the input data in experiment series 9. Monitoring of the gas utilisation degree is conducted by the calculation of H_2 utilisation degree. The amount of inlet oxygen via supplied CO_2, the amount of reduced oxygen and the reduction rate are evaluated through the following equations:

$$m_{O,CO_2inlet.} = \sum_{c=1}^{n} V_{CO_2}^{inlet} \cdot \frac{32}{22.41} \ [g] \quad (58)$$

$$m_{O,tot.} = m_{O,H_2O} + m_{O,H_2O,corr} + m_{O,CO} + m_{O,CO_2} - m_{O,CO_2inlet} \ [g] \quad (59)$$

$$dm_{O,red.}/dt = (V_{H_2O} + V_{H_2O,corr} + V_{CO} + 2.V_{CO_2} - 2.V_{CO_2}^{inlet}).\frac{16}{22.41} \ [g/cycle] \quad (60)$$

7.3.3.5 H_2O-H_2-Ar reduction experiments

Inlet flow of H_2O ($V_{H_2O}^{inlet}$), Nl/cycle is set within the input data in experiment series 10. The following changes in the equations were carried out:

$$V_{H_2O,corr.} = V_{H_2}^{inlet} + V_{H_2O}^{inlet} - V_{H_2O} - V_{H_2} \ [Nl/cycle] \quad (61)$$

$$m_{O,H_2Oinlet.} = \sum_{c=1}^{n} V_{H_2O}^{inlet} \cdot \frac{16}{22.41} \ [g] \quad (62)$$

$$m_{O,tot.} = m_{O,H_2O} + m_{O,H_2O,corr} + m_{O,CO} + m_{O,CO_2} - m_{O,H_2Oinlet} \ [g] \quad (63)$$

$$dm_{O,red.}/dt = (V_{H_2O} + V_{H_2O,corr} + V_{CO} + 2.V_{CO_2} - V_{H_2O}^{inlet}).\frac{16}{22.41} \ [g/cycle] \quad (64)$$

7.3.3.6 H_2-Ar reduction with coke additions

Inlet amount of coke, g or g/min are set within the input data in experiment series 11. There is no change in the calculation procedures. However, carbon utilisation degree is defined as follows:

$$\eta_C = \frac{0.5.V_{CO} + V_{CO_2}}{coke,inlet} \cdot 100 \ [\%], \quad (65)$$

where V_{CO}, V_{CO_2} and coke inlet are in moles/cycle.

7.3.3.7 Continuous feeding of ore during reduction

The dosage rate of ore, r, g/cycle and the percentage of reducible oxygen in the ore, p, %, are additionally set to the input data in experiment series 12. The total reducible oxygen is not constant in these experiments but increases over the time of the experiment due to the continuous feeding of the ore. Therefore, the reducible oxygen is the summation of the oxygen content in the ore existing in the crucible before further feeding of ore, $m_{O,red.,batch}$ and that fed continuously, $m_{O,red.,cont.}$.

$$m_{O,red.,cont.} = (r.p)/100 \ [g/cycle] \quad (66)$$

$$m_{O,red.,cont.,tot.} = \sum_{c=1}^{n} m_{O,red.,cont.} \ [g] \quad (67)$$

$$m_{O,red.} = m_{O,red.,batch} + m_{O,red.,cont.,tot.} \ [g] \quad (68)$$

7.4 Results of experiments

All experiments started by melting 100 g fines through transferred argon plasma in a low carbon steel crucible (0.03-0.05 % C). The melting phase was run for approximately 3 minutes with argon flow of 3 Nl/min, voltage between 30 and 35 V and current between 95 and 100 A. This corresponded to an electrical power of almost 3 kW that increased up to 8 kW by using, for instance, 60 % H_2 in the plasma gas. During the melting progression, some conversion of hematite into magnetite took place. However, a degree of ore reduction (2-3 %) was only found in the results of the gas analysis, whereas the minimum achievable reduction degree in the case of complete melting is 11%. This limited reduction rate was due to the partial melting of the ore. Moreover, an obvious decrease in the Fe^{3+} concentration was observed. For example, a shift from 68 % to approximately 30 % Fe^{3+} in the molten portion of the Carajas ore was found [10]. This was due to the melting of the ore and the reaction of the ignition pin with the molten portion according to the following reaction:

$$Fe_{liq} + 2Fe^{3+} \leftrightarrow 3Fe^{2+} \quad (69)$$

After the melting phase, the plasma gas was switched from argon to a mixture of argon and other gases, e.g. H_2, CH_4, CO, CO_2 and H_2O, where complete melting and reduction took over.

7.4.1 Reduction by H_2 plasma, graphite versus tungsten electrodes

To have a fingerprint for the new MS, reduction experiments using various concentrations of H_2 in H_2-Ar mixture and graphite electrode were carried out. Evaluation of the reduction rate and the H_2 utilisation degree was conducted. However, the exact evaluation of the H_2 utilisation degree was not possible in experiments which used graphite electrodes due to the contribution of carbon in the reaction and the water gas shift reactions. Therefore, reduction experiments with same concentrations of H_2 have been conducted in another test run but with the usage of a lanthanated tungsten electrode rather than a graphite electrode. With such facility, the contribution of carbon in the reduction process was ruled out.

7.4.1.1 H_2-Ar reduction using graphite electrode

7.4.1.1.1 Assessment of the reduction rate

The influence of H_2 flow on the reduction behaviour has been monitored in this test run. The total flow was set at a constant value of 5 Nl/min and a charge of Carajas ore used was 100 g in all experiments. The duration of one measuring cycle was approximately 2.4 s. A change in the H_2 – Ar concentrations in a series of experiments of 30 %, 40 % and 50 % H_2 was conducted. To guarantee the completion of the reduction, it was decided to operate

within this range of H_2 concentrations as an optimum range. At some lower values of % H_2, the voltage was less than 50 V and the current exceeded 100 A. Such high current has led to the overheating of the transformer. While, at some higher values of % H_2, the voltage exceeded 100 V as a result of the increasing enthalpy of H_2 (more difficult to be ionised with respect to Ar) and the plasma device automatically cut off.

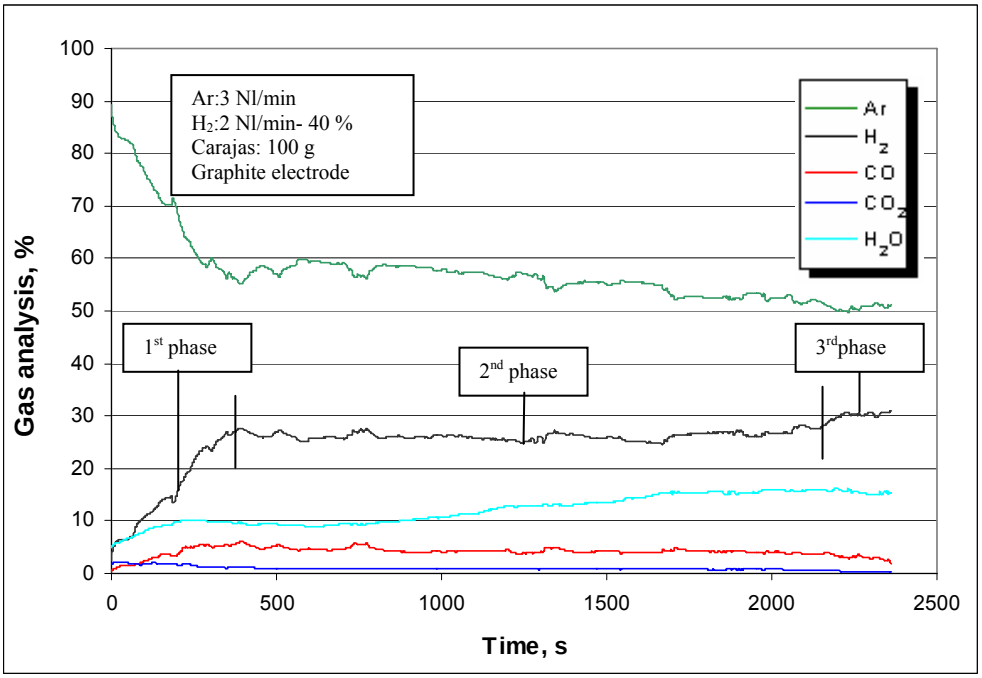

Fig. 49. Off-gas analysis of 40 % H_2 experiment

Consistent reduction began by the switch from pure Ar to a mixture of Ar-H_2. At the same time, the measuring of the gas analysis by the MS and assessment of the process started. An example of the gas analysis of Ar-H_2 reduction experiment with 40 % H_2 concentration is shown in figure 49. It should be mentioned that the H_2O shown in the gas analysis was less than the actual H_2O (calculated via the H_2 balance) at the beginning of the experiment. At advanced stage of the experiment where the lining temperature is high enough, the analysed H_2O showed higher values than the actual one. This was due to the condensation of the H_2O on the cold furnace lining in the beginning of the experiment and its evaporation at a later stage. The start of reduction completion was witnessed by the increase of H_2 and the decrease of CO analysed in the off-gas (beginning of 3rd phase). Another assessment tool of the reduction completion was the floatation of the slag droplets (stemming from the gangue material in the ore) and that was monitored via a sight glass.

The reduction behaviour was evaluated by calculating the reduction degree, H_2 utilisation degree, total utilisation degrees and the oxygen reduction rate. As clarified earlier in section

7.3.3 the reduction degree is the oxygen reduced by the reducing gases from iron oxide during the experiment, divided by the oxygen content of iron oxide existed in the ore. H_2 utilisation degree is the used or utilised portion of the H_2 supplied (H_2O produced) while the total utilisation degree comprises in addition to the produced H_2O, the CO and CO_2 developed.

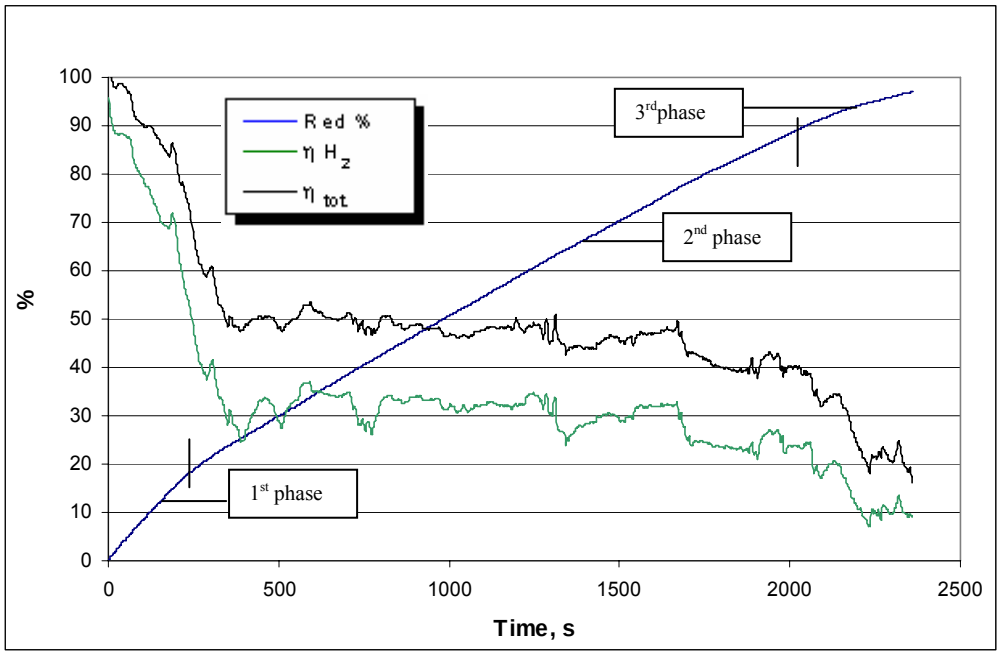

Fig. 50. Reduction and utilisation degrees of 40 % H_2 experiment using graphite electrode

Figure 50 shows the development of the reduction degree, H_2 utilisation degree and the total H_2 utilisation degree versus time. It is clear that the reduction trend shows three phases as shown in the figure. The first phase was mainly during the reduction of trivalent iron which was characterised by the highest reduction rate over the duration of the experiment. The second phase, the main stable phase, was mainly the result of the divalent iron reduction which is bonded with the corresponding amount of oxygen. In this phase, the Fe^{2+} was reduced to metallic iron by a constant rate. Finally, the third phase started when the slope of curve began to decrease. This is due to the diminishing amount of reducible oxygen in the melt and the reaction rate limitation by the transport of oxygen to the melt-plasma interface.

The average observed H_2 utilisation degree was some 32 % while the average total H_2 utilisation degree was approximately 48 %. However, the actual H_2 utilisation degree is some value between the shown two experimental results. Assessment of the actual H_2 utilisation degree was conducted and presented in the tungsten electrode experiments. It is worth mentioning that such low value of H_2 utilisation degree with respect to thermodynamic equilibrium (~40 %) was mainly due to the contribution of the graphite electrode in the reduction reactions, reaction (22). The erosion rate of the electrode was assessed through

the gas analysis and found to be 0.15 g/min. Considering this, it should be noted that by the conduction of carbon balance to the electrode used in some of the experiments, it was found that the measured erosion was ~7 % higher than the weighted erosion. This deviation was mainly due to the slag droplets splashed on the electrode during the experiment and could not be ruled out during the weighing of the electrode.

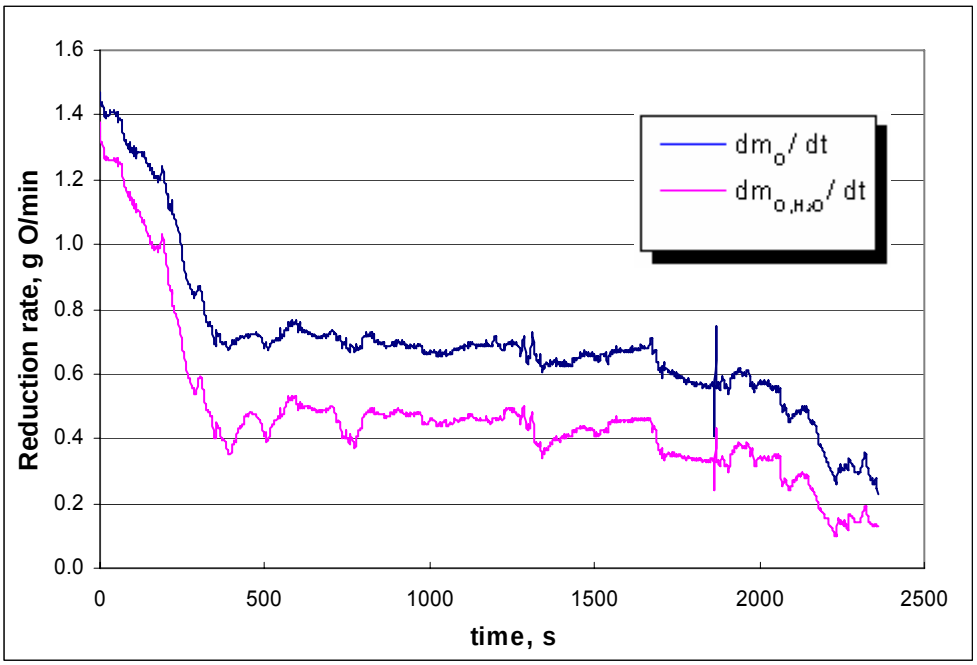

Fig. 51. Reduction rate of 40 % H_2 experiment using graphite electrode

Figure 51 shows the total reduction rate (dm_O / dt) including the oxygen carried by CO and CO_2. Moreover, the apparent reduction rate obtained by H_2 ($dm_{O,H_2O} / dt$) is also plotted. It was found that the reduction contribution by H_2 is some 65 % of the total reduction rate. Averaging the total reduction rate during the 2nd phase, mainly iron (II) oxide reduction phase, 0.7 g O /min was obtained. Combining this result with those obtained from the experiments with other H_2 concentrations (30 and 50 %), figure 52 is plotted. Results of the other Ar-H_2 experiments are attached in the appendix. It is clear from figure 52 that the reduction rate increases with increasing H_2 flow rate on a first order relationship basis. However, exact passage of the trend line through the origin could not be obtained due to two factors. The first factor is the contribution of carbon (stemming from the graphite electrode) in the reduction process. The second factor that could not be ruled out is the possible error of measurement caused by the MS and the gas flow controllers.

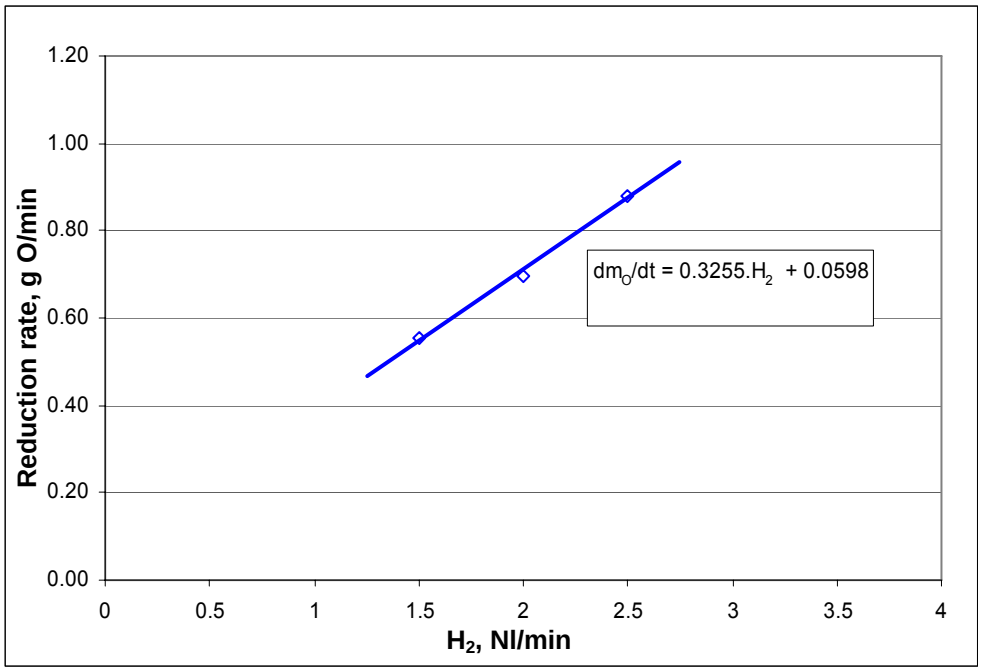

Fig. 52. Reduction rate versus H_2 flow using graphite electrode

7.4.1.1.2 Metal analysis

Metal was analysed by a spark spectrometer after each experiment. Table 2 shows the chemical analysis of a fully reduced Carajas under 40 % H_2. The carbon shown was due to some melting of the crucible and the total melting of the ignition pin.

	% Fe	% C	% Si	% Mn	% P	% S
Metal	99.73	0.0215	0.0282	0.118	0.0138	0.0092
crucible	99.47	0.0455	0.0182	0.354	0.0119	0.0170
Ignition pin	99.44	0.0361	0.0254	0.364	0.0084	0.0174

Table 2. Metal, crucible and ignition pin analyses with H_2, wt. %

Accompanying elements (Si, Mn, P and S) have been monitored in the metal analysis due to their partial reduction to the melt. Moreover, the partial melting of the crucible and melting of the ignition pin took place in the presence of those elements.

Looking at the microstructure of the metal produced, ferrite phase with obvious numbers of non metallic inclusions was observed, figure 53. SEM analysis was carried out [10] and it was found that the size of inclusions was mainly between 1 and 3 μm. These inclusions were mainly FeO_x and multiphase components (MnO, SiO_2), figure 54.

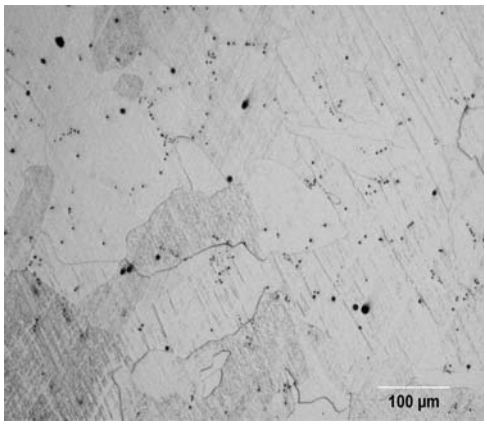

Fig. 53. Ferrite structure

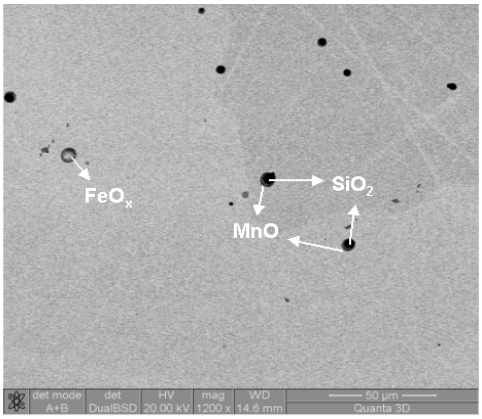

Fig. 54. Non metallic inclusions

7.4.1.2 H_2-Ar reduction using tungsten electrode

As shown in the last series of experiments (conducted with graphite electrode), exact evaluation of the H_2 potential in the ore reduction was not possible due to the graphite electrode interference in the process. The current series of experiments was conducted to rule out the carbon contribution in the reduction process. A 1 % La_2O_3 (lanthanated) tungsten electrode has been adopted. The process parameters were set to be the same as the last series for comparison purposes. A change in H_2 – Ar concentrations of 30 %, 40 % and 50 % H_2 was conducted.

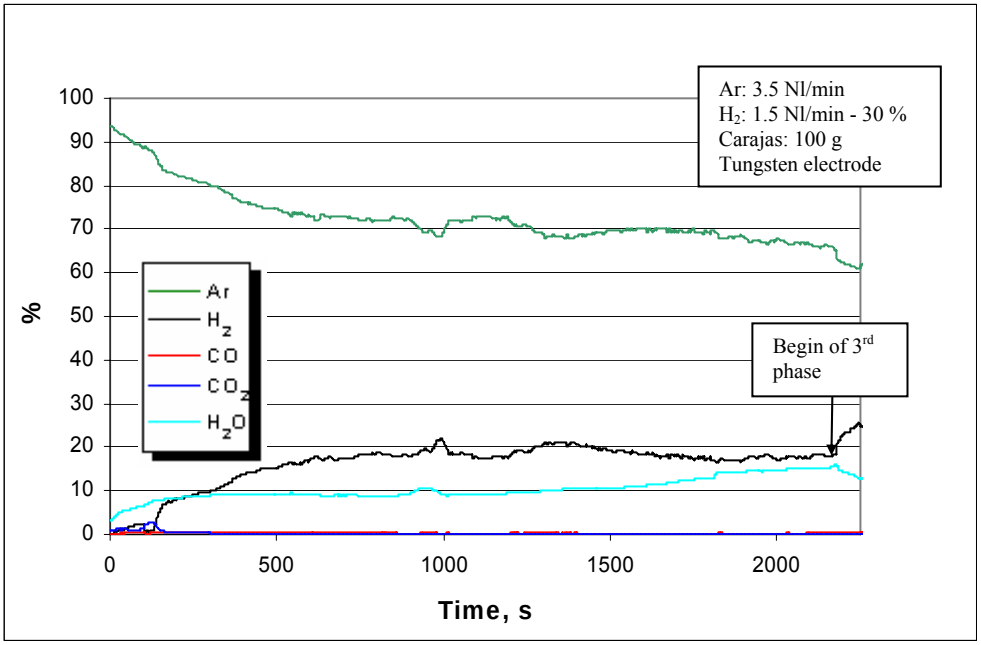

Fig. 55. Off-gas analysis of 30 % H_2 experiment using tungsten electrode

Figure 55 shows the gas analysis of an experiment with 30 % H_2 in Ar-H_2 mixture. It is clear that via the tungsten electrode usage, the formation of CO and CO_2, found in the case of the

graphite electrode, were ruled out. On the other hand no significant change has been witnessed in the electrical energy used with respect to the graphite electrode experiments.

In the conducted experiments, a lateral shift of the plasma arc towards the crucible was monitored and witnessed on the crucibles sidewall, figure 56. The formation of an arc column between the cathode and the crucible sidewalls, rather than between the cathode and the oxide melt, has led to the solidification of the melt. The same phenomenon was observed previously in Plaul's work [10].

Fig. 56. Lateral shift of the arc column and melting of crucible sidewall

The inconsistency in plasma behaviour will be discussed later in the discussion section, 7.5. However, although the encountered plasma instability during the reduction, the maximum reduction rate in the stable phase was determined and assessment of the reduction rate at various concentrations of H_2 was carried out.

Figure 57 shows the reduction degree, H_2 utilisation degree and total H_2 utilisation degree.
It is clear that the H_2 utilisation degree was significantly fluctuating. This was due to the instability of the plasma and its intermittent shift to the lateral side of the crucible. An extreme case was witnessed at the end of the experiment when complete sparkover on the crucible sidewall occurred and then solidification of the melt has been observed. At that time, the reduction degree curve levelled off and the H_2 utilisation degree dropped to 0 %.

The H_2 and total utilisation degrees were almost superimposed due to the disappearance of CO and CO_2 in the gas analysis. The average value in the stable 2nd phase showed some 40 % which agrees with the thermodynamic equilibrium.

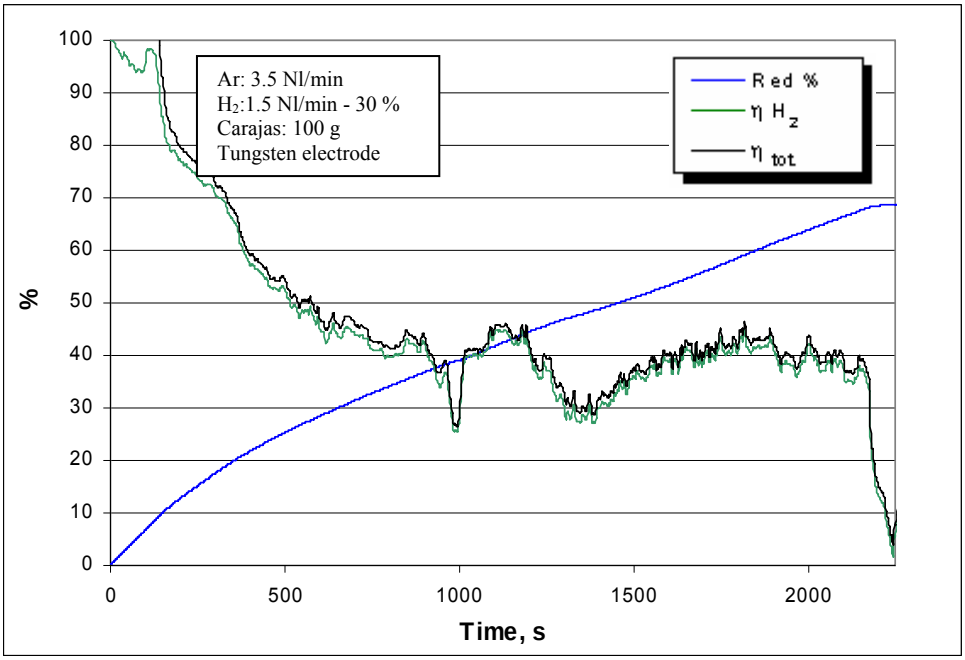

Fig. 57. Reduction and utilisation degrees of 30 % H_2 experiment using tungsten electrode

Evaluation of the reduction rate during the 2nd phase for the conducted experiments is shown in figure 58. Moreover, the reduction rate results of Ar-H_2 experiments conducted by graphite electrode, shown earlier on, have been presented on the same figure for comparison purposes. It was found that the reduction rate in the experiments done by graphite electrode was 1.25 times faster than that done by tungsten electrodes.

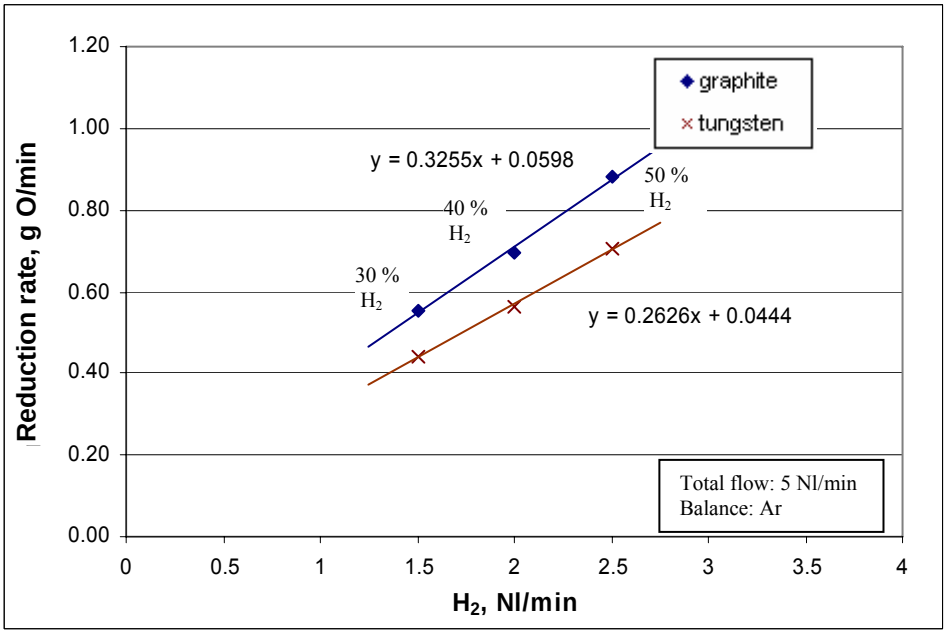

Fig. 58. Reduction rate by H_2, graphite and tungsten electrodes

7.4.2 Impact of lateral H_2 supply on the reduction behaviour

In the previous experiments, H_2 was mixed with Ar before entering the hollow electrode. As an alternative way, the H_2 was partially supplied in this test run through a ceramic lance. As shown earlier on in the schematic diagram, figure 45, the lance was laterally fixed so that the H_2 was blown above the melt at the edge of the crucible (not influenced by the plasma). The lance was approximately 20 mm above the melt surface.

In the conducted experiments, the flow of H_2 (over the lance) has been varied between 0.75 – 1.25 Nl/min. The rest of total required H_2 flow (2 Nl/min) was fed through the hollow electrode. The total H_2 flow was kept constant to compare the results with the reference parameters (100 g Carajas, H_2: 2 Nl/min and Ar: 3 Nl/min).

Figure 59 shows the results of the reduction and H_2 utilisation degrees in the case of lateral flow of H_2 (0.75 Nl/min) and that fed via the electrode (premixed H_2). It is clear that the rate of reduction did not change as both reduction degree curves overlap. In other words, this means that changing the method of H_2 supply did not deteriorate the reduction kinetics. Moreover, the H_2 utilisation degrees were within the same range. The contribution of carbon from the graphite electrode was slightly less than the pre-mixed H_2 experiments, 0.13 g /min, but without clear effect on the reduction rate.

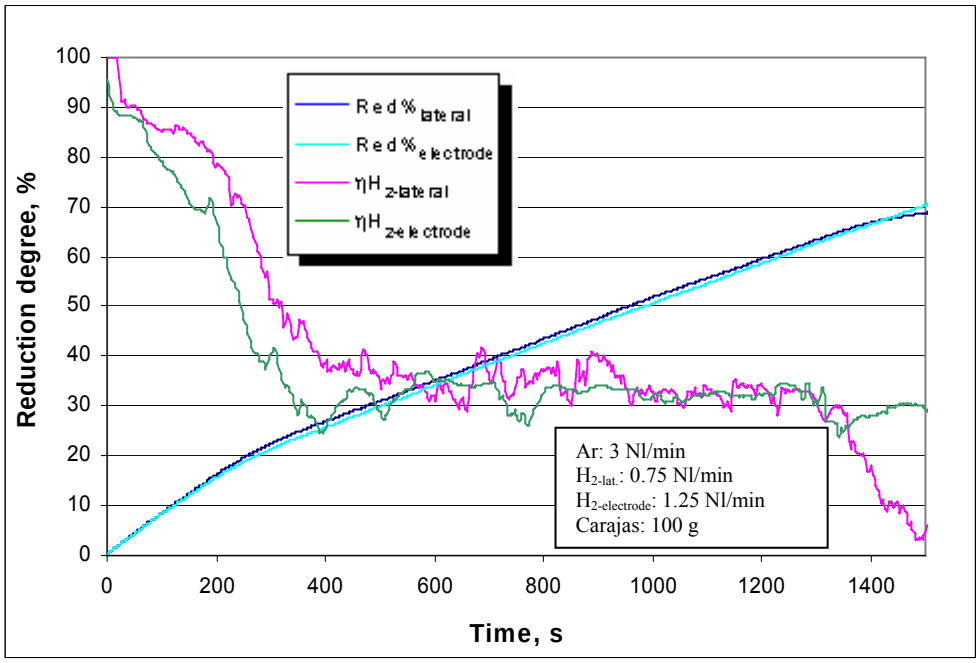

Fig. 59. Reduction and H_2 utilisation degrees, lateral supply and via the electrode

It should be mentioned that the experiment was driven only to 70 % reduction degree. This was attributed to abandoning the usage of the refractory ring to fit the ceramic lance. This consequently led to the sparkover (between the electrode and the crucible side wall) and the flow of the oxide melt out of the crucible.

Figure 60 shows the reduction degrees at various flows of H_2. Achievement of high reduction degree was not attainable at high lateral H_2 flow, i.e. more than 0.75 Nl/min. At 1 Nl/min and 1.25 Nl/min, a reduction degree of only 50 % and 26 %, respectively, were achieved. However, it is clear from the figure that varying the lateral flow of H_2 did not influence the reduction kinetics (same slope for all curves).

Moreover, it was noticed that the input power in both series of experiments (premixed H_2 and laterally fed H_2) were within the same range ~ 6 kW. This fact indicates that the laterally fed H_2 has been homogeneously mixed with the plasma gas to raise the power up to the premixed H_2-Ar case. In that sense, it should be noted that some drop in the input power was expected due to the high viscosity of the plasma gas that could in turn hinder its mixture with the laterally fed H_2 or the H_2O produced, but obviously this was not the case.

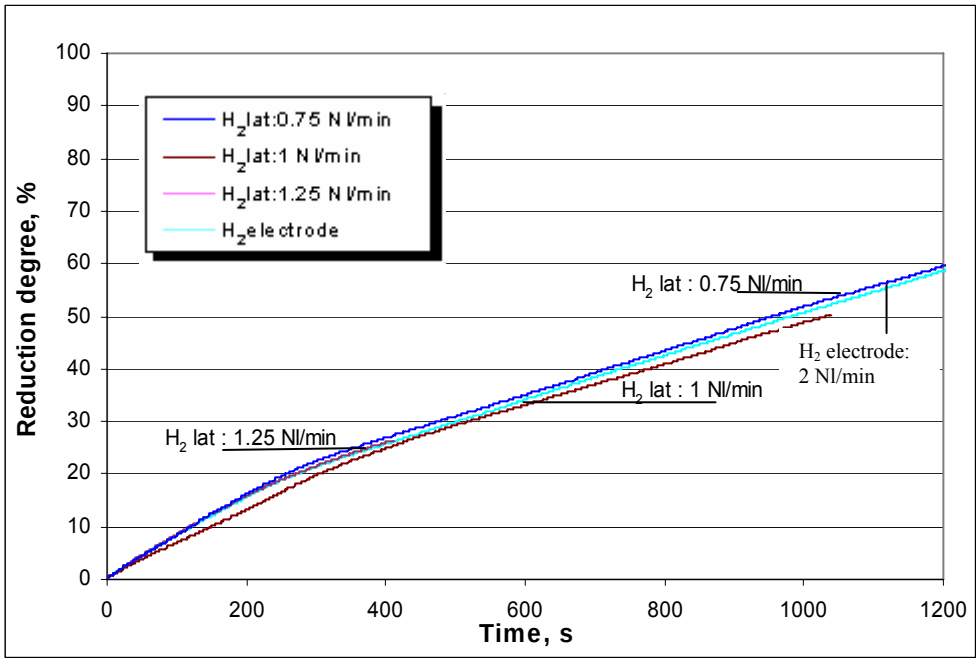

Fig. 60. Reduction degree, lateral supply at various flow rates using graphite electrode

It is believed that the depression shape (cavity) formed by the momentum of the plasma was the same in both series of experiments. According to Maecker's law, section 4.4.2, the depression shape is a function of the current intensity, which was almost the same in the conducted experiments. On the other hand, no depression effect has been noticed from the

sight glass by the lateral blow of H_2. This was obviously justified by the absence of current density /plasma effect in this lateral zone. An additional experiment at 40 mm apart from the bath was carried out and no deterioration in the reduction kinetics compared with the 20 mm ones has been witnessed, results shown in the appendix.

7.4.3 CH_4 – Ar reduction

7.4.3.1 Reduction rate

The current experiments were aiming at using a CH_4–Ar mixture instead of a H_2–Ar mixture as a plasma gas to assess the feasibility of using CH_4 as a substitute to H_2 in the plasma process. In all experiments, 100 g Carajas ore was placed in the furnace under a constant total flow of 5 Nl/min. The CH_4-Ar concentrations of 10 %, 15 %, 20 % and 25 % CH_4 were carried out. A trial to increase the CH_4 concentration in the mixture to 30 % was attempted but the experiment failed due to the plasma power supply limitations. The flow meter was calibrated to measure and control CH_4 rather than H_2, by using Fluidat software [83] in calculating the CH_4 conversion factor. The MS was set to measure the slip methane in the off-gas. However, the monitored CH_4 did not exceed the 0.05 % in the gas analysis, where it was fully cracked during the experimentation.

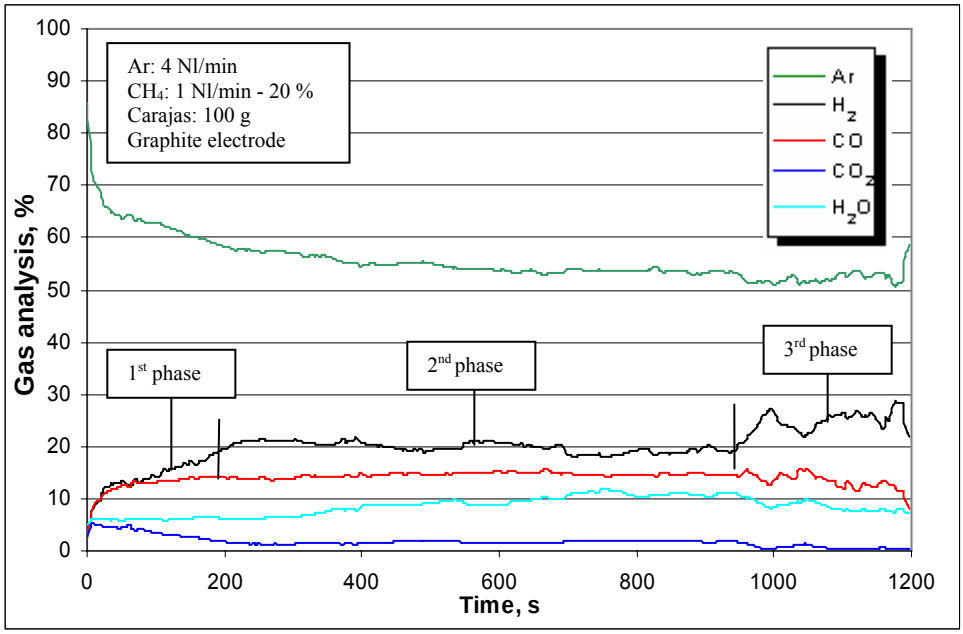

Fig. 61. Off-gas analysis of a 20 % CH_4 in a CH_4-Ar mixture

Figure 61 shows the gas analysis of a 20 % CH_4 in a CH_4–Ar mixture. Comparing this experiment with that in figure 49, where the supplied H_2 is the same (2 Nl/min), the CO and CO_2 produced are approximately 3 and 2 times, respectively, of that found in the H_2

experiment. It is clear that the cracked carbon contributed in the reduction process and sped up the reduction rate.

Some carbon soot was observed in the experiments of low CH_4 concentrations (10, 15 %). This soot was clearly visible at the colder zones of the furnace roof and the crucible refractory side wall. At higher concentrations of CH_4, 20, 25 %, carbon deposition inside the electrode tip was faced. This led to a reduction of the hollow electrode diameter during the experiment.

To evaluate the reduction behaviour, H_2 and C utilisation degrees were assessed as per the equations set under section 7.3.3.2. Examining the 2nd phase of the experiment, the utilisation degrees were almost constant but with some drops. This was due to the previously mentioned non uniform distribution of plasma gas. The average ηC and ηH_2 (during a stable phase) was found to be almost 70 % and 30 % respectively, figure 62.

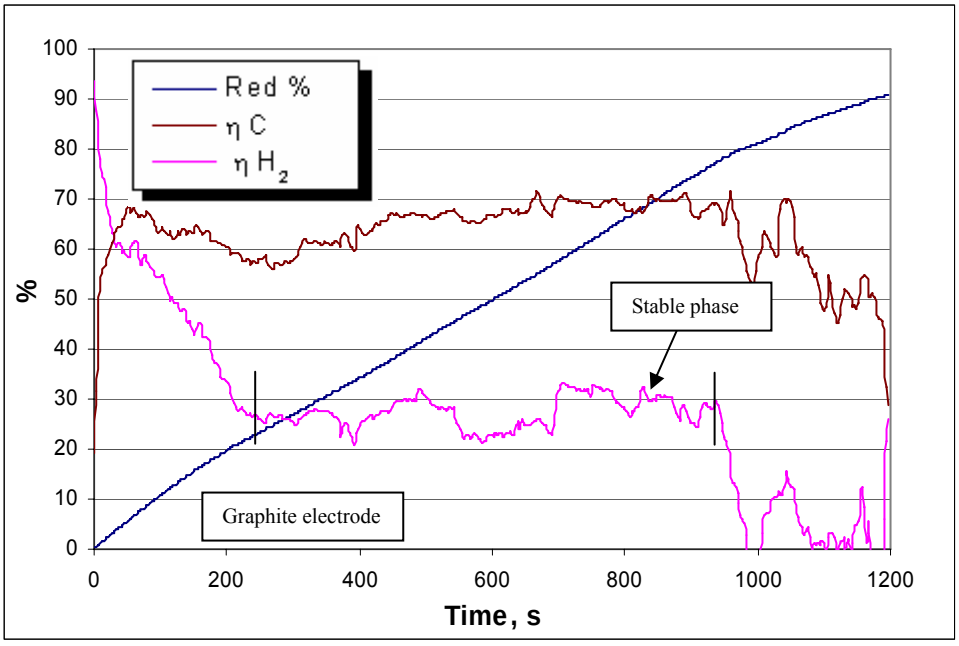

Fig. 62. Reduction and utilisation degrees of 20 % CH_4

Figure 63 shows the reduction degrees attained by the conducted experiments versus time. It should be noted that the slope of the reduction curves represents the various reduction rates. In other words, the greater the CH_4 content within the Ar-CH_4 mixture, the greater the slope/reduction rate. Nevertheless, the completion of reduction was, most of the times, not attainable. It is presumed that the resulting carbon soot and deposition led to the intermittent

instability of plasma gas on the melt. This non consistency in the heat distribution caused sometimes partial solidification of the melt (non completion of the reduction).

The electrode erosion rate was calculated (via the gas analysis) for the experiments done. It was found that the average erosion rate of the H_2 experiments was almost 1.6 times that of the CH_4 experiments at the same amount of supplied H_2. This means that the carbon, from the electrode, has more contributed in the reduction process of H_2 experiments with respect to CH_4.

The potential of CH_4 plasma as an alternative reduction process with respect to H_2 plasma in terms of reduction rate was evaluated as shown in figure 64. The linear regression analyses were determined by averaging the reduction rate in the 2nd phase of the reduction (mainly Fe (II) phase). It was found that the CH_4 reduction rate is almost 3.5 times faster than H_2 reduction rate. However, a correction to this ratio has been done by subtracting the oxygen reduced by the generated gases (CO, H_2), produced by reaction (22), in both sets of experiments. A corrected reduction rate ratio was found to be 4. This ratio is agreeing with the stoichiometric ratio and relatively conforming to the thermodynamic ratio 4.8 calculated by the FACTSAGE program, [9].

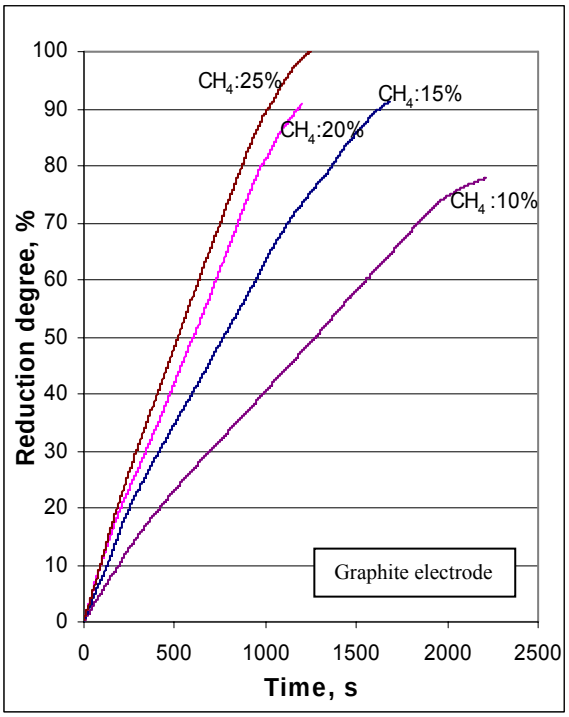

Fig. 63. Effect of % CH_4 on the reduction degree

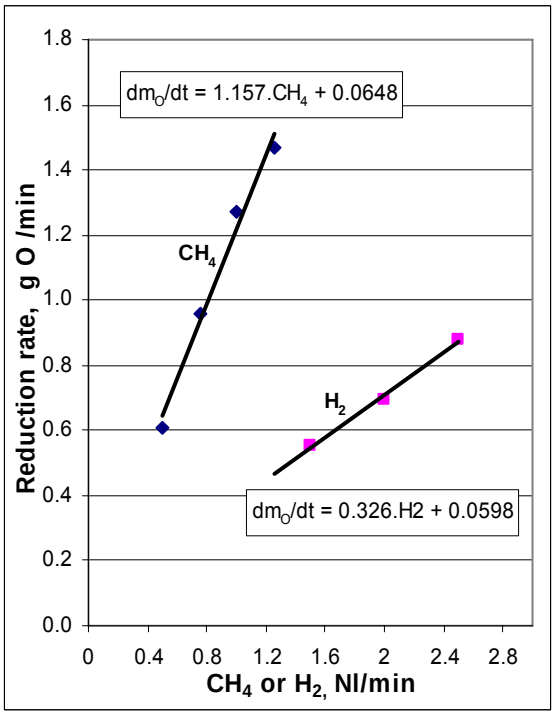

Fig. 64. Reduction rate of CH_4 and H_2

7.4.3.2 Metal analysis

Although the conducted experiments were carried out under CH_4 plasma reduction, the metal analyses showed slightly more carbon content than that of the H_2 plasma experiments as can be seen in table 3**.**

	% Fe	% C	% Si	% Mn	% P	% S
CH_4: 10 %	99.60	0.075	0.035	0.182	0.012	0.013
CH_4: 15 %	99.37	0.169	0.024	0.312	0.018	0.016
CH_4: 20 %	99.54	0.049	0.021	0.250	0.016	0.017
CH_4: 25 %	99.47	0.069	0.040	0.293	0.018	0.014

Table 3. Chemical analysis of the reduced metal with CH_4, wt. %

It should be mentioned that the remaining slag was glassy in structure and brown in colour. Wet chemical analysis was not possible due to small quantities obtained after the reduction.

7.4.4 Reduction at various basicities

7.4.4.1 Reduction behaviour

In this series of experiments, the effect of increasing basicities (CaO additions) on the dephosphorisation of the reduced metal has been assessed. 100 g Hamersley ore (0.075 % P) and a constant flow of H_2 (2 Nl/min) in a H_2-Ar mixture were used in all experiments. Previous work has been carried out [10] to study this relationship but no correlation was found between the added CaO and the phosphorous reduced. The previous work was conducted at lower basicities with respect to the current experiments.

The basicity B_2 was varied between 0.06 and 2.5 (0.33 – 13.17 g CaO additions) without any notable difficulties in the slag dissolution. The experimentation time was set to 42.5 minutes for all experiments to rule out the influence of time that might affect the phosphorus reduction.

Figure 65 shows the reduction degrees attained in the conducted experiments. A linear correlation between the basicity and the reduction rate was not obvious. However, due to the CaO additions, a small decrease in the reduction rate (slope of curves) and earlier levelling off of the reduction curves was noticed. At advanced stages of the reduction, a partial

solidification of the oxide melt at the side wall was monitored from the sight glass. This was due to the raised melting point of the CaO enriched slag.

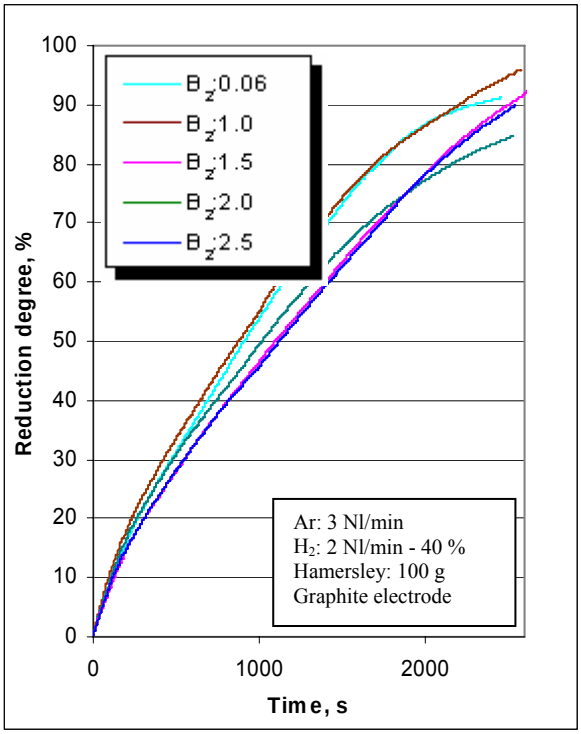

Fig. 65. Effect of basicity, B_2, on the reduction behaviour

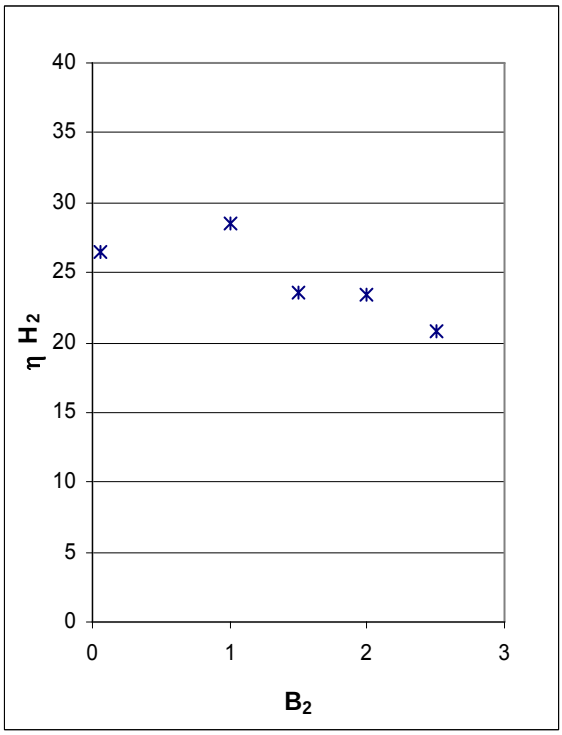

Fig. 66. Effect of basicity, B_2, on the H_2 utilisation degree

On the other hand, the stable phase of the conducted experiments was generally short as shown in detail in the appendix. However, by averaging the results of the H_2 utilisation degree, figure 66 was obtained. It is clear that some decrease in the H_2 utilisation degree was found at higher amounts of CaO (B_2:1.5-2.5) but again without obvious correlation versus basicity.

7.4.4.2 Phosphorous behaviour

From the conducted experiments, chemical analyses were carried out and % P was found to be as shown in figure 67. It is clear that the phosphorous levels in the metal decreased in experiments with a higher basic slag content.

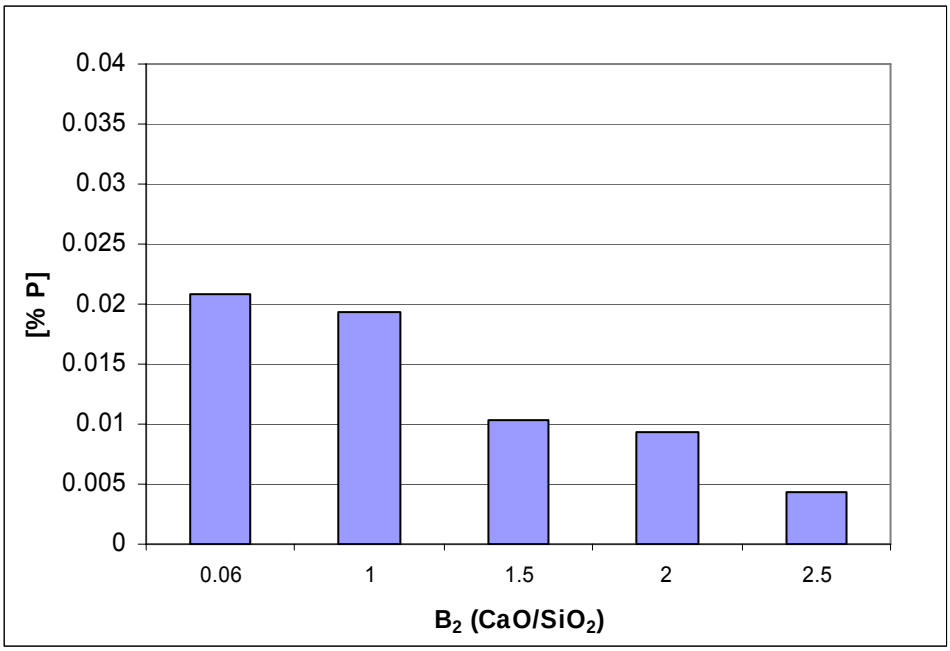

Fig. 67. Effect of the basicity, B_2, on the phosphorous content in the metal

Wet chemical analysis was carried out on the slag obtained. The captured phosphorous in terms of P_2O_5 increased in the slag with increasing CaO contents, table 4. MgO showed higher values at lower basicities with respect to the ore composition. This was attributed to the slight failure of the MgO refractory ring which fell into the melt during the reduction process.

	% Fe_{tot}	% Fe^{2+} (*)	% Fe^{3+}	% CaO	% SiO_2	% MnO	% MgO	% Al_2O_3	% P_2O_5	B_2 (actual)
B_2: 0.06	11.69	11.50	0.19	2.50	30.20	7.99	30.24	13.77	<0.01	0.08
B_2: 1.0	14.44	13.95	0.49	21.97	22.56	4.36	23.82	10.0	0.073	0.97
B_2: 1.5	14.96	14.71	0.25	35.05	19.98	3.68	9.33	9.02	0.176	1.75
B_2: 2.0	17.41	16.71	0.70	38.98	19.36	2.78	7.54	8.41	0.371	2.01
B_2: 2.5	16.27	16.05	0.22	42.35	17.98	2.36	6.37	8.47	0.332	2.35

*: metallic Fe is included in Fe^{2+}

Table 4. Slag analyses at various % CaO, wt. %

By conducting a phosphorous balance for the experiments, with basicity B_2=0.06 and B_2=2.5, figure 68 was obtained. The share of phosphorous found in the slag increased to 40.23 % at a basicity of B_2=2.5 whilst the phosphorous, which was reduced into the metal and the phosphorous evaporated decreased to 6.17 % and 53.60 % respectively. The change in

phosphorus concentrations in the shown phases was obviously dependant on the slag basicity.

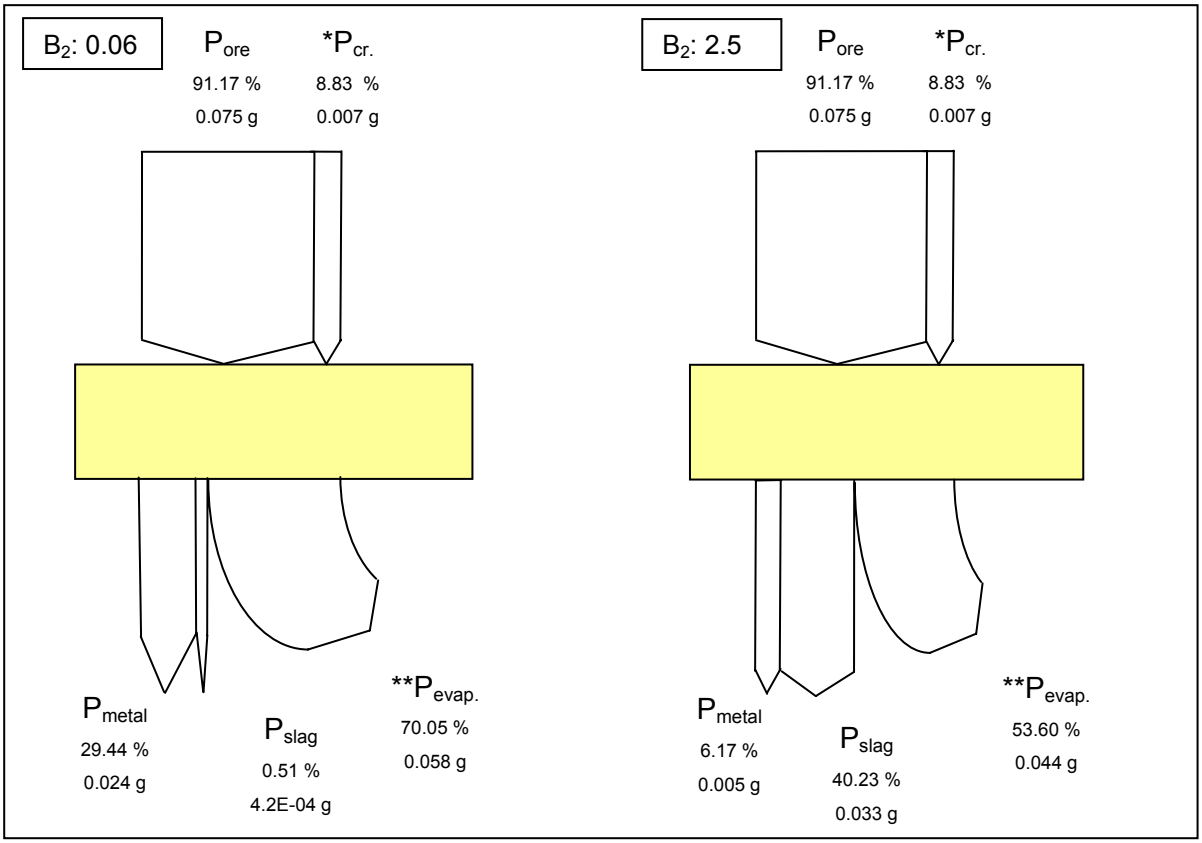

*$P_{cr.}$: phosphorous from the crucible
**$P_{evap.}$: phosphorous evaporated (including dust)
Fig. 68. Phosphorous balance

A fraction of the phosphorous evaporated was found in the dust. This dust was deposited on the refractory of the reactor and weighed to be approximately 1.5 g. From the SEM analysis, P_2O_5 between 0.59 and 1.16 % in the experiments were found. This corresponds to approximately 10 % of the evaporated phosphorous. However, tracing the evaporated phosphorus in the form of P_2, P_2O_3 and PH_3 was tried but not witnessed by the MS.

7.4.5 Reduction of magnetite

Kiruna ore with a Fe_3O_4 content of 92.26 % was adopted in this series of experiments. The objective of this series of experiments was to explore the difference in reduction behaviour between the hematite ores (Fe_2O_3) and the magnetite ores (Fe_3O_4). The experiments, therefore, were conducted with the same boundary conditions of those used in Carajas experiment (total flow of 5 Nl/min and the same concentrations of H_2 % in the H_2/Ar mixture, of 30 %, 40 % and 50 %).

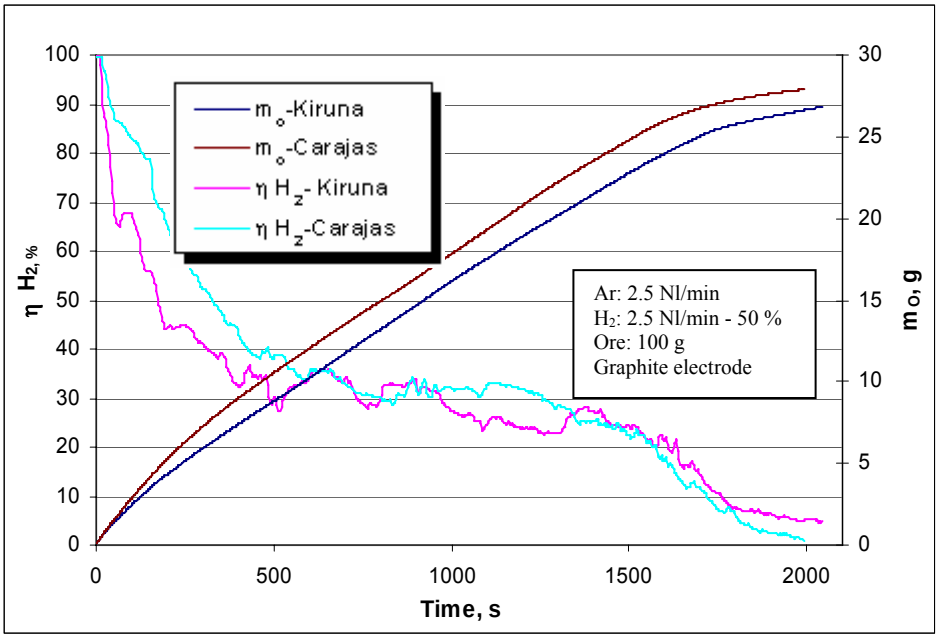

Fig. 69. Kiruna against Carajas reduction

Figure 69 shows the amount of reduced oxygen and the H_2 utilisation degree of both ores for a 50 % H_2 experiment. Examining the first phase of the reduction, it is clear that the removal rate of oxygen was higher in the Carajas experiment. This was attributed to the high ratio of Fe^{3+}/Fe^{2+}, in the Carajas ore with respect to the Kiruna. The influence of this high ratio on the H_2 utilisation degree during the first phase was apparent, i.e. a higher H_2 utilisation degree in the case of the Carajas ore.

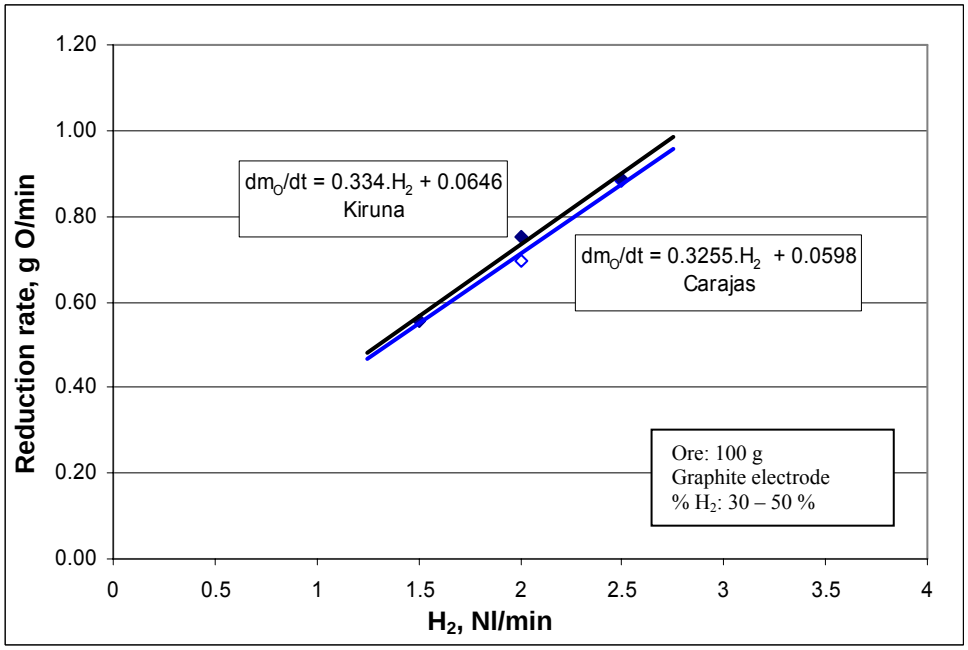

Fig. 70. Reduction rate obtained for Kiruna and Carajas fines

In the linear stable phase (the 2nd phase), where the majority of Fe^{3+} is already reduced, it was found that the slope of both m_o curves were the same (same reduction rate). This was attributed to the presence of same controlling reactants during this phase (Fe^{2+}-H_2). This was evidenced in the results of the H_2 utilisation degree where the values were almost the same.

To summarize results of the conducted experiments, figure 70 shows the reduction rate obtained in the Kiruna with respect to the Carajas experiments during the 2nd phase. Due to the overlapping of trend lines, some of the experimental results are not visibly clear. The input power in both series of experiments was within the same range ~ 6-8 kW. Detailed results of the experiments are shown in the appendix. Finally, a chemical analysis was conducted on the Kiruna reduced metal which showed similar results to the Carajas after the completion of reduction, table 5.

	% Fe	% C	% Si	% Mn	% P	% S
H_2: 30 %	99.63	0.0187	0.0161	0.167	0.0150	0.0118
H_2: 40 %	99.53	0.0191	0.0268	0.258	0.0105	0.0112
H_2: 50 %	99.50	0.0217	0.0335	0.275	0.0107	0.0112

Table 5. Chemical analysis of the reduced metal in Kiruna experiments, wt. %

7.4.6 Reduction of pre-reduced ore

LKAB ore has been reduced mainly to FeO to facilitate experimentation using divalent iron pre-reduced ore. It was adopted within a set of experiments under various concentrations of hydrogen (20 – 60 % H_2), with a total flow: 5 Nl/min and 100 g charge. The objective of this series was to investigate the influence of the scarcity of Fe^{3+} on the reduction kinetics.

Figure 71 shows the amount of reduced oxygen and the H_2 utilisation degree for Carajas and pre-reduced LKAB fines for a 50 % H_2 experiment. Examining the first phase of the reduction, it is clear that the reduction rate of oxygen was higher in the Carajas experiment which is a Fe^{3+} containing ore. Having mainly Fe^{2+}, the oxygen removal rate in the LKAB pre-reduced fines was obviously less so that the 1st phase in this series of experiments shortened considerably and the 2nd phase started earlier. The influence of Fe^{3+} scarcity on the decrease of H_2 utilisation degree of the pre-reduced LKAB fines with respect to the Carajas ore was also clear from the figure in the period corresponding to the 1st phase. It should be mentioned that the 100 % utilisation degree obtained at the beginning of all

experiments, including the pre-reduced ore, was unrepresentative. This was evident from the current experiments where the reduction was primarily between Fe^{2+} and H_2 (100 % utilisation degree could not be attainable from a thermodynamical point of view).

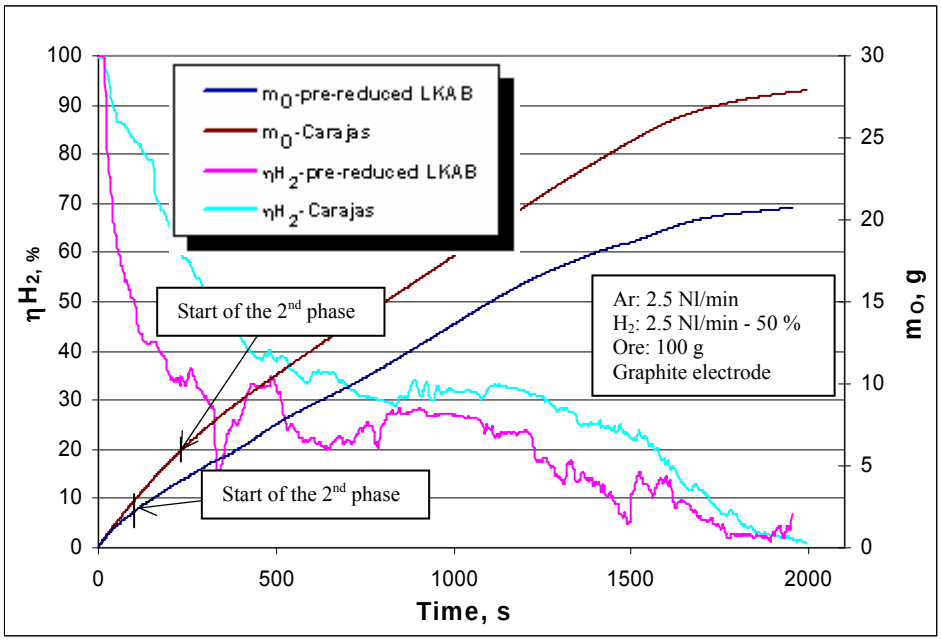

Fig. 71. Comparison between pre-reduced LKAB and Carajas fines

In the 2nd phase of reduction, where most of the Fe^{3+} was reduced, the slope of m_o–pre-red. LKAB was obtained as clear in the figure. It was slightly less than the slope of Carajas. This slight difference was due to the residual Fe^{3+} effect, which existed in Carajas experiments. The effect of the Fe^{3+} content in Carajas was also clear with slightly higher H_2 utilisation degree with respect to the pre-reduced ore.

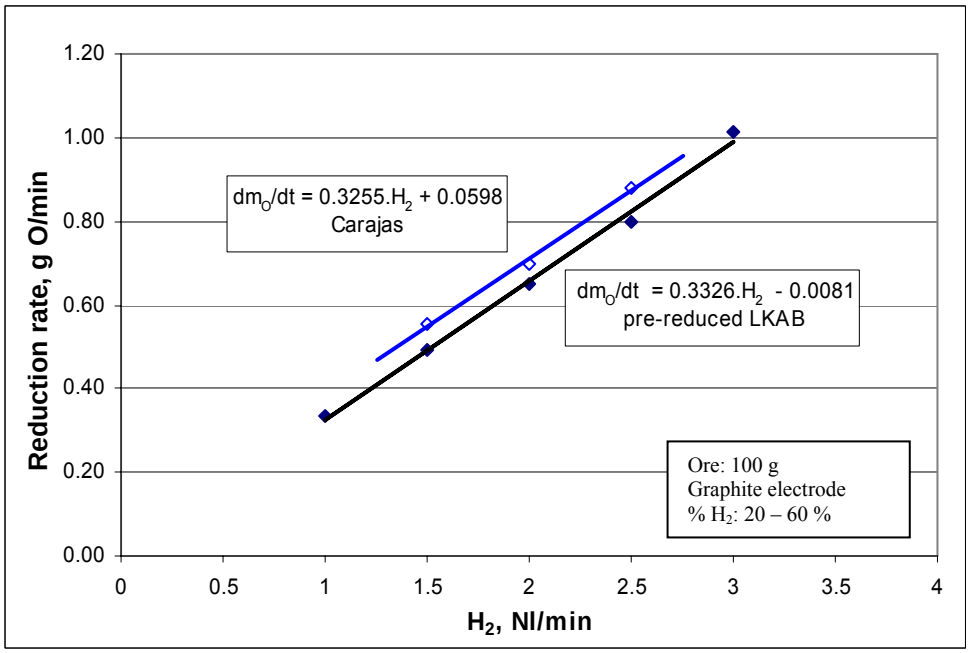

Fig. 72. Reduction rate obtained in pre-reduced LKAB and Carajas fines

Figure 72 shows the reduction rate of the wustite equivalent fines versus the hematite ore in the 2nd phase of the experiment. It was found that the reduction rate of the pre-reduced LKAB fines was slightly lower than the Carajas ore, i.e. the reduction rates showed 91 % of that of Carajas due to the previously stated reason. Chemical analysis of the samples from the conducted experiments showed the following results, table 6. Detailed results of the experiments are shown in the appendix.

	% Fe	% C	% Si	% Mn	% P	% S
H_2: 20 %	99.76	0.0196	0.0115	0.016*	0.0295	0.0042
H_2: 30 %	99.72	0.0192	0.0128	0.088*	0.0150	0.0091
H_2: 40 %	99.54	0.0185	0.0156	0.231	0.0136	0.0123
H_2: 50 %	99.58	0.0196	0.0154	0.197	0.0149	0.0111
H_2: 60 %	99.51	0.0197	0.0179	0.274	0.0101	0.0098

*: Mn was relatively low due to the non completion of the reduction in these experiments

Table 6. Chemical analysis of the reduced metal in the pre-reduced LKAB experiments, wt. %

7.4.7 Reduction with CO-H_2-Ar mixture

In all previous experiments where the graphite electrode was used, CO was found in the off-gas. The formation of CO was due to the reaction between H_2O and carbon, stemming from reaction (22). The reduction potential of CO was investigated in the current experiments under a H_2-Ar plasma atmosphere. 100 g Carajas ore was charged.

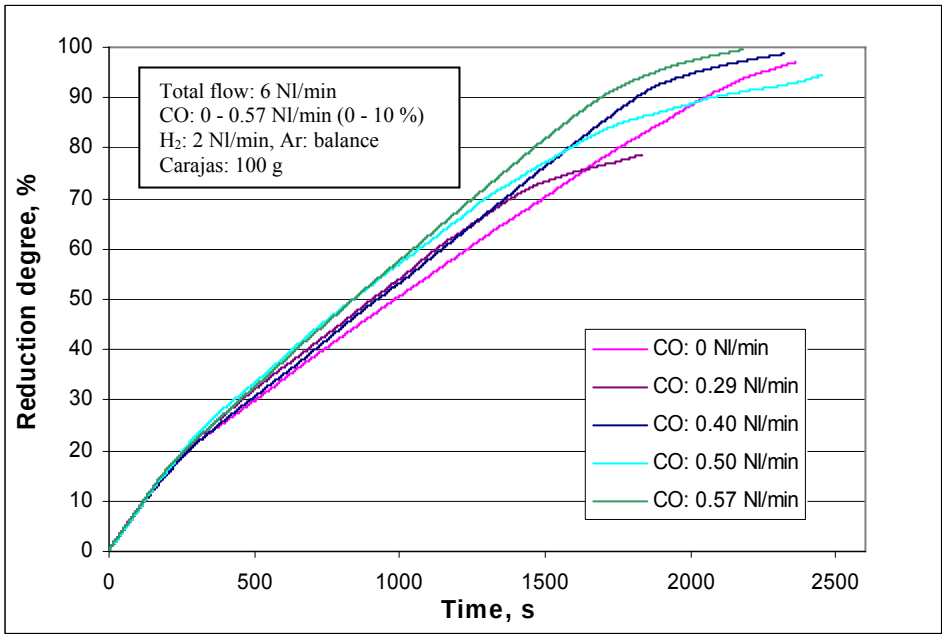

Fig. 73. Reduction degrees attained with CO-H_2-Ar mixtures

CO concentration was varied between 0.29 and 0.57 Nl/min (5 -10 %) in a total flow of 6 Nl/min. H_2 flow was kept always constant (2 Nl/min) to evaluate the increasing effect of CO on the ore reduction rate. The mentioned concentration of CO in the total flow corresponded to a CO/H_2 ratio of 0.14 – 0.29. The CO concentration was set within this limited range in order not to go beyond the expected CO/H_2 ratio in a real H_2 plasma (experimental / up-scaled) process.

Figure 73 shows the reduction degrees at various CO concentrations. It is clear that the CO contributed in the reduction, with the slopes of all CO experiments greater than the experiment conducted without the use of CO. It is clear from the figure that one experiment (CO: 0.29 Nl/min) did not achieve high reduction degree. This was attributed to the high amount of melt splashed on to the refractory ring during the course of the experiment as was determined from the mass balance. This melt splash led to a shortage in the available oxide melt and accordingly to the decrease in the reduction degree attained. However, exact evaluation of the CO reduction rates was conducted by the assessment of the reduction rate during the stable phase (2nd phase).

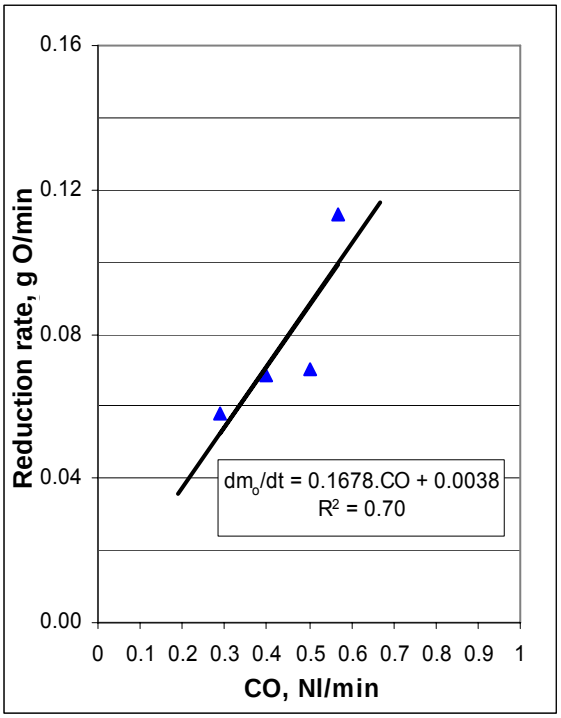

Fig. 74. Reduction rate against CO flow

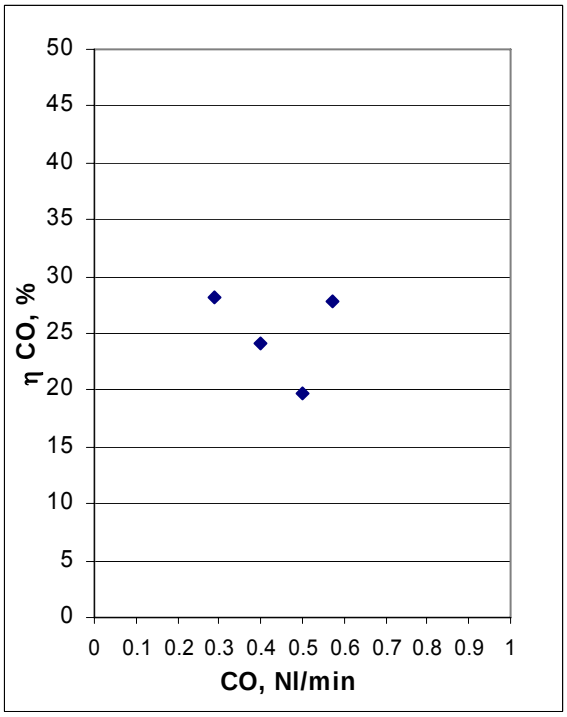

Fig. 75. Calculated CO utilisation degrees

Figure 74 shows the rate of reduction versus CO flow rate in the 2nd stage (the stable phase) of the experiments. The shown values are calculated by subtracting the portion of the reduced oxygen by H_2. This subtracted portion is known from previous experiments carried

out by only using H_2 as a reducing gas. However, working within this limited range and low flow rates of CO (0.29 – 0.57 Nl/min) was not feasible in terms of the results reproducibility and correlation (coefficient of determination, R^2 = 0.70). The CO utilisation degree was also calculated as the reduced oxygen divided by the inlet CO in the stable phase. It was found out that the utilisation degree is between 20 – 30 %, figure 75, which is obviously higher than the calculated thermodynamic equilibrium results (~15 %). This was again attributed to the low CO flow used with respect to H_2 (2 Nl/min). In the end it was agreed to assess the CO reduction potential in another series of experiments at higher flow rates and without H_2 usage, in order to have more correlative results that are better comparable to thermodynamic calculations.

Looking at the rate of electrode erosion in that range of CO flow, it was found that the average erosion rate was almost like that of the H_2 experiment (without supply of CO), 0.16 g /min. On the other hand, no influence on the chemical analysis in terms of carburisation was evident by using CO, table 7.

	% Fe	% C	% Si	% Mn	% P	% S
CO: 5 %	99.68	0.0163	0.0123	0.167	0.0180	0.0188
CO: 7 %	99.58	0.0187	0.0150	0.255	0.0162	0.0173
CO: 8 %	99.62	0.0155	0.0108	0.217	0.0161	0.0177
CO:10 %	99.56	0.0243	0.0303	0.247	0.0171	0.0185

Table 7. Chemical analysis of the reduced metal in CO-H_2-Ar experiments, wt. %

7.4.8 Reduction with CO-Ar mixture

In the current series of experiments, higher concentrations of CO (50 – 70 %) have been adopted. The reduction degrees attained were generally low (< 60 %) due to the limitation of the experimentation period. This was attributed to the absence of high enthalpy gas like H_2, which caused lower plasma voltages (higher current) and consequently rapid heating of the transformer winding. On-line monitoring of the temperature of the winding was undertaken and the current supply was manually shutoff whenever the temperature exceeded 150^{o}C.

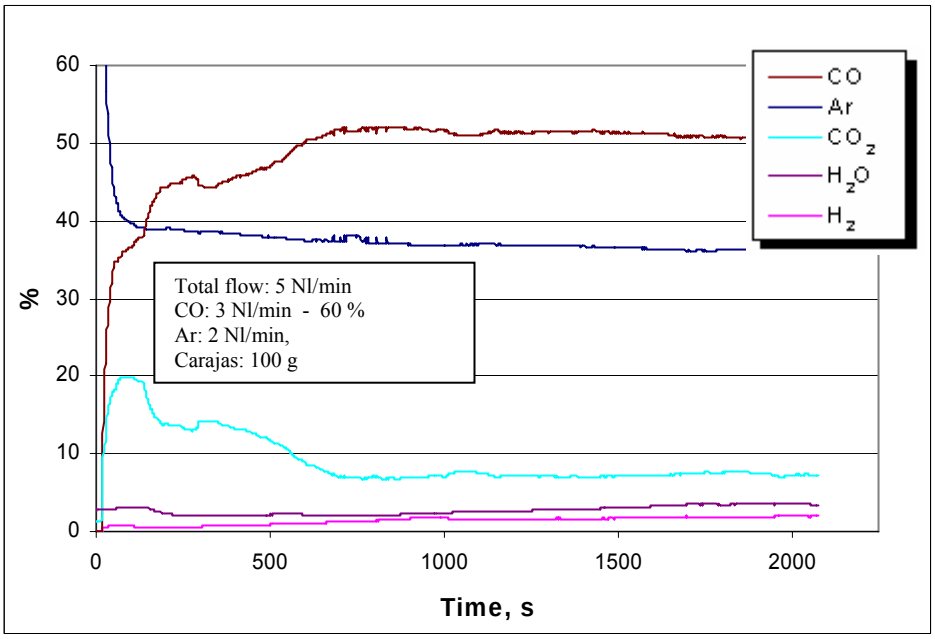

Fig. 76. Off-gas analysis of 60 % CO in Ar-CO mixture

Figure 76 shows an experiment with 60 % CO concentration (3 Nl/min). CO reacts with the oxide melt to give CO_2. It was noticed in all experiments that although no H_2 was used, H_2O and H_2 existed in the system. This was due to the stored H_2O in the refractory that appeared throughout the experiments. Moreover, the plasma gas showed bright bluish colour in this set of experiments, varying to the H_2 experiments where a yellowish colour of the plasma showed up. The sealing of the system was confirmed before each experiment.

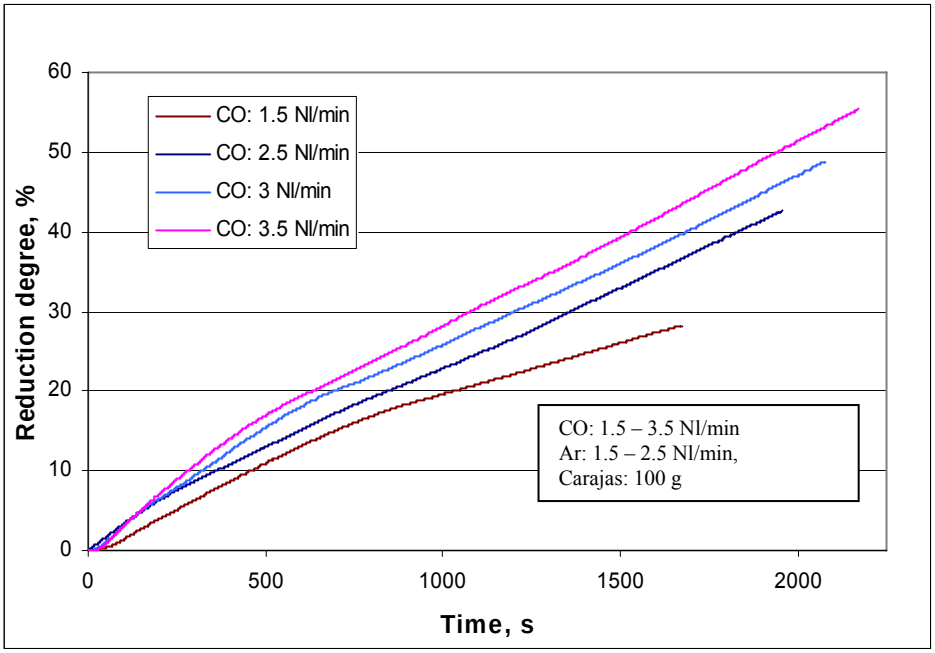

Fig. 77. Reduction degrees of CO – Ar experiments

The reduction degrees attained for various amounts of supplied CO are presented in figure 77. Despite the relative low reduction degrees, the 2nd phase duration was long enough to calculate the average reduction rate. A first order relationship between the reduction rate and the increasing flow of CO was observed, figure 78. It is clear from the regression analysis that the correlation of the results is much better (R^2 = 0.93) than the CO-H_2-Ar experiments (R^2 = 0.70). It is evident through this correlation that the CO supply is the rate limiting factor for this set of experiments.

The CO utilisation degree was also calculated as the reduced oxygen divided by the inlet CO in the stable phase. These results showed comparable values (16 – 20 %) relative to the CO-H_2-Ar experiments, figure 79. However, these results were slightly higher than the expected maximum contribution of CO (15 %), when equilibrium calculations are considered. This was attributed to the additional reducing gases (H_2, CO) stemming from the graphite electrode reactions, i.e. average graphite erosion rate 0.06 g/min.

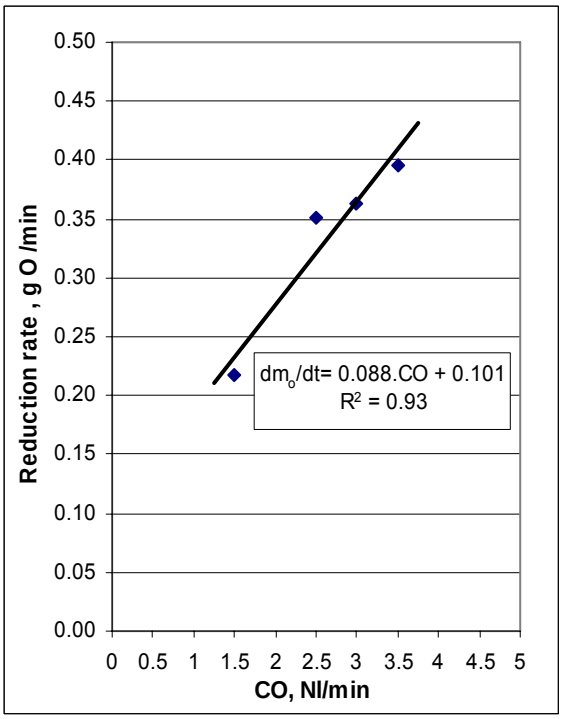

Fig. 78. Reduction rate against CO flow

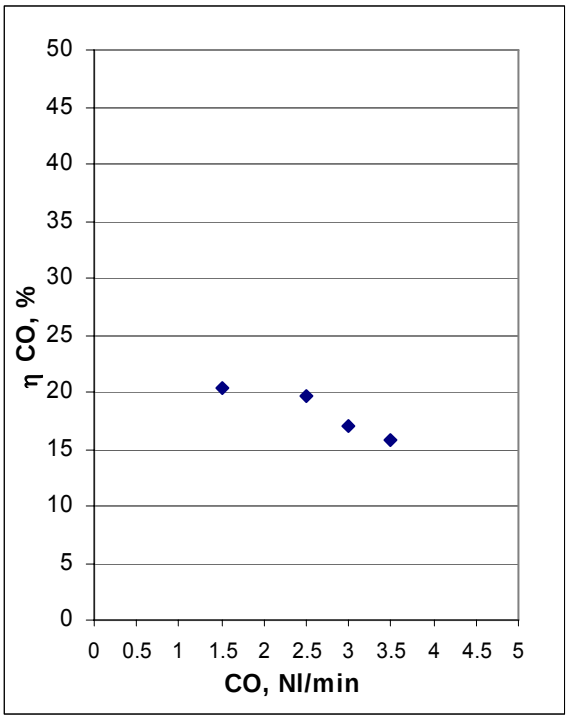

Fig. 79. Calculated CO utilisation degree

Finally, it should be mentioned that the specific reduction rate of liquid iron oxide by CO has been evaluated in the discussion section, section 7.5, and presented with respect to the corresponding results of H_2 under the application of plasma. The results are also presented with respect to the published reduction results of H_2 and CO at lower temperature ranges.

7.4.9 Reduction with CO_2-H_2-Ar mixture

CO_2 is an accompanying gas in the graphite electrode based experiments. As a permanent gas produced from electrode and water gas shift reactions and calcinations of carbonates, it was decided to carry out the current set of experiments to assess its negative influence on the H_2 reduction rate. The partial pressure of CO_2 has been varied between (3 – 8 %) in a H_2-Ar mixture. 100 g Carajas, H_2 flow of 2 Nl/min and total flow of 6 Nl/min were kept constant in all experiments.

Figure 80 shows the results of the conducted experiments against that of H_2 (CO_2: 0 Nl/min). It is clear that the CO_2 supply to H_2 retarded the reduction rate in all experiments, resulting in curves less steep than that of H_2 (CO_2: 0 Nl/min). On the other hand, it is clear from the figure that some experiments did not achieve high reduction degrees. This was attributed to the high amount of melt splashed on to the refractory ring during the course of the experiment as was determined from the mass balance. It is presumed that the increasing flow of CO_2 played a role in the amount of splash obtained. A justification for this phenomenon was nevertheless not clear. However, it should be mentioned that this limitation in the reduction degrees faced in some experiments did not cause a problem in the reduction rate assessment as the duration of the stable phase was long enough to conduct an evaluation.

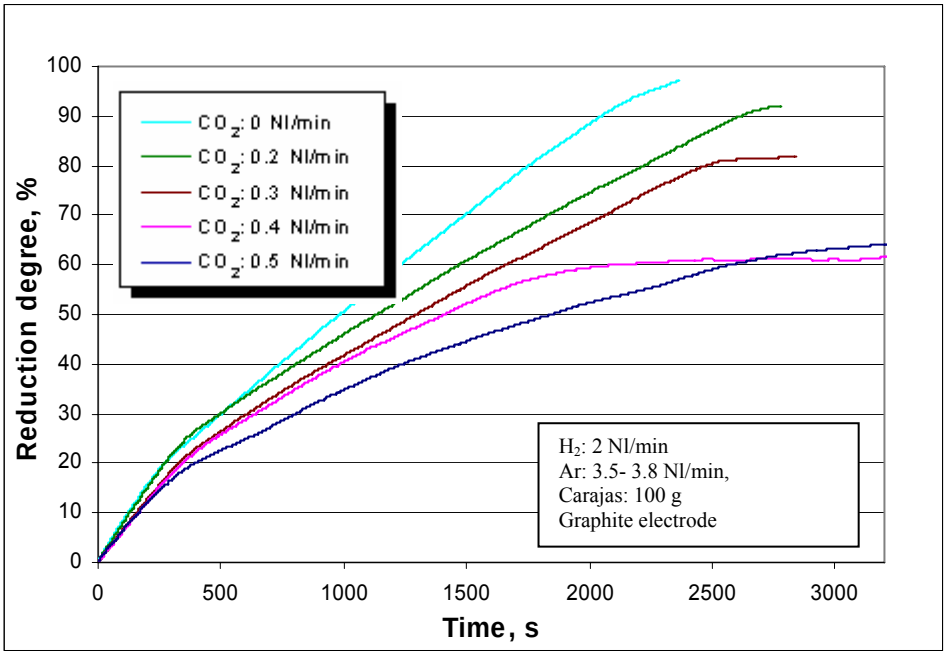

Fig. 80. Reduction degrees of CO_2-H_2-Ar experiments

The decrease in reduction rate due to CO_2 was evaluated by subtracting the results of reduction rates obtained in the 2nd stage, from that of the experiment with H_2 (2 Nl/min) and

CO_2 (0 Nl/min). Figure 81 shows that the more CO_2 flow is used, the greater the effect on the reduction retardation. Moreover, a first order relationship between the drop in reduction rate and the increasing flow of CO_2 was observed.

By quantifying the drop in reduction rate of the liquid iron oxide with respect to the H_2 experiment (without supply of CO_2), it is clear from the figure that a drop of about 50 % at 0.5 Nl/min CO_2 was attained. This oxidising effect of CO_2 was evaluated later in the discussion section, section 7.5, and compared with the apparent rate constants found in the literature for the oxidation of liquid iron oxide by CO_2.

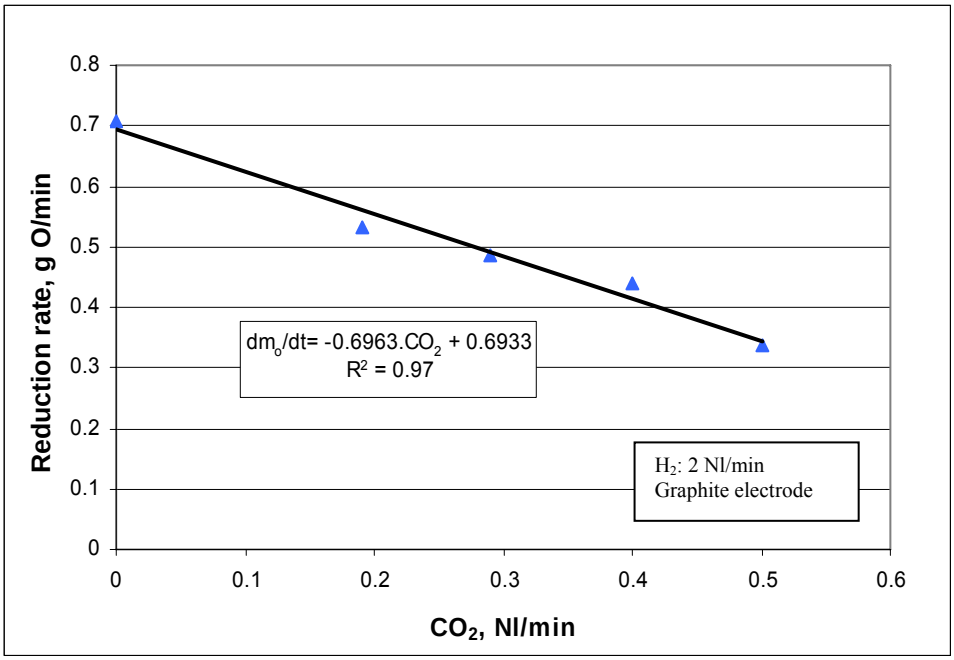

Fig. 81. Reduction rates against CO_2 flow rate

Examining the rate of electrode erosion in the applied range of CO_2 flow, it was found that the average rate was slightly higher, 0.18 g /min, than that of the H_2 and CO-H_2 experiments, i.e. the CO_2 reaction with the graphite of the electrode contributed in its consumption.

	% Fe	% C	% Si	% Mn	% P	% S
CO_2: 3 %	99.72	0.019	0.014	0.130	0.018	0.018
CO_2: 5 %	99.66	0.020	0.014	0.173	0.018	0.017
CO_2: 7%	99.62	0.020	0.015	0.223	0.015	0.017
CO_2: 8 %	99.65	0.018	0.013	0.194	0.016	0.019

Table 8. Chemical analysis of the reduced metal in CO_2-H_2-Ar experiments, wt. %

Finally, it is worth mentioning that from the conducted chemical analysis, no carburisation by the CO_2 took place as was expected, table 8.

7.4.10 Reduction with H_2O-H_2-Ar mixtures

The objective of this series of experiments was to investigate the effect of H_2O supply on the reduction kinetics in a H_2-Ar plasma atmosphere. The concentration of H_2O was varied between (3 – 11 %) in a H_2O-H_2-Ar mixture. 100 g Carajas, H_2 flow of 2 Nl/min, Ar flow of 3 Nl/min and total flow of (5.15 – 5.62 Nl/min) were set in these experiments.

Steam was produced as explained previously in section 7.2.3. Maintaining the vapour phase between the evaporator outlet pipe and the heated hose was guaranteed by superheating the steam (+ 20 °C higher than the required evaporation temperature). The heated hose was then used to transfer the steam until the feeding port of the furnace. The steam inlet temperature was maintained at a temperature of 120 °C by setting the temperature of the heated hose.

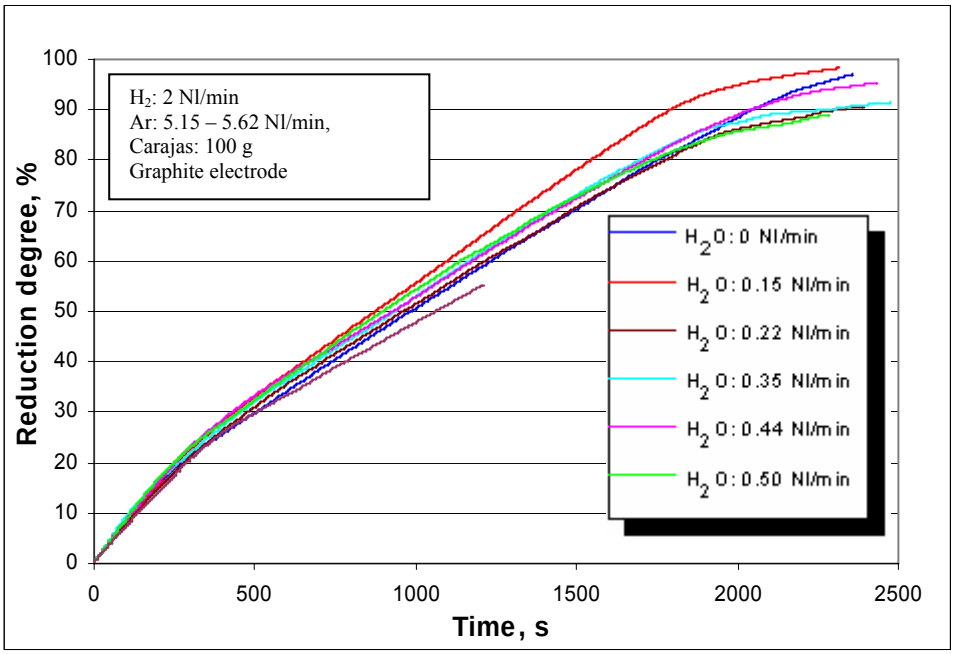

Fig. 82. Reduction degrees of H_2O-H_2-Ar experiments

Figure 82 shows the results of the conducted experiments including the experiment undertaken without H_2O usage. It is clear that all experiments behaved almost identically regardless of the H_2O flow, i.e. the deviation between the slopes of the reduction curves was not so obvious. Reduction was almost completed up to an inlet H_2O flow of 0.5 Nl/min. At higher flow rates (H_2O: 0.62 Nl/min), the completion of reduction failed due to the plasma

power supply limitations. However, it should be mentioned that this convergence in the reduction kinetics contradicted the thermodynamic principles of the H_2-H_2O reactions where a decreasing reduction rate with an increasing supply of H_2O was expected.

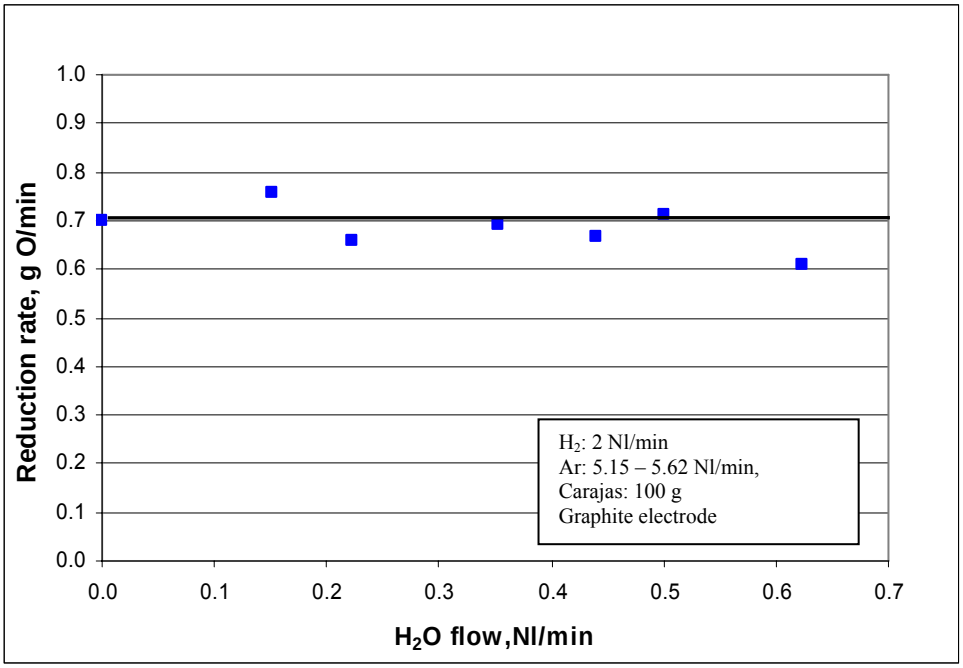

Fig. 83. Reduction rates of H_2O-H_2-Ar experiments at various H_2O flows

For a closer approach to the results of the current experiments, the reduction rates during the 2nd stage have been plotted against the H_2O flow, figure 83. No clear influence of the H_2O flow rate on the reduction rate was found, where the results were within the same range. To study the influence of inlet H_2O on the electrode erosion, the evaluation of the average erosion rate during the 2nd stage of the experiments was carried out. It was found that it is generally high in this series of experiments as a result of the increasing reaction between the inlet H_2O and carbon from electrode. Internal erosion at the tip of the electrode (hollow side) was also observed, figure 84, and it was ~ 25 % of the total erosion (as determined by the geometry of the electrode).

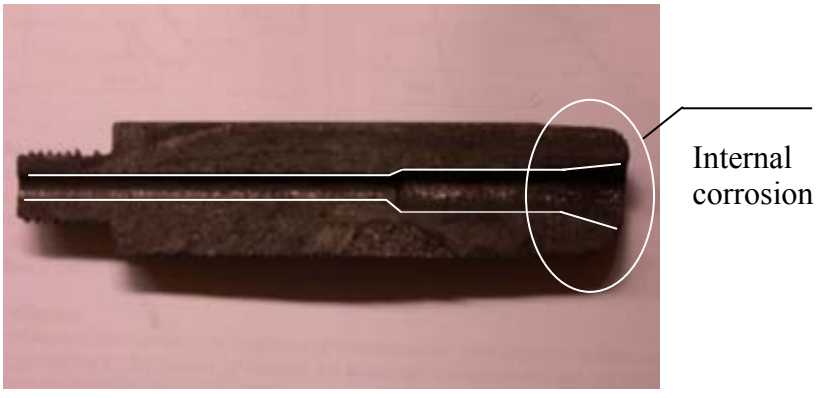

Fig. 84. Corrosion of the electrode, from the hollow side, by the supplied H_2O

The rate of carbon eroded in the stable phase was calculated from the gas analysis and plotted against the inlet H_2O, figure 85. It is clear from the regression analysis that there was a linear relationship between the inlet H_2O and the eroded carbon. In other words, the more H_2O supplied, the more CO and H_2 to the system was delivered via the H_2O – $C_{electrode}$ reaction, reaction (22).

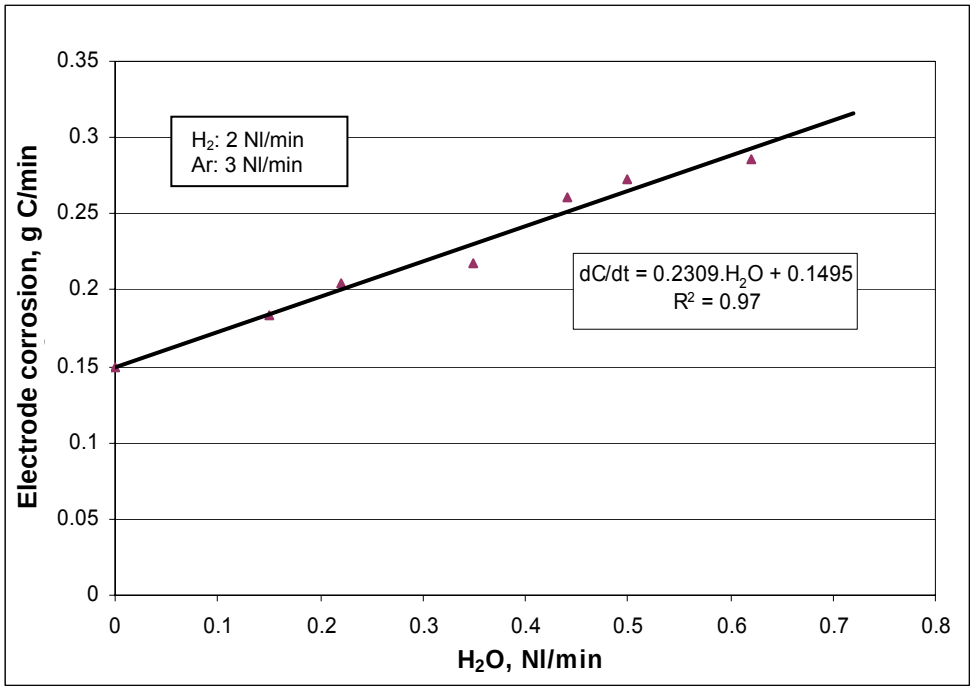

Fig. 85. Electrode erosion rate against H_2O flow

The contribution of the generated CO and H_2 was obviously high so that additional reduction of the oxide melt took place. It is presumed that this was a reason for the absence of the negative effect of H_2O on the reduction within the applied range of inlet H_2O. However, it is believed that at higher flows of H_2O, the H_2O retardation influence on the reduction rate could be observed.

7.4.11 H_2 - Ar reduction with coke additions

7.4.11.1 Coke additions – batch wise

Hybrid application of coke and hydrogen plasma was put as an option to widen the application of the H_2-plasma. Dried coke with the chemical analysis shown in table 9, was mixed with the ore and placed in the crucible in a series of experiments to evaluate the influence of coke on the reduction behaviour of hydrogen plasma. Coke between 2.5 and 15 g in mass and 0.5 – 3 mm in size was used. 100 g Carajas, H_2 flow of 2 Nl/min and Ar flow of 3 Nl/min were set in the current experiments.

% H_2O	% Ash	% C	% H	% N	% $S_{tot.}$	% VM
15.11	14.20	83.40	0.36	0.98	0.47	2.37

Table. 9. Chemical analysis of the coke, wt. %

Figure 86 shows the gas analysis from a H_2-Ar experiment with 5 g coke added. A significant increase during the first minute in the CO and CO_2 was observed due to the coke contribution. A decreasing trend in CO and increasing trend in H_2 were then observed. These trends and the decreasing reduction rate (figure 87) indicated that no stable phase was obtained during the course of the experiment.

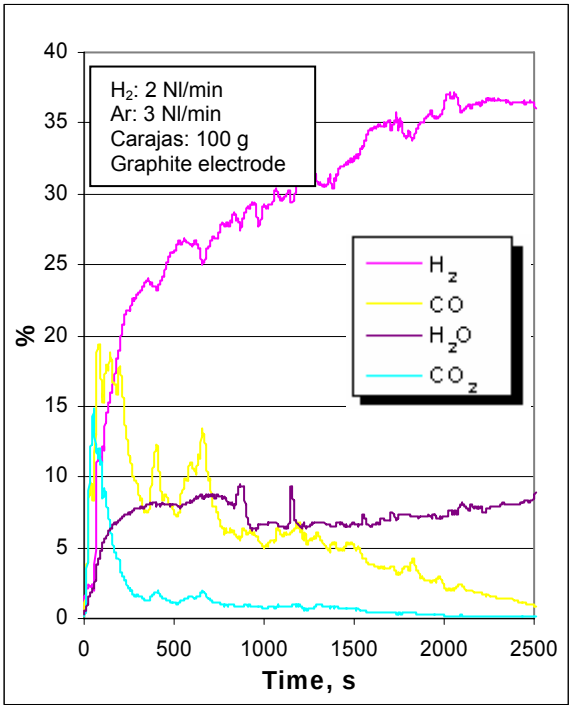

Fig. 86. Gas analysis with 5 g coke

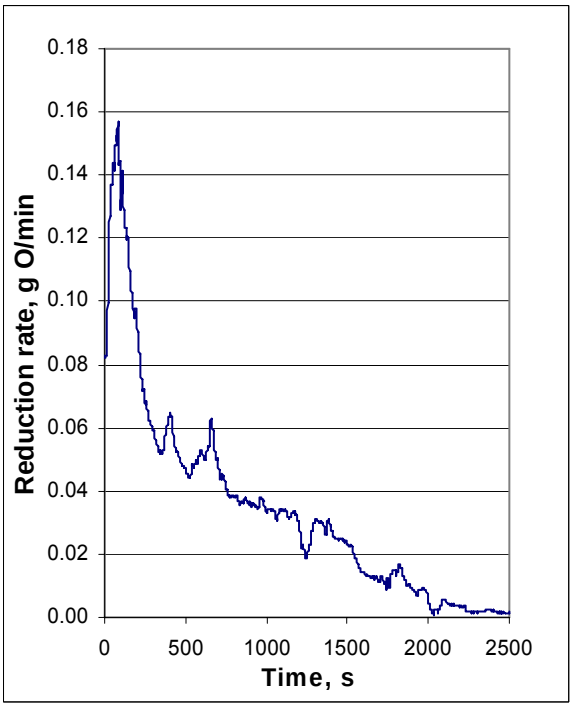

Fig. 87. Reduction rate with 5 g coke

In the conducted experiments, the melting phase under Ar did not exceed 45 s. After that, H_2 was supplied to evaluate the coke behaviour in the reduction process. It is worth mentioning that despite the usage of coke, no obvious slag foaming was observed in any of the experiments. On the other hand, it was observed from the sight glass that no homogeneous melting of the mix occurred. Moreover, the melt was significantly solidifying (except at the melt plasma interface) after ~75 % reduction degree. This solidification phenomenon led to the non removal of the remaining oxygen which results accordingly in the limitation of the

reduction degree (< 90 %) as shown in figure 88. From the conducted metal analysis, no carburisation took place and an average carbon content of 0.021 % was found.

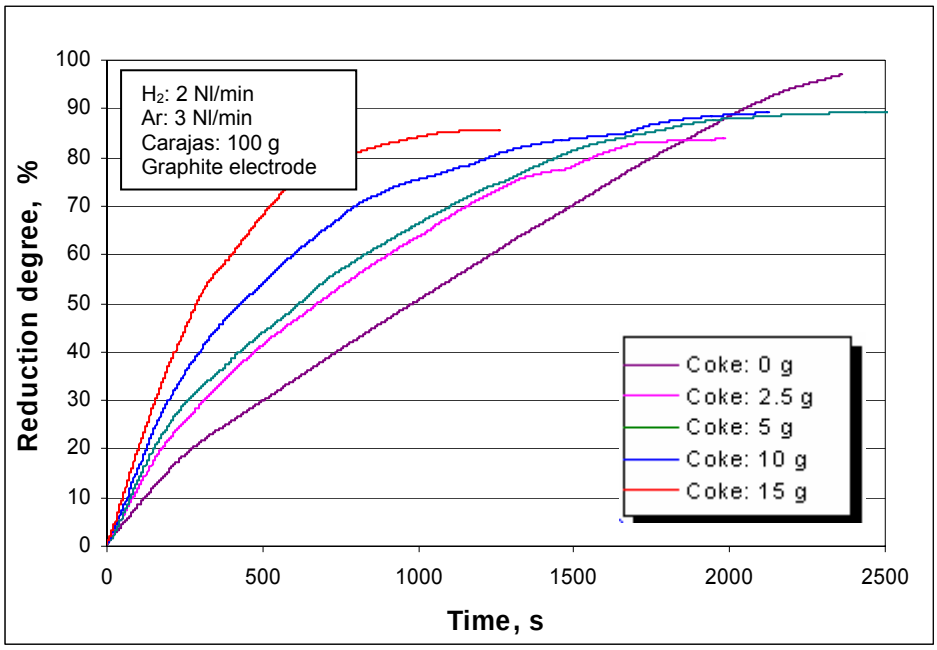

Fig. 88. Reduction degrees for various coke additions

In the end, it was decided to assess the coke reduction potential by feeding it continuously via a prepared screw conveyor, thereby ensuring a stable phase for investigation rather than a decreasing reduction rate trend as was shown in the previous section.

7.4.11.2 Coke additions – continuous feeding

Coke fines have been continuously fed with the above shown boundary conditions rather than mixing it with the ore. The coke was fed through the hollow electrode via a screw conveyor. A fixed rate of 1.33 g/min was conveyed almost 3 minutes after the H_2 supply during the conducted experiments.

It is clear from figure 89 that CO increases significantly as soon as coke is added to the system. The CO development was characterised by an increasing trend over time until reaching a stable phase. However, even within the stable phase a fluctuation in CO values has been noticed, i.e. 25 – 32 %. This fluctuation was attributed to the intermittent feeding of coke caused by the irregular discharging of the screw conveyor. CO also decreased significantly before the end of the reduction where solidification took place, as for the coke batch wise experiments. This solidification obviously hindered reduction development and led to the rise of H_2. However, a peak in CO was again noticed due to the partial resumption of the molten phase. In the end, coke supply was stopped after the reduction was completed.

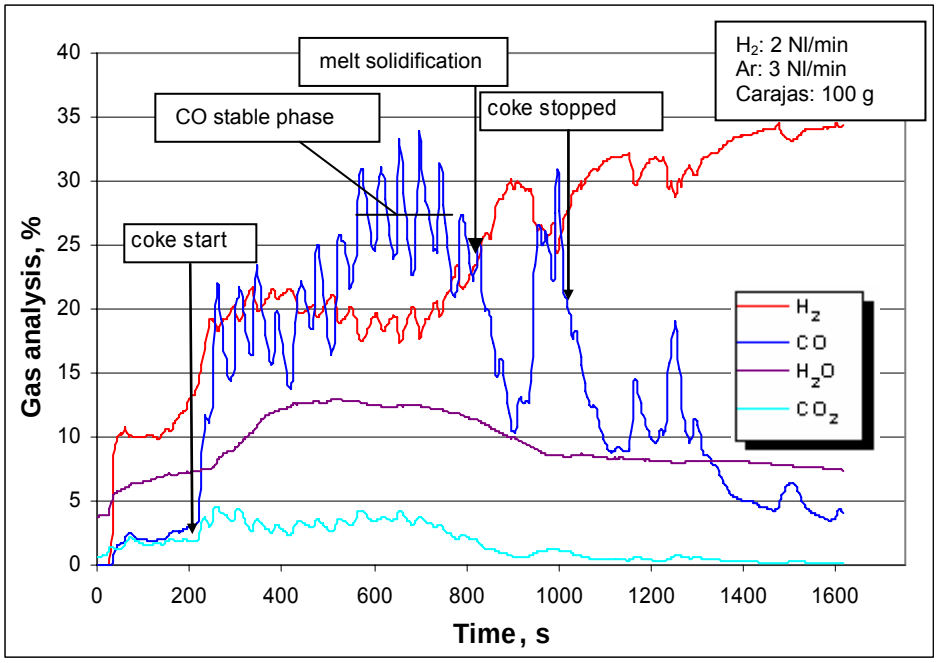

Fig. 89. Gas analysis for H_2-Ar experiment with continuous coke addition (1.33 g/min)

It should be mentioned that although coke fines was fed through the hollow electrode, no plasma deterioration was observed. The turbulent characteristics of the plasma and the surrounding gases were observed sometimes via the blackish colour of the coke. Moreover, slag foaming was hardly noticeable. At the end phase of reduction, full reduction in the remaining molten zones was evident by monitoring of the floating tiny films that were silver in colour (presumably cementite).

Figure 90 shows the reduction degree, carbon and H_2 utilisation degrees. Completion of reduction was very fast due to the contribution of coke. The carbon utilisation degree in the stable phase varied between ~55 – 90 %. The large fluctuation and high carbon utilisation degree were due to the mentioned intermittent feeding of the coke. This behaviour led to an instantaneous discrepancy between the actual and theoretical feeding rate. It should be noted that the intermittent feeding is mainly dependant on the geometry of the screw and the sticking behaviour of the material fed. However, an average carbon utilisation degree of 67 % was calculated.

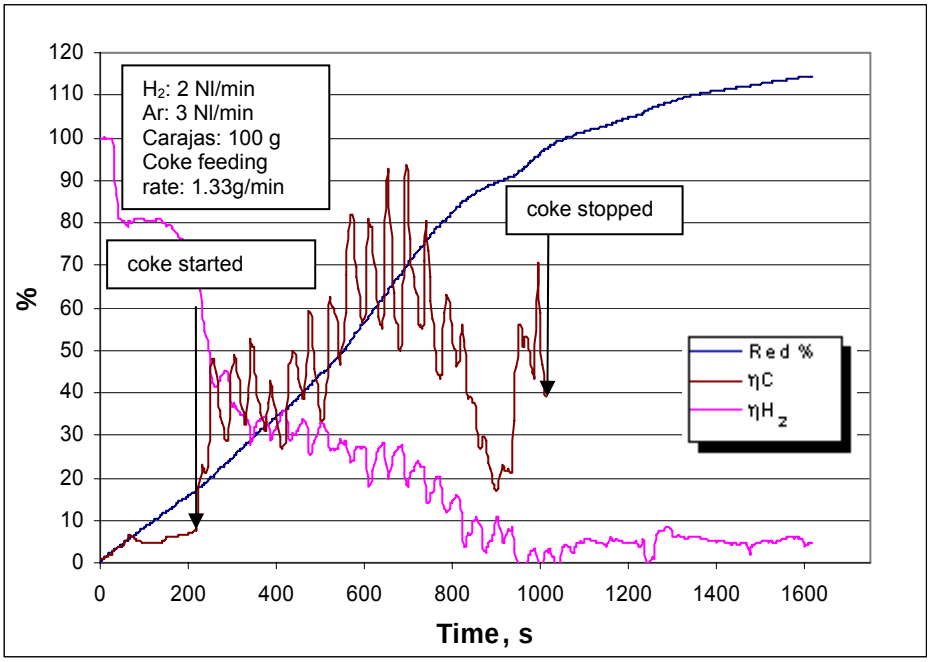

Fig. 90. Reduction and utilisation degrees for H_2-Ar experiment with continuous coke addition

According to the definition of carbon utilisation degree, section 7.3.3.6, and the utilisation degree obtained, the fed coke was fully utilised and converted mainly to CO and partially to CO_2. However, it should be mentioned that the actual carbon utilisation degree should be less than that observed in the results and that the deviation was attributable mainly to the water gas shift reaction, reaction (26). Exact contribution of carbon in the reduction is assessed in the discussion section, 7.5. Finally, as is clearly evident from figure 90, the reduction degree exceeded 100 %. It was found that this increase in reduction degree was attained over CO existed in the off-gas. It is believed that the formed CO was due to the reaction of stored H_2O in the refractory and remaining coke in the system. However, there is no clear evidence to support this hypothesis.

Due to the existence of surplus carbon during the end phase of reduction, metal carburisation was observed in the current experiments. This is evident from the chemical analysis, table 10 , and the pearlite-secondary cementite microstructure obtained, figure 91.

	% Fe	% C	% Si	% Mn	% P	% S
Coke: 1.33 g/min	98.43	1.08	0.044	0.291	0.011	0.020

Table 10. Chemical analysis of the reduced metal using coke, wt. %

Fig. 91. Pearlite-secondary cementite structure

7.4.12 H_2 - Ar reduction of continuous fed ore

All the previous conducted experiments, except coke continuous feeding experiments, were batch wise based experiments, (ore was charged in the crucible before starting the experiment). In the current experiments, continuous feeding of fines ore through the hollow electrode was carried out. The objective of this series of experiments was to investigate the plasma stability and the reduction behaviour under continuous ore feeding. The boundary conditions were identical to the batch wise H_2-Ar experiments. A change in H_2 concentrations of 30 %, 40 %, 50 % and 55 % H_2 in a total H_2-Ar flow of 5 Nl/min was conducted. 100 g Carajas was charged in the crucible before each experiment. The ore was melted, H_2 was then supplied, followed by the feeding of fresh ore.

The preparation of a screw conveyor system for the continuous feeding of the ore was conducted in-house as explained previously in section 7.2.4 . The control of the system was not ideal, especially in the first experiments. It was important to confirm the soundness of the sealing system and ensure the optimum alignment between the screw element and the housing. Typical problems faced throughout the experiments were confined in the gas leakage from the o-ring side and the stuck of the screw element with its housing during rotation.

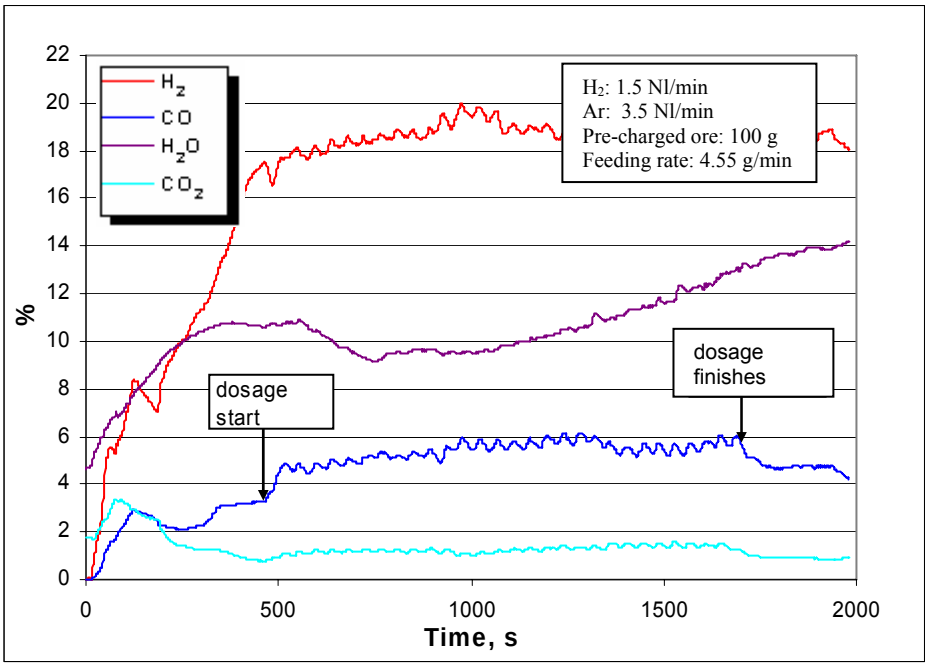

Fig. 92. Gas analysis for H_2-Ar experiment with continuous ore feeding (4.55 g/min)

Figure 92 shows the gas analysis from a 30 % H_2 experiment under continuous feeding of Carajas ore with a rate of 4.55 g /min. It is clear from the figure that as soon as the ore was fed to the furnace, saw-tooth shaped peaks in the analysed gases appear. These peaks were attributed to the intermittent feeding of the ore caused by the irregular discharging of the screw conveyor. A comparison of the gas analysis with that of a batch wise experiment at the same conditions (gas flow and concentration of H_2) was carried out as shown in the appendix. It was found that an increase in H_2O, CO and CO_2 in the current experiments was obtained.

The slope of the reduction degree curve was lower than that for all the previous conducted experiments, figure 93. This was due to the increasing amount of the dominator (the reducible oxygen) caused by feeding ore throughout the experiment. Whereas, in the previous experiments, the reducible amount of oxygen in the ore was constant from the beginning of the experiment. The slope, however, increased again in the conducted experiments, when ore feeding (reducible oxygen source) stopped, as it is clearly shown in the figure. On the other hand, the average H_2 utilisation degree did not show a clear change (~ 32 %) while the total utilisation degree showed a higher utilisation of approximately 10 % (~60 %) with respect to the corresponding batch wise experiment.

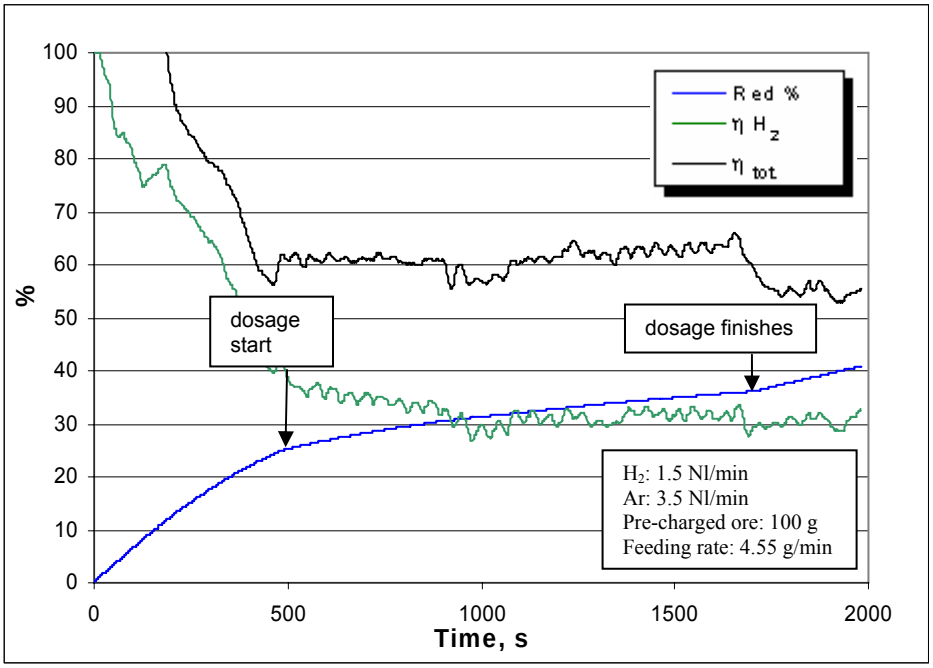

Fig. 93. Reduction and utilisation degrees for H_2-Ar experiment with continuous ore feeding

Figure 94 shows the reduction rate of the conducted experiments and those of batch wise experiments in the stable phase with the same flow rate of H_2. It is clear that the reduction rates in the current experiments are higher. An average increase of almost 20 % was found. This increase was justified by the continuous supply of trivalent iron via the fresh ore fed. It should be mentioned that the erosion rate of the graphite electrode used was about 1.7 times that of the batch wise experiments, 0.29 g/min.

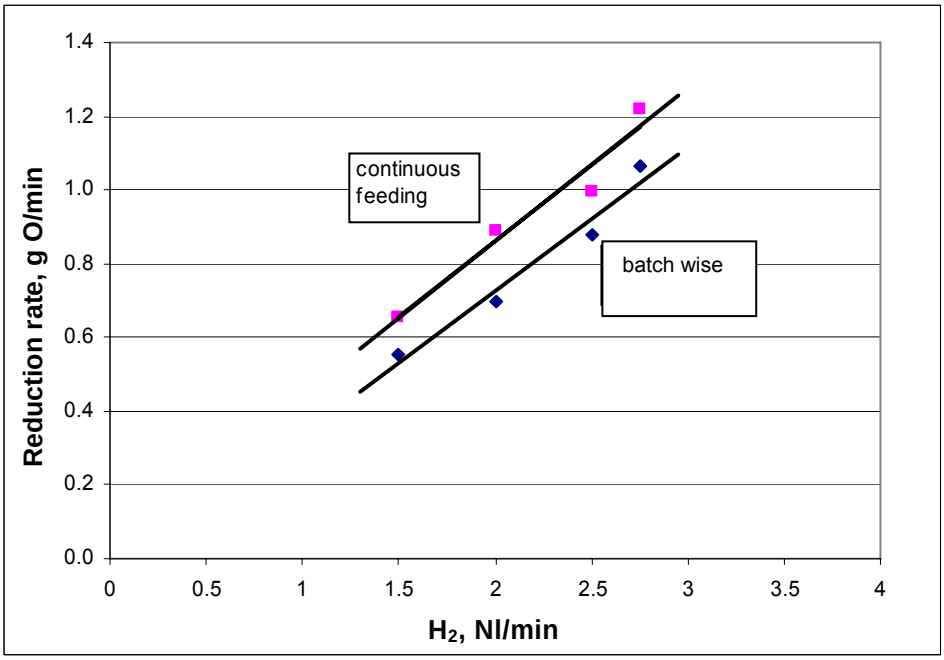

Fig. 94. Reduction rate, continuous feeding versus batch wise

It was debated that the high erosion rate of the electrode was not only due to the higher amount of produced H_2O, but, it might also be due to extra carbon that might has been eroded by the ore fed from the hollow side. An experiment, however, with an upper graphite electrode threaded to a lower tungsten electrode was carried out. This sequence was chosen to avoid the H_2O – $C_{electrode}$ reaction, reaction (22). It was found that neither CO nor CO_2 was obtained in the off-gas from the graphite part of the electrode, for which results are shown in the appendix. This experiment confirmed that no electrode erosion by the action of the fed ore was obtained. Visual check of the electrode was also conducted to show its soundness (erosion free) from the hollow side

Fe (II) and Fe (III) concentrations in the slag of the current experiments were analysed. The results obtained have been presented with those of the ore (Carajas), the ore after melting and after partial reduction to the pre-charged ore (batch wise experiments). The fines ore initially contained 0.31 % of Fe (II) and 66.82 % of Fe (III).

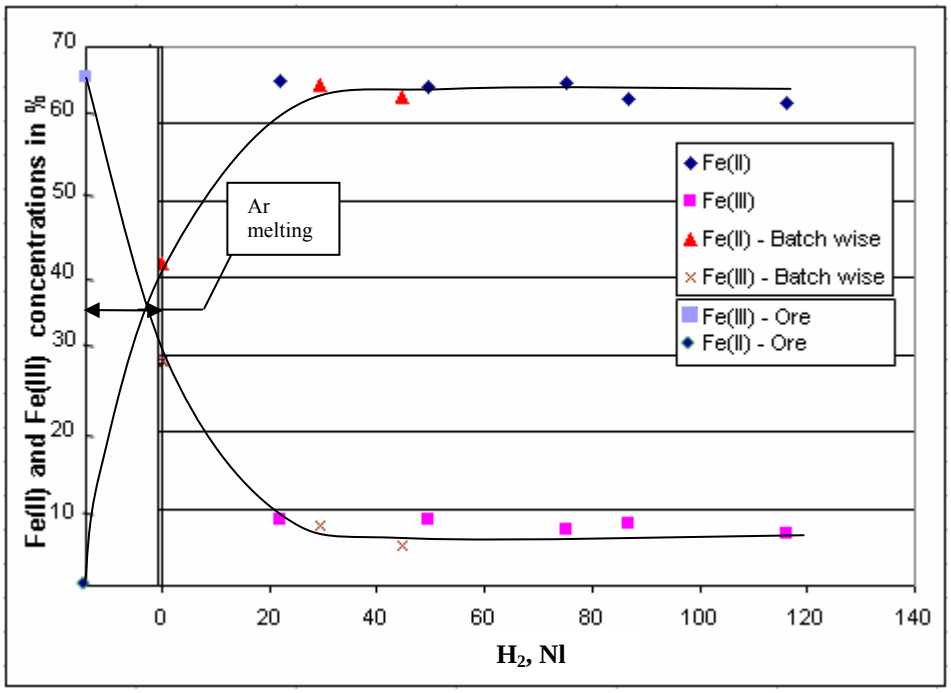

Fig. 95. Change of Fe (II) and Fe (III), in wt. %, in the slag against H_2 flow

After 3 minutes melting duration with Ar, Fe(III) and Fe(II) changed by thermal decomposition to 29.1 % and 41.9 % respectively [10]. By the addition of H_2, the Fe (III) decreased significantly and showed average results of 7.85 %. This decrease was witnessed in the batch wise experiments as well. It should be noted that significant deviations of Fe (III) concentrations in both series of experiments were not observed, figure 95.

One of the most important findings in the current experiments was the stable behaviour of the plasma despite the ore feeding via the hollow electrode. This was observed from the sight glass where the plasma had its own pattern which was separate from that of the fines ore. The phenomenon of two separate patterns was attributed to the high viscous characteristics of the plasma. The pattern of ore was, however, sometimes showing turbulent flow that was presumably due to the usual changing shape of the arc column and the accompanying fluctuation in arc stability.

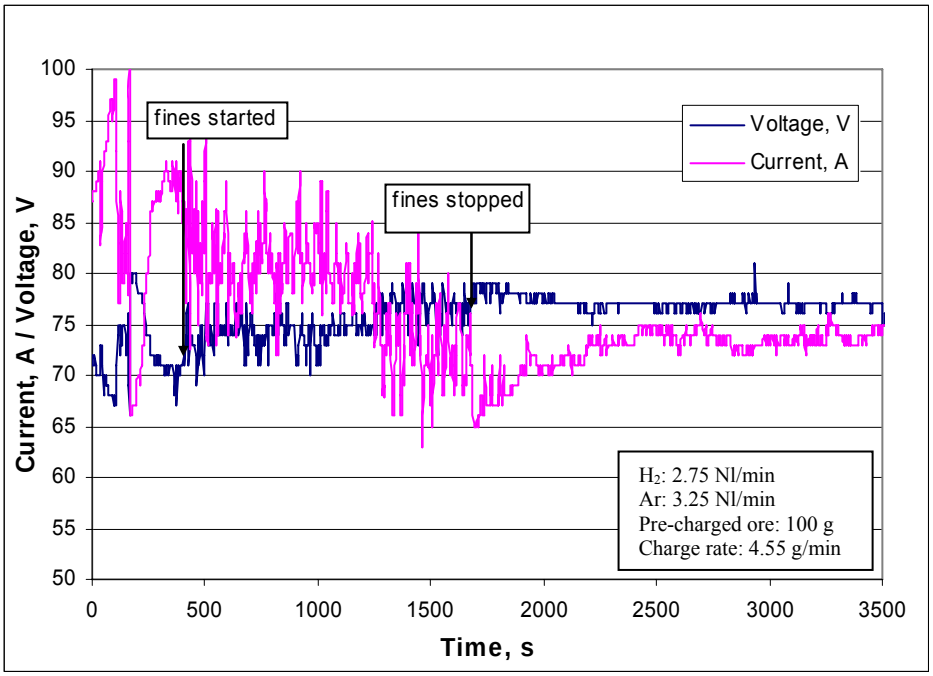

Fig. 96. Voltage and current changes during ore feeding

On line monitoring of the current and voltage of the plasma was carried out and is shown in figure 96. As mentioned earlier on, the plasma stability did not deteriorate. However, some fluctuations in both voltage and current were noticed when compared to a period where no ore feeding took place.

7.5 Discussion

7.5.1 Reduction by H_2-Ar plasma

The mechanism of H_2-Ar plasma reduction was explained in detail in previous work [10,14]. However, a brief description of the process, as shown in figure 97, is worth mentioning before discussing the details of the present experimental program.

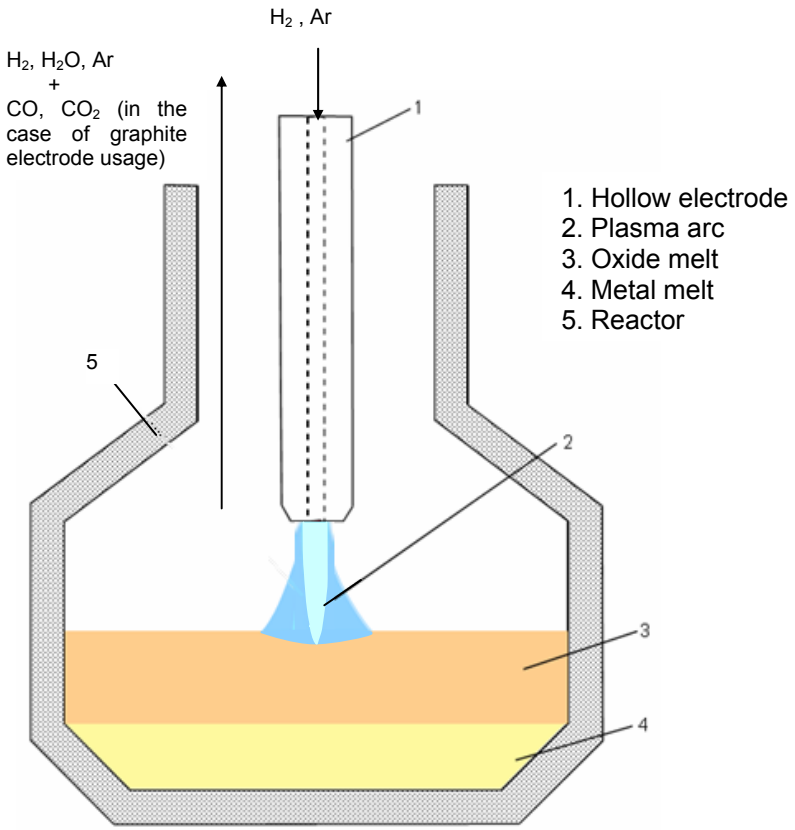

Fig. 97. Schematic diagram of the reduction process

The plasma gas (H_2+Ar) is supplied through a hollow electrode. At the interface between the plasma arc and the oxide melt, the melt temperature reaches high temperatures (2000 – 2600 ^oC). The supplied hydrogen reacts (at the surface) with Fe^{2+}, O^{2-} and Fe^{3+} in anion complexes that exist in the oxide melt according to the chemical reactions below, [13]:

$$Fe^{2+} + O^{2-} + H_2 \Leftrightarrow Fe\ (l) + H_2O\ (g) \quad (70)$$

$$2FeO_2^- + 2e^- \Leftrightarrow 2Fe^{2+} + 4O^{2-} \quad (71)$$

$$2FeO_2^- + H_2\ (2H) \Leftrightarrow 2Fe^{2+} + 3O^{2-} + H_2O\ (g) \quad (72)$$

$$Fe_2O_5^{4-} + H_2\ (2H) \Leftrightarrow 2Fe^{2+} + 4O^{2-} + H_2O\ (g) \quad (73)$$

When reduction of the oxide melt starts and coalescence of reduced iron takes place, the iron melt settles (as a metal bath layer) beneath the oxide melt layer. During progression of the experiment, the quantity of the oxide melt decreases whilst that of the metal bath increases. At the end of the reduction, when the oxide melt quantity extremely lessens, the plasma arc is positioned directly on to the metal bath and the reduction rate obviously drops. Some partial reduction and evaporation of the gangue elements to the metal bath and atmosphere are respectively possible.

7.5.1.1 Reduction using graphite electrode

As a product of the reduction process, H_2O goes to the off-gas but a fraction is missed as it is condensed in the refractory lining. Moreover, suction of some of the evolving gas takes place at the tip of the electrode. This suction is caused by the effect of plasma jet where the H_2O react with the graphite electrode, reaction (22). The resultant products are led back to the oxide melt where further reduction by H_2 and CO takes place. On the way from the melt to the off-gas, the gas temperature decreases and consequently water gas shift reaction, reaction (26), to the direction of CO_2 and H_2 is expected, [14].

In previous work [10,14] it was believed that H and H^+, stemming from the dissociation and the ionisation within the plasma region, take place in the reduction process at the plasma melt interface. This concept was adopted especially as the overall reduction rates obtained from the conducted experiments were higher than that which could be obtained by the molecular H_2. However, justification of the contribution of H and H^+ in the reduction was not possible due to the interference of CO and H_2, from reaction (22), and their contribution in further reduction.

7.5.1.2 Reduction using tungsten electrode

In the current research work, H_2 plasma experiments were conducted using 1 % lanthanated tungsten electrode. In these experiments, the contribution of H_2O-$C_{electrode}$ reaction, reaction (22), has been ruled out, as only Ar, H_2 and H_2O was detected in the off-gas. From the experimental results, an utilisation degree of H_2 of ~40 % was assessed. This result conformed to the thermodynamic equilibrium of the molecular H_2 rather than that of H or H^+. In other words, it is evident from these results that the higher reduction rates obtained in the graphite electrode experiments were exclusively due to the contribution of the generated CO and H_2 in the reduction and that no novel reaction by the hydrogen plasma took place. Correction of the results found using the graphite electrode was conducted to eliminate the

effect of reaction (22). This correction was achieved by subtracting the oxygen portion reduced by the generated gases (CO, H_2) which were based on CO and H_2 utilisation degrees of 15 and 40 % respectively. These utilisation degrees were adopted according to the equilibrium calculations and H_2 and CO experiments. It is worth mentioning that the results obtained after the correction were in good agreement with that of the tungsten electrode results as is shown in figure 98. Through this conformance in results, the perception of the contribution of the generated gases (CO and H_2) in the reduction based on the adopted utilisation degrees was validated.

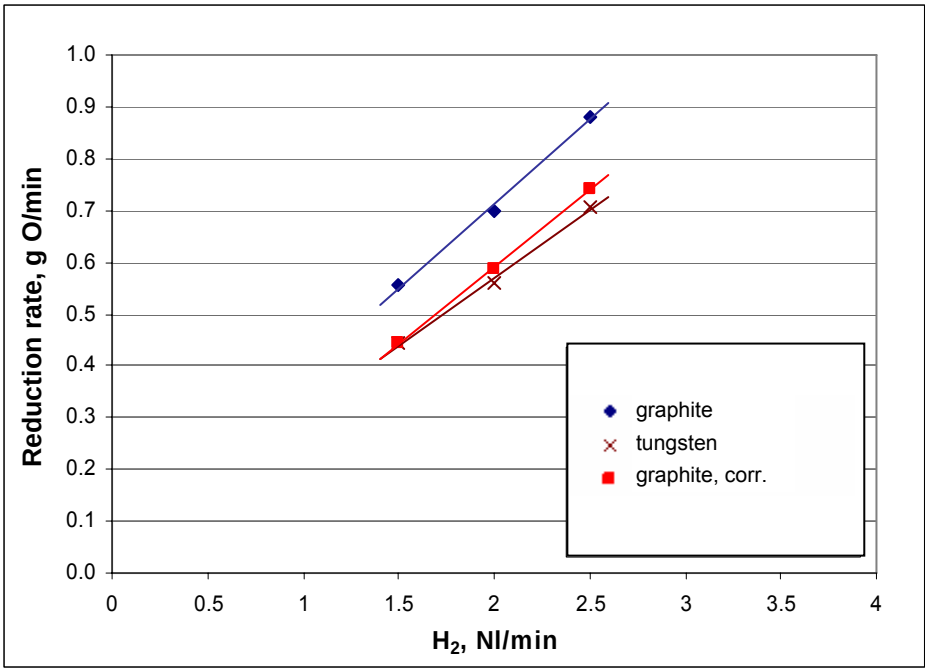

Fig. 98. Effect of the elimination of the graphite electrode effect on the reduction rate

In practice, tungsten is widely used along with graphite in the production of cathode electrodes as both materials can deliver sufficiently high current density at temperatures below their respective sublimation or melting points. In case of the usage of tungsten electrodes, about 2 % ThO_2 is added to reduce the work function needed for electrons to leave the emitting surface. However, as a substitute for the radioactive thorium, 1 % La_2O_3 was applied in the electrode used.

Plasma instability in the conducted experiments, lateral shift to the side walls, was mentioned in the experimental part. This plasma instability hindered both the consistency and the completion of the experiment. This is mainly attributed to the less surface roughness of the tungsten electrode with respect to the graphite electrode. This difference leads to an easier mobility of the arc on the graphite electrode where the arc looks continuously for sharp points with higher stable conditions and less resistive path. During the arc movement on the melt, it

sparks over sometimes to the metal crucible. In case of the graphite electrode, the easy mobility of the arc renders its contact to the melt while it is not the case in the tungsten electrode. In other words, the less mobility of the arc on the tungsten electrode leads to the relative stagnation of the arc at the crucible and the found stagnant lateral shift of the arc.

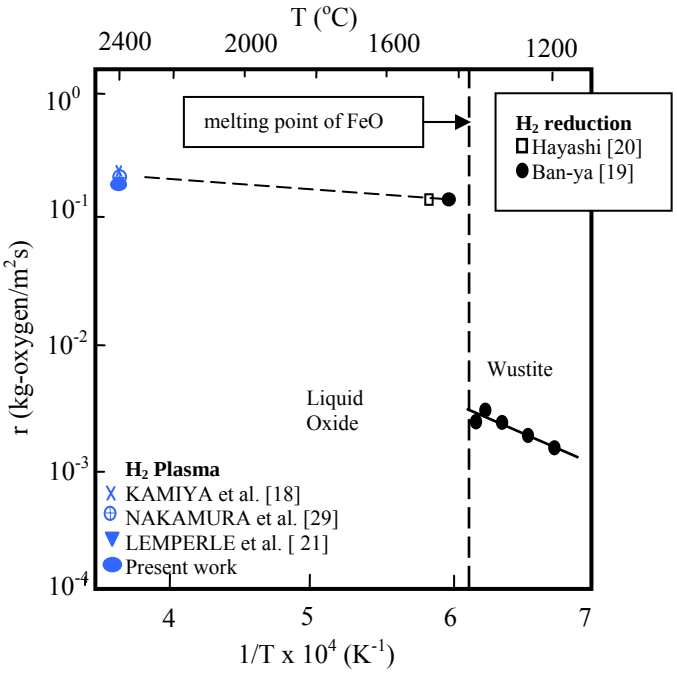

Fig. 99. Reduction rate of wustite and liquid oxide by H_2 as a function of temperature

Finally, the specific reduction rates of both sets of experiments were calculated based on a reaction area of 1 cm^2. This area corresponds to the plasma melt interface and was visually estimated during the experimentation. The calculations from the experiments using graphite and tungsten electrodes showed 30 x 10^{-2} and 25 x 10^{-2} kg-oxygen/m^2s respectively. Having the results obtained, the average results of the published H_2 plasma smelting (using tungsten electrode), [18,21,29], and the work of Ban-Ya [19] for a H_2 reduction rate at 1400 °C, a straight line is plotted, figure 99. It should be noted that, according to Arrhenius equation [84], the slope of the plotted straight line is defined as (- E_a/R) where,

E_a: the activation energy for the reaction in Joules
R: the ideal gas constant in J/mol K

The activation energy was calculated to be 23 kJ/mol and from a regression analysis, the following empirical equation was obtained:

$$ln\ r = -0.15 - 2811 / T \ (kg\text{-}oxygen/m^2s) \qquad (74)$$

Where *r* is the specific reduction rate and T is the temperature in K.

7.5.2 Impact of lateral H_2 supply on the reduction behaviour

As an alternative way to premixing the plasma gases, H_2 was partially fed via a ceramic lance. The lance was positioned above the melt and slightly towards the edge of the crucible. The objective of this positioning was to keep the blown gas at approximately the room temperature before the reaction takes place. In other words, this was done to rule out the influence of plasma on the blown gas, and accordingly the dissociation and ionisation of H_2.

Completion of experiments with high lateral hydrogen flow rate (more than 0.75 Nl/min) was not possible as mentioned in the experimental section. This was due to the abrupt fluctuations of voltage found during the experiments, which caused break up of the power supply. However, the results were generally satisfying and obviously agreed with the premixed hydrogen argon experiments. This means that no contribution of H and H^+ in the hydrogen plasma experiments take place, as previously proved in section 7.5.1.2. On the other hand, it should be noted that the possibility of feeding H_2 through separate lances rather than hollow electrodes could be utilized as an option when a scaled-up process is considered. By having such a possibility, the amount of H_2 (plasma gas) fed via the hollow electrode could be decreased.

7.5.3 CH_4 – Ar reduction

The objective of this series of experiments was to assess the CH_4 reduction behaviour with respect to H_2. Through the application of plasma, CH_4 is fully cracked to solid carbon and hydrogen molecules according to the reaction (50). From a stoichiometric point of view, it is clear that the products of 1 mole of CH_4 can reduce 4 atoms of oxygen (CO_2, $2H_2O$) while 1 mole of H_2 can only reduce 1 mole of oxygen (H_2O). Therefore, the usage of CH_4 in comparison to H_2 will result in a higher reduction rate (i.e. 4 times higher reduction rate). However, this value should increase to 4.8 when thermodynamics is considered, as clarified in section 6.1.2.

From the experimental results, the average erosion rate of the H_2 experiments was more than that of CH_4 experiments at the same amount of supplied H_2. It is presumed that this was attributed to the increasing amounts of CO, produced from CH_4, which increased the rate of water gas shift reaction, reaction (26), towards more CO_2 and less H_2O. This subsequently decreased the rate of H_2O-$C_{electrode}$ reaction, reaction (22), i.e. less erosion rate of the electrode.

The methane reduction rate was found to be 4 times that of the hydrogen reduction rate. This reduction rate ratio was calculated by using a correction term as conducted in the H_2 experiments, section 7.5.1.2, to eliminate the contributing carbon (from reaction (22)) in the reduction results. From the calculated ratio, it is apparent that the reduction rate of 1 mole of carbon was equivalent to that of 2 moles of H_2. Moreover, it is clear that this ratio conforms relatively to the thermodynamical ratio of 4.8. However, this deviation might be due to the non full contribution of carbon from the CH_4 in the reduction. This was evident from the deposited carbon inside the hollow electrode and the carbon soot formation. It should be stressed that the encountered carbon deposition inside the hollow electrode has led to non uniform distribution of the plasma gas over the melt. This consequently led to a partial solidification of the melt and an inconsistency in reduction, with some zones fully reduced whilst other zones were not. However, it is believed that the hollow electrode susceptibility to the carbon deposition was significantly high due to the limitations of the hollow diameter (8 mm), whereas such a phenomenon is not expected to occur in larger diameters in the up-scaled process.

From the chemical analysis results, a slight carburisation has been found. This was due to carbon pick-up by excessive CH_4. However, for an up-scaled process with continuous operation no carburisation is expected due to the existence of the protecting slag layer with high oxygen potential.

Finally, it should be mentioned that CH_4 is a potential alternative to H_2 when up-scaling is considered. On one hand, saving the investment and running cost of H_2 production is a great advantage by applying CH_4-plasma. On the other hand, the gas volume in the prospective flow-sheet will be decreased with respect to H_2-plasma due to the higher reduction potential of the existing carbon in the CH_4.

7.5.4 Reduction at various basicities

This set of experiments was carried out to study the effect of CaO addition on the phosphorous behaviour. CaO additions slightly influenced the reduction rate but have captured to a great extent the phosphorous in the slag. This was evident from the experimental results where the phosphorous in the slag obviously increased at higher basicities whilst the phosphorous reduced into the melt and that evaporated decreased. The evaporated phosphorus was obviously high in the conducted experiments. This shows the potential of the H_2-plasma in terms of phosphorous evaporation up to a basicity of $B_2 = 2.5$.

7.5.5 Reduction of magnetite

Kiruna ore with a Fe_3O_4 content of 92.26 % was reduced in this set of experiments by H_2 to assess its reduction behaviour with respect to Carajas ore. It was found that after first phase of the reduction process, where most of the Fe^{3+} in the melt was reduced, the reduction rate of both charges exhibited identical results. This was attributed to the reduction characteristics of the 2nd phase where the Fe^{2+} reduction is the rate limiting factor. This identical behaviour of magnetite with respect to hematite showed the potential of bath smelting process with respect to solid phase reduction process. In other words, the characteristics of low reduction rate in the case of magnetite, as a solid phase, disappeared in the molten phase process by the usage of the H_2 plasma. This obviously widens the range of ore selection when up-scaling process is considered.

7.5.6 Reduction of pre-reduced ore

A 69.43 % FeO and 28.14 % Fe_3O_4 pre-reduced ore was reduced in this set of experiments by H_2 to assess its reduction behaviour with respect to the Carajas ore. In the main phase of the conducted experiments, slight decreases in the reduction rates of ~7 % with respect to the Carajas ore were found. This slight deviation was attributed to the full conversion of Fe^{3+} to Fe^{2+} in the first phase of reduction (contrary to the hematite and magnetite experiments).

On the other hand, it was evident that the starting H_2 utilisation degree of 100 % was an unrepresentative result from a thermodynamic point of view. It is believed that this high value was due to the highly estimated $\dot{V}_{H_2O,corr.}$, equation (39).

7.5.7 Reduction with CO-H_2-Ar mixture and CO-Ar mixture

The objective of the CO experimental work was to assess the reduction rate of liquid iron oxide by CO under an Ar plasma atmosphere. The reduction rate was evaluated in the stable phase of the experimentation. This phase was characterised as the reaction between the CO and the divalent iron Fe^{2+} existing in the oxide melt. A first trial to derive experiments at low flow rates of CO up to 0.57 Nl/min in an Ar-H_2 mixture was carried out. H_2 was used as high enthalpy gas to sustain the current of the plasma at low values. However, due to the low CO supplied, the exact reduction contribution of CO against H_2 was not possible for reliable evaluation; higher reduction rates by CO in the experimental results were found in comparison to the equilibrium calculations. Another set of experiments at higher flow rates of

CO up to 3.5 Nl/min in an Ar-CO mixture was carried out and better results with respect to the equilibrium calculations were obtained.

Based on the experimental results, a specific reduction rate in the conducted experiments was calculated to be 1.09 x 10^{-1} kg-oxygen/m^2s. However, this reduction rate was corresponding to the results presented in section 7.4.8 where the calculated CO utilisation degree was slightly higher than the equilibrium one. This was attributed to the contribution of H_2O-$C_{electrode}$, reaction (22), in the reduction process. A correction to these additional reactions has been made to rule out the effect of the additional oxygen due to the reduction of H_2 and CO. This correction was approximated by subtracting the contribution from the gases based on their utilisation degree as conducted in the H_2 experiments. A corrected reduction rate for the conducted experiments was calculated to be 0.89 x 10^{-1} kg-oxygen/m^2s. The deviation, however, between both results was not so significant. Combining the work of Soma [37] for a CO reduction rate at 1600 ^oC with the current work at an average temperature of 2400 ^oC, an activation energy of 150 kJ/mol was calculated and a regression analysis of both works gave the following empirical equation:

$$ln\ r = 4.34 - 18059 / T\ (kg\text{-}oxygen/m^2s) \quad (75)$$

Where *r* is the specific reduction rate and T is the temperature in K.

By dividing the presented reduction rate results from H_2 with respect to those from the CO in the plasma region, a factor of 3.4 was obtained. This convergence in the reduction potential of both gases at high temperatures of the plasma is justified by the increasing diffusion coefficient versus temperature, where the influence of molecules mass is diminishing. A summary of these results with respect to the results of H_2 and CO at lower temperatures is given in figure 100.

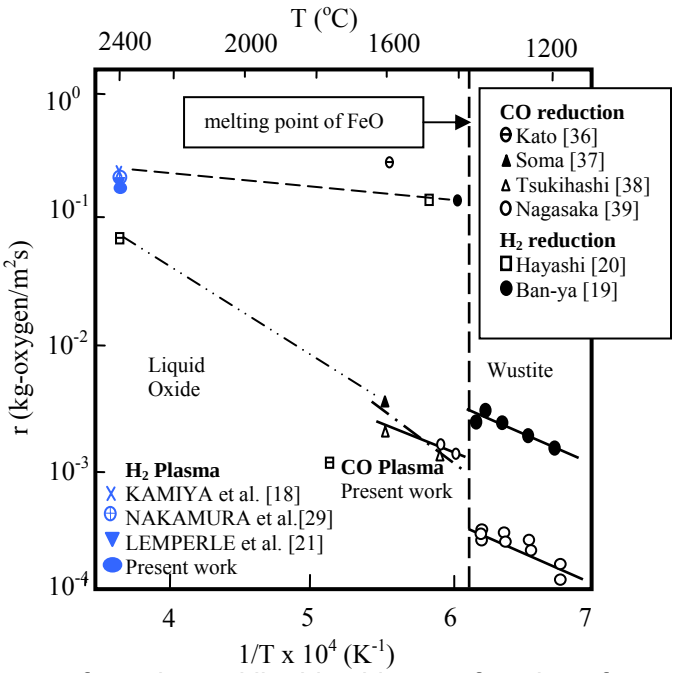

Fig. 100. Reduction rate of wustite and liquid oxide as a function of temperature, [34]

7.5.8 Reduction with CO_2-H_2-Ar mixture

In these series of experiments, the CO_2 flow rate was varied up to 0.5 Nl/min under an Ar-H_2 atmosphere. The results showed that the greater the CO_2 flow used, the larger the effect on the reduction retardation. However, such high flows for inlet CO_2 have been adopted to determine the relationship between the CO_2 flow and the reduction retardation whereas in an up-scaled process the concentration of CO_2/H_2 should be much less. Using the results obtained, the rate of the reduction drop (k) has been calculated. It was found that the drop rate at 1 atm CO_2 was 5.09 x 10^{-3} mole O cm^{-2} s^{-1} at the plasma temperature zone, (~2400 °C).

The influence of graphite electrode reactions was corrected in a similar manner to those of the CO experiments to give a corrected rate k of 6.73 x 10^{-3} mole O cm^{-2} s^{-1}. Another influence on the reduction process was the share of the water gas shift reaction, reaction (26). It took place in this series of experiments, where a partial shift of the supplied CO_2 and H_2 towards CO and H_2O was obtained at higher temperatures at the plasma-melt interface. In that sense, it should be noted that a slight share of the reduction retardation was due to the replacement of H_2 by the lower potential reducing CO in the reduction process. The influence of this water gas shift reaction was corrected by calculating the amount of contributing CO (from the equilibrium point of view) and its corresponding reduced amount of oxygen. A net drop in the reduction rate at 1 atm CO_2 was found to be 4.91 x 10^{-3} mole O cm^{-2} s^{-1}.

Figure 101 shows the rate constant for the reduction drop (log k) as determined in the present work, -2.32 mole O cm^{-2} s^{-1}.atm^{-1}, with respect to the apparent rate constants of the oxidation of iron oxide by CO_2 at low temperature ranges, which were presented by Li [85]. By extrapolating the straight line in the figure further up to the plasma temperature (~2400°C), it is clear that the published results are in good agreement with the present work.

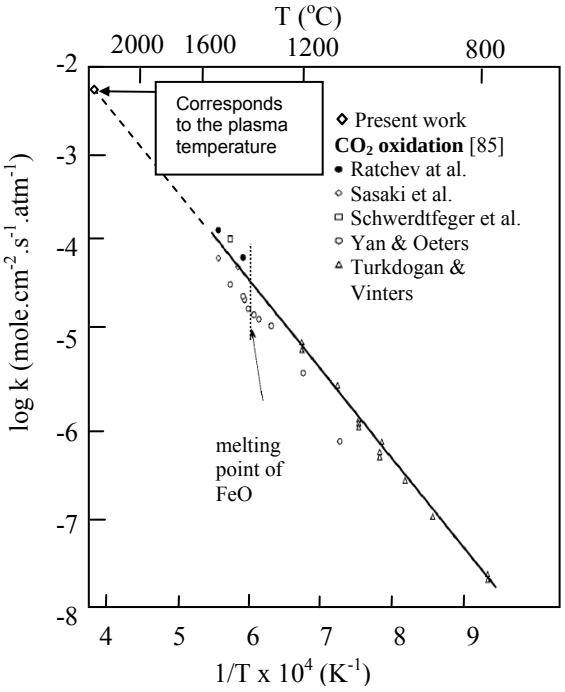

Fig. 101. Comparison of the apparent rate constants for the oxidation of liquid iron oxide by CO_2 with results from the H_2-CO_2 reduction experiments, [34]

7.5.9 Reduction with H_2O-H_2-Ar mixtures

A relationship between the H_2O supplied in a H_2O-H_2-Ar mixture and the reduction rate of the molten iron oxide by H_2 was investigated. Contrary to the CO_2 experiments, discussed in the last section, no H_2O influence has been monitored. This discrepancy between H_2O and CO_2 in the reduction behaviour was firstly attributed to the less negative influence of H_2O on the reduction behaviour of H_2 against that of CO_2, as clarified from the equilibrium point of view in section 6.1.5 Secondly, a significant contribution of the generated gases (H_2 and CO) that stemmed from the H_2O-$C_{electrode}$ reaction, reaction (22), in the reduction of the oxide melt as ,an additional reducing gases beside the supplied H_2, took place.

Quantification of the generated gases was carried out to justify the difference in reduction behaviour between H_2O and CO_2. It should be mentioned that in the case of full conversion of the inlet H_2O or CO_2 to the generated gases, a value for the $(CO+CO_2)_{off\text{-}gas}$:$H_2O_{inlet}$ ratio of

1 and $(CO+CO_2)_{off\text{-}gas}$:$CO_{2\ inlet}$ ratio of 2 are expected. However, from the averaged results at the same inlet flow of gases, a $(CO+CO_2)_{off\text{-}gas}$: H_2O_{inlet} ratio of 0.44 and $(CO+CO_2)_{off\text{-}gas}$:$CO_{2\ inlet}$ ratio of 0.16 were found. This means that H_2O is 2.75 times more likely to react with the graphite electrode than CO_2. This was clear evidence to indicate the significant contribution of the H_2 and CO in the reduction experiments of H_2-H_2O.
Looking at the previous work done on the kinetics of oxidation of the graphite material by CO_2 and H_2O was carried out to analyse the above mentioned reactions. It was found that the rate constant at 1500°C of the H_2O reaction compared to that of CO_2 is slightly greater by a factor of about 1.35 for He as a carrier gas and is approximately equal in the case of Ar, [86]. This has indicated that the molecular diffusion was a primary transport mechanism and that the kinetics of H_2O-$C_{electrode}$ reactions might further develop at different circumstances like carrier gas compositions and temperature.

It should be mentioned that despite the finding that almost half the inlet H_2O did not react with the electrode, the negative effect of H_2O on the reduction has not been observed at the shown range for inlet H_2O. However, it is believed that at higher flows of H_2O, deterioration in the reduction rate would appear. In that sense, limitations in the plasma power supply and evaporator capacity should be considered.

7.5.10 H_2 - Ar reduction with coke additions

Coke was mixed with the ore fines in a series of experiments (batch wise) to assess its reduction behaviour. The coke showed a fast reduction rate in the first period of the experiments which slowed down as soon as the coke was consumed. In other words, a stable phase for coke reduction evaluation was not attainable. On the other hand, slag foaming was not observed even during the first period of reduction where CO development in the off-gas was relatively high. It is believed that the reason for not attaining foaming in the slag was the low viscosity of the slag (FeO rich slag).

To evaluate the coke reduction rate in a stable phase, coke fines was fed continuously by a screw conveyor via the hollow electrode in H_2-Ar reduction experiments. Ruling out the usage of H_2 in these experiments, to evaluate individually the coke reduction behaviour, has not been adopted to avoid the transformer overheating (obtained by using low enthalpy gases like Ar). Over the stable phase, the total reduction rate was evaluated. The coke reduction rate was calculated by subtracting the amount of oxygen reduced by H_2 which was obtained from the H_2 experiments. It was found that 1.64 g /min of oxygen was reduced by the supplied coke of 1.33 g/min, i.e. O/C = 1.11. This ratio corresponds to an actual carbon

utilisation degree of ~ 55 %. It should be mentioned that using coarser grains of coke could decrease the reduction rate, where the interface area between the coke and the oxide melt might be a rate limiting factor.

Based on the experimental results, a specific reduction rate of the conducted experiments was calculated to be 9.19 x 10^{-1} (kg-oxygen/m^2s). By dividing this reduction rate result by that of H_2 in the plasma region, a factor of ~ 3 has been obtained.

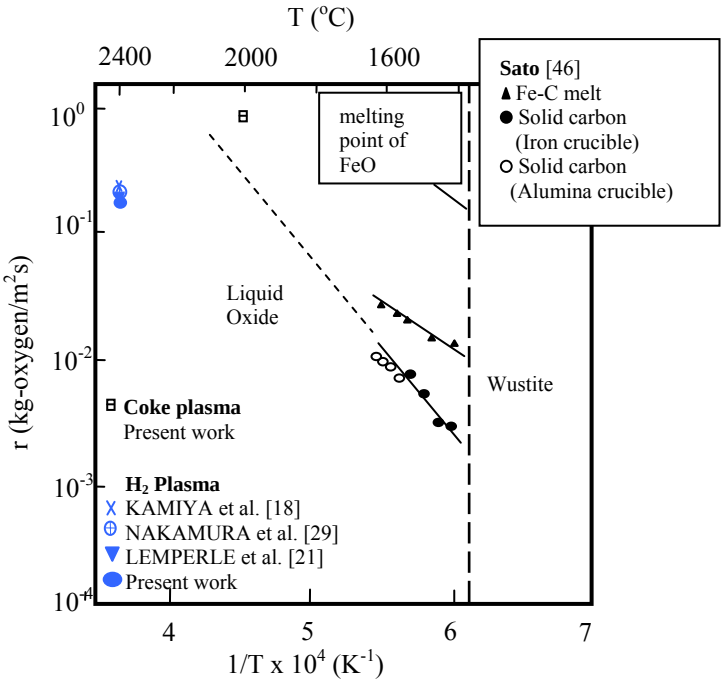

Fig. 102. Comparison of the reduction rates for coke plasma with respect to C melt and solid carbon

By extrapolating the published reduction rates at lower temperatures [46] to higher temperatures, some agreement with the present experimental result is observed, as shown in figure 102. However, it should be mentioned that the evaluated experimental result is not completely reliable. This is due to the rough assumption that the reaction took place at the plasma-melt interface, where the exact reaction area between the coke and oxide melt could not be figured out. A lower operating temperature of 2000 °C with respect to that of H_2 plasma (~2400 °C) was selected in the figure. This is due to the fact that the coke can react at lower temperatures within the whole bulk of the oxide melt. In summary, coke has a good reduction potential with respect to H_2 at higher temperatures. Furthermore, no plasma deterioration was witnessed during coke continuous feeding.

7.5.11 H_2 - Ar reduction of continuous fed ore

In the current series of experiments, the continuous feeding of fines ore instead of charging it in the crucible before the experiments was carried out. One of the most important findings in the current experiments was the plasma stability despite the ore feeding via the hollow electrode, where the plasma gas had its own pattern which was separate from that of the fines ore. The phenomenon of two separate patterns was attributed to the high viscous characteristics of the plasma. A greater reduction rate with respect to the batch wise experiments was also observed due to the continuous feeding of the ore which led to a higher Fe^{3+}/Fe^{2+} ratio in the oxide melt. Examining the slag analysis, the concentration of Fe^{3+} in the continuous feeding experiments was almost identical to that of the batch wise. This was against the expectations of higher Fe^{3+} in the slag in the case of the continuous feeding of ore. However, this was attributed to the H_2 potential in reducing most of the Fe^{3+} in the ore fed at the given ore feeding rate.

From the results obtained, an increase in the reduction rate of approximately 20 % was found. However, the larger quantities of H_2O produced obviously led to a higher reaction rate of the H_2O – $C_{electrode}$ and consequently to more generated gases (CO, H_2) as was observed in section 7.4.12. By ruling out the generated gases contribution via a correction term, as practiced in section 7.5.1, an increase in the reduction rate of almost 10 % was calculated.

7.5.12 Experimental results overview

The conducted experimental program was characterised by comprising wide range of process parameters, i.e. fines ores, reducing agents, reducing gas injection port, batch wise / continuous feeding. As main outcomes of the experiments, the specific reduction rates, the reduction potential of each test run with respect to the standard H_2 experiment and the gas utilisation degrees were summarized in table 11. Examining CH_4, CO and coke, it was worth finding that their reduction potentials with respect to H_2 are 3.5, 0.35 and 2.97 respectively. On the other hand, the oxidation effect of CO_2 was evident from the experimental results and the gas utilisation degrees whilst this effect did not appear in H_2O experiments. A summary of the specific reduction rates of the conducted experiments is also plotted in figure 103.

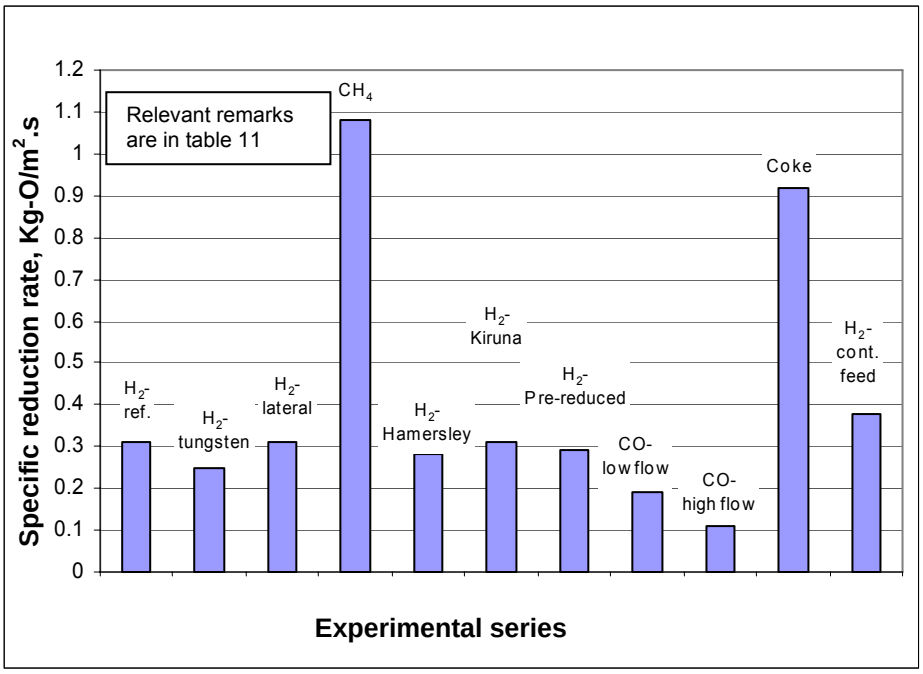

Fig. 103. Summary of the specific reduction rates of the conducted experiments

experiment #	Fines ore	Reducing agent	Specific reduction rate, kg-O/m^2.s	Reduction potential factor with respect to H_2 (1a)	Gas utilisation degree	Remarks
1a	Carajas	H_2	3.10×10^{-1}	1	ηH_2: 32 %, $\eta_{tot.}$: 48 %	reference (with graphite electrode)
1b	Carajas	H_2	2.5×10^{-1}	0.83	ηH_2 : 40 %	with tungsten electrode
2	Carajas	H_2	3.10×10^{-1}	1	ηH_2: 32 %, $\eta_{tot.}$: 48 %	lateral supply of H_2
3	Carajas	CH_4	1.08	3.5	ηH_2: 30 %, ηC: 70 %	reduction factor increases to 4 when carbon contribution, from the electrode, is ruled out in CH_4 and H_2 (1a) experiments
4	Hamersley	H_2	2.8×10^{-1}	0.9	ηH_2: 26 %, $\eta_{tot.}$: 45 %	average results without CaO additions
5	Kiruna	H_2	3.1×10^{-1}	1	ηH_2: 32 %, $\eta_{tot.}$: 48 %	magnetite reduction rate is identical to that of hematite
6	Pre-reduced LKAB	H_2	2.9×10^{-2}	0.93	ηH_2: 27 %, $\eta_{tot.}$: 45 %	corresponds to the reduction rate of Fe(II) - H_2
7	Carajas	H_2-CO	1.9×10^{-1}	0.61	ηCO (calculated) : 25 %	results correspond to CO reduction only, ηCO was higher than equilibrium calculations due to low flow rates of CO
8	Carajas	CO	1.1×10^{-3}	0.35	ηCO (calculated) : 18 %	ηCO (calculated) : 15 %, when carbon contribution, from the electrode, is ruled out
9	Carajas	H_2 (under supply of CO_2)	-	-	ηH_2: 22 %, $\eta_{tot.}$: 24 % (at maximum applied CO_2 flow: 0.5 Nl/min)	Rate of oxidation due to supplied CO_2 : 4.91×10^{-3} mol O/ bar.cm^2.s
10	Carajas	H_2 (under supply of H_2O)	-	-	ηH_2: 20 %, $\eta_{tot.}$: 50 % (at maximum applied H_2O flow: 0.5 Nl/min)	Rate of oxidation due to supplied H_2O: not witnessed in this range of supplied H_2O
11	Carajas	H_2-Coke	9.20×10^{-1}	2.97	ηC (calculated) : 55 %	results correspond to coke reduction only
12	Carajas	H_2	3.77×10^{-1}	1.22	ηH_2: 32 %, $\eta_{tot.}$: 60 %	Continuous feeding of ore

Table 11. List of the experimental results

8 Up-scaling of the H_2/CH_4 plasma process

8.1 Introduction

The demand for new technologies in steelmaking, to meet environmental and economic concerns, has recently increased. Iron making as well as being a major energy and resource consumer is also a major CO_2 producing process during the steel production. Therefore, the idea of directly smelting iron ores in a furnace avoiding the cost intensive process steps of ore agglomeration, coking and sintering have shown high potential for further research and development. In that sense, the concept of up-scaling the H_2/ CH_4 plasma smelting reduction (HPSR / MPSR) have been explored in the research program ULCOS [4]. A conceptual design for an up-scaled steel production process of 1Mt/y was conducted by presenting a relevant flow-sheet and a corresponding heat and mass balance.

8.2 Process flow-sheet

Optimisation of the HYDROMET flow-sheet that was presented by Wiesinger [87] was carried out as a first step in the current up-scaling study. The flow-sheet basically comprised an iron ore pre-heater/pre-reduction unit and a smelting reactor and other units as explained below, figure 104.

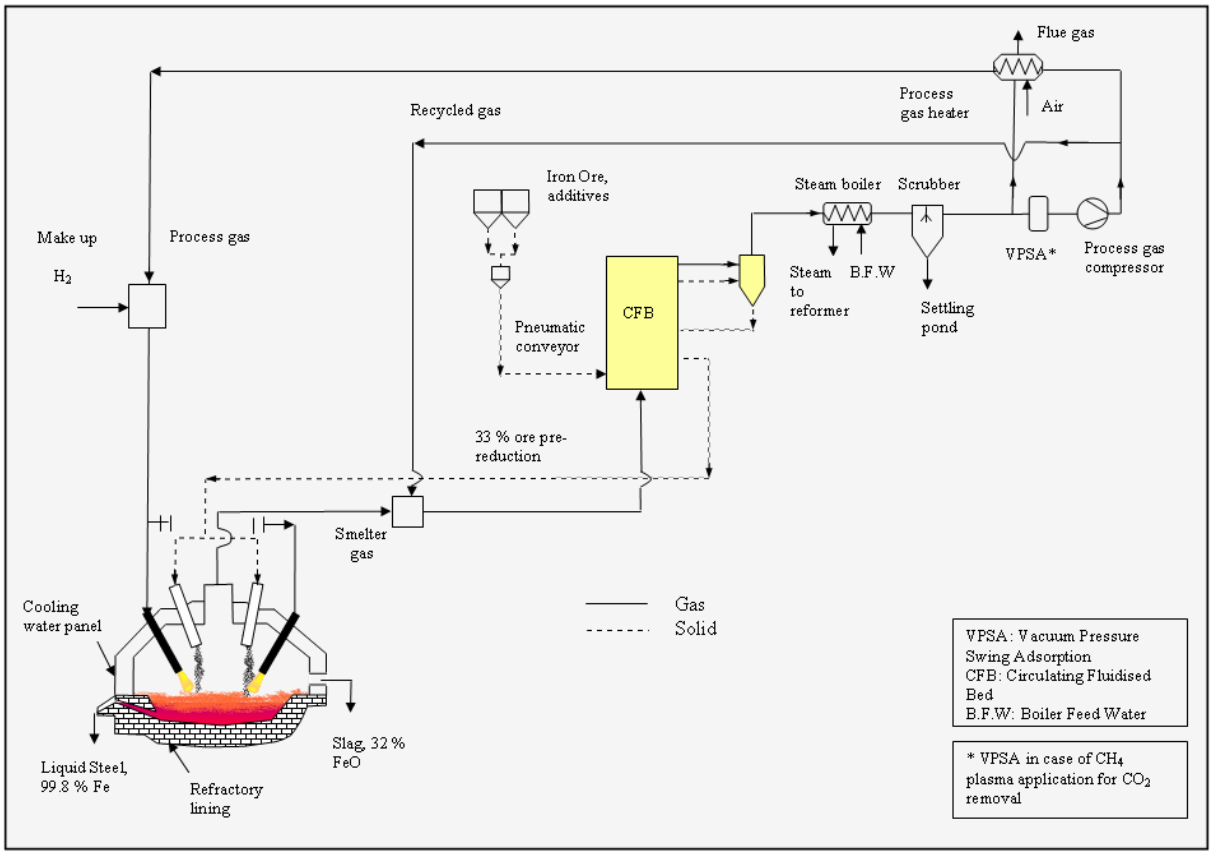

Fig. 104. Hydrogen Plasma Smelting Reduction Process, HPSR

8.2.1 Iron ore pre-heater

An iron ore fines pre-heater has been adopted despite the whole reduction process could be conducted at higher reduction rate at the molten phase in the smelter. However, the strength of choosing a pre-heater is to utilise the significant sensible heat of the smelter off-gas and minimise the energy input to the system.

According to the flow-sheet, iron ore fines are preheated prior to feeding them into the smelting reactor. The selection of the CFB principle is adopted as it showed successful operation on a semi-commercial basis, [88]. The circulating fluidised bed (CFB) system consists of a reactor, a recycle cyclone and two stage venturi pre-heater with the necessary gas/solids separation cyclones. The pre-heating will take place in the circulating fluidised bed reactor to dry and calcine the material, and pre-reduce the ore fed. The highly possible achieved pre-reduction degree (33 % in the current case) within this type of fluidised bed (CFB) is due to the high slip velocity attained (difference between the gas and particles velocity). This high slip velocity renders great heat and mass transfer rates which is much higher than that showed in a bubbling fluidised bed and transport reactor.

8.2.2 Smelting reactor

The reactor is chosen with a refractory lining within the hearth and a water cooled free board. The refractory hearth contains a metal bath and above it a layer of slag. Envisaging an approximate diameter for the reactor, the relationship between the electrode diameter, minimum pitch circle diameter and the applied current of the AC-EAF has been adopted in the diameter calculations. The limiting factor in that sense is the irregular interference between the arcs electromagnetic forces. A diameter of 6 - 7 m and an overall height of 3.3 m are found relevant for the process. No stirring facility is planned in the flow-sheet due to the satisfactory effect of the plasma impulse. However, a closer investigation of the implementation of a stirring facility might be useful. The advantage of stirring in that sense is to increase the amount of splashed slag on the water cooled free board and accordingly utilise it as a self liner.

8.2.3 Electrical energy

Electrical energy is supplied by separate DC power supply units over non-cooled hollow graphite electrodes. The advantage of the graphite electrodes is the characteristic high power capacity in comparison to the water cooled plasma torches. The DC plasma is

maintained under transferred arc mode and connected to the bottom anode via the melt. The electrodes, cathodes, are side positioned (inclined) to increase the view factors from the plasma arc and accordingly improve the net heat flux via radiation to the bath. However, due to the immaturity of the current plasma technologies with graphite electrodes, maximum permissible energy transferred per electrode could not be defined. Nonetheless, a figure between 3 and 6 electrodes (based on the permissible energy) is adopted.

8.2.4 Feeding of fines ore

Feeding of the pre-reduced ore is conducted through feeding pipes that are distributed evenly across the roof. In the case of a vertical oriented electrode, the feeding process can be carried out through the hollow of the electrode as proven by the experimental work or through fixing a plasma jacket around the electrode and feeding the pre-reduced ore through the annular space between them. The advantage of feeding the pre-reduced ore through the electrode or around it is the possibility to deliver it to the hottest areas, possible in-flight reduction and the decrease of the heat load to the furnace walls.

8.2.5 Reducing gas

H_2 rich gas is supplied to the smelter via the hollow electrodes. H_2 will be produced by a steam reformer due to its advanced state of the art in terms of cost effectiveness and production capacity compared with the other existing alternatives like oil partial oxidation and coal gasification. In that sense, H_2 temperature has been accordingly set at 760 ^oC. However, it should be mentioned that CH_4 has great potential to be used as an alternative to H_2 as a reducing gas. The strengths of CH_4 against H_2 will be described later in this chapter.

8.2.6 Products

The carbon free liquid iron produced by the process is batch tapped approximately every 1 hour while the slag is tapped every 5 hours due to the low quantity of generated slag. The steel produced can be post treated in the secondary metallurgy to remove dissolved hydrogen and oxygen to the required limits. The slag as an FeO containing product can also be used as a valuable material (without free CaO) in road construction work.

8.3 Process description

8.3.1 Operation parameters

The feed materials (fines ore and lime additives) are heated to 700 °C and reduced up to 33 % (wustite). The pre-reduced ore is subsequently fed to the smelter, where it is heated to 1600 °C and reduced up to an iron yield of 98 %. To fulfil high iron yields and low FeO content in the slag, a clear drop in the H_2 utilisation degree is attained. The negative consequence of having a lower H_2 utilisation degree is obviously the necessity to recycle more H_2 in to the process.

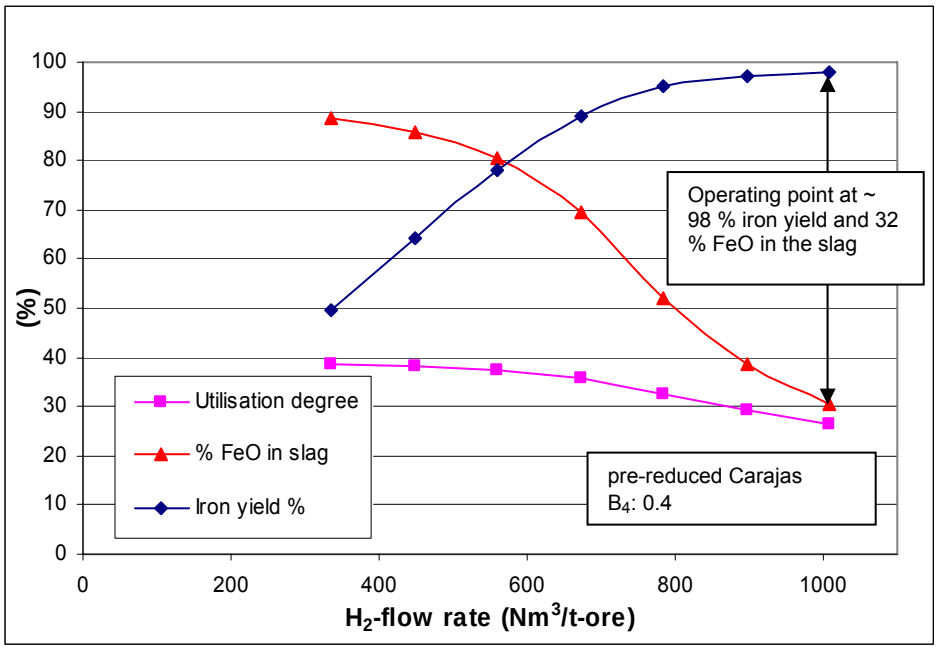

Fig. 105. H_2 flow rate versus the iron yield, % FeO in the slag and the utilisation degree

Figure 105, calculated by the Factsage program [9], was presented to simulate the changing behaviour of various parameters in the smelter by increasing the supplied H_2 per the pre-reduced ore contained in 1 ton of Carajas and the corresponding inlet additives. It is clear from the figure that by fulfilling the required figures of iron yield and FeO content in the slag, at the operating point, the amount of supplied H_2 should increase to 1000 Nm^3/t-ore. The H_2 utilisation degree will subsequently decrease to approximately 26 %.

Mass balance to the up-scaled process was conducted to study the impact of varying the process parameters on the process outcomes. From the mass balance, the required specific ore and the generated specific slag versus the iron yield were calculated as shown in figure 106. The influence of increasing the iron yield up to 98 % on decreasing the required specific ore and slag to 1.52 t/t and 0.08 t/t respectively is evident. Furthermore, the slag

basicity, B_4, was varied to study its impact on the FeO content in the slag and the generated specific slag. It is clear from figure 107 that by increasing B_4 up to 1, the FeO content in the slag decreased to only 26 %.

Despite the lime additives showing a positive contribution in phosphorous removal, as witnessed earlier on in the experimental chapter, it was preferred to operate the process at low basicity as justified in the slag diagram calculations in section 6.2. The potential of working at low basicity is firstly to decrease the negative effect of lime on the reduction rate as also clarified in the experimental chapter, secondly to decrease the slag quantity to save the input energy that would be consumed by the extra slag. Back to figure 107 at a chosen basicity (B_4=0.4), a slag quantity of 81 kg/t-steel and 32 % FeO in the slag was obtained. The slag generated is generally much less than that of the blast furnace (250 kg/t-hot metal).

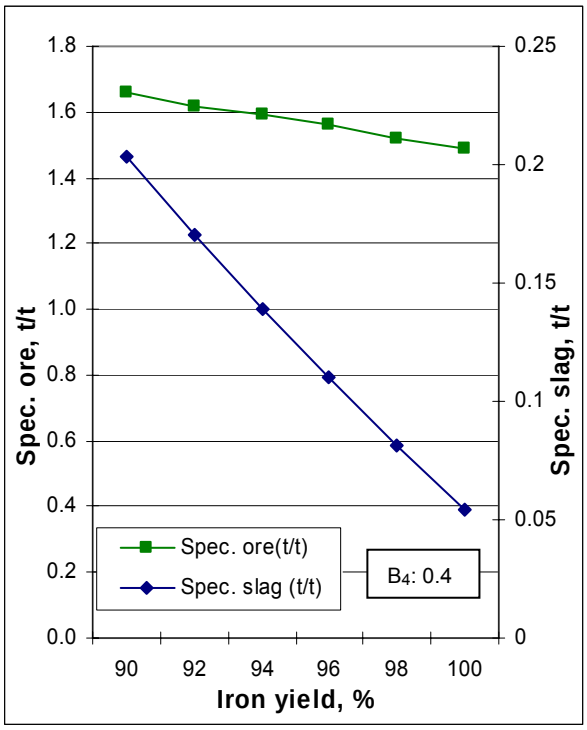

Fig. 106. Iron yield versus the specific ore, and the specific slag

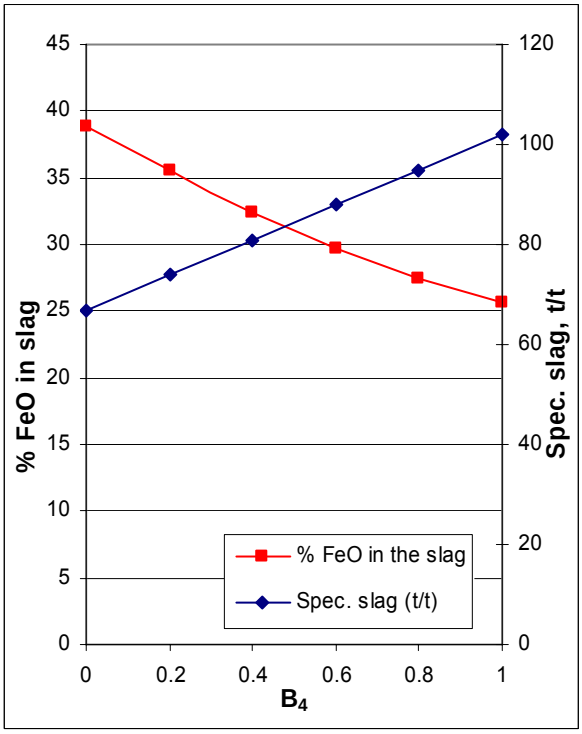

Fig. 107. Slag basicity (B_4) versus % FeO in the slag and the specific slag

8.3.2 Flow-sheet

It is clear from figure 104 that the feed materials are fed to the pre-heater by a pneumatic conveyor. Pre-heater inlet gas preheats and partially reduces the fines ore. Moreover, calcination of the lime added is partially carried out in the pre-heater. The top gas (outlet gas from the pre-heater) goes to a boiler to make use of its sensible heat. The steam generated from the boiler can be utilised as a reactant in the steam reformer for the further production of H_2. The top gas is then washed in a scrubber to get partially rid of the formed steam and

clean the gas from the accompanying dust. The exit water is conveyed by pipe lines to a settling pond. After that, a small portion of the gas is exported to the atmosphere. The objective of this export gas is to limit the enrichment of the top gas by the produced CO and CO_2 that stem from the graphite electrode and calcination reactions. Furthermore, air is injected to the export gas in order to burn the contained combustibles. The subsequent heat produced will be utilised through a process gas heater.

The process gas (top gas after being washed and compressed) is then split in two branches. The first branch is mixed with the smelter off-gas to cool down the temperature of the pre-heater inlet gas to ~ 900 ^{o}C in order to avoid ore sticking problems. The second branch is heated by the process gas heater through combusting the exported gas. It is then mixed with the make-up H_2 to be fed through the hollow electrode to the smelter.

In the context of the ULCOS project [4], a heat and mass balance model was developed based on an iron productivity of 1 ton at Corus (research and development department). This iron making model, called IRMA [89], was developed to compare the outcomes of various smelting reduction processes. Calculations were based on a mix of thermodynamic equilibrium and empirical relationships.

The model has used the previously shown flow-sheet and the operation parameters stated in section 8.3.1 to build the total process from simple building blocks, figure 108. A total electrical energy of 3703 MJ/t-steel and feed H_2 of 690 Nm^3/t-steel were required as found from the model. It should be mentioned that the results obtained were under the conditions shown in table 12.

		Assumption	**Remarks**
1	**Heat losses of the smelter**	15 % of the electrical energy input	the assumed figure is less than that found in the publications for Ar plasma [55,60]
2	**Heat losses of the pre-heater**	16.5 % of the electrical energy input	unreliable assumption where the ore pre-heater heat losses should be much less
3	**Boiler energy**	19 % of the electrical energy input	the energy produced has not been utilised in the process
4	**Water removal unit**	100 % of water is removed	provided that a VPSA unit will be used after the scrubber to adsorb the rest of the steam

Table 12. Set assumptions

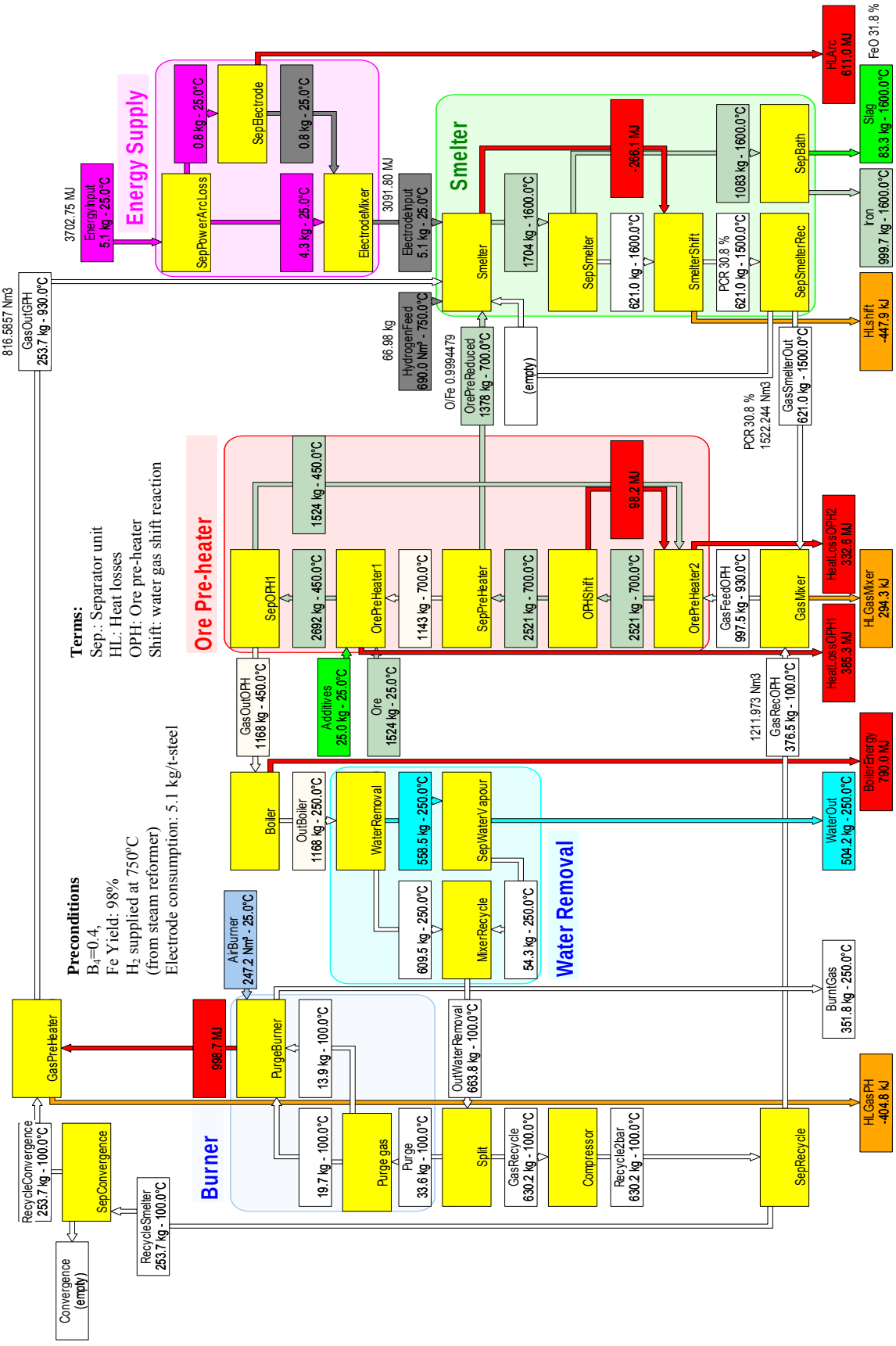

Fig. 108. HPSR heat & mass balance, IRMA model

8.3.3 Process parameters

From that model and preliminary assumptions, a list of the prospective process parameters for 1 Mt/y steel was obtained as clear in table 13.

				Nominal	Reference & Comments
Capacity			----		
Productivity	Annual Production		kt/y	1,040	
	Steel productivity		ton/h	125	to meet the 1 Mt/y
	Capacity per day		ton/d	3,000	
Availability	Scheduled repairs		%	2.5%	assumption
	Unscheduled repairs		%	2.5%	assumption
Principal data	Operating pressure		bar abs	2	no pressure preference
	Number of tap holes		-	2	metal , slag
	Number of electrodes		-	4	assumption, choosing less number of electrodes entails higher operating current and voltage which might not be possible for normal sized hollow electrodes
	Electrical power per electrode		MWh	36	calculated, corresponding to a voltage of 600 V and current of 60 kA
Dimensions	Diameter at metal bath level		m	6.40	calculated based on the chosen # of electrodes and considering the minimum permissible pitch circle diameter to avoid arc interferences
	Diameter at slag level		m	6.40	
	Top metal bath elevation		m	0.80	assumption
Metal bath	Volume		m^3	17.75	
		Height	m	0.80	referring to metal bottom level
		Metal residence time	h	0.99	
		Mass	t	124.25	
		Surface area bottom	m^2	65.12	
		Surface area walls	m^2	6.03	
	Temperature		°C	1600	
	Heat losses		----		
		Heat flux	kW/m^2	10	assumption, based on EAF
		Heat loss	MW	0.71	
Slag layer		Slag volume	m^3	16.08	
		Slag height	m	0.50	assumption
		Slag density	t/m^3	3.50	assumption
		Slag mass	t	56.30	
	Temperature		°C	1600	
	Heat losses		----		
		Heat flux walls	kW/m^2	100	assumption, based on EAF

Table 13, Process Parameters

				Nominal	Reference and comments
Freeboard		Surface area walls	m^2	10.05	
	Volume		m^3	74.79	
		Height	m	2.00	**assumption**
	Temperature		°C	1500	
	Heat losses		----		
		Heat flux walls	kW/m^2	500	**assumption, to agree with the total heat losses set in the model**
		Surface area walls	m^2	40.21	
		Heat loss walls	MW	20.11	
Self lining (Freeboard)	Thickness		mm	7.65	**calculated via the conduction heat transfer law at the solidus temperature of the slag obtained (T: 1057°C), T_{stave}: 100°C and 500 kW/m^2**
Inputs					
Reductant		Type	-	H_2	
		Temperature	°C	760	**steam reformer**
		Consumption	Nm^3/t-steel	690	
Electrical Energy			MJ/t-steel	3702	**~ 1.03 MWh/t-steel**
			MWh	144	**Energy needed for the hourly production, assuming 90 % electrical supply efficiency (~1.15MWh/t-steel)**
Burden	Ore (type)		-	Carajas	
		Temperature	°C	25	
		Consumption	kg/t-steel	1524	
Flux	Type		-	Lime	
		Temperature	°C	25	
		Consumption	kg/t-steel	25	
Outputs					
Hot Metal production	Temperature		°C	1600	
	Composition		----		
		Fe	%	99.78	
		Others	%	0.22	
Slag production			kg/t-steel	80.87	
	Temperature		°C	1600	
	Composition		----		
		CaO	%	15.87	
		MgO	%	1.21	
		SiO2	%	16.6	
		Al_2O_3	%	25.22	
		FeO	%	32.37	
		MnO	%	6.09	

Table 13, Process Parameters, cont.

				Nominal	Reference and comments
Slag production	Basicity (2) CaO/SiO_2		-	0.96	
	Basicity (4)			0.41	assumption, above solidification zone
Process gas	Temperature		°C	930	Before being mixed with inlet H_2
	Composition		----		
		CO	%	8.58	
		CO_2	%	5.25	
		H_2	%	82.97	
		H_2O	%	3.16	
	Volume		Nm^3/t	816	
Cooling losses overview	Heat flux				
		Metal bath	kW/m^2	10	
		Slag zone	kW/m^2	100	
		Freeboard zone	kW/m^2	500	
	Surface area		m^2		
		Metal bath	m^2	71.15	
		Slag zone	m^2	10.05	
		Freeboard zone	m^2	40.21	
	Heat loss				
		Net heat losses	%	15.18	of the input electrical energy
	Heat loss fractions				
		Metal bath	%	3.26	heat losses by each zone divided by the total heat losses
		Slag zone	%	4.61	
		Freeboard zone	%	92.13	

Table 13. Process parameters, cont.

It is clear from the table, that a total heat loss of 15 % was adopted in the model. It should be noticed the heat losses via radiation in the freeboard are almost two times higher than the set assumptions as generally found in the published modelling work, [55,60]. However, not enough published work has examined the quantification of the heat brought back to the bath via wall radiation to the melt. Moreover, it is debated how long the self lining refractory would be sustainable at this high heat flux especially as the thickness of the self lining could drop to less than 10 mm as shown in table 2.

8.3.4 Methane plasma

The model has been adapted to use CH_4 instead of H_2 as an alternative reducing gas. The corresponding flow-sheet is attached in the appendix while the process parameters in terms of make-up gas, electrical energy and smelter gas are presented in table 14. As a result of the significant amount of CO and CO_2 produced by the CH_4 reduction process, a CO_2

separation unit (with separation up to 97 %) has been installed after the scrubber to minimize the negative impact of these gases on the reduction process. Vacuum pressure swing adsorption (VPSA) technology is adopted for H_2O and CO_2 separation due to its potential advantage with respect to the chemical absorption technology in terms of cost effectiveness and ease of operation. H_2O and CO_2 are separated over one adsorber with a layered bed where H_2O is firstly adsorbed and then CO_2. However, operating an adsorption unit entails a low temperature (less than 50^oC) and high pressure (more than 4 bar abs.), [90]. It should be noticed that these operating parameters have not been considered in the conducted flow-sheets.

It is clear from the table that the consumed electrical energy in the methane plasma is higher than that of the hydrogen plasma process. This was due to the required additional energy for the methane cracking. The CO_2 emissions were also high due to the usage of carbon containing methane as a reducing agent. However, the CO_2 emissions showed significant lower values in comparison to that of the BF-BOF route (1850 kg-CO_2/t-steel).

	H_2 plasma	**CH_4 plasma**
Make-up gas, Nm^3	690	157
Electrical Energy, kWh	1030	1440
*CO_2 emissions, kg	29	345
Gas volume (smelter outlet), Nm^3	1522	924

*: CO_2 emissions resulting from the production of electricity are not considered

Table 14. H_2/CH_4 plasma process parameters corresponding to 1 ton of steel produced and approximately 30 % FeO in the slag

Beside the simplicity of the CH_4 plasma flow-sheet due to the saving of the steam reformer, the significant saving in the off-gas volume produced from the smelter is counted as an additional advantage. However, the problems encountered with the CH_4 usage (the behaviour of the carbon soot and carbon deposition) have to be assessed furthermore in a bigger reactor.

8.4 SWOT analysis

From the conducted up-scaling work, some advantages were presented like the obvious low CO_2 emissions, flow-sheet simplicity and low slag produced. However, some weaknesses have been determined as clarified in the SWOT (Strengths-Weaknesses-Opportunities-Threats) analysis, figure 109. Further development through a pilot plant is therefore quite sensible to improve our perception of the process and find out mature solutions for the weak points raised. One important issue to tackle is the investigation of a proper reactor lining (refractory / cooling system), under the influence of the high heat flux in the freeboard zone and the high FeO content in the slag.

Strengths	**Weaknesses**
▪ Low CO_2 iron making process ▪ Simple flow-sheet ▪ Carbon free product ▪ Low slag generation ▪ Non post combustion process	▪ High radiation to the furnace walls (non foaming slag process) ▪ Slag aggressiveness to the refractory due to its high FeO content ▪ Necessity of a gas tight operation ▪ High cost of hydrogen/methane versus coal as a reducing agent
Opportunities	**Threats**
▪ Dedication to breakthrough steel making technologies for CO_2 mitigation ▪ Dedication to eliminating coke ovens, sintering and pelletizing plants ▪ Hybrid application with coal-oxygen injection	▪ Existence of more mature coal based smelting processes with satisfactory CO_2 mitigation results and advanced state of development ▪ Immaturity of the existing transferred arc plasma technologies in steel processing

Fig. 109. SWOT analysis

From the SWOT analysis, a sum-up of the characteristics of the process has been carried out. Some opportunities have become evident to develop the process due to the CO_2 mitigation policies while the advanced progress of other coal based smelting processes and the immaturity of the plasma production have hindered further development of the process.

9 Conclusion and future work

9.1 Conclusion

The objective of the present work was to introduce a fair concept of the characteristics of hydrogen based smelting process using plasma technology. Better understanding of the process characteristics (thermodynamics and kinetics) was obtained by a series of experiments adopting various reducing agents like H_2, CH_4, CO and coke for the reduction of mainly hematite fines ore (Carajas). Moreover, CO_2 and H_2O gases were used in a mixture of H_2-Ar to study their influence on the ore reduction rate. An investigation of the plasma stability under the continuous feeding of ore through a hollow electrode was also carried out. A conclusion of the work conducted is summarized as following:

- Reduction experiments of Carajas ore by H_2 with a tungsten electrode were conducted and showed less reduction rate with respect to those experiments done using graphite electrode, i.e. approximately 20 % less reduction rate. The obtained 40 % utilisation degree of hydrogen, in the case of the tungsten electrode experiments, conforms to the FeO-H_2 equilibrium calculations rather than that of FeO-H or FeO-H^+.

- An empirical equation was derived statistically for the work published on the reduction rates of molten iron oxide using H_2 at low temperatures (just above the melting point of FeO) and that done by hydrogen plasma (~ 2400 ^oC) to show:

  $ln\ r = -0.15 - 2811 / T$ *(kg-oxygen/m^2s)*

  Where *r* is the specific reduction rate and T is the temperature in K.

- Hydrogen was partially fed via a ceramic lance, rather than through the hollow electrode, in a series of experiments to decrease the amount of hydrogen dissociated via the plasma and examine the reduction potential of molecular hydrogen. The results agreed completely with those experiments supplying hydrogen only through the electrode. This finding confirms the first conclusion: H and H^+ do not influence the reduction process. Secondly, these experiments show the possibility to partially feed the reducing gases in separate pipes rather than being totally fed through the hollow electrodes. This possibility would be important in the case that the reacting area (melt-plasma interface) turned to be a rate limiting factor.

- CH_4 showed, in general, high reduction rate of the iron ore with respect to H_2, i.e. 3.5 – 4 times that of H_2. Although there was deposited carbon observed inside the hollow electrode and carbon soot formation, it is believed that these phenomena will be diminished when the up-scaling process is considered. In that sense, CH_4 will be a potential alternative to H_2 where the burden of H_2 production will be ruled out and less gas volume compared to that in the case of hydrogen process will be handled.

- The positive influence of CaO additions to the ore on the phosphorus stability in the slag was proven in a series of experiments. A minimum phosphorous content of 0.004 % in the metal was found at a slag basicity of B_2 = 2.5. However, further investigation has to be done to study the feasibility of the phosphorous removal in the plasma reactor, rather than in a separate reactor. An obvious importance of the CaO additions (except for phosphorous removal) is not observed, where fluxing the slag with high amounts of CaO is not as meaningful as found in section 6.2.

- Magnetite ore (Kiruna) and pre-reduced ore (reduced almost to FeO at “LKAB”) were used in two series of experiments for comparison purposes with the used hematite ore (Carajas). In the pre-reduced LKAB experiments, an agreement with the results of Carajas experiments, but with slight less reduction rates, was observed. This slight difference was due to the effect of the retained Fe^{3+} that existed in the stable phase of Carajas experiments. In the case of Kiruna experiments, the influence of morphology, as expected, did not take place. This is a significant advantage, when up-scaling process is considered, where wider range of ore can be selected.

- To study the up-scaling potential of the hydrogen based smelting reduction process within ULCOS project; the details of the proposed flow-sheet were described. Moreover, a heat and mass balance, based on 1 ton liquid steel, using Corus designed model was carried out. Expected low CO_2 emissions in both H_2 and CH_4 plasma process were found. However, complete removal of CO, CO_2 and H_2O in the system could not be achieved. Moreover, FeO content in the slag, even at a set high iron yield of 98 %, will be relatively high, i.e. ~ 30 % FeO.

- The experimental results obtained in the reduction of Carajas ore by CO under Ar plasma atmosphere showed values that are in the same order of magnitude with that of H_2 plasma, i.e. reduction rate by H_2 plasma is approximately 3 times that of CO plasma. While the reduction rate of liquid iron oxide using H_2 at lower temperatures

(above the melting point of FeO) is almost two orders of magnitude faster than CO, as found in the literature. This means that the increase of the reduction rate using H_2 is less compared to CO with increasing temperatures. This convergence in the reduction potential of both gases at higher temperatures is due the higher rate of increase of CO diffusion coefficient with respect to that of H_2.

- An empirical equation was derived statistically for the work published on the reduction rates of molten iron oxide using CO at low temperatures (above the melting point of FeO) and that done by CO plasma (~ 2400 ^oC) to show:

  $ln\ r = 4.34 - 18059 / T$ *(kg-oxygen/m^2s)*

  Where *r* is the specific reduction rate and T is the temperature in K

- The reduction rates of Carajas using a mixture of H_2-CO_2-Ar were evaluated through a series of experiments. Reduction retardation was obtained due to the supply of CO_2. Using the results obtained, the rate of the reduction drop has been calculated. It was found that the drop rate at 1 atm CO_2 was 4.91 x 10^{-3} mole O cm^{-2} s^{-1} at the plasma temperature zone, (~ 2400 ^oC). This result was found to be in a good agreement with the extrapolation of the published work at lower temperatures. In other words, the plasma application did not show, via CO_2 dissociation, an increase in the reduction rate drop with respect to the published work.

- H_2O was supplied to H_2-Ar mixture in a series of experiments to investigate its influence on the reduction rate of Carajas ore. Contrary to the CO_2 experiments, no influence on the reduction was monitored. This was attributed to the less negative influence of H_2O against that of CO_2 on the reduction behaviour of H_2 from the equilibrium point of view. Moreover, the contribution CO and H_2 (generated from the reaction of graphite electrode with the produced H_2O) played an obvious role in further ore reduction and the disappearance of H_2O influence on H_2 reduction behaviour.

- Reduction of Carajas ore in H_2/Ar plasma atmosphere using continuously fed coke was also evaluated. From the experimental results, a specific reduction rate of iron oxide via coke was found to be 9.19 x 10^{-1} (*kg-oxygen/m^2s).* This means that the reduction potential of coke compared to that of H_2 is approximately a factor of 3 at high temperatures of the plasma application. An important advantage of coke usage

in H_2 plasma up-scaled process is the possibility to suppress FeO content in the slag such that the problem of slag aggressiveness to the refractory lining (due to high FeO) could be ruled out.

- Continuous feeding of Carajas fines ore throughout the experiment, rather than conducting batch-wise experiments, was examined in a series of experiments. It was concluded that ore feeding through the hollow electrode does neither deteriorate the plasma arc stability nor the behaviour of ore reduction.

- A SWOT (Strengths-Weaknesses-Opportunities-Threats) analysis was presented during the study of the up-scaling potential of the process. Some advantages were emphasized like the obvious low CO_2 emissions, flow-sheet simplicity and low slag produced. However, some weaknesses were introduced. Two important points that have to be deeply investigated in future work are the influence of the high heat flux via radiation in the freeboard zone on the total heat losses of the process and determination of a proper reactor lining in the slag zone (refractory / self lining). However, the option of self lining by water cooling system could be ruled out in the case of coke usage as a control tool for % FeO reduction in the slag. In that case, the refractory is a sensible option for the reactor lining.

In conclusion, it should be noted that despite that H_2/CH_4 plasma smelting reduction process shows a potential advantage, from the environmental point of view, the economics of plasma metallurgy processes do not yet show a significant advantage over other comparable techniques. Therefore the development of the plasma in the field of ore reduction is unlikely to happen unless electricity becomes much cheaper. A second scenario could be the growing shortage of fossil fuels and the increasing burden of reducing CO_2 emissions, which might force the steelmakers, at some time, to abandon the conventional steelmaking processes. A third scenario is the development of plasma technology one day so that the contribution of radicals (H and H^+) would exist, improving dramatically the reduction kinetics and driving the process to a novel economics standard.

9.2 Future work

Plasma processing, in general, has a high potential even at the present status. More work has to be done to find the strengths of the plasma metallurgy. During the execution of the present work, the following topics were found to be valuable for further work:

- During the last two decades, much work [91-93] has been done to develop processes based on plasma technology for recovering valuable metals from waste dusts and slag. However, all projects conducted have adopted only carbonaceous reducing agent for waste treatment. In that sense, it is believed that plasma application using hydrogen and coke (supplied by the existing screw conveyor facility) could be a potential alternative for the reduction of solid wastes, i.e. electric arc furnace (EAF) dust and EAF stainless steel dust.

- Continuous feeding of coke (using the screw conveyor facility) can be carried out in another series of experiments. In this work, a partial reduction of the oxide melt by H_2 plasma could be conducted. A switch to the reduction by coke is then proposed to investigate the coke behaviour (as a single reducing agent) and the possible carburisation in the remaining period of the experiment.

- The variation of the degree of reduction of iron oxide could be experimentally controlled in a series of experiments. The objective of these experiments is to investigate the reduction behaviour of the accompanying elements like phosphorous at various reduction degrees.

- Modelling work in the field of hydrogen plasma smelting reduction has not yet been conducted. The present status is still immature in the fundamentals of the technology like plasma arc heat distribution, melt temperature and heat losses. Some modelling work on the plasma arc, however, has recently started in conjunction with the chair of modelling and simulation of metallurgical processes (CMSMP). A primary validation to the simulation program with respect to the published work was conducted (shown in the appendix). The validation of the model with respect to the experimental results is planned as a next step.

List of figures

List of tables

List of literature

[1] International Iron and Steel Institute (IISI): Steel in figures, http://www.worldsteel.org/index.php

[2] Still, G., ThyssenKrupp Steel: Practical solutions for steel to national allocations plans, 5. June 2003, www.ceps.be/files/TF/SchulzeThyssenkrupp.ppt

[3] Birat, J. P., Arcelor Research: Overview of the results & conclusions of ULCOS program's phase I and of the scientific & technical program for phase II, second year-confidential report, August 2006.

[4] Sixth Framework Programme (FP6) Home Page: http://cordis.europa.eu/fp6/projects.htm, ULCOS.

[5] Boon, W. and Denys, M.: New smelting reduction, ULCOS 1st annual conference, Bilbao 11-12 February 2004.

[6] Sormann, A.: Doctoral thesis, Untersuchungen zur Schmelzreduktion von Eisenoxiden mit Wasserstoff als Reduktionsmittel. Montanuniversität Leoben, 1992.

[7] Sormann, A.; Hiebler, H.; Presslinger, H.: Smelting reduction of iron oxide by hydrogen. In: International Conference on New Smelting Reduction and Near Net Shape Casting Technologies for Steel. Vol. 1: pp.57-74, 1990.

[8] Hatarascu, O.: Besonderheiten der Thermodynamik und Kinetik der Eisenoxidreduktion mit Kohlenmonoxid und Wasserstoff: Archiv für das Eisenhüttenwesen. Vol. 51, Nr. 11: pp. 445-448, 1980.

[9] C.Bale, W.Pelton, K. Hack et al.: www.factsage.com, © Thermfact 1976-2007, GTT-Technologies.

[10] Plaul, J.F.: Doctoral thesis, Schmelzreduktion von hämatitischen Feinerzen im Wasserstoff-Argon-Pasma, Montanuniversität Leoben, 2005.

[11] Milner, D. R.: A survey of the scientific principles related to wetting and spreading, British welding journal, vol.5, no.3, pp. 90-105, 1958

[12] Coudurier, L.; Hopkins, D. W.; Wilkomirsky, I.: Fundamentals of metallurgical processes, Oxford, New York, Toronto, Sydney, Paris, Frankfurt: Pergamon Press, 1978.

[13] Robino, C.V., Representation of mixed reactive gases on free energy (Ellingham-Richardson) diagrams, Metallurgical and Materials Transaction B, vol 27B, pp 65-69, 1996.

[14] Bäck, E.: Doctoral thesis, Schmelzreduktion von Eisenoxiden mit Argon-Wasserstoff-Plasma, Montanuniversität Leoben, 1998.

[15] Dembovsky, V.: Zu Fragen der Thermodynamik und Reaktionskinetik in der Plasmametallurgie, Neue Hütte. Vol. 32: pp. 214-219, 1987.

[16] Dembovsky, V.: Plasma Metallurgy -The Principles, Materials Science Monographs, 23, Elsevier Science Ltd, 1985.

[17] Dembovsky, V.: How the polarity of a surface reacting with a low temperature plasma affects the thermodynamic variables in metallurgical reactions, acta phys. slov. 34, No.1, 1984.

[18] Kamiya, K.; Kitahara, N.: Reduction of molten iron oxide and FeO bearing slags by H_2-Ar plasma, Transactions ISIJ. Vol. 24: pp. 7-16, 1984.

[19] Ban-ya, S.; Iguchi, Y.; Nagasaka, T.: Rate of reduction of liquid iron oxide with hydrogen, Transactions ISIJ, Vol. 23, pp. 197, 1983.

[20] Hayashi, S.; Yoshiaki, I.: Hydrogen reduction of liquid iron oxide fines in gas-conveyed systems, ISIJ International, Vol. 34, No. 7, pp.555-561, 1994.

[21] Lemperle, M.; Weigel, A.: On the smelting reduction of iron ores with hydrogen argon plasma. steel research, Vol. 56, No. 9: pp. 465-469,1985

[22] Müller, H.: Doctoral thesis, Entwicklung von induktiven und Lichtbogen-Plasmaanlagen und ihre experimentelle Erprobung bei der Reduktion von Eisenerz. Aachen, RWTH-Aachen, 1982.

[23] Müller, H.; Weigel, A.; Wilhelmi, H.: Verfahrenstechnische Grundlagen der Plasma-Schmelzreduktion, Arch. Eisenhüttenwesen 54, No. 12, pp. 481-486, 1983.

[24] Plaul, J. F.; Krieger, W.: Wasserstoff-Plasma-Schmelzreduktion: Ein alternativer Weg zur Stahlerzeugung, BHM. Vol. 194, No. 7: pp. 235-239, 2004.

[25] Plaul, J. F.; Krieger, W.; Bäck, E.: Reduction of fine ores in argon-hydrogen plasma, steel research international. Vol. 76, No. 8: pp. 548-554, 2005.

[26] Bäck, E.; Schneider, R.; Hiebler, H.: Vergleich der Schmelzreduktionsverfahren, BHM. Vol. 142, No. 5: pp. 195-203, 1997.

[27] Bäck, E., Hiebler, H. (1998): Schmelzreduktion von Eisenoxid mit Wasserstoff in einem Plasmaofen, BHM. Vol. 143, No. 5: pp. 153-158, 1998.

[28] Bäck, E.,Sormann A.: Stand der Schmelzreduktion von Eisenoxid mit Wasserstoff als Reduktionsmittel, BHM. Vol. 145, Nr. 1: pp. 14-21, 2000.

[29] Nakamura, T.; Shibata, K.; Takeda, K.: Reduction and dephosphorisation of molten iron oxide with hydrogen-argon plasma, Plasma Chemistry and Plasma Processing. Vol. 1: pp. 149-160, 1981.

[30] Gilles, H. L.; Clump, C. W.: Reduction of iron ore with hydrogen in direct current plasma jet.: Ind. Eng. Chem. Process Des. Dev. Vol. 9: pp. 194-207, 1970.

[31] Gold, R. G.; Sandall; W. R., Cheplick P. G.: Plasma reduction of iron oxide with hydrogen and natural gas at 100 kw and 1 MW, Ironmaking and Steelmaking, No.1, pp. 10-14, 1977.

[32] Pateyron, B.; Aubreton, J.; Kassabji F.; Fauchais P.: New design of reduction plasma furnaces including the electrical transfer to the bath and the falling film, ISPC5, Edinburgh, pp. 167-177, 1981.

[33] Akashi, K.; Ishizuka, R.; Mutobe, T.: Reduction of metal oxide in a direct current plasma arc. Proceedings of the 4th International Conference on Vacuum Metallurgy, Vol. 3: pp. 165-169, 1974.

[34] Badr, K.; Bäck, E.; Krieger, W.: Reduction of iron ore by a mixture of Ar-H_2 with CO and CO_2 under plasma application; 18th International Symposium on Plasma Chemistry, August 26-31, Kyoto, Japan, 2007.

[35] Badr, K.; Bäck, E.; Krieger, W.: Plasma Reduction of Iron Oxide by Methane Gas and its Process Up-scaling; steel research int., 78, No. 4, pp. 275-280, 2007.

[36] Kato, K.; Sasaki, Y.; Soma, T.: Reduction of molten iron oxide with carbon monoxide gas, Trans. Iron Steel Inst. Jpn., Vol. 17, pp. 532-33, 1977.

[37] Soma, T.: Molten state reduction of iron ore, Bull. Jpn. Inst. Met., vol. 21, pp. 620-25, 1982.

[38] Tsukihashi, F.; Kato, K.; Ohtsuka, K.; Soma, T.: Reduction of molten iron ore with carbon Trans, Iron Steel Inst. Jpn., Vol. 22, pp. 688-95, 1982.

[39] Nagasaka, T; Iguchi, Y.; Ban-ya, S.: 5th Int. Iron and Steel Congr.: Process Technology Proc., ISS, Washington, DC, Vol. 6, pp.669-78, 1986.

[40] Nagasaka, T; Mitsutaka, H.; Ban-ya, S.: Interfacial kinetics of hydrogen with liquid slag containing iron oxide, Metall. Mater.Trans.B, Vol. 31B, pp.945-55, 2000.

[41] Ryzenkov, D.I.; Golenko, D.M.; Chelyadunov, L.M.: Izv. VUZ Chern. Met., No. 4, pp. 19-22, 1960.

[42] Kondakov, V.V. ; Ryzenkov, D.I. ; Golenko, D.M.: Izv. VUZ Chern. Met., No. 4, pp. 23-28, 1960.

[43] Takahashi, K.; Amatatsu, M.; Soma, T.: Reduction of molten iron ores with solid carbon, Tetsu-to-Hagane, vol. 61, pp. 2525-30, 1975.

[44] Sasaki, Y.; Okamoto, K.; Soma, T.: Tetsu-to-Hagane, Vol. 64, pp. 367-75, 1978.

[45] Tsukihashi, F.; Amatatsu, M.; Soma, T.: Reduction of molten iron ore with carbon, Tetsu-to-Hagane, Vol. 68, pp. 1880-88, 1982.

[46] Sato, A.; Aragane, G.; Kamihira, K.,; Yoshimatsu, S.: Reduction rate of molten iron oxide by the solid carbon or the carbon in molten iron, Tetsu-to-Hagane, 1987, Vol. 73, pp. 812-19.

[47] Dancy, T.E.: The kinetics of the reduction of iron oxide above 1400°, J. Iron Steel Inst., Vol. 169, pp. 17-24, 1951.

[48] Mac Rae; Donald, R.: Kinetics and mechanism of the reduction of solid iron oxides in iron-carbon melts from 1200 to 1500°, J. Met., Vol. 17, pp. 1391-95, 1965.

[49] Lloyd, G.W.; Young, D.R.; Baker, L.A.: Reaction of iron oxide with iron-carbon melts, Ironmaking and Steelmaking, Vol. 2, pp. 49-55, 1975.

[50] Sato, A.; Nakagawa, R.; Yoshimatsu, S.; Fukuzawa, A.; Ozak, F.: Melting rate of iron oxide pellets into iron melt, Tetsu-to-Hagane, Vol. 67, pp. 303-12, 1981.

[51] Feinman, J.: Plasma Technology in Metallurgical Processing, Iron and Steel Society, Chapter 3, 4, 7, ISBN 0-932897-12-6,1987.

[52] Murphy, A.B.; Arundell, C.J.: Transport coefficients of argon, nitrogen, oxygen, argon-nitrogen, and argon-oxygen Plasmas, Plasma Chem. Plasma Process, 14, pp. 451-490, 1994.

[53] Murphy, A.B.: Transport coefficients of hydrogen and argon-hydrogen plasmas, Plasma Chem. Plasma Process, 20, pp. 279-297, 2000.

[54] Murphy, A.B.; Tanaka, M.; Tashiro, S.; Satoh, T.; Lowke, J.J.: Modelling of the influence of welding gas composition on arc properties and weld depth in TIG welding, 18th International Symposium on Plasma Chemistry, August 26-31, Kyoto, Japan, 2007.

[55] Tanaka, M.; Lowke, J.J.: Predictions of weld pool profiles using plasma physics, J. Phys. D: Appl.. Phys. 40, pp.1-23, 2007.

[56] Murphy, A.B.: Demixing in free-beurning arcs, Physical Review E, Vol. 55, 6, pp. 7473, 1997.

[57] Coudert, J.F.; Delalondre, C.; Roumilhac, P., Simonin, O.; Fauchais, P.: Modeling and experimental study of a transferred arc stabilized with argon and flowing in a controlled-atmosphere chamber filled with argon at atmospheric pressure, Plasma Chem and Plasma Process, 13, pp. 399, 1993.

[58] Hur, M.; Hwang, T.H..; Ju, W. T.; Lee C. M.; Hong, S.H.: Numerical analysis and experiments on transferred plasma torches for finding appropriate operating conditions and electrode configuration for a waste melting process, Thin Solid Films, Vol. 390, pp. 186-191, 2001.

[59] Sci-Tech Encyclopedia, McGraw-Hill Encyclopedia of Science and Technology**,** 5th edition, McGraw-Hill Companies, Inc**.,** Principles of radiation transfer, www.Answers.com.

[60] Holt, N. J.; Bakken, J. A.: Transferred argon arc reactor with emphasis on radiation heat transfer, 1993 Electric furnace conference proceedings, pp.177-86, 1993.

[61] Esser, F.; Fiedler, H.; Lachner, W.: On the theory of remelting solid metallic charges in plasma torch furnaces, Proceedings 4th ICVM, pp.145-48, 1968.

[62] Bini, R.; Boulos, M.I.: Energy distribution in argon transferred arcs, 18th International Symposium on Plasma Chemistry, August 26-31, Kyoto, Japan, 2007.

[63] Lowke, J. J.: Prediction of arc temperature profiles using approximate emission coefficients for radiation losses, J. Quant. Spectrosc. Radiat. Transfer, 14, 111, 1974.

[64] Cram, L. E.: Statistical evaluation of radiative power losses from thermal plasmas due to spectral lines, J. Phys. D: Appl. Phys. vol. 18, pp. 401, 1985.

[65] Murphy, A.B.: Net emission coefficients tables using Cram method, not published yet.

[66] Bakken, J. A., Modelling of fluid flow, heat transfer and diffusion in arcs, High Temp. Chem. Processes 3, pp. 677-688, 1994.

[67] Essoltani, A.; Proulx, P.; Boulos, M.I.: Radiation and self absorption in argon – iron plasmas at atmospheric pressure, J. of Analytical Atomic Spectrometry, Vol. 5, pp. 543-546, 1990.

[68] Tanaka, M.; Ushio, M.; Lowke, J.J.: Numerical study of gas tungsten arc plasma with anode melting, Vacuum 73, pp. 381-389, 2004.

[69] Jones, R.T.; Reynolds, Q.G.; Alport, M.J.: DC arc photography and modelling, Minerals Engineering, V. 15, pp. 985-991, 2002.

[70] Fruehan R., The making, Shaping and Treating of Steel, 11th Edition, Steelmaking and Refining Volume, ISBN: 0-930767-02-0, pp. 61, 89, 1998.

[71] Turkdogan, E.T.: Fundamentals of Steelmaking, The Institute of Materials, London, 1996.

[72] Dembovsky, V.: Thermodynamics of dissolution and liberation of gases in the atomization of molten metals by plasma-induced expansion, J of Mat. Proc. Tech. 64, pp. 65-74, 1997.

[73] Gedeon, S. A; Eagar, T.W.: Thermochemical Analysis of Hydrogen Absorption in Welding, Welding Research Supplement, pp.264-271, 1990.

[74] Grigorian, V. A. et al.: Research on interaction of nitrogen with liquid iron in electric arc heating, Interactions of gases with metals (in Russian), pp. 146, 1973.

[75] Suh, D.; Eagar, T.W.: Mechanistic understanding of hydrogen in steel welds, Proceedings of international workshop conference on hydrogen management for welding applications, Ontario, Canada, pp.105-10, 6-8 Oct. 1998.

[76] Iguchi, Y.; Ban-ya, S.; Fuwa, T.: The solubility of water in liquid CaO-SiO_2 with Al_2O_3, TiO2, and FeO at 1550oC, Transactions ISIJ, Vol. 9, pp. 189-95, 1969.

[77] Wahlster, M.; Reichel, H.: Die Wasserstofflöslichkeit von Schlacken des Systems CaO-FeO-SiO_2, Archiv für das Eisenhüttenwesen, Heft 1, 1969.

[78] Ban-ya, S.; Hino, M.; Nagasaka, T: Estimation of water vapour solubility in molten silicates by quadratic formalism based on the regular solution model, ISIJ International, Vol. 33, pp. 12-19, 1993.

[79] Sung-Koo, J.; Seon-Hyo, K.: The solubility of water vapour in CaO- SiO_2-Al_2O_3-MgO slag system, steel research 71, pp. 15-21, 2000.

[80] Imai, M.; Ooi., H.; Emi, T.: Tetsu to Hagane 48, pp.111/17, 1962.

[81] Larson, H.: Chipman, J.: Oxygen activity in iron oxide slags, Journal of Metals, pp. 1089-96, 1953.

[82] Jung, In-Ho: Thermodynamic modelling of gas solubility in molten slags (II)-water, ISIJ International, Vol. 46, No.11, pp. 1587-93, 2006.

[83] Bronkhorst High-Tech B.V.: Bronkhorst software for physical properties and flow calculations of liquids and gases, http://www.fluidat.com.

[84] Purdue University, College of Science: Review of the activation energy of chemical reactions, http://chemed.chem.purdue.edu/genchem/topicreview/

[85] LI, Y.; Ratchev, I. P.; Belton, G.R.; et al.: Rate of interfacial reaction between liquid iron oxide and CO-CO_2, Metall. and Mater.Trans.B, Vol. 31B, pp. 1049-1057, October 2000.

[86] Story, S.R.; Fruehan, R.J.: Kinetics of oxidation of carbonaceous materials by CO_2 and H_2O between 1300°C and 1500°C, Metall. and Mater.Trans.B, Vol. 31B, pp. 43-54, February 2000.

[87] Wiesinger, H.: Doctoral thesis: Bewertung der Wasserstoffschmelzreduktion zur Stahlherstellung, Montanuniveristät Leoben, 2000.

[88] Elmquist, S.; Weber, P; Eichberger, H: Operational results of the Circored fine ore direct reduction plant in Trinidad, stahl und eisen 122, No.2 , 2002.

[89] R. Speets: Iron Making Model User Manual – IRMA version 1.1, Corus Research, Development & Technology, Confidential within ULCOS Project, 2005.

[90] Vincent, G.: Vacuum and Pressure Swing Adsorption by AIR LIQUIDE, Confidential presentation within ULCOS Project, September 2006.

[91] Herlitz, H.G.: Plasma technology for metal recovery from oxidic waste, Vacuum Metallurgy Conference on Special Metals Melting and Processing, Pittsburgh, PA, June 1984.

[92] Page, D.C.; Heanley, C.P.: Non ferrous metals extraction using Tetatronics Plasma Systems with particular emphasis on Zinc and Lead, Mintek 50, International conference on Plasma in Extractive Metallurgy, Sandton, South Africa, March1984.

[93] Denton, G.M.; Barcza, N.A.; Scott. P.D.; Fulton, T.: EAF stainless steel dust processing, John Floyd International Symposium on Sustainable Developments in Metals Processing, Melbourne, Australia, pp. 273-283July 2005.

Smelting of Iron Oxides Using Hydrogen Based Plasmas

Appendix

10 Appendix

A. Thermodynamic calculations of slag diagrams at various % CaO

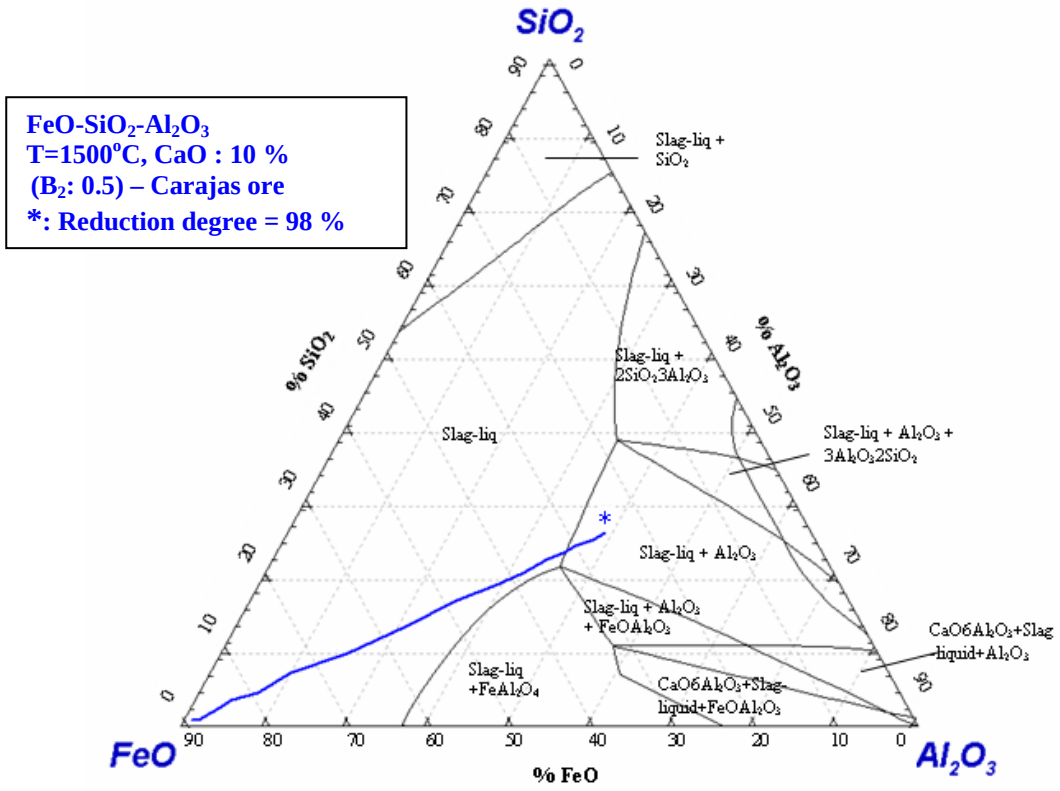

Fig. A.1 Quaternary oxide system $FeO\text{-}SiO_2\text{-}Al_2O_3\text{-}CaO$ and the calculated slag line during reduction at temperature: 1500 °C and CaO: 10 %

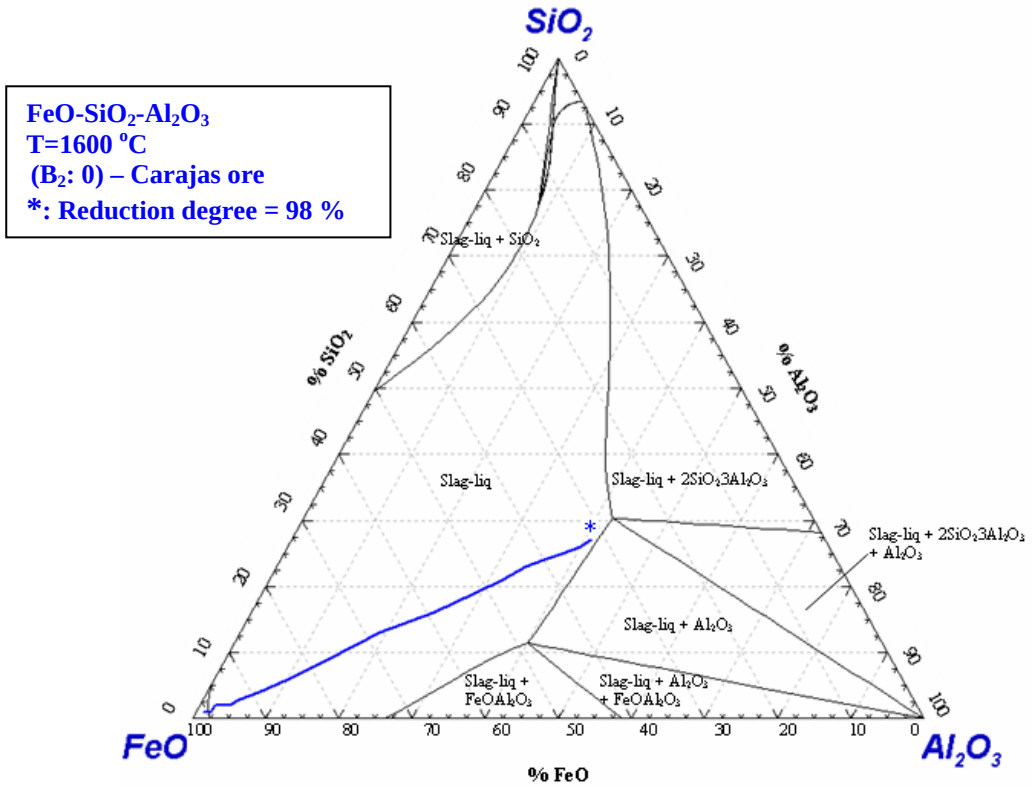

Fig. A.2 Ternary oxide system $FeO\text{-}SiO_2\text{-}Al_2O_3$ and the calculated slag line during reduction at temperature: 1600 °C and CaO: 0 %

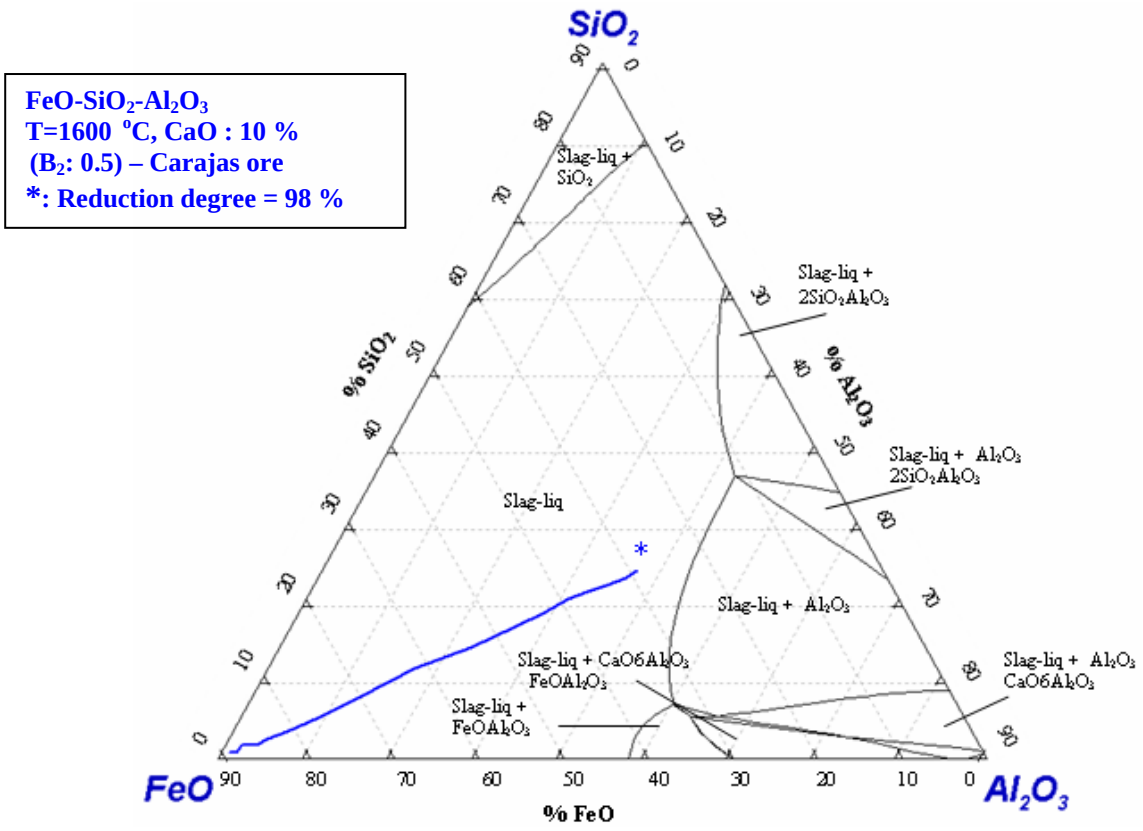

Fig. A.3 Quaternary oxide system $FeO\text{-}SiO_2\text{-}Al_2O_3\text{-}CaO$ and the calculated slag line during reduction at temperature: 1600 °C and CaO: 10 %

B. Experimental work

CaO	Insoluble in HCl	LOI	Heavy metals (as Pb)	Fluoride	Mg and alkali salts
min. 93.48 %	max. 0.5 %	max. 3.5 %	0.003 %	0.015 %	max. 2.5 %

Table B.1 Chemical analysis of the lime used in the basicity experiments, wt.

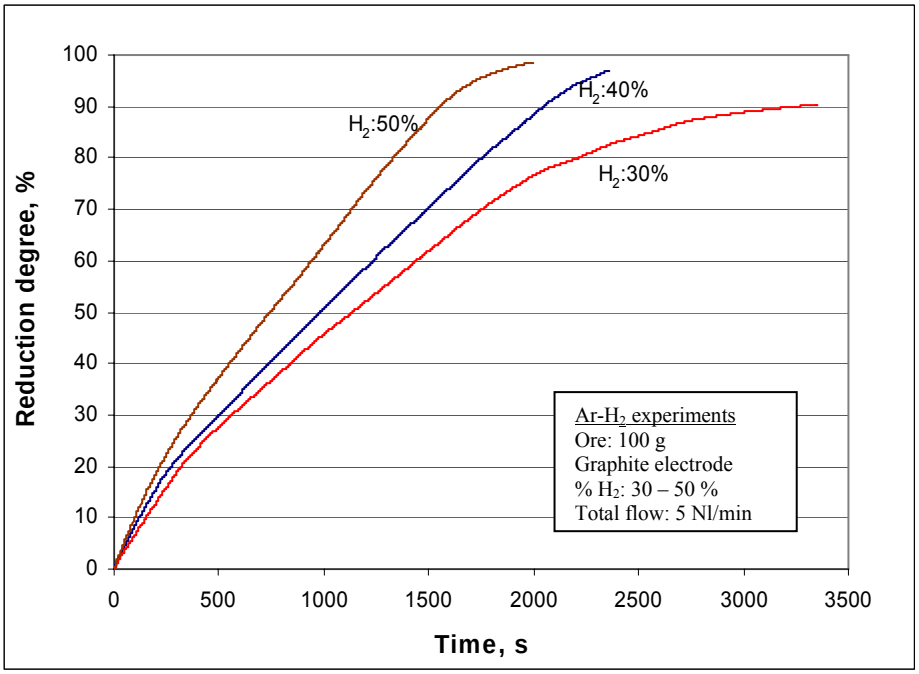

Fig. B.1 Reduction degrees of Carajas ore at various concentrations of H_2 in Ar-H_2 mixture

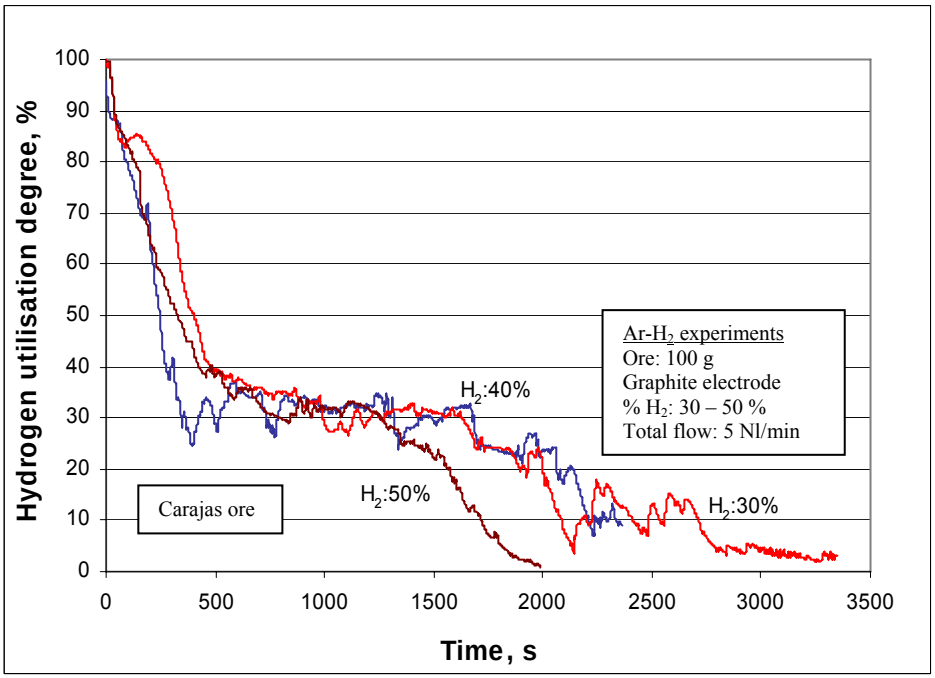

Fig.B.2 Utilisation degrees of hydrogen at various concentrations of H_2 in Ar-H_2 mixture

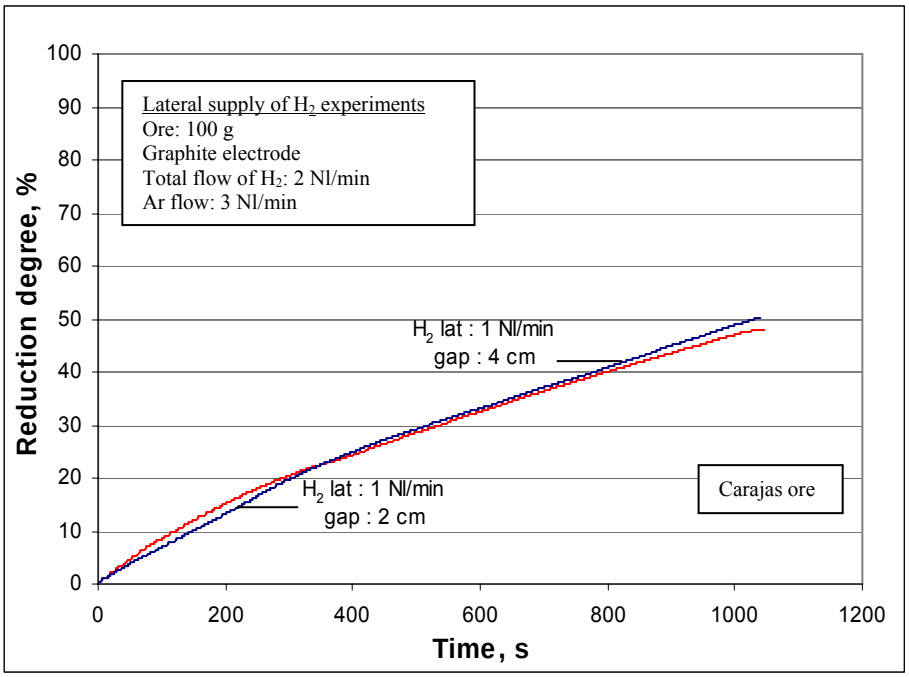

Fig. B.3 Reduction degrees of hydrogen at two different gaps; distance between the lance tip and the melt surface

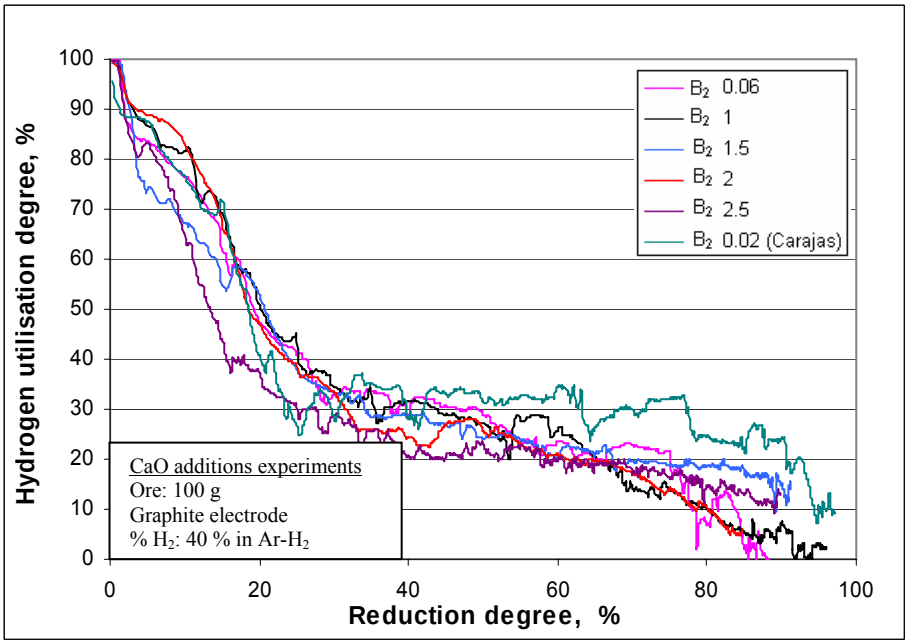

Fig. B.4 Utilisation degrees of hydrogen versus reduction degree; using Hamersley ore at various basicities (B_2= 0.06 - 2.5) and Carajas ore without CaO additions

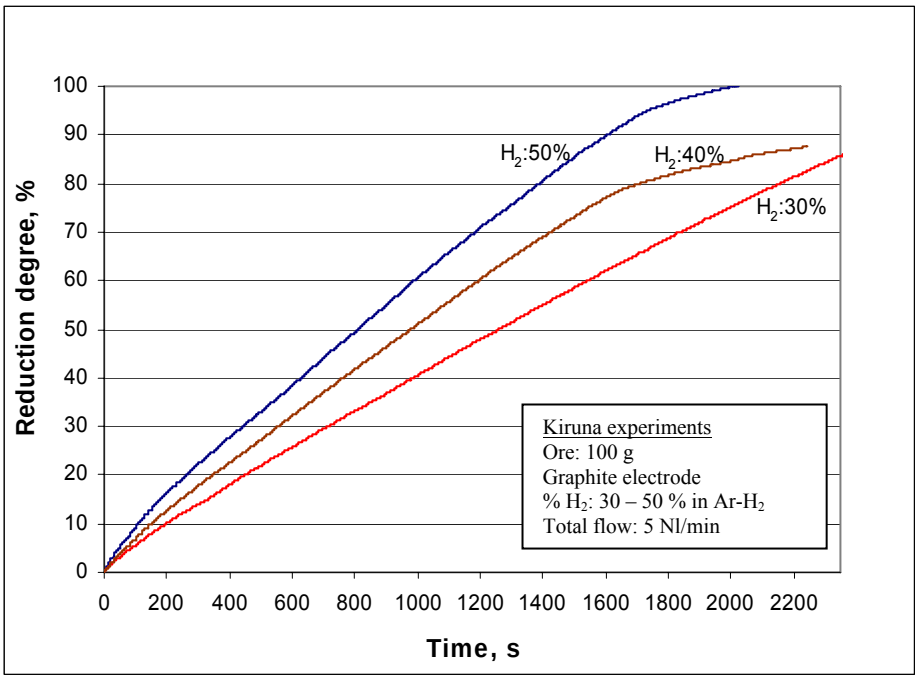

Fig. B.5 Reduction degrees of Kiruna ore at various concentrations of H_2 in Ar-H_2 mixture

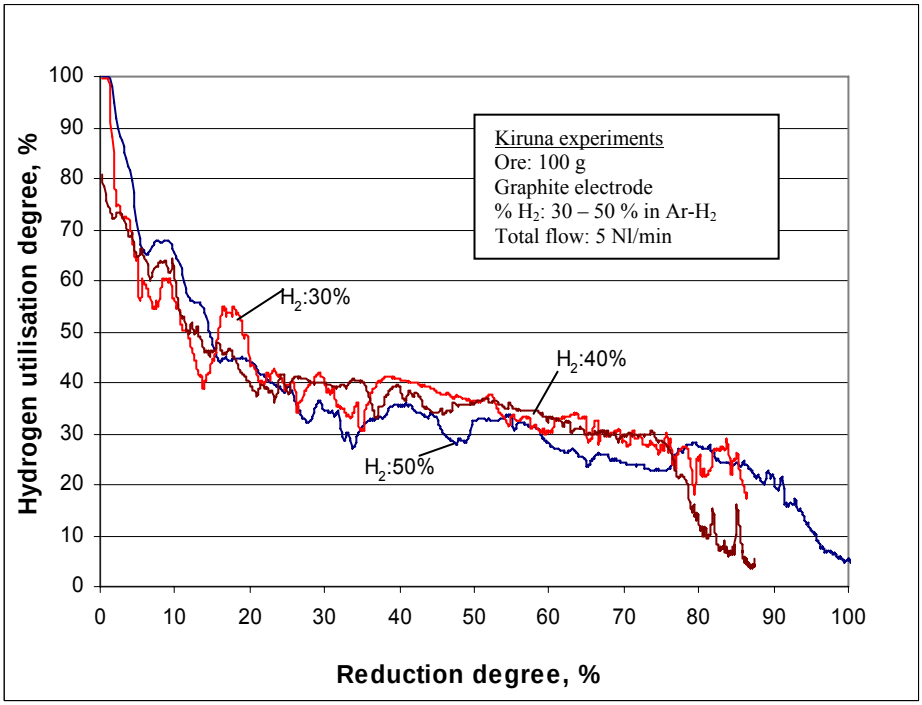

Fig. B.6 Hydrogen utilisation degrees using Kiruna ore at various concentrations of H_2 in Ar-H_2 mixture

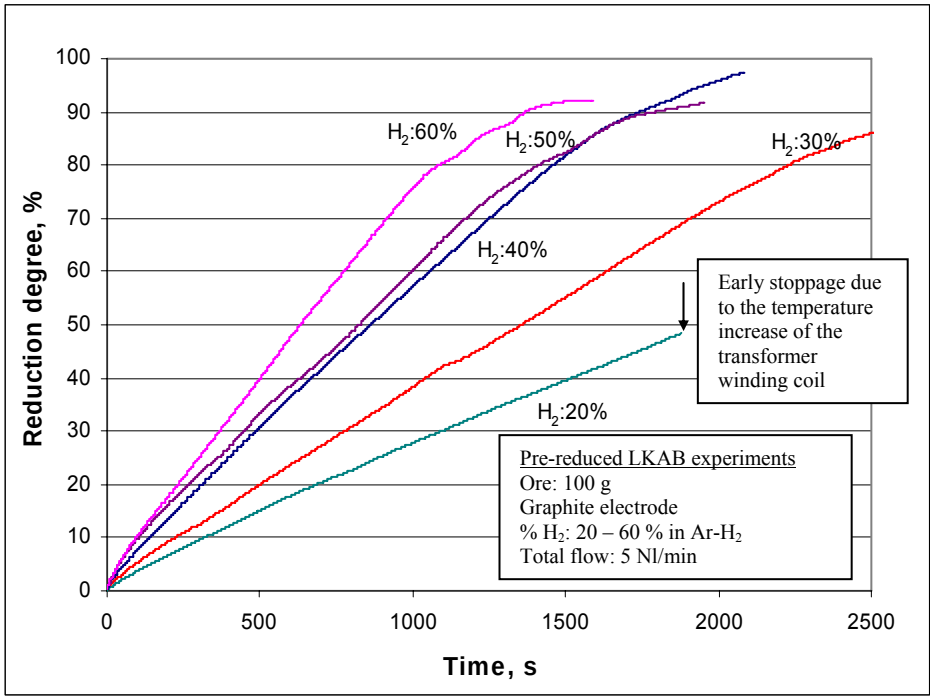

Fig. B.7 Reduction degrees of Kiruna ore at various concentrations of H_2 in Ar-H_2 mixture

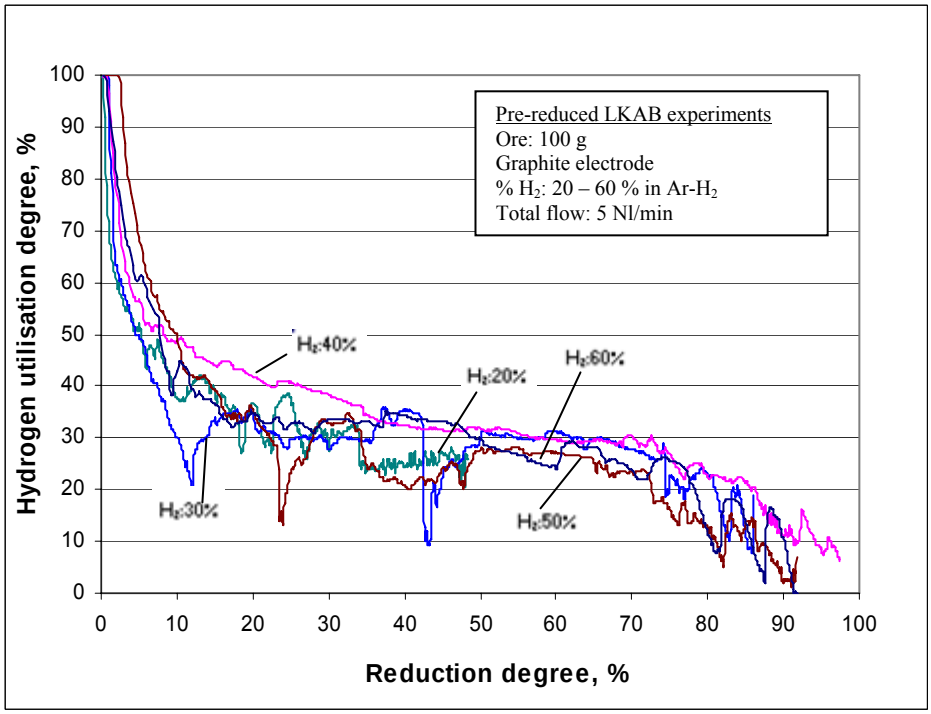

Fig. B.8 Hydrogen utilisation degrees using pre-reduced LKAB ore at various concentrations of H_2 in Ar-H_2 mixture

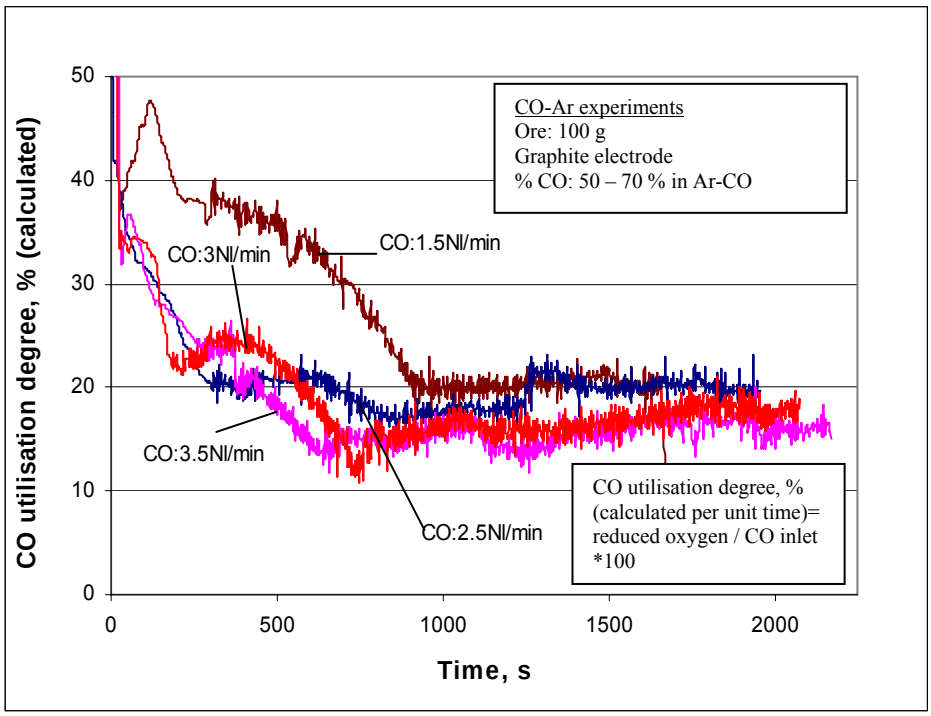

Fig. B.9 CO utilisation degrees (calculated) using Carajas ore at various concentrations of CO in Ar-CO mixture

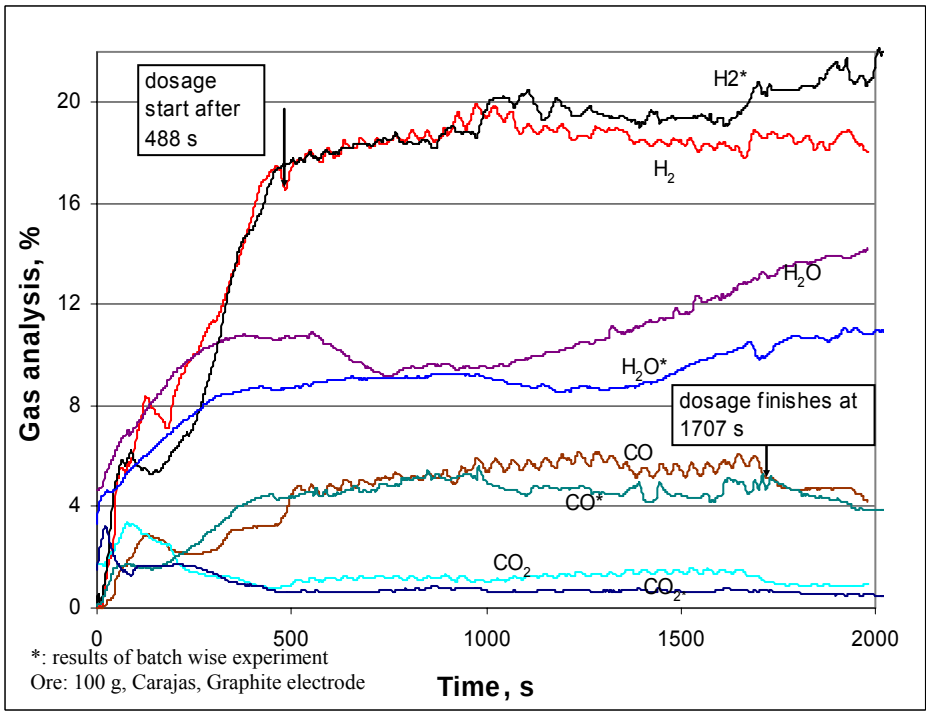

Fig. B.10 Gas analysis at 30 % H_2 in Ar – H_2; ore continuous feeding against batch wise results

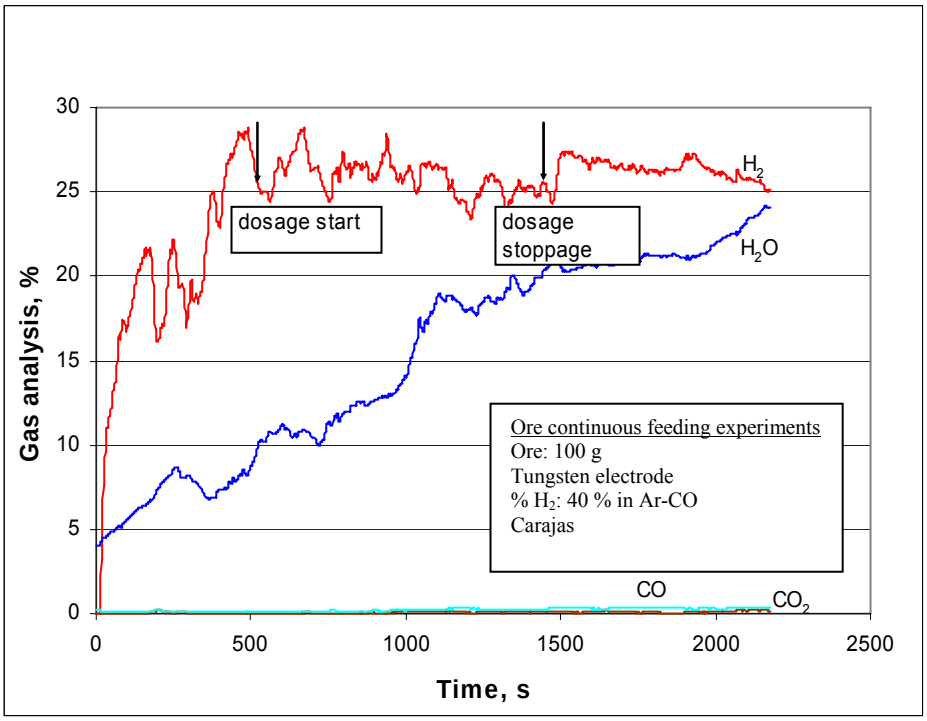

Fig. B.11 Gas analysis at 40 % H_2 in Ar – H_2; ore continuous feeding using tungsten electrode

C. CH_4 heat and mass balance, IRMA model

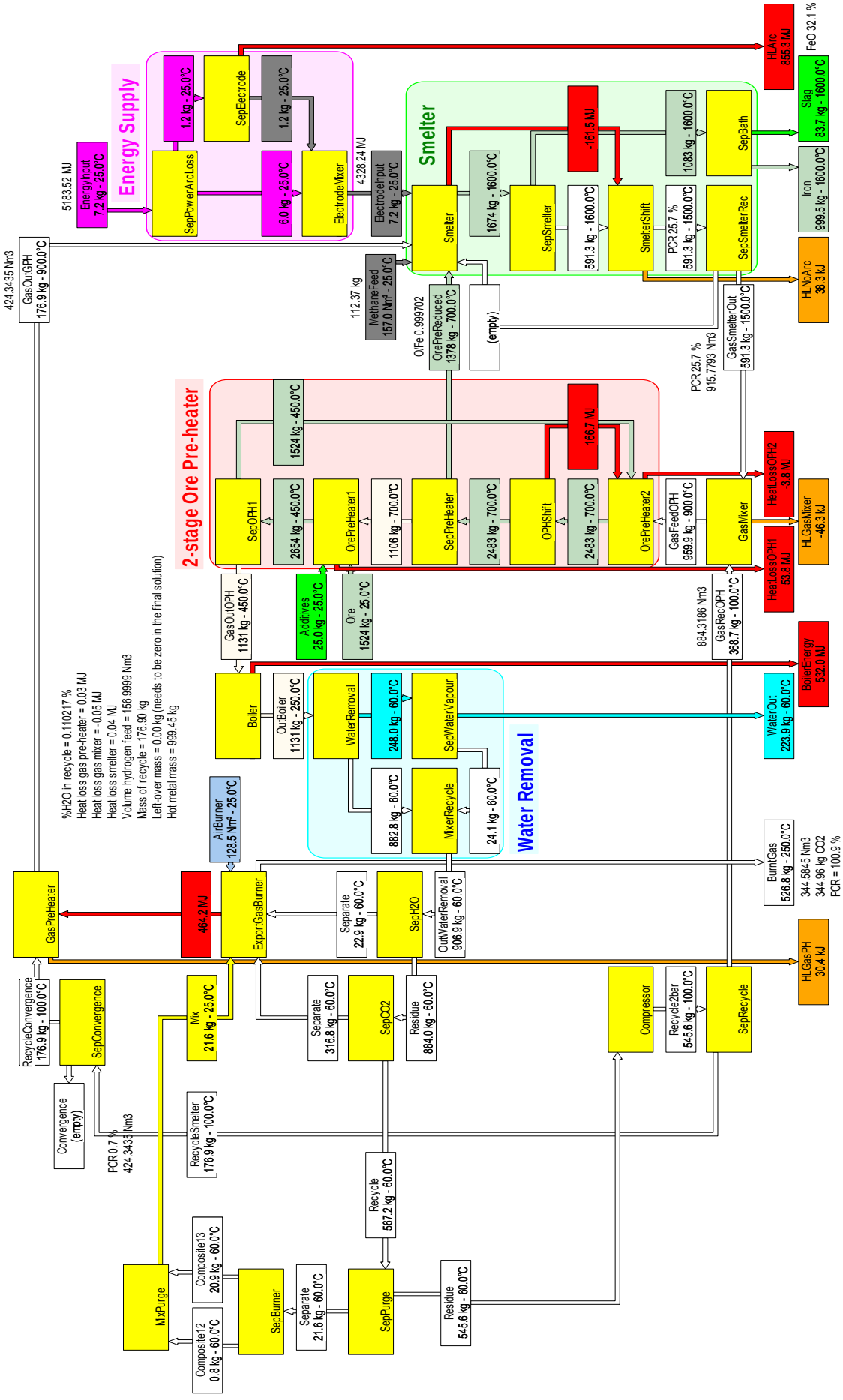

Fig. C.1 Methane Plasma Smelting Reduction, MPSR heat & mass balance, IRMA model

D. Numerical simulation of pure hydrogen arc with FLUENT program

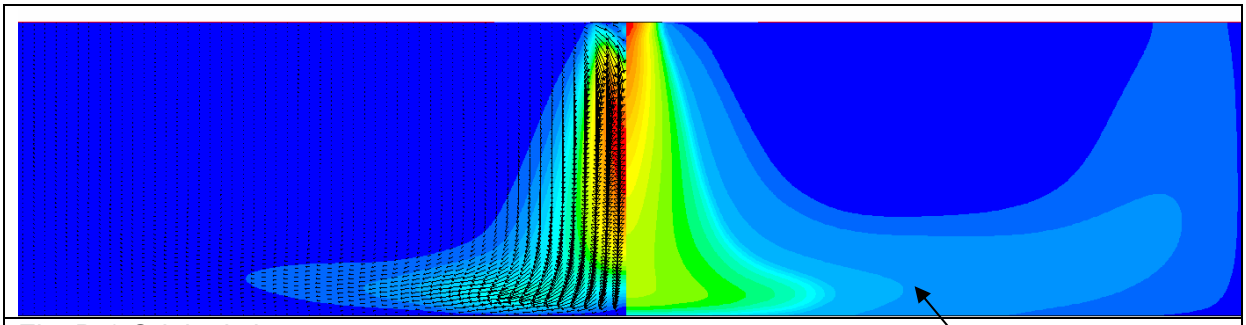

Fig. D.1 Original size

Arc gap: 5 mm, Arc current: 150 Amp, Melt width: 20mm

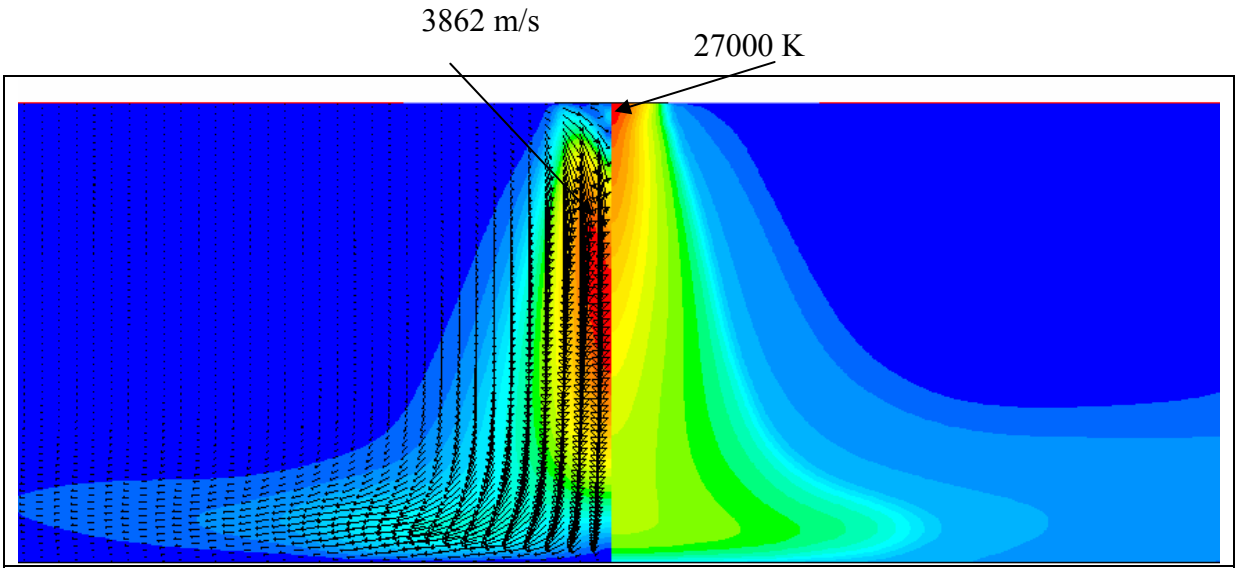

Fig. D.2 Corped and zoomed: maximum velocity 3862 m/s maximum temperature 27000 K

Equations solved

- **Momentum:** Navier-stokes with Lorentz force
- **Turbulence:** RNG k-epsilon (Renormalisation group)
- **Energy:** Enthalpy with Joule heating
- **Electric current**: Electromagnetic induction
- **Radiation:** Discrete ordinates

Boundary conditions

	Solid electrode	Open top	Lateral wall	Melt
Momentum	Velocity = 0 m/s	Pressure = 1 atm	Velocity = 0 m/s	Velocity = 0 m/s
Energy	T=3500 K	Entering flow T=300 K	h=1000 Watt/m^2K Tc = 300 K	h = 5000 Watt/m^2K Tc = 1500 K
Electric current	$J_z = B(1-(r/r_e)^2)$ (A/m^2) r = radius, r_e is the electrode radius B=f(I_0), I_0 total current	$J_z = 0$ (A/m^2) J_z: axial current density	$J_r = 0$ (A/m^2) J_r: radial current density	$J_r = 0$ (A/m^2)

Table D.1 Boundary conditions

Validation of the results against Murphy* [54]

	Maximum temperature (K)	Maximum Velocity (m/s)
Murphy	27000	4332
Present work	27000	3862

*: same boundary conditions (arc current, arc gap, pure H_2)

Table D.2 Comparison between the present work and Murphy's work